

L

AD B 005191

NWC TP 5319
Part 1

Plume-Signal Interference

Part 1. Radar Attenuation

by
Andrew C. Victor
Production Development Department

JUNE 1975

DDC
RECEIVED
JUL 21 1975
RECEIVED
B

Distribution limited to U.S. Government agencies only; test and evaluation; 22 May 1975. Other requests for this document must be referred to the Naval Weapons Center.

Naval Weapons Center

CHINA LAKE, CALIFORNIA 93555



Naval Weapons Center

AN ACTIVITY OF THE NAVAL MATERIAL COMMAND

R. G. Freeman, III, RAdm., USN Commander

G. L. Hollingsworth Technical Director

FOREWORD

This report (combined with Part 2 which was published in May 1972) is the final publication of a plume signal interference research program initiated at the Naval Weapons Center (NWC) over ten years ago. Funding for the program was canceled in January 1974, causing a reduction in the number of sample problems included in Section 5, *Problem Solving*. No other recognized reduction in quality has resulted.

This report goes beyond the scope of the NWC studies in order to present a balanced compendium which can be used for the solution of practical problems. Support for the preparation of this report was provided by the Naval Air Systems Command (NASC) through AirTask A3303300/216-B/IF-19332302. Other significant support during the preceding decade was provided by the Naval Ordnance Systems Command (NOSC)(now Naval Sea Systems Command) and by the joint NASC-NOSC consortium which once formed the Bureau of Naval Weapons.

This report is intended for use at the working level and does not reflect the official view or final judgment of NWC.

Released by
D. H. WILLIAMS, *Head*
Advanced Technology Division
1 December 1974

Under authority of
G. W. LEONARD, *Head*
Propulsion Development Department

NWC Technical Publication 5319, Part 1

Published by Propulsion Development Department
Collation Cover, 132 leaves
First printing 270 unnumbered copies

UNCLASSIFIED

SECURITY CLASSIFICATION OF THIS PAGE (When Data Entered)

REPORT DOCUMENTATION PAGE		READ INSTRUCTIONS BEFORE COMPLETING FORM
1. REPORT NUMBER NWC TP 5319, Part 1	2. GOVT ACCESSION NO.	3. RECIPIENT'S CATALOG NUMBER
4. TITLE (and Subtitle) PLUME-SIGNAL INTERFERENCE PART. 1. RADAR ATTENUATION		5. TYPE OF REPORT & PERIOD COVERED
		6. PERFORMING ORG. REPORT NUMBER
7. AUTHOR(s) Andrew C. Victor		8. CONTRACT OR GRANT NUMBER(s) AirTask A3303300/216-B/1F-19332302
9. PERFORMING ORGANIZATION NAME AND ADDRESS Naval Weapons Center China Lake, California		10. PROGRAM ELEMENT, PROJECT, TASK AREA & WORK UNIT NUMBERS
11. CONTROLLING OFFICE NAME AND ADDRESS Naval Air Systems Command Naval Ordnance Systems Command Washington, DC 20361		12. REPORT DATE June 1975
		13. NUMBER OF PAGES 262
14. MONITORING AGENCY NAME & ADDRESS (if different from Controlling Office)		15. SECURITY CLASS. (of this report) UNCLASSIFIED
		15a. DECLASSIFICATION/DOWNGRADING SCHEDULE
16. DISTRIBUTION STATEMENT (of this Report) Distribution limited to U.S. Government agencies only; test and evaluation; 22 May 1975. Other requests for this document must be referred to the Naval Weapons Center.		
17. DISTRIBUTION STATEMENT (of the abstract entered in Block 20, if different from Report)		
18. SUPPLEMENTARY NOTES		
19. KEY WORDS (Continue on reverse side if necessary and identify by block number) Exhaust Plume Rocket Exhaust Rocket Plume Radar Attenuation Plume Signal Interference Plume Models Electron Suppression		
20. ABSTRACT (Continue on reverse side if necessary and identify by block number) See reverse side of this form.		

DD FORM 1473
1 JAN 73EDITION OF 1 NOV 65 IS OBSOLETE
S/N 0102-014-6601 1

UNCLASSIFIED

SECURITY CLASSIFICATION OF THIS PAGE (When Data Entered)

UNCLASSIFIED

SECURITY CLASSIFICATION OF THIS PAGE(When Data Entered)

(U) *Plume-Signal Interference, Part I. Radar Attenuation* by Andrew C. Victor. China Lake, Calif., NWC, June 1975. 262 pp. (NWC TP 5319, Part I, publication UNCLASSIFIED.)

(U) A number of analytical techniques for predicting radar attenuation by tactical rocket exhausts in flight and static tests are assembled and described in this report. The results of many attenuation measurements are included for comparison with the calculations. These data also form a data base which may be used for preliminary estimates of attenuation and other plume properties on unmeasured propulsion systems.

UNCLASSIFIED

SECURITY CLASSIFICATION OF THIS PAGE(When Data Entered)

NWC TP 5319, Part 1

CONTENTS

1.0 Introduction	3
2.0 Plume Models	5
2.1 Chamber Reactions and Nozzle Expansion	9
2.2 Equilibrium Exhaust-Air Mixtures	11
2.3 Static Versus Flight Conditions	13
2.4 Base Recirculation and Reactions	13
2.5 Inviscid Plume	16
2.6 Compute Mixing and Afterburning Plume	27
2.7 Plume Mixing Models Incorporating Chemical Kinetics	38
2.8 Prediction of the Effects of Attenuation-Reducing Additives	43
3.0 RF Interaction Models	53
3.1 Line-of-Sight Attenuation Calculations	56
3.2 Diagonal Refraction	62
3.3 Diagonal Diffraction	66
3.4 Dispersion of Focused Microwave Beams in Transverse Attenuation Measurements	78
3.5 Pulse Distortion by a Rocket Exhaust Plume	83
4.0 Plume-RF Attenuation Data Summary	89
4.1 Static Transverse Attenuation Data	91
4.2 Static Diagonal Attenuation Data	93
4.3 Dynamic Transverse Attenuation Data	102
4.4 In-Flight Attenuation Data	108
4.5 RF Attenuation Suppressing Additive Data	112
5.0 Problem Solving	123
5.1 Use of the BYU Plume Model	124
5.2 Use of the AeroChem Plume Model	126
5.3 Concluding Remarks on Problem Solving	135
References	137
Appendices	
A. Diagonal Line-of-Sight and Ray Trace Refraction Computer Programs	151
B. Diagonal Diffraction Computer Programs	173
C. Transverse Attenuation Data	187
D. Plume Properties and Radar Attenuation for Six Rocket Motor Firings	249

1.0 INTRODUCTION

Afterburning exhaust plumes of rocket propulsion systems interfere with radio frequency (RF) transmission. This interference is caused by absorption, refraction, diffraction, reflection, and modulation effects of the plumes on RF transmissions through them. Such interference can prevent guided missiles from achieving their operational objectives. Other problems arise from plume interference with range telemetry and range command-destroy signals.

This publication is concerned with signal interference by low- to medium-altitude plumes (less than 75,000 feet) in which mixing and afterburning with air constitute a major source of heat in the plume. Some of the chemical reactions occurring at the resulting high temperature release free electrons into the plume flow, predominantly by reactions related to ionization of alkali metal impurities in the propellant. A minor degree of ionization is due also to chemi-ionization, but this source of free electrons needs to be considered only in very pure liquid propellant systems with no chamber or nozzle ablation effects.

Plume signal interference at higher altitudes falls beyond the range of most of our work at the Naval Weapons Center (NWC). In such cases the plume does not afterburn, and plume structure and other properties can be calculated by inviscid techniques. From this point, the calculation of interactions with RF radiation is similar to that for afterburning plumes.

Theoretically, all RF/plume interactions are contained in the solution to Maxwell's wave equations in a time-dependent lossy medium. However, since this solution has proved intractable for any real cases of interest, it has been necessary to subdivide the problem into several specific types of interactions and deal with each of those individually. In this manner, theoretical assumptions and approximations can be applied to the phenomena for which they seem reasonable without oversimplifying the general problem. Thus, we may treat absorption, refraction, diffraction, and reflection separately, although it is their combined effect which results in what we observe as attenuation. We further separate modulation effects (and those closely-related ones which appear as radar cross section) into a special category of time-dependent or turbulence-related effects.

While it is not assumed that the reader necessarily has any prior experience in plume-signal interference technology, a familiarity with interference problems is presumed. Therefore, the preceding discussion of the problem has been brief.

Although the "arcane art" of predicting rocket exhaust plume RF/interference has grown vigorously over the past decade, no prior effort other than a recent review paper (Ref. 1) has been made to summarize the techniques available for dealing with the problem. When this report was originally conceived six years ago, it was envisioned as a primer in radar attenuation by rocket plumes. The original draft was partially completed when progress was rudely jarred by the following realizations:

NWC TP 5. 4 Part 1

1. Existing plume models did not account for flight effects in a realistic manner. Most notably, the important effects of missile base geometry were ignored in the models.
2. Existing RF interaction models based on line-of-sight propagation failed to accurately predict diagonal attenuation for static tests of many high-energy propellants.
3. There were inconsistencies between attenuation data on the same propellant fired in different size motors. These inconsistencies could not be explained by existing models.
4. There was lack of agreement between transverse attenuation measurements and analytical predictions.
5. Plume-induced noise data did not fit predictions based on plume turbulence models.
6. No chemical models existed for predicting the suppression of electron density by propellant additives.

These difficulties have been attacked in the intervening years. While it would be foolish to think these difficulties have been conquered, we now have tools for dealing with all of them. Further improvements in plume technology are being sought; in the future, some of the techniques described here will be superceded. Nevertheless, the time for collecting the technology and presenting it in one place now seems opportune.

This report is intended to serve as a guidebook for solving plume-signal interference problems. An earlier paper (Ref. 1) summarized the problem, available data, and analytical models. This report (Part 1) takes the next step and leads the reader through the use of analytical models by actually solving realistic attenuation problems. In Part 2, (Ref. 2) modulation or noise induced on RF signals by plumes is discussed in terms of experimental data and a predictive model. Additional aspects of plume technology will be treated in workbook fashion in the JANNAF Plume Technology Handbook now in preparation (Ref. 3).

Analytical models of both plume dynamics and electromagnetic wave interactions with plumes range from the trivially simple to formulations which are too complex to have yet been solved. Between these extremes is a wide range of models which have been used with varying degrees of success to predict and explain the results of plume-signal interference measurements in a variety of test and flight situations. Those models which have been developed and/or used at NWC are described in detail with examples of their use. Other models, with which we have little or no working experience, are discussed with reference to their sources.

The approach used in this publication follows that recommended in Ref. 4. Figure 1 is a logic diagram to the solution of interference problems and to tools available for their solution. Sections 2.0 and 3.0 of this report follow the logic diagram through the techniques of plume property determination and calculation of electromagnetic interactions. Section 4.0 is a summary of available data and Section 5.0 presents the solution of sample problems.

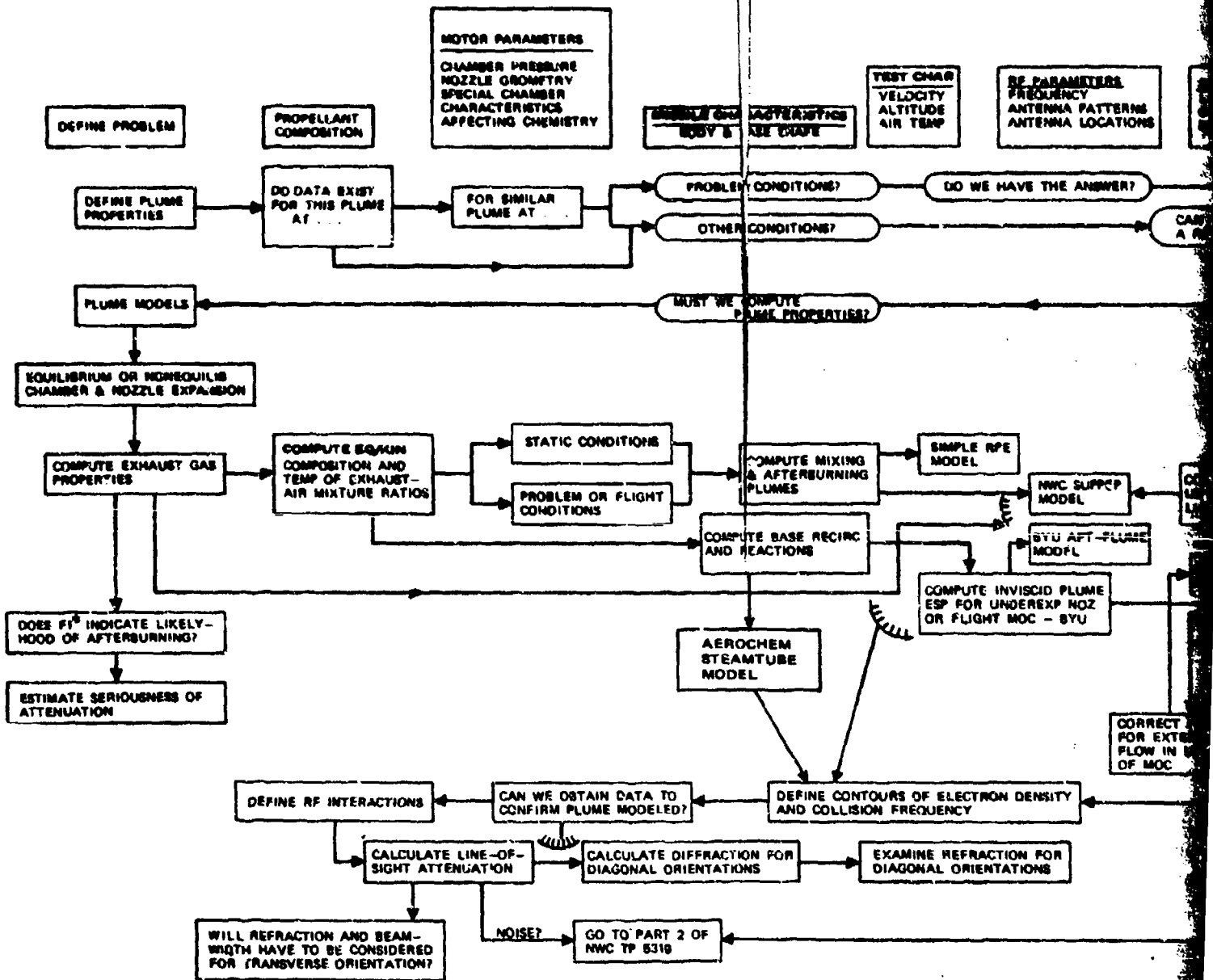
2.0 PLUME MODELS

Predictions of plume-induced RF attenuation based entirely on calculated plume structures and properties have been made since about 1965 (Ref. 5 through 10). Prior to that time, the predictions were usually made for calculated exit plane conditions or for data correlations in which electron-density and electron-neutral collision frequencies were "backed out" of measured attenuation values.

In order to calculate *steady state* attenuation, one must first map the plume electron density and collision frequency contours in space. Because of the complexities of plume chemistry, this requires sophisticated calculations of other plume properties including temperature, pressure, velocity, density, major neutral species and minor (but critically important) ionic species. In some cases, especially where reaction rate chemistry is included, some minor neutral species concentrations may also be very important. The physics and chemistry of plume mixing and afterburning with air must also be accounted for in the low-to-intermediate altitude (below 75,000 feet) plumes of tactical missiles with which this report deals.

Because the theory of plume flow fields has been dealt with many times in many places (Ref. 2 through 18), it will not be repeated here. For afterburning plumes, it is often unnecessary to consider the shock intersection structure which has a minor effect compared with the much larger volume of high-temperature high-electron density gas due to afterburning. Even for low attenuating systems, very good agreement has been obtained between data and theory by simple superposition of independently calculated inviscid and afterburning plume properties (Ref. 8) (Figure 2).

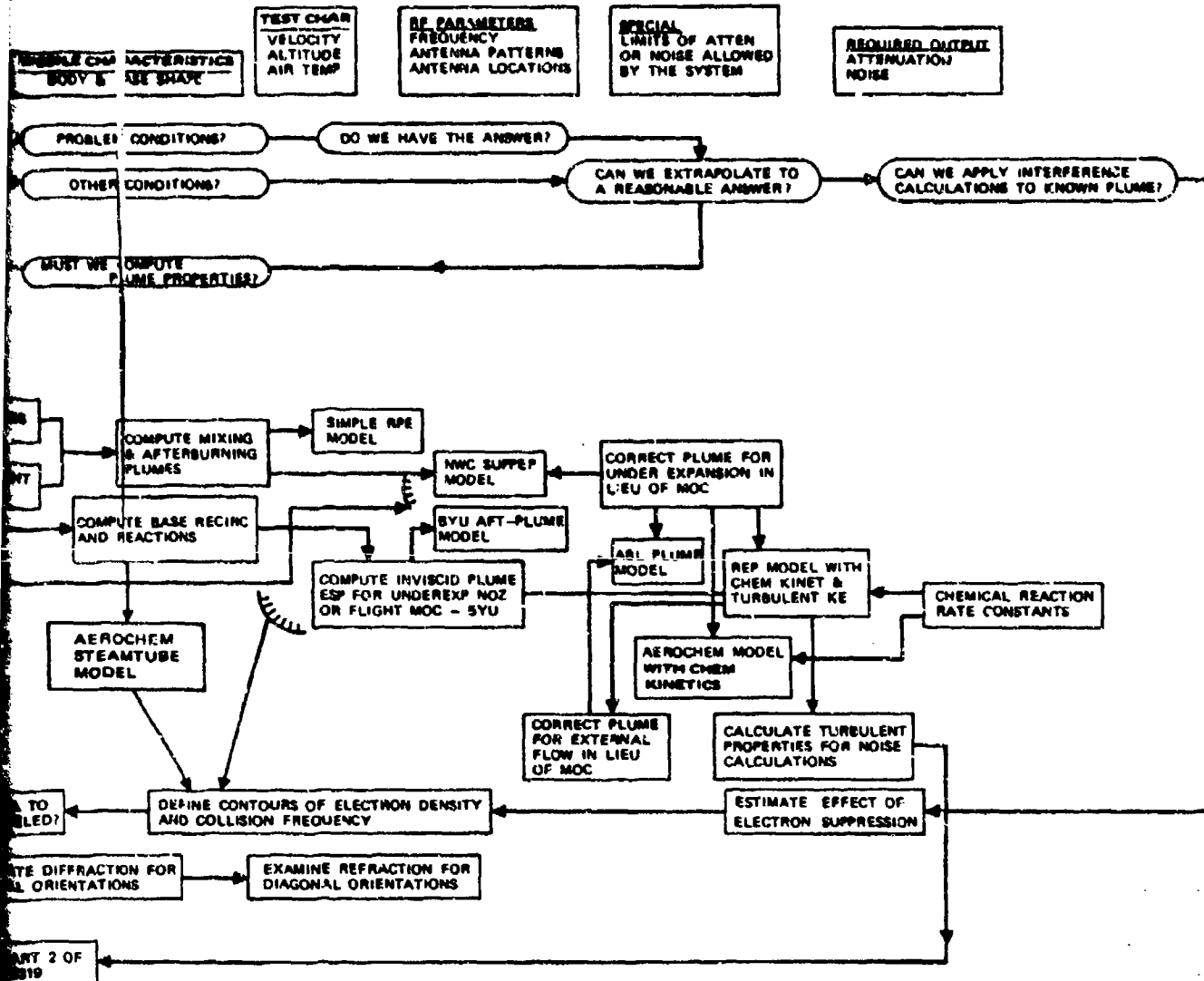
The total plume structure model is outlined in Figure 3. For some cases, several factors may be eliminated. For example, for a plume exhausting into still air, the free-stream velocity is zero and the base recirculation is negligible. For optimally expanded nozzles with small exit cone angles, the shock structure may be ignored without serious error. Multiphase flow is generally ignored in plume calculations used for RF interaction predictions. This approximation has not caused any failures that we know of. However, it is well-known that high concentrations of fine particles have a major effect on the gas properties in a jet (Ref. 19, 20).



$FI^2 = \text{FUEL INDEX} = (CO + H_2) / (CO + H_2 + CO_2 + H_2O + HCL)$. HIGHER VALUES INDICATE MORE OXIDIZABLE SPECIES.

FIGURE 1. Logic Diagram for Solution of Plume Signal Interference Problems.

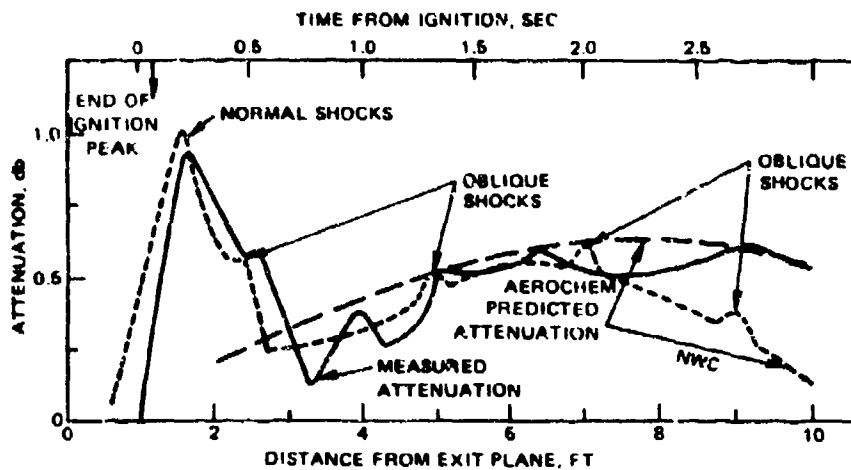
NWC TP 5319, Part 1



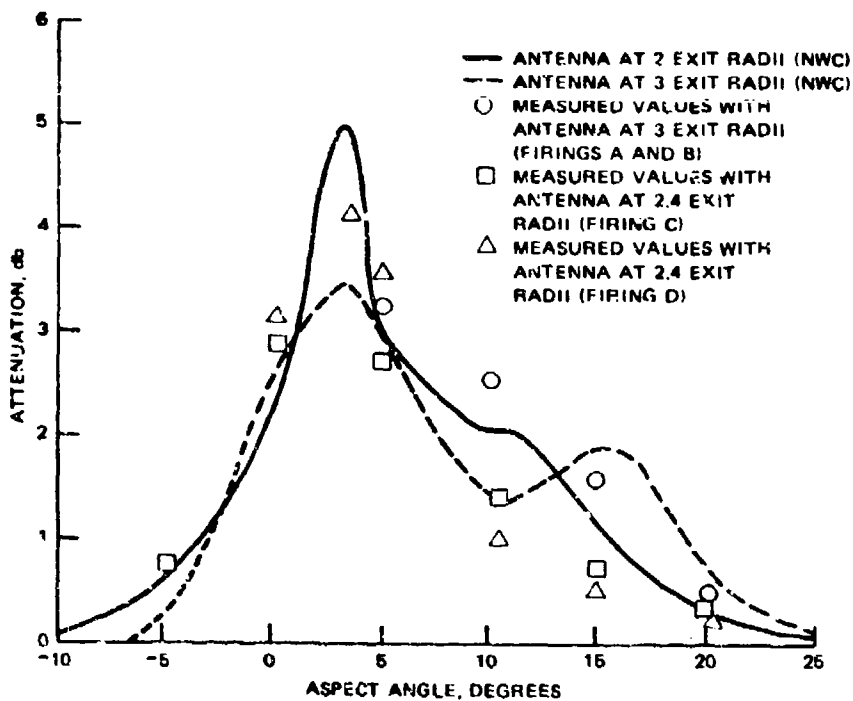
INDICATE MORE

Logic Diagram for Solution of Plume Signal Interference Problems.

NWC TP 5319, Part I



(a) Transverse attenuation.



(b) Diagonal attenuation.

FIGURE 2. Comparison of Measured and Calculated Attenuation for Rocket Motor With 5% Al/88% Solids Propellant. (NWC predictions include effect of shock structure added to simple plume calculation.) From Ref. 8. Thrust level was approximately 8,000 pounds.

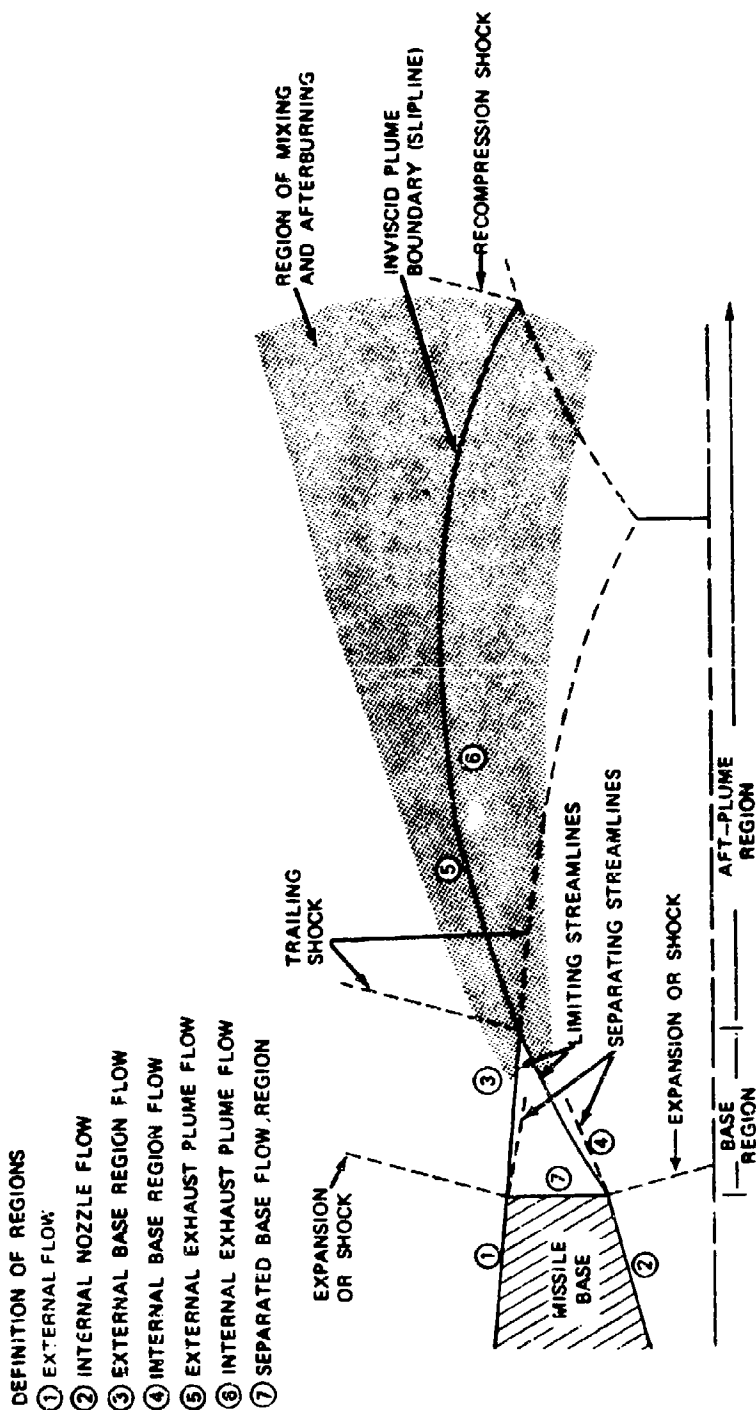


FIGURE 3. Schematic of the Flow Regions of a Flight Missile System.

NWC TP 5319, Part 1

In the remainder of this section, the various methods used at NWC for calculating plume properties preparatory to making RF interaction predictions are described. Several other methods are also referenced. The reader is referred to original sources for computer programs and user manuals.

2.1 CHAMBER REACTIONS AND NOZZLE EXPANSION

All plume computations require as input the temperature and species at the nozzle exit. The NWC plume model (Section 2.6.2) and the Brigham Young University (BYU) base recirculation model (Section 2.4) have internal subroutines which compute the exit properties from propellant composition and chamber pressure for later use within the programs. When working with the other plume programs described under Sections 2.6 and 2.7, it is necessary to first perform the chamber and nozzle calculations with an appropriate computer program. Several computer programs are available for performing this one-dimensional calculation assuming chamber and nozzle chemical equilibrium with isentropic expansion (Ref. 21 through 23). At NWC we use the Propellant Evaluation Program (PEP) (Ref. 21) since it was developed here and expertise in its use and modification is locally available.

More sophisticated treatment of the chamber combustion may be desired in some liquid systems. For example, the CONTAM program (Ref. 24) developed by McDonnell Douglas Astronautics Company provides analysis of transient combustion processes in the chamber, including feedline dynamics, injection, atomization, droplet drag, heat-up/vaporization, gas-phase combustion, deposition on combustion walls, and ejection of gas- and liquid-phase propellant into the nozzle throat. We believe that this precise a calculation is rarely needed for tactical missile RF problems, although it can be of major importance for plume impingement or contamination studies.

Chamber chemical non-equilibrium was suspected several times in the past when the failure of calculations to reproduce measured attenuation data was attributed to characteristic exhaust velocity (c^*) inefficiency (Ref. 25). Since c^* varies as the square root of nozzle inlet temperature, theoretical attenuation values could be widely adjusted by small percentage changes in c^* . In addition to lacking strong experimental evidence, this method of adjusting theoretical nozzle exit properties should be frowned on because measured c^* values usually belie their theoretical basis (Ref. 26).

The CONTAM program also provides an improved treatment of nozzle flow by accounting for multi-phase transport including momentum and energy coupling between the phases. Additional sophistication can be obtained by including chemical reaction rate effects (kinetics) in the reactions occurring during nozzle expansion. Both one- and two-dimensional kinetic nozzle analysis programs are available (Ref. 27, 28). The principal differences between the two programs are that the one-dimensional solution ignores nonaxial streamlines and shocks within the nozzle. These limitations are overcome in the two-dimensional solution. A two-dimensional equilibrium nozzle program is available in Ref. 29, and a turbulent boundary layer nozzle analysis computer program in Ref. 30.

For plume-signal interference problems, it is essential that ionization chemistry also be considered so that the calculated properties at the nozzle exit include ionized species concentrations (e.g., Na^+ , Cl^- , OH^- , and e^-) as well as concentrations of neutral species, temperature, gas constant, and the other gas properties output by all of the nozzle programs.

2.1.1 The Fuel Index

The fuel index was proposed (Ref. 31) as a convenient index of the relative capability of a fuel-rich rocket exhaust to afterburn with atmospheric oxygen. The fuel index is defined as the proportion of combustible gas to total gas at the nozzle exit.

$$\text{FI} = (\text{H} + \text{H}_2 + \text{CO}) / (\text{H} + \text{H}_2 + \text{CO} + \text{CO}_2 + \text{H}_2\text{O} + \text{HCl}) \quad (1)$$

As indicated in Figure 4, the transverse microwave attenuation increases rapidly with increasing fuel index. This correlation can serve as a guide for determining the relative merits of several propellant compositions. It seems unlikely that fuel index could serve as a basis for an empirical scheme for predicting in-flight attenuation because too many other variables are involved. The exit temperature, metal (Al) concentration, binder and oxidizer type, missile shape and trajectory will all have a major influence on attenuation level. Thus, although fuel index can be used to estimate the relative attenuation to be expected for propellants within a given propellant family, from the standpoint of the remainder of this report the concept has little use.

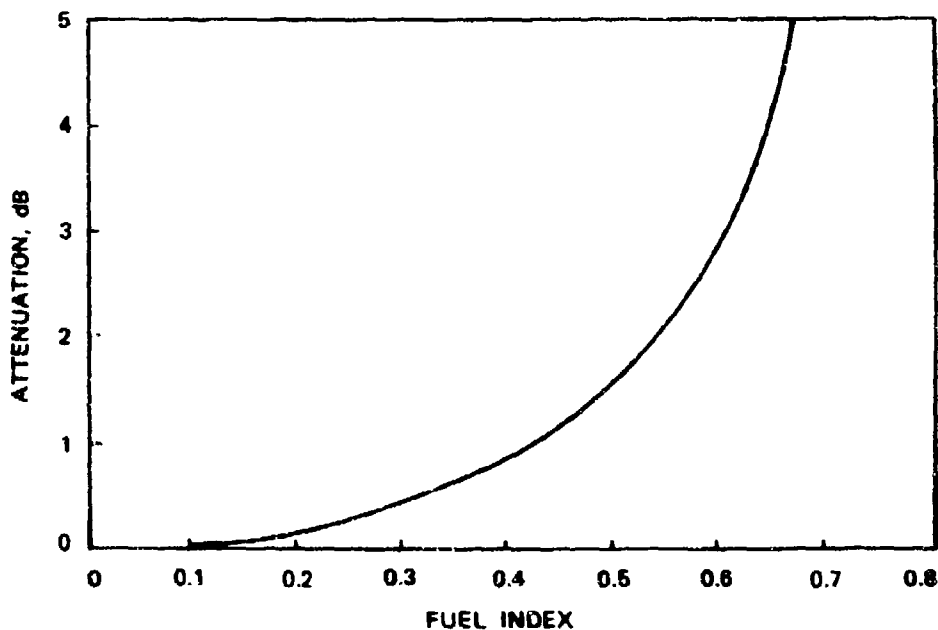


FIGURE 4. Effect of Fuel Index on Attenuation for Typical Solid Propellant.

2.2 EQUILIBRIUM EXHAUST-AIR MIXTURES

All equilibrium plume mixing and afterburning models yield (1) the ratio of exhaust gas to air at each point in space, (2) the temperature and species concentrations at each point, which result from allowing the mixed gas to achieve thermochemical equilibrium, and (3) electron-neutral collision frequencies (if plume-signal interference calculations are to be made).

Since equilibrium chemistry is independent of the path which constituents have taken to a given spacial point, it is practical to consider making this calculation prior to commencing the equilibrium plume calculation. The chemical calculation is performed within the NWC plume computer program: SUPPEP (Section 2.6.2), BYU base recirculation (2.4), ABL plume (2.6.3) and BYU aft-plume (2.6.4) models. The simple RPE model (2.6.1) contains no chemical computations and so, if that plume model is used, the results of equilibrium exhaust-air afterburning calculations must be input.

It is important that energy, mass, and momentum be conserved in performing the afterburning calculations. In the past, workers have occasionally forgotten to include the contribution of mixing to the energy (enthalpy) equation. The basis of that calculation follows.

The enthalpy in contours of constant f (exhaust gas mass fraction) is assumed to be equal to the sum:

$$\begin{aligned}
 & \text{(Exhaust gas static enthalpy within the contour)} \\
 & + \text{(Free stream static enthalpy within the contour)} \\
 & + \text{(Enthalpy recovered by reducing the exhaust velocity to the mixing} \\
 & \quad \text{contour velocity)} \\
 & - \text{(Enthalpy lost by increasing the free stream velocity to the mixing contour} \\
 & \quad \text{velocity)} \\
 \hline
 & = \text{Static enthalpy in mixing contour}
 \end{aligned}$$

The equilibrium thermochemical computer program used in conjunction with an afterburning program usually treats a total mass of 100 grams. Consequently, it is convenient to use a fractional factor (f) in the afterburning calculation and retain the 100-gram basis of the calculation. Use is made of the following nomenclature:

$$\begin{aligned}
 f &= \text{mass fraction of exhaust gas in a contour of the mixing region} = m_e / (m_e + m_j) \\
 H &= \text{stagnation enthalpy of 100 grams of exhaust jet gas (calories)} \\
 h_j &= \text{static enthalpy of 100 grams of exhaust jet gas at exit plane (calories)} \\
 h_e &= \text{static enthalpy of 100 grams of free stream air (calories)} \\
 h &= \text{static enthalpy of 100 grams of mixed gas in a mixing contour (calories)} \\
 u_j &= \sqrt{2c(H - h_j)} \text{ (for 100 grams) = exhaust velocity at exit plane (meters/sec)}
 \end{aligned}$$

NWC TP 5319, Part 1

u_e = free stream velocity (meters/sec)

u = velocity in a mixing contour (meters/sec)

c = conversion factor = $41.86 \frac{\text{m}^2 - 100 \text{ g}}{\text{cal} - \text{sec}^2}$

m = 100 grams = total mass in mixing contour

m_j = mass of exhaust gas in a mixing contour = fm

m_e = mass of free stream air in a mixing contour = $(1 - f)m$

From conservation of momentum (with unity Prandtl (Pr) and Schmidt (Sc) numbers)

$$mu = m_j u_j + m_e u_e$$

$$mu = fm u_j + (1 - f)mu_e \quad (2)$$

or

$$u = f u_j + (1 - f)u_e$$

and

$$(1 - f) = \frac{u_j - u}{u_j - u_e}; \quad f = \frac{u - u_e}{u_j - u_e}$$

For a static firing (quiescent free stream), $u_e = 0$ and $u = f u_j$.

From conservation of energy

$$m(h + u^2/2) = m_j(h_j + u_j^2/2) + m_e(h_e + u_e^2/2) \quad (3)$$

and the general equation for enthalpy at velocity (u) is

$$h = h_j(f) + (1 - f)h_e + \frac{(f)u_j^2}{2c} \left(1 - \frac{u^2}{u_j^2}\right) + \frac{(1 - f)u_e^2}{2c} \left(1 - \frac{u^2}{u_e^2}\right) \quad (4)$$

For a static firing Eq. 4 becomes:

$$h = h_j(f) + (1 - f)h_e + \frac{u_j^2}{2c} (f)(1 - f)$$

or

$$h = h_j(f) + (1 - f)h_e + f(1 - f)(H - h_j)$$

NWC TP 5319, Part I

When it is assumed that $Pr = Sc = 1$, the relationship $\frac{u - u_e}{u_j - u_e} = f = \frac{h - h_e}{h_j - h_e}$ is true.

For non-unity Pr and Sc numbers, the relationship must be altered to

$$\frac{u - u_e}{u_j - u_e} = f^{1/Sc} = \left(\frac{h - h_e}{h_j - h_e} \right)^{1/Pr} \quad (5)$$

Under these conditions, for which there is a considerable body of evidence (Ref. 32), a contour for a given mass fraction (f) will not be the contour for the same value of velocity and enthalpy ratio. Thus, the simplifying relationships which underlie the NWC SUPPEP plume model do not hold in general and in the newer, more sophisticated programs (Sections 2.6.3, 2.6.4, 2.7.1 and 2.7.2), these simplifications are not necessary.

2.3 STATIC VERSUS FLIGHT CONDITIONS

There are major differences between modeling static and dynamic mixing plumes. For one thing, the six mixing plume models which follow have been used to adequately predict static transverse attenuation, with no consideration given to inviscid structure. The addition of inviscid structure has provided additional improvement by predicting local increases in attenuation due to shock intersections. One would expect that mixing models based on the inviscid plume boundary or slip line should be superior since they have a physical basis for locating the mixing region (Figure 3).

The situation is much more complicated for predicting plume structure and properties with a moving free stream. The base region, which separates the exhaust gas and free stream at the nozzle exit, can make a major contribution to the aft-plume geometry and chemistry. Mixing starts in the base region and, under some conditions, ignition of the plume may also start there.

Downstream of the base, the flow conditions are no longer those of free stream and nozzle exit. An inviscid plume must be defined and both internal and external pressures and velocities are needed, point-to-point. A mixing model can then be superimposed on the inviscid plume. Ideally the whole plume, *inviscid* and viscous, should be solved simultaneously downstream of the base region (Ref. 15).

2.4 BASE RECIRCULATION AND REACTIONS

It has been demonstrated that recirculation and combustion in the base region of a flying missile can seriously modify the structure and properties of the rocket plume (Ref. 33, 34). The work of Beheim, et al., (Ref. 35, 36) and Dixon, et al.,

NWC TP 5319, Part 1

(Ref. 37) served as the basis for a computer model of base recirculation and reactions developed by Hedman, Smoot, and Simonsen (Ref. 38, 13). Other work has been reported by Addy (Ref. 39) and Baughman and Kochenderfer (Ref. 40).

In the base region, jet-air mixing forms chemical and physical inputs to the inviscid and aft-plume calculations. It provides ionic, species, thermal, and pressure conditions in the base region. It determines the trailing shock geometry, the aft-external and internal pressures and the effective plume size.

The base model of Ref. 13, as modified in Ref. 32, is used at NWC.¹ Several sample base calculations are shown in Figure 5. It is easily seen that the greater the ratio of the base to nozzle diameter, the greater the effect of the base both in increasing the plume radius and increasing the temperature resulting from equilibrium reactions in the base region. The "flower pot" base of Figure 5d causes particularly high base temperatures. Neglecting base chemical reactions decreases the calculated base pressure and temperature in Figure 5a by factors of 1/5 and 1/3, respectively. Lowering the recompression efficiency to 90% increased base pressure 13%, but caused little change in base temperature. Increasing base ratio (r_n/r_b) from 0.6 to 0.9, increased the base pressure (+21%) and decreased the base temperature (-33%) as shown in Figure 5b. Reducing the boat-tail angle from -10 degrees to 0 degree reduced base pressure (-32%), with little change in base temperature (+7%) as shown in Figure 5c. These examples are taken from Ref. 32.

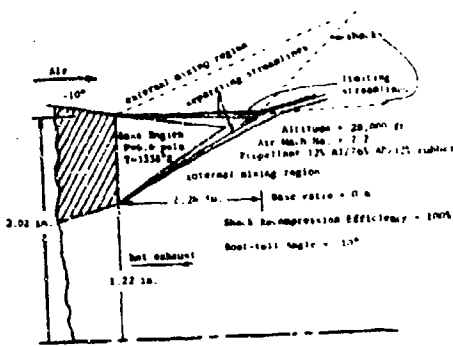
In addition to providing input for a method of characteristics (MOC) inviscid plume program (Section 2.5) and for the aft-mixing and afterburning plume program (Section 2.6.4), the base model also has built into it several earlier versions of the BYU aft-plume model (Ref. 13). The base program can be run with any of the following options:

1. Complete Program. All components of the program are run, with all input parameters for the aft-plume being obtained internally from the base region computation. Runs can be made with or without line-of-sight radar attenuation computations.

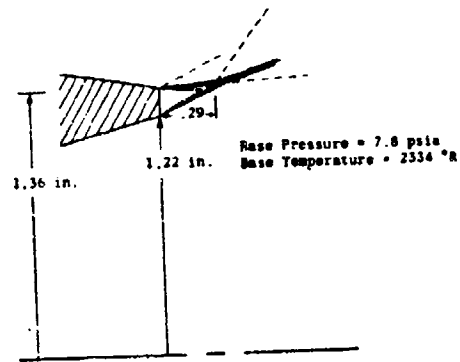
2. Without Base Effects. Components of the program for the chamber, nozzle, and aft-plume regions (with or without a radar attenuation computation) can be run separately without computing base region structure, (e.g., to describe a jet where base flow can be ignored).

3. Specified Aft-Plume Input. All components of the program can be run, with any of several input parameters for the aft-plume subroutine being input directly, rather than being obtained from the base region computation (e.g., to determine effects of varying static pressure, free stream velocity, etc.).

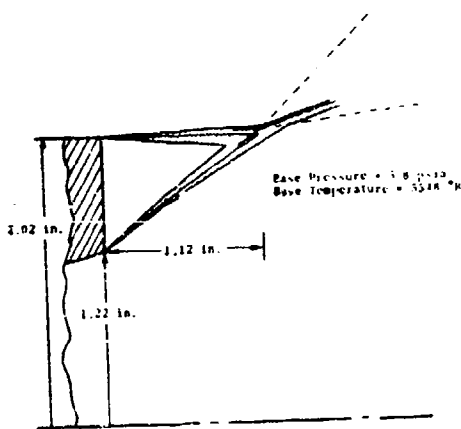
¹ Developed for the Naval Weapons Center on Contract No. N00123-70-C-0274.



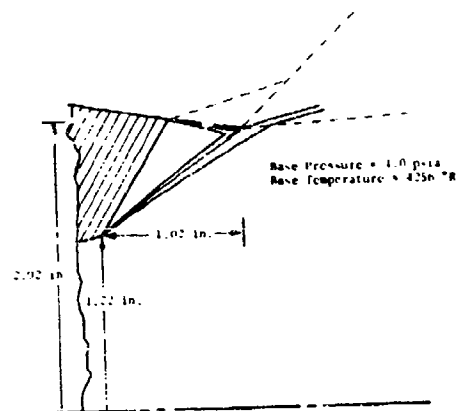
(a) Reference case-simulated flight test 1.



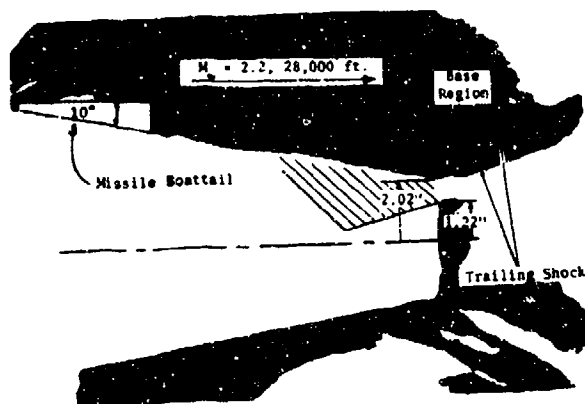
(b) Base ratio = 0.9.



(c) Zero degree boat-tail angle.



(d) Boat-tail lip aft of nozzle exit.



(e) Schlieren photograph of base region for simulated flight missile system.

FIGURE 5. Effect of Base Parameters on Predicted Base Structure, Pressure and Temperature.

4. Base Region Only. Components of the program for chamber, nozzle, and base region can be run separately without computing the aft-plume properties or radar attenuation (e.g., to obtain base pressure or base drag computations).

The program has a major weakness as a total plume program since the species computed in the base region do not flow into the aft-plume. However, the calculated base pressure and temperature and the calculated external environment do become input to the aft-plume. If Option 4 of the base model is used (base region only), the calculated base properties can be input directly (with ambient conditions) to the internal-external MOC program (Ref. 32) of Section 2.5. Both the base and MOC program outputs become input for an improved aft-plume model (Ref. 32) described in Section 2.6.4 which can use the radially varying base properties as input, and can also use the longitudinally varying pressure and velocities obtained from the MOC program.

2.5 INVISCID PLUME

Whereas an inviscid plume model (complete absence of viscous effects) describes the entire flow field of higher altitude rocket exhausts, it is only part of the solution for plumes at the lower altitudes at which tactical missiles travel. The inviscid plume describes the boundary across which air and jet gases mix as well as the shock locations within the jet. In this section, some simple models are explained in enough detail so that the reader can use them without reference to additional sources.

Love, et al., (Ref. 41) summarized the results of inviscid plume calculations for a wide range of initial conditions in the form of graphs, which are useful for predicting plume boundaries.

Several simple empirical models for predicting normal shock (Mach disc) location in jets have been published (Ref. 42 through 45). Lewis and Carlson (Ref. 42) reported excellent agreement between data and theory for normal shock locations using the equation

$$x/r_e = 1.38M_j \left(\frac{\gamma P_j}{P_\infty} \right)^{1/2} \left(1 + 0.197M_j^{1.45} \phi^{0.65} \right)^{-1} \quad (6)$$

for underexpanded¹ pure- or gas-particle jets where x is the distance to the normal shock, r_e is the nozzle exit radius, M_j is the nozzle exit Mach number, P_e and P_∞ are the jet exit and ambient static pressures respectively and ϕ is the particle-to-gas mass fraction. According to this equation, jets laden with 10 and 50% particle mass will have shock locations reduced to 82 and 62%, respectively, of the distance for a pure gas jet. Williams, Hartsock, and Buckley (Ref. 14) have shown that Eq. 6 also applies to locating the Mach disc for a jet in a dynamic environment. It should be noted that the Mach disc diameter will be reduced for a jet with a moving free stream and with increased external Mach number, the Mach disc could completely disappear.

Buckley and Myers (Ref. 46) described a model to correct a parallel-mixing plume model for nozzle underexpansion. As illustrated in Figure 6, the jet flow expands through an angle $(\delta_o - \theta_n)$ to a pressure P_{b_o} equal to the pressure reached when the external flow is compressed from P_∞ through an angle δ_o to P_o . Downstream of the first plume wavelength, it is assumed that the flow is uniform and the pressure is atmospheric.

It is assumed in the Buckley-Myers model that the inviscid boundary can be described by

$$(r - r_m)/(r_j - r_m) = e^{-bx} \quad (7)$$

where r_m is the maximum radius of the inviscid plume boundary and $b = \tan(\delta_o)/(r_m - r_j)$. It is further assumed that

$$(P_b - P_\infty)/(P_{b_o} - P_\infty) = e^{-cx} \quad (8)$$

where it is assumed that $c \cong b$. Assuming uniform flow conditions at the nozzle exit and at the downstream location where the plume pressure is that of the environment, conservation of momentum yields

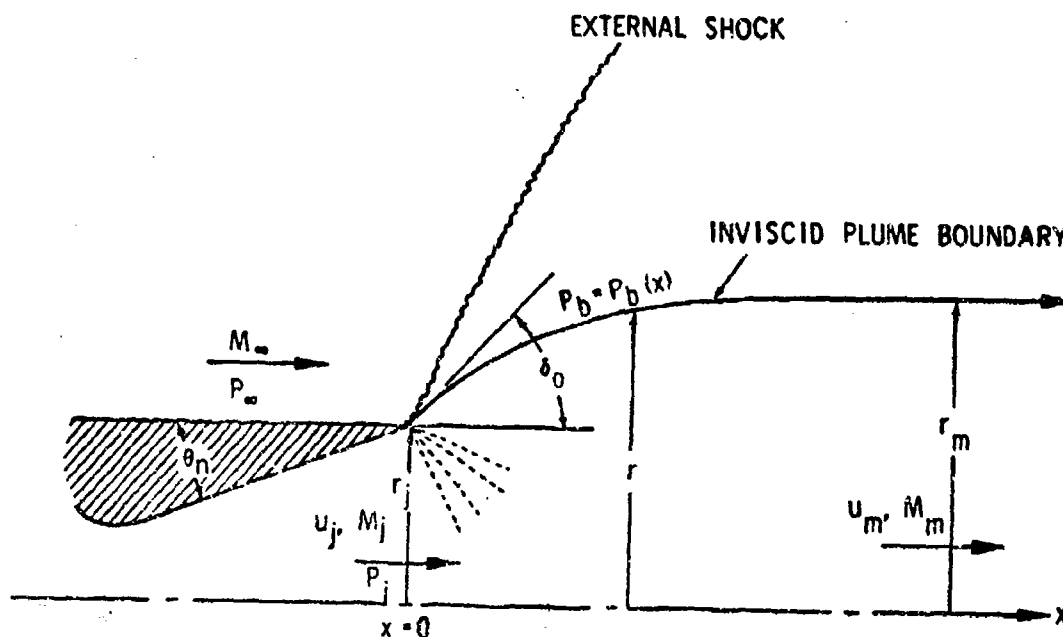


FIGURE 6. Low-Altitude Inviscid Plume Model (Ref. 46).

$$\begin{aligned} & \left(\frac{P_j}{P_m} - 1 \right) + \left(\frac{P_{b_0}}{P_\infty} - 1 \right) \left(r_m^2/r_j^2 + r_m/r_j - 2 \right) / 3 = \\ & = \gamma_j M_j^2 P_j / P_\infty \left\{ \frac{M_m}{M_j} \sqrt{ \left[1 + (\gamma_j - 1) M_j^2 / 2 \right] / \left[1 + (\gamma_j - 1) M_m^2 / 2 \right] } - 1 \right\} \end{aligned} \quad (9)$$

where

$$\begin{aligned} M_m = & \left\{ \sqrt{ 1/(\gamma_j - 1)^2 + 2(r_j/r_m)^2 (P_j/P_\infty)^2 \left[M_j^2 + (\gamma_j - 1) M_j^4 / 2 \right] (\gamma_j - 1) - } \right. \\ & \left. - 1/(\gamma_j - 1) \right\}^{1/2} \end{aligned} \quad (10)$$

Buckley and Myers (Ref. 46) also discussed the effect of free stream flow on inviscid plume boundaries. The results are shown for $M_j = 3.0$, $\gamma_j = 1.2$, $\theta_n = 15$ degrees and $\gamma_\infty = 1.4$ for a range $0 < M_\infty < 5$ in Figures 7 through 10. The dynamic effect is readily apparent in Figures 7 and 8 where the inviscid plume is seen to compress as M_∞ is increased. Figure 9 indicates that the plume compression is accompanied by an increase in u_m (velocity at r_m), which is particularly significant at higher P_j/P_∞ . These relationships can be used as inputs to modify perfectly expanded plume models to account for the effects of underexpansion in static or dynamic environments.

Two different techniques, illustrated in Figure 11, were used to correct the input to the perfectly expanded flow model to account for the effects of underexpansion. In Figure 11a, three different plume contours are shown for the same value of P_j/P_∞ . The thickest plume results if the nozzle exhausts into a static environment; the plume boundary pressure being equal to P_∞ . If external flow is added, the maximum plume radius decreases from r_{m_0} to r_{m_1} , and the pressure along the plume boundary now varies, decreasing from P_{b_0} at the exit to P_∞ further downstream. The third contour is for a situation in which the boundary pressure is not allowed to fall in the downstream direction but is maintained at P_{b_0} (corresponding to $M_\infty = 0$). This condition results in a plume of even smaller radius (r_{m_2}). The effect of the streamwise pressure gradient associated with the flow accounts for the difference between the last two contours.

The first, and simplest, underexpansion correction is shown in Figure 11b. It is assumed that the effect of underexpansion in a dynamic environment can be accounted for through use of an effective jet having a radius equal to r_{m_1} and a velocity of u_{m_1} obtained from Figures 7 and 9 at the appropriate values of P_j/P_B and M_∞ . The effective jet exit pressure, and that throughout the plume, is equal to P_∞ .

NWC TP 5319, Part 1

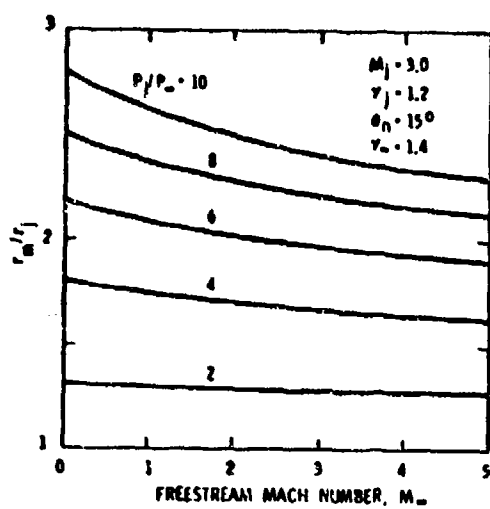


FIGURE 7. Effect of Freestream Mach Number on Maximum Radius of Model Plume (Ref. 46).

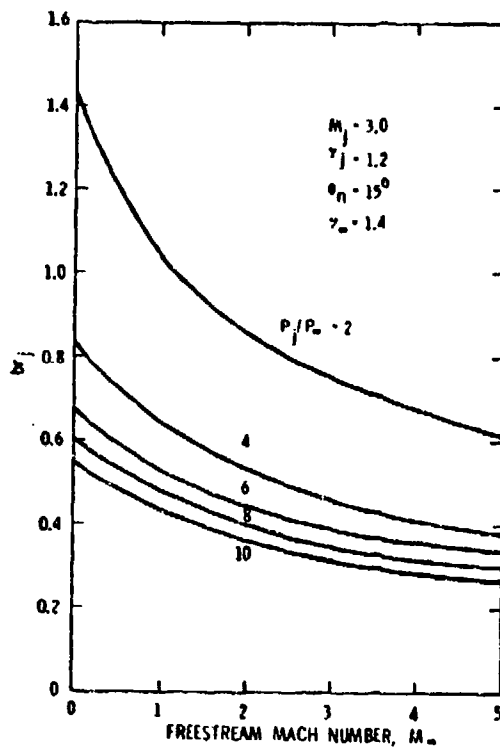


FIGURE 8. Effect of Freestream Mach Number on Shape Factor of Model Plume (Ref. 46).

NWC TP 5319, Part 1

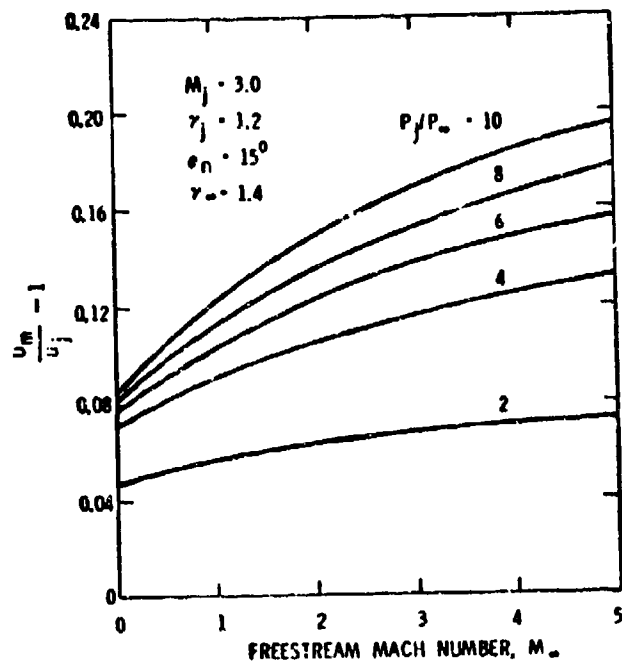


FIGURE 9. Effect of Freestream Mach Number on Velocity at Maximum Radius of Model Plume (Ref. 46).

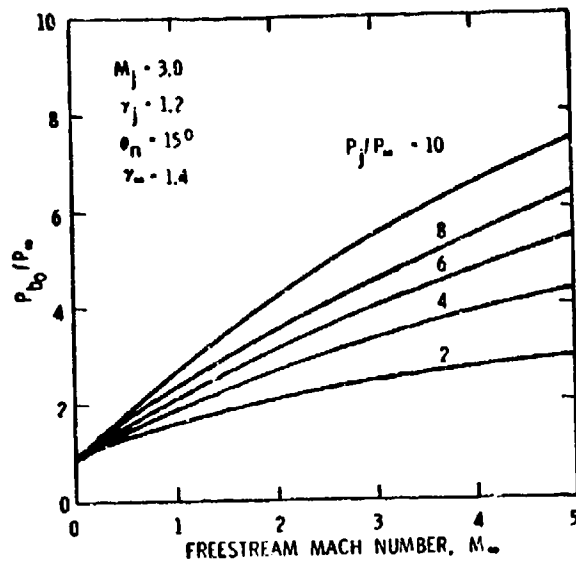


FIGURE 10. Effect of Freestream Mach Number on Initial Boundary Pressure of Model Plume (Ref. 46).

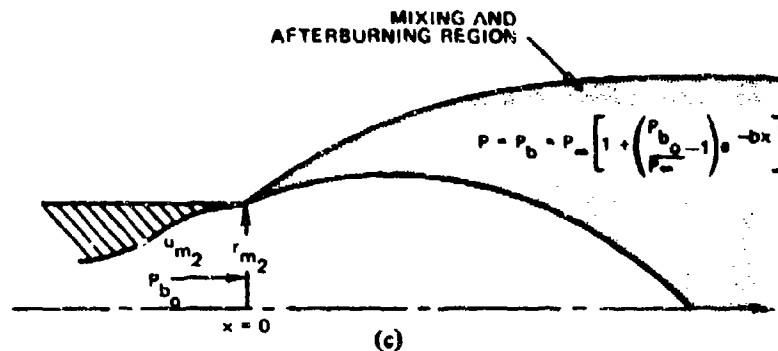
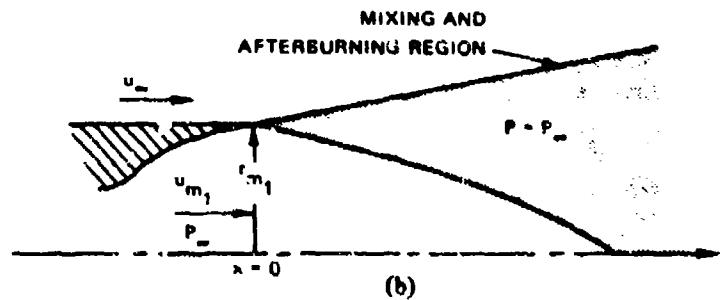
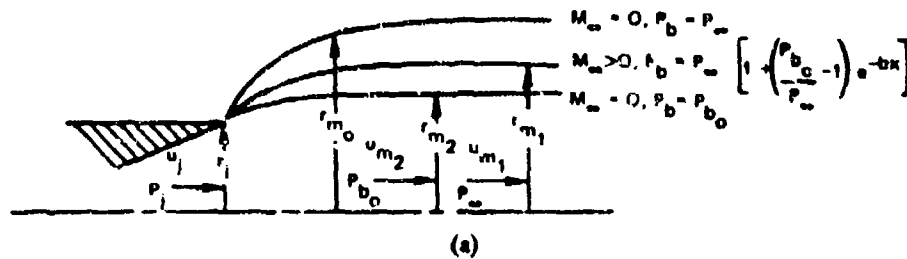


FIGURE 11. Scheme for Correction Due to Effects of Underexpansion in a Dynamic Environment (Buckley and Myers, Ref. 46).

The second correction scheme is shown in Figure 11c. Here, an attempt has been made to include the pressure gradient effect. If a flow effect had been present to compress the flow to P_{b_0} at $x = 0$, but no gradient had existed, the plume radius would have been r_{m_1} . Thus, an effective jet with a radius equal to r_{m_1} and a velocity equal to u_{m_2} (obtained from Figures 7 and 9 at $M_a = 0, P_j/P_a, P_j/P_{b_0}$) is used to represent this situation. The effective jet exit pressure is taken as P_{b_0} . Now, to include the pressure gradient effect, the plume pressure is allowed to decrease from P_{b_0} at the exit plane to P_a further downstream, in accordance with Eq. 8. The values of b and

P_{b_0} are determined from Figures 8 and 10 for the appropriate values of M_∞ and P_j/P_∞ . The actual jet radius is used in the computation of b . Through use of this technique, the radial location of the jet edge streamline in the far field should be close to that achieved with use of the zero pressure gradient correction. The temperature in the external flow at the jet edge is also varied in the downstream direction by using $T_b = T_\infty [1 + (T_{b_0}/T_\infty - 1) \exp(-bx)]$.

The results of attenuation computations for flow from an underexpanded nozzle into a supersonic stream, with the two different pressure corrections given above, are presented in Figure 12. Inclusion of a pressure gradient effect decreases the peak attenuation and shifts its location further downstream. Also, the two attenuation profiles are markedly different. Further study is required to fully assess the validity of the underexpansion correction schemes presented and to completely analyze the pressure gradient effect.

Another approach for determining the radius of an expanding plume is presented by Draper and Moran (Ref. 47). Although this technique was developed for high-altitude plumes, Rothschild and Stanford (Ref. 48) have used it in lower altitude plumes. However, there is no experimental information on its validity for this case. For an exhaust expanding into air:

$$R_j = 0.364 \frac{D^{1/2}}{q_\infty}$$

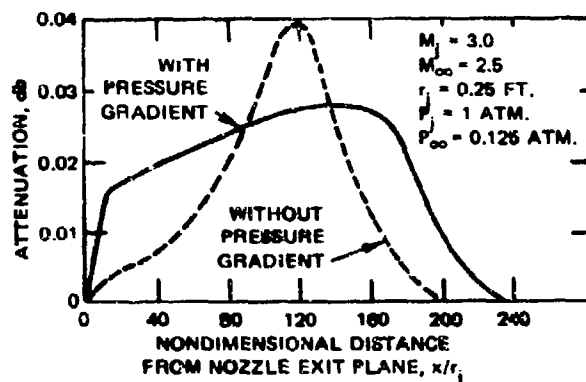


FIGURE 12. Comparison of Attenuation Calculations in a Dynamic Environment With and Without Consideration of Nozzle Expansion Correction (Buckley and Myers, Ref. 46).

NWC TP 5319, Part 1

The free stream dynamic pressure, q_∞ , is calculated from missile flight velocity and altitude.

$$q_\infty = \frac{\rho_\infty v_\infty^2}{2g_c}$$

where

ρ_∞ = free stream density, lb_m/ft^3

v_∞ = free stream velocity, ft/sec

g_c = gravitational conversion, $32.17 \frac{\text{lb}_f\text{-ft}}{\text{lb}_m\text{-sec}^2}$

Plume drag, D , is calculated from exhaust gas thrust, T_g , and a plume spreading parameter, λ (see Figure 13).

$$D = \frac{T_g}{\lambda \sqrt{\pi} - 1}$$

The exhaust gas thrust is that portion of the total engine thrust which is not produced by particulates in the two-phase flow of solid propellant rocket plumes

$$T_g = T \left(1 - \dot{m}_{\text{solid}}/\dot{m}_{\text{total}} \right)$$

The plume geometric structure is scaled by (Ref. 47):

$$\bar{L} = \left(\frac{T_g}{q_\infty} \right)^{1/2}$$

so that x/\bar{L} and R/\bar{L} are the respective units of length and radius. This technique has only been shown to be valid for conditions in which the missile body has negligible effect on the plume/air interaction.

For overexpanded jets, an approximate method for calculating the shock and separating streamline was given in Ref. 49. The following equations determine the radius of curvature, R_s , of the shock and r'_s of the separating streamline (see Figure 14) by means of a first-order expansion about the separation point.

$$r'_s = M_{1s}^{-1} \left[\frac{2}{(\gamma+1)} \left(1 + \frac{(\gamma-1)}{2} M_{1s}^2 \right) \right]^{\frac{\gamma+1}{2(\gamma-1)}} \frac{1}{\alpha}$$

NWC TP 5319, Part 1

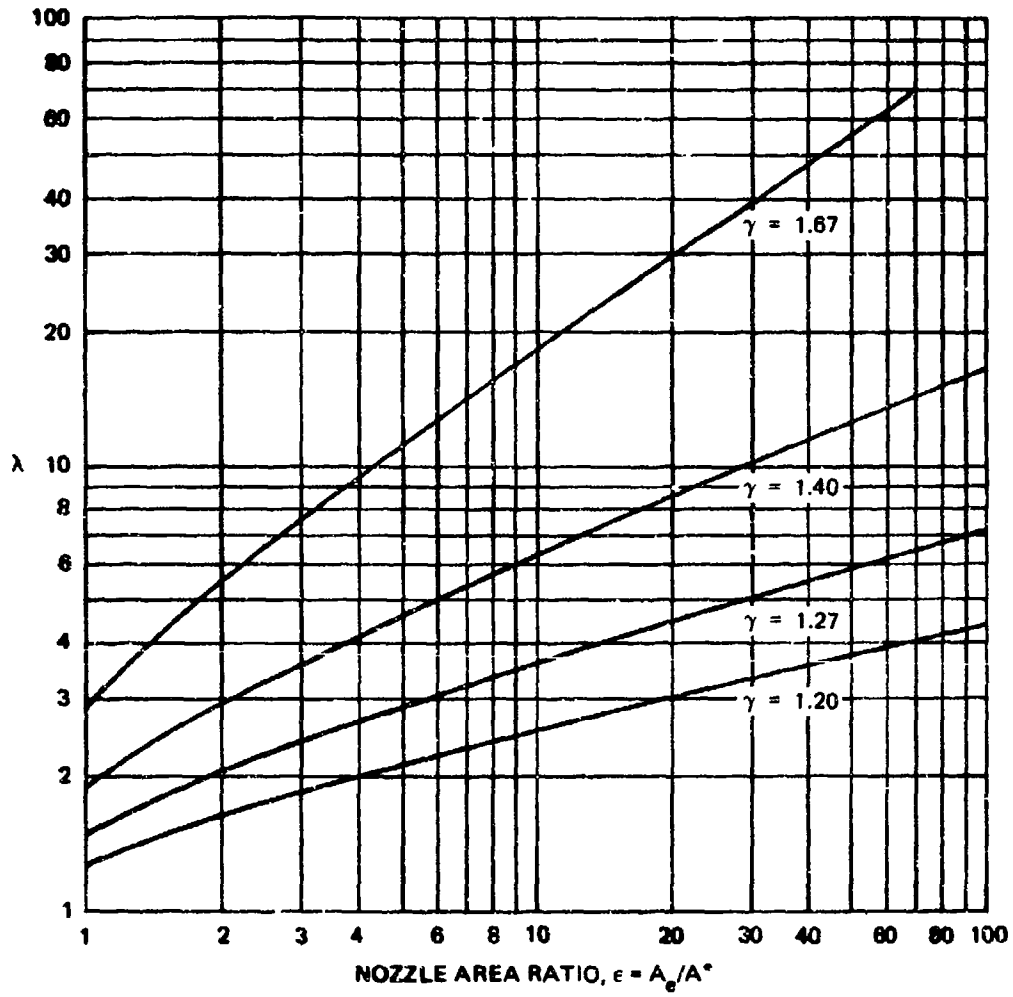


FIGURE 13. Plume Spreading Parameter, λ .

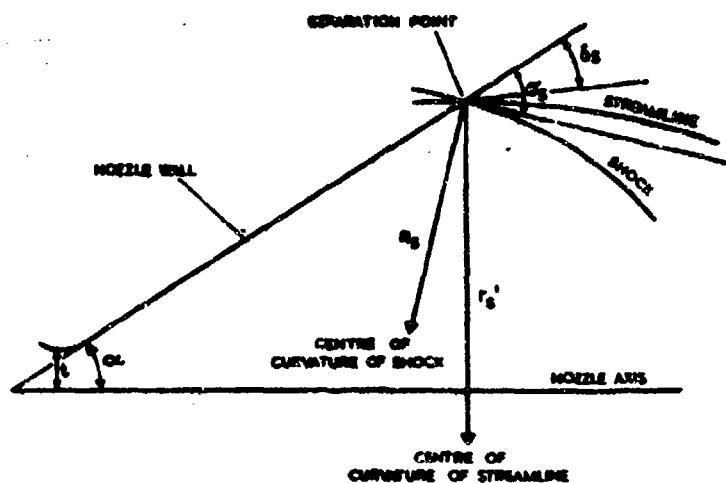


FIGURE 14. Determination of Flow Separation Point (Ref. 47).

$$R_s = x r_s$$

$$r'_s = \frac{R_s}{y}$$

where

$$x = \frac{b_0 c_2 + b_2 c_0}{b_2 c_1 - b_1 c_2}$$

$$y = \frac{b_0 c_1 + b_1 c_0}{b_2 c_1 - b_1 c_2}$$

$$b_0 = \sin \delta_s \cos \delta_s [-A + B + c] \cot \delta_s$$

$$b_1 = (1 - \sin \delta_s \cos \delta_s [-A + BD + cE] \cot \sigma_s) \sin \sigma_s$$

$$b_2 = \cos (\sigma_s - \delta_s)$$

$$c_0 = F \cot \sigma_s$$

$$c_1 = (G + FD) \cos \sigma_s$$

$$c_2 = H \sin (\sigma_s - \delta_s)$$

$$A = \sec^2 \sigma_s$$

$$B = \frac{2M_{1s}^2 \sin^2 \sigma_s}{(M_{1s}^2 \sin^2 \sigma_s - 1)}$$

$$C = \frac{2M_{1s}^2 \sin^2 \sigma_s}{\left(1 + \frac{(\gamma+1)}{2} M_{1s}^2 - M_{1s}^2 \sin^2 \sigma_s\right)}$$

$$D = 1 - \frac{\left(1 + \frac{(\gamma-1)}{2} M_{1s}^2\right)}{(M_{1s}^2 - 1)}$$

$$E = 1 + \frac{\left(1 + \frac{(\gamma-1)}{2} M_{1s}^2\right)}{(M_{1s}^2 - 1)} \left[\frac{(\gamma+1)}{2} \operatorname{cosec}^2 \sigma_s - 1\right]$$

$$F = \frac{2\gamma M_{1s}^2 \sin^2 \sigma_s}{\left(\gamma M_{1s}^2 \sin^2 \sigma_s - \frac{\gamma-1}{2}\right)}$$

$$G = \frac{\gamma M_{1s}^2}{(M_{1s}^2 - 1)}$$

$$H = \gamma M_{2s}^2$$

M_{1s} is the Mach number in the flow upstream of the shock; M_{2s} is the Mach number in the flow downstream of the shock. The relationships between M_{2s} , M_{1s} , σ_s , and δ_s are obtained from the oblique shock relations:

$$\sigma_s = \sin^{-1} \left[\frac{1}{M_1} \sqrt{\frac{(\gamma+1) \frac{P_2}{P_1} + (\gamma-1)}{2\gamma}} \right]$$

$$\delta_s = \tan^{-1} \left[\left(\frac{\frac{P_2}{P_1} - 1}{\gamma M_2^2 - \frac{P_2}{P_1} + 1} \right) \sqrt{\frac{2\gamma M_1^2 - (\gamma-1) - (\gamma+1) \frac{P_2}{P_1}}{(\gamma+1) \frac{P_2}{P_1} + (\gamma-1)}} \right]$$

$$M_{2s} = \frac{1}{\sin(\sigma_s - \delta_s)} \sqrt{\frac{(\gamma - 1) \frac{P_2}{P_1} + (\gamma + 1)}{2\gamma \frac{P_2}{P_1}}} = \sqrt{\frac{M_1^2 \left[(\gamma + 1) \frac{P_2}{P_1} + (\gamma - 1) \right] - 2 \left(\frac{P_2}{P_1} \right)^2 - 1}{\frac{P_2}{P_1} \left[(\gamma - 1) \frac{P_2}{P_1} + (\gamma + 1) \right]}}$$

$$M_{1s} = \sqrt{\left[\left(\frac{P_1}{P_1} \right)^\gamma - 1 \right] \frac{2}{\gamma - 1}}$$

If more accuracy is desired, a computer-generated inviscid plume solution must be used. Ideally, the inviscid and mixing plume computations should be made simultaneously. Such an approach has been developed by Edelman and Weilerstein (Ref. 15). Unfortunately, this method-of-characteristics with viscous effects (MOCV) program is not available for general use. The elements of a similar program have been described by Hoffman (Ref. 24, 50). A stream tube method for solving the problem has been developed by Kelley and Pergament (Ref. 51).

In lieu of a combined inviscid-viscous solution, one must superimpose mixing on a calculated inviscid plume. The Lockheed MOC program, in fairly wide use (Ref. 52, 53, 54), has been expanded by Simonsen (Ref. 32) to generate the external flow-field properties as well as the internal plume and the separating slipline.² The results of using this program are shown in Figure 15. Hoffman has also described a MOC program (Ref. 55).

2.6 COMPUTE MIXING AND AFTERBURNING PLUME

Six models used for computing the structure and properties of exhaust plumes with jet-air-mixing and afterburning are discussed in the following section. Each of the models is self-contained in that it functions independently of any prior base or inviscid plume calculation, except for the model described in Section 2.6.4. This model (BYU aft-plume) is used with inputs from a base mixing calculation and a MOC inviscid plume calculation previously described (Sections 2.4 and 2.5).

For problems involving nozzle under- or over-expansion, some correction of the other models has to be made. This is done internally in the NWC model. The other models require some adjustment of the inviscid plume boundary. This can be obtained from Love's figures (Ref. 41) or by the method of Buckley and Myers (Ref. 46) given in Section 2.5. It is also possible to adjust the boundaries of the finite difference models (Sections 2.6.3, 2.7.1, and 2.7.2) by imposing longitudinal pressure gradients which match an inviscid plume solution.

² Developed for the Naval Weapons Center on Contract No. N00123-72-C-0274.

All of the plume models except for the REP-1 model (Section 2.7.2) use an eddy viscosity mixing model based upon input assumptions about the eddy viscosity coefficient (K). All of the models might be improved by incorporating the recent correlations of eddy viscosity coefficients described by Stowell and Smoot (see Ref. 56 and Eq. 11). The model recently developed by Kelly and Pergament (Ref. 51) uses a stream tube technique to compute inviscid plume properties and the conditions downstream of the Mach disc. This program also computes the effects of nozzle underexpansion and particle flow in a completely coupled non-equilibrium chemistry model. The Stowell-Smoot eddy viscosity correlations are incorporated in this model.

2.6.1 Simple RPE Plume Model

Cummings, Williams, and Wilson (Ref. 49) of the Rocket Propulsion Establishment (RPE), United Kingdom, described a very simple model of a rocket plume which they used earlier for attenuation calculations. Although the model is designed only for use with a static environment, proper adjustment of the core length (L) and the maximum radius of the inviscid boundary (r_m) would allow its use for crude calculations in dynamic environments. For non-optimum nozzle expansion, the jet gas is allowed to expand inviscidly from the nozzle lip until the tangent to the inviscid jet boundary is parallel to the jet axis (Figure 16). At this point, x_m , the plume radius is r_m . The inviscid boundary can be obtained by any of the methods mentioned in Section 2.5.

The simple RPE plume model is made quantitative by introducing several empirical relationships. The core length, L , is assumed to be a function of the Mach number, M_m on the axis at x_m and is given by

$$L/r_m = 2.1(M_m)^2$$

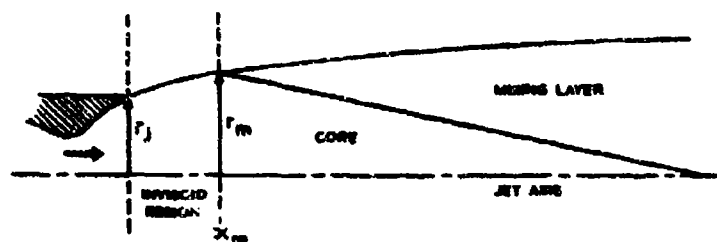


FIGURE 16. Method of Correction When Nozzle Exit Pressure is Not Equal to Ambient Pressure (Ref. 47).

NWC TP 5319, Part 1

The core (defined as the constant velocity, u_j , unmixed region of the plume) is assumed to be cone-shaped, centered on the jet axis, of base radius r_m and height L , so that the generator is given by

$$r_i/r_m = 1 - x/L$$

where r_i is the core radius at x . The velocity in the core (u_j) is constant, but beyond the core, the centerline velocity, u_c , varies inversely with x .

$$u_c/u_j = L/x$$

The radial variation of the longitudinal velocity component in the mixing region is expressed as

$$u/u_j = \exp \left[- \ln(2) \left(\frac{r - r_i}{r_5 - r_i} \right)^2 \right]$$

where

$$\begin{aligned} u_i &= u_j & \text{if } x \leq L \\ u_i &= u_c & \text{if } x > L \\ r_i &= 0 & \text{if } x > L \end{aligned}$$

r_5 is the half velocity radius, i.e., where $u = u_i/2$. The half velocity radius is determined from the equation

$$u_i^2 r_i \sqrt{\pi}/2a + u_i^2/2a^2 = \frac{u_i^2}{2} (r_j^2 + r_i^2)$$

where

$$a^2 = 2 \ln(2)/(r_5 - r_i)^2$$

If $x \leq L$, then $u_i = u_j$ and r_5 can be found in terms of r_j , which is given above as a function of x . If $x > L$, then $r_i = 0$ and $u_i = u_j L/x$, so that r_5 can be found directly as a function of x . In this way contours of constant velocity can easily be defined.

The mass fraction of jet gas for this case was given in Eq. 5 as

$$f = (u/u_j)^{Sc}$$

It is also true that

$$\frac{f}{f_i} = \left[\frac{u}{u_i} \right]^{Sc}$$

where the i subscript signifies the value at the edge of the core for $x \leq L$, or the centerline value if $x > L$. If one further simplifies by assuming unity Schmidt number (Sc), then

$$f = f_i \exp \left[- \ln(2) \left[\frac{r - r_i}{r_s - r_i} \right]^2 \right]$$

$$f_i = 1 \quad x \leq L$$

$$f_i = L^2/x^2 \quad x > L$$

With $Sc = 1$, the species concentration contours (f) will coincide exactly with the velocity contours (u/u_j). Therefore, composition of the contours can be computed by the technique given in Section 2.2. The results of such computations are compared for the simple RPE model, the NWC model (Section 2.6.2) and a BYU aft-plume model (Option 2 of Section 2.4) in Figure 17.

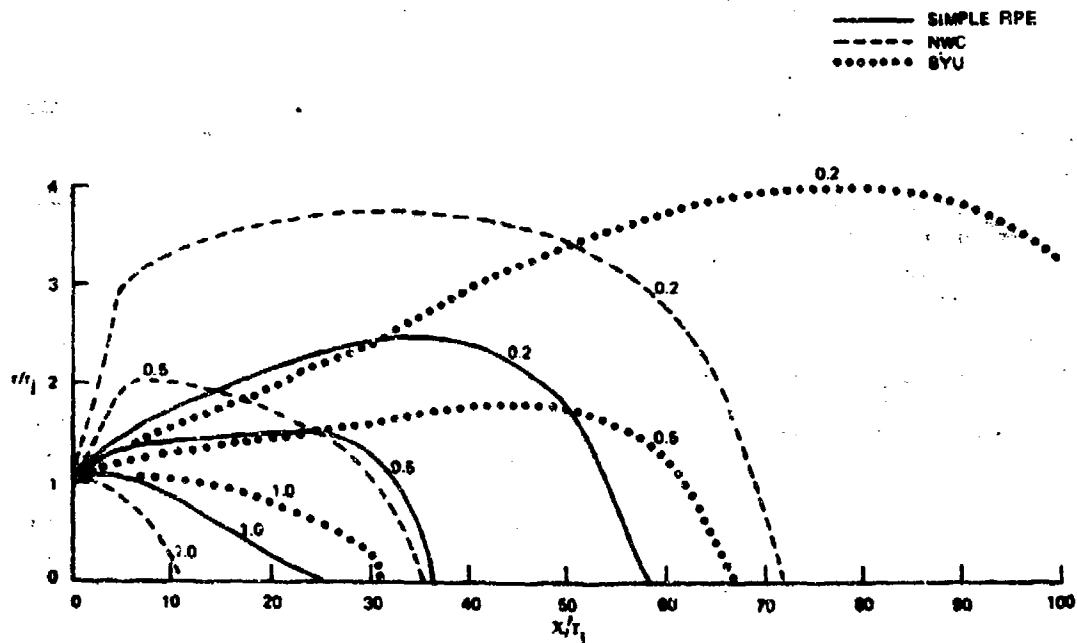


FIGURE 17. Comparison of Simple RPE Plume Model with NWC and Old BYU Models for Static Sea-Level Exhaust of Propellant Containing 88% Solids/20% Al (88/20). Numbers on graph refer to value of $f = \text{mass jet gas/mass air}$.

NWC TP 5319, Part 1

If equilibrium electron density and electron-neutral collision frequencies are computed for the contours, the model can be the basis for line-of-sight attenuation computations or for any of the other electromagnetic interaction computations described in Section 3.0 of this publication. In Figure 18 the models of Figure 17 are compared for attenuation predictions.

In the use of this model as described in Ref. 49, the electron density in the core has been assumed to be frozen at a level above equilibrium; the level is assumed to exist at the nozzle exit. This value is allowed to persist into the mixing region to the radius at which the equilibrium electron density exceeds the core value (Figure 19).

2.6.2 The NWC Plume Model

The NWC mixing and afterburning plume model has been described in two reports (Ref. 57, 58). Based on the model presented by Libby (Ref. 16), several of the variables are linearized to simplify the computation. The validity of the linearized model evaporates beyond the regions of significant electron density ($f < 0.1$) and modifications would be required to use the model for radiation or impingement calculations. The model predicts core lengths which seem too short when compared with other models and constant property contours (velocity, species concentration, and temperature) which are too fat, especially near the nozzle (see Figure 17). Nevertheless, predicted axial temperatures and velocities seem to fit measured data well (Ref. 59).

Following a Von-Mises transformation, contours of constant velocity are described by the cylindrical heat flow equations of Carslaw and Jaeger (see Ref. 16). The result is a grid of constant velocity (also temperature and concentration) contours in Von-Mises space (Figure 20). The NWC plume computer program transforms these contours back to physical ($x-y$) space according to the values of density predicted from equilibrium combustion for each concentration ratio. (Generally, ten equally-spaced contours of $f = (u - u_e)/(u_j - u_e)$, between 1.0 and 0.1, are used.) Since Sc and Pr are assumed to be unity, calculated contours of temperature, concentration and velocity ratio are coincident in space for the same ratios.

Unlike the computer programs given in Ref. 55 and 56, the current NWC plume computer program (SUPPEP) includes the thermochemical equilibrium calculations for the contours of interest. In addition, changes have occasionally been made in the ratios for contours in order to study contours further downstream than the 0.1 contour. This has been done for calculations of smoke generation (water condensation), gaseous impingement pressures, and IR emission.

The program includes two options to correct the plume geometry for nozzle underexpansion. The first of these (called "Continued Expansion to Optimum") simply continues the expanding nozzle flow at the nozzle half-angle to ambient pressure, and

NWC TP 5319, Part 1

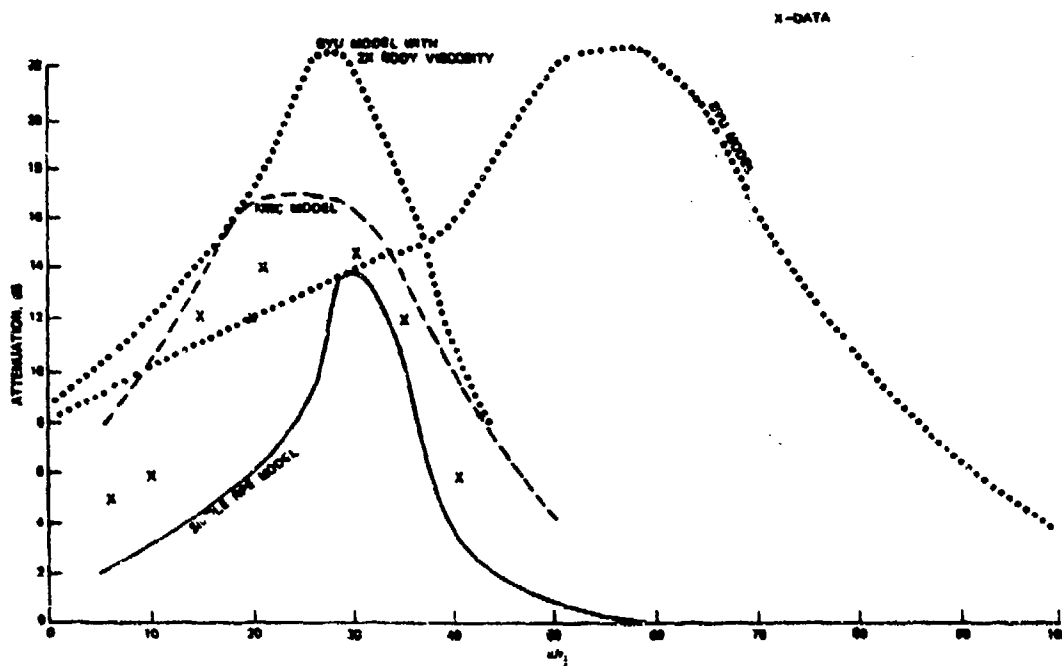


FIGURE 18a. Comparison of Simple RPE, NWC, and Old BYU Plume Model Attenuation Predictions with Data for 88/20 Composite Aluminized Propellant.

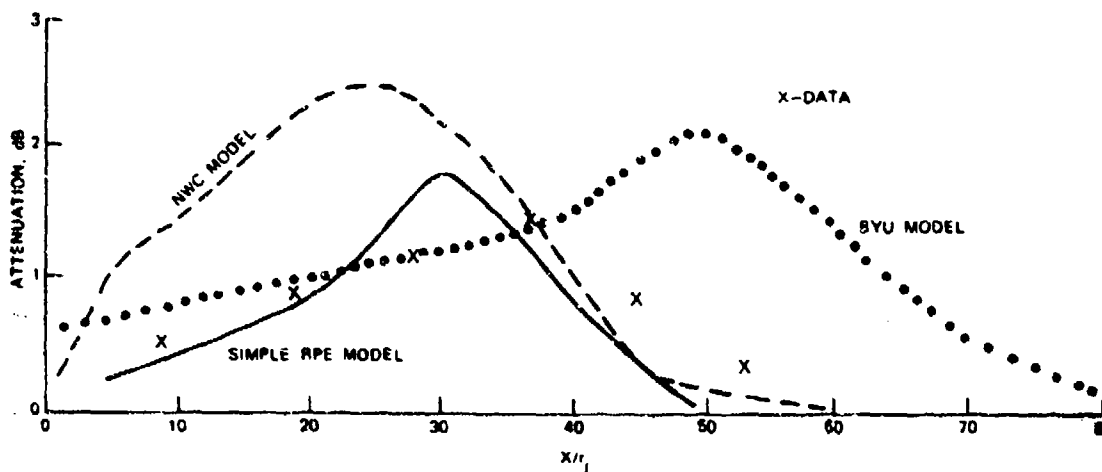


FIGURE 18b. Comparison of Simple RPE, NWC, and Old BYU Plume Model Attenuation Predictions with Data for 88/12 Composite Aluminized Propellant.

NWC TP 5319, Part I

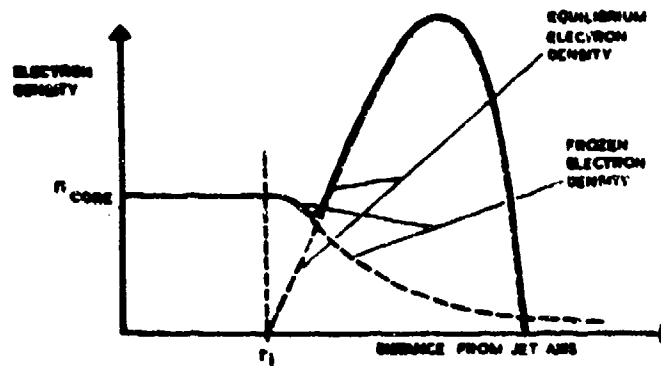


FIGURE 19. Diagram of a Typical Electron Density Profile (Ref. 47).

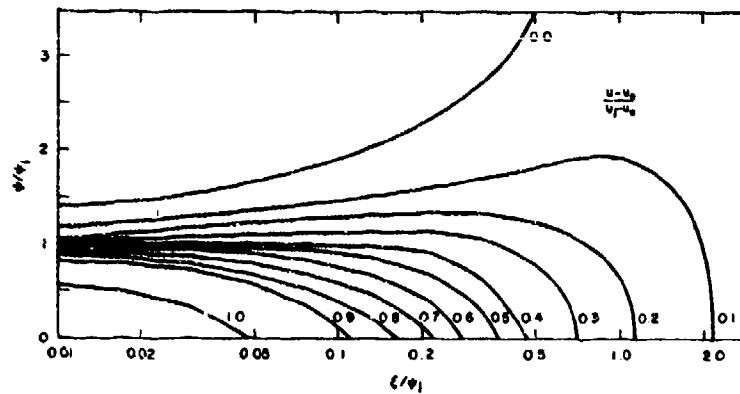


FIGURE 20. Velocity Distribution (in Transformed Coordinates) at Various Downstream Locations (Ref. 57).

assumes that final radius to be the effective jet radius for parallel mixing. Mixing calculations are started at that complete expansion point. The second correction technique for underexpansion (called "Jet Radius Correction") uses the values of inviscid plume boundaries given by Love (Ref. 41) for a nozzle half-angle of 15 degrees, a nozzle exit Mach number of 3.0, and a jet specific heat ratio of 1.2 to describe the growth of the plume to an effective jet radius given by the maximum radius of the first plume wavelength. With this latter technique, the mixing calculation starts at the nozzle exit and continues along the expanding plume boundary.

Buckley (Ref. 14) has pointed out that the NWC "Jet Radius Correction" defines an effective jet having mass flux greater than could actually exist. The "Continued Expansion to Optimum" correction is also in error because it assumes the expansion to be isentropic. Furthermore, neither correction technique accounts for the effects of dynamic environment on the radius of the effective jet. These flaws may be partially responsible for the prediction of too fat a plume by the model. It is also possible that the mathematical formulation which led to Figure 20 is basically incorrect as a description of plume-air mixing.

The NWC plume model uses an eddy viscosity mixing model. In the original formulation of the plume model the Libby (Ref. 16) equations for eddy viscosity were used. In the near field, eddy viscosity was assumed to follow

$$\epsilon = 0.00137 \times |u_j - u_w|$$

In the far field, eddy viscosity was assumed to behave as

$$\epsilon = K_5 r_s |u_G - u_w|$$

with $K_5 = 0.025$.

Subsequently, both the Donaldson-Gray (Ref. 60) eddy viscosity (K varies with $M_{1/2}$, half velocity Mach number) shown in Figure 21 and a selectable variable viscosity have been used. But no extensive study of the effect of eddy diffusivity coefficients has been made with the NWC model as has been done by Pergament for the AeroChem model (Ref. 12). Of course, it goes without saying that for any plume mixing model, the higher the eddy viscosity coefficient, the faster the mixing and the shorter the plume.

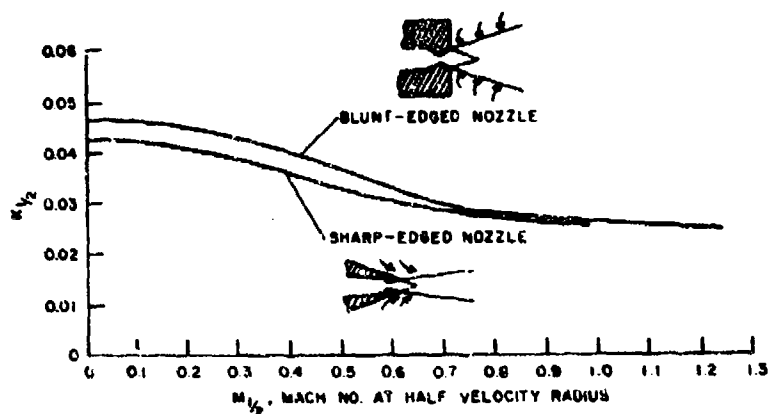


FIGURE 21. Local Mixing Rate Constant Versus Local Mach Number at the Half-Velocity Radius.

NWC TP 5319, Part 1

Despite its weaknesses and many simplifying assumptions, the NWC plume model has been shown by Webb and Smoot (Ref. 61) to be about equal in accuracy to the other models in common use for most attenuation predictions. The critical variable in comparing the different models appears to be the eddy diffusivity values selected.

2.6.3 The ABL Plume Model

The plume computer program developed by Allegany Ballistics Laboratory (ABL) of Hercules, Inc. (Ref. 14, 48, 62) has not been distributed for general use; hence, we cannot report first-hand experience, but only what has been reported previously in the literature.

The ABL model is different from other parallel axisymmetric mixing and equilibrium afterburning programs in that it uses a finite difference solution to the equations of conservation and motion. The BYU model (Section 2.6.4) uses an integral solution; the simple RPE (Section 2.6.4) and the NWC models (Section 2.6.2) use linearized solutions. The non-equilibrium AeroChem (Section 2.7.1) and REP-1 models (2.7.2) also use finite difference solutions. Use of a finite difference solution lends a flexibility which is not possible with the other methods.

The ABL program can handle non-unity Prandtl and Schmidt numbers. Afterburning ignition can be delayed any desired distance downstream of the nozzle. The Donaldson-Gray eddy viscosity model (Figure 21) is used in the ABL program.

Calculated temperature and species contours and values of predicted transverse attenuation are similar to those for the other programs (Ref. 12, 13, 57). Differences between the programs can generally be adjusted by modifying the eddy viscosities and turbulent transport coefficients (Pr and Sc).

The most unique feature of Ref. 14, 49, and 62, which describe the ABL model, has been the discussion of underexpansion and free stream flow correction factors (see Section 2.5).

In a recent report, Williams, Hartsock and Buckley (Ref. 14) have described the development of a new ABL Flight Plume Model, a single computer program incorporating base structure, inviscid plume structure, free-shear and axisymmetric mixing. Although described as being essentially complete, the program has not been checked out by performing sample calculations.

2.6.4 The BYU Aft-Plume Model

The latest version of the BYU aft-plume model (Ref. 32)³ starts the plume calculation at the point where the trailing shock intersects the limiting streamline (Figure 3). Features of the model include (1) axial pressure gradient effects, coupled with non-zero (but small) radial flow effects, (2) an improved mixing coefficient for treating systems with finite secondary flows, (3) inclusion of the extent of air/jet mixing in the base region as initial conditions in the aft-plume models, and (4) non-unity turbulent Prandtl and Schmidt numbers.

Unfortunately the integral solution technique chosen by BYU for solution of the equations of continuity and motion is not well-suited to inclusion of non-equilibrium chemistry. In describing the model (Ref. 32), Smoot, et al. have shown that equilibrium and non-equilibrium chemistry have about the same effects on gas mixture density versus reduced velocity $[(u - u_\infty)/(u_j - u_\infty)]$. Therefore, it would be possible to superimpose chemical kinetics upon the results of the integral calculation to obtain a second approximation which would modify the temperature and species distributions while maintaining the mixture ratio and velocity distributions calculated by the equilibrium technique. However, existing numerical schemes (Sections 2.6.3, 2.7.1, and 2.7.2) are more appropriate for incorporating non-equilibrium chemistry.

The earlier BYU aft-plume model (Ref. 13), which has been used for comparison with other models and with data (Figures 17, 18, and Ref. 61, 63), is described briefly in Section 2.4.

Associated with the development of the BYU plume-mixing and afterburning models, Tufts and Smoot (Ref. 64), and more recently Stowell and Smoot (Ref. 56) have developed empirical correlations of the eddy viscosity coefficient for turbulent mixing.

The Tufts and Smoot correlation shows that the difference between measured (x_p) and predicted (x_u) velocity and concentration (x_c) core lengths can be represented by:

$$x_p - x_u = 67.6/(UR)^{1.07}$$

$$x_p - x_c = 87.8/(UR)^{1.23}$$

where $UR = u_j/u_\infty$ or u_∞/u_j , whichever is greater than unity, and the x 's are in dimensionless units (x/r_j).

³ Developed for the Naval Weapons Center on Contract No. N00123-72-C-0274.

The more recent Stowell and Smoot correlation is based on the data of Harsha (Ref. 65) in addition to all the data used by Tufts and Smoot. As a result of this correlation, a new formulation of the eddy viscosity coefficient has been defined.

$$K = c_1 (M_m)^{c_2} (\rho_6/\rho_5)^{c_3} \left[(u_6 + u_5)/(u_6 - u_5) \right]^{c_4} \quad (11)$$

where the coefficients c_1 , c_2 , c_3 , and c_4 , are defined in Table 1. M_m is the average of the internal and external Mach number $(M_5 + M_6)/2$. The subscripts 5 and 6 refer to properties external to, and internal to, the flow slipline (Figure 3). For the parallel mixing case, u_5 and u_6 become u and u_j , respectively. For application to the ABL model, they become u and u_m , respectively.

Since Stowell and Smoot correlated temperature and concentration data jointly, no differences are apparent for turbulent Schmidt and Prandtl numbers.

$$Pr = Sc = 1.08 (M_m)^{-0.01} (\rho_6/\rho_5)^{0.089} \left[(u_6 + u_5)/(u_6 - u_5) \right]^{-0.228} \quad (12)$$

These values for K , Pr and Sc were used in the latest BYU aft-plume model (Ref. 32). This model is intended for use with the BYU MOC and BYU base recirculation models described in Sections 2.5 and 2.4.

2.7 PLUME MIXING MODELS INCORPORATING CHEMICAL KINETICS

Until recently the most general model in existence for possible use in describing aft-plume structure supersonic missiles was the MOCV program developed by Edelman and Weilerstein (Ref. 15). This model considers fully coupled, nonparallel, viscous flows of supersonic external and internal streams with arbitrary initial conditions. A technique for rapid, non-equilibrium chemical computations (Ref. 66) is formally included for hydrocarbon combustion schemes. While a chlorinated solid propellant kinetic package could presumably be added to this program, such kinetics are not presently part of the system. Unfortunately, this program is neither fully documented in the literature nor available for general use.

The AeroChem plume model (Ref. 12) and the several REP models developed by the RPE (Ref. 67) utilize a finite difference technique and finite rate chemistry. Both of these programs have a general chemical reaction capability in that they can handle for neutral or ionic species any reactions of the following types:

- (1) $A + B \rightleftharpoons C + D$
- (2) $A + B + M \rightleftharpoons C + M$
- (3) $A + B \rightleftharpoons C + D + E$
- (4) $A + B \rightleftharpoons C$
- (5) $A + M \rightleftharpoons C + D + M$

TABLE 1. Summary of Mixing Coefficient Correlations for Free Jet Data.

Type data	$K = c_1 (M_m)^2 (\rho_1 / \rho_2)^{c_2} [(u_6 + u_3) / (u_6 - u_3)]^{c_4}$				Number of experiments	Deviation of predicted and measured values	
	c_1	c_2	c_3	c_4		Average absolute	Average relative, %
Core region mixing coefficients (K_c)							
Velocity data						$\frac{X_p - X^*}{X^*}$	$\frac{(X_p - X^*)}{X^*}$
With secondary flow	0.0342	-0.369	-0.186	0.519	37	2.64	23.4
Without secondary flow	0.0343	-0.010	-0.071	^a	46	1.76	12.3
Concentration and temperature data							
With secondary flow	0.0316	-0.359	-0.276	0.747	50	2.26	27.7
Without secondary flow	0.0317	-0.110	-	^a	20	7.57	14.8
Decay region mixing coefficients (K_d)							
Velocity data						$\frac{m_p - m_c}{m_c}$	$\frac{(m_p - m_c)}{m_c}$
With secondary flow	0.0453	0.024	-0.210	0.734	37	0.258	20.4
Without secondary flow	0.0299	-0.163	-0.097	^a	46	0.125	11.2
Concentration and temperature data							
With secondary flow	0.0534	-0.029	-0.258	0.827	50	0.2166	17.6
Without secondary flow	0.0366	-0.077	0.025	^a	20	0.183	16.3

^a Since $u_3 = 0$, $u_6/u_6 = 1$ and no exponent needs to be specified.

NWC TP 5319, Part 1

where M is an arbitrary third body. The AeroChem program has the added feature of being able to freeze a reverse reaction by specifying "forward reaction only" for any of the five reaction types above.

Both computer programs utilize reaction rate coefficients of the general type:

$$K_f = AT^n \exp(B/RT)$$

in ml/molecule/sec units ($\text{ml}^2/\text{molecule}^2/\text{sec}$ for termolecular reactions).⁴

The two programs have reasonably economical computer run-times and both seem to require about one minute of computer time per foot of tactical missile plume on a UNIVAC 1108 computer. Temperature contour plots for a particular plume are compared in Figure 22 for NWC, REP-1, AeroChem and AeroChem TKE programs. The JANNAF Plume Technology Handbook (Ref. 3) contains additional discussion of plume chemical kinetics.

In the latest AeroChem plume program, a stream tube inviscid structure calculation and particle flow are coupled to the existing capability (Ref. 51).

2.7.1 AeroChem Plume Model

The AeroChem plume model (Ref. 12) is a reasonably rapid, finite difference solution for a co-flowing, parallel, axisymmetric, turbulent, free jet with rate dependent chemistry. The chemical reaction rate data of Ref. 68 are used. The mixed implicit/explicit scheme used for the solution eliminates instability problems on the computer. Implicit differences are used for the solution of species conservation equations and explicit differences are used for the momentum and energy equations. Since the program is designed to handle axial pressure gradients, it is possible to adjust the plume calculation for a non-optimally expanded nozzle or for the effects of base recirculation and inviscid flow by proper pre-selection of the axial pressure curve and proper radial variation of the input species concentrations.

Prandtl and Schmidt numbers are assumed to be constant throughout the plume but need be neither unity nor equal to each other. Turbulent transport is described by an eddy viscosity model. Any one of six different eddy viscosity models contained in the program can be selected for use. In addition, Cashen⁵ has modified the

⁴ Jensen and Jones have published an extensive list of chemical reaction rate data (Ref. 68).

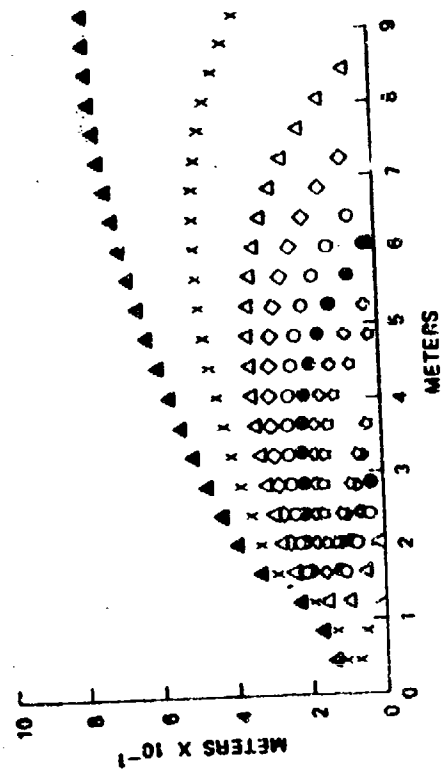
⁵ Dr. John Cashen, Hughes Aircraft Co., private communication, used:

$$K_{\text{momentum}} = 0.0284(M_m)^{-0.416} \left(\frac{u_o + u_w}{u_o - u_w} \right)^{0.609} \left(\frac{\rho_o}{\rho_m} \right)^{-0.213}$$

and

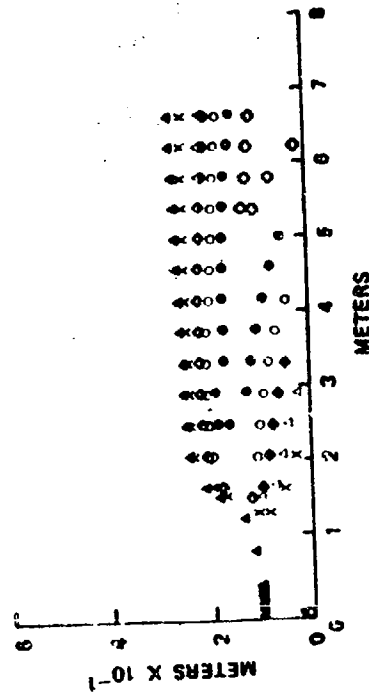
$$K_{\text{temperature}} = 0.0276(M_m)^{-0.375} \left(\frac{u_o + u_w}{u_o - u_w} \right)^{0.823} \left(\frac{f_o}{f_m} \right)^{-0.288}$$

Also see Hughes Aircraft Company Technical Internal Correspondence 2773.1/80, D. Bregman, 16 August 1973.



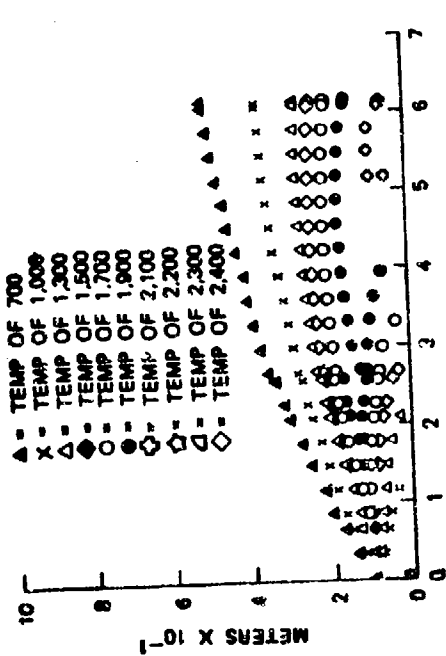
(a) AeroChem model

(b) REP-1 model (TKE)



(c) NWC model

(d) AeroChem TKE model



(a) AeroChem model

FIGURE 22. Comparison of Plume Temperature Contours Calculated by Four Plume Models.

NWC TP 5319, Part 1

Donaldson-Gray eddy viscosity coefficient in the AeroChem model by incorporating the results of the Stowell-Smoot correlation (Ref. 56 and Section 2.6.4). This new eddy viscosity coefficient yielded excellent agreement with an empirical model previously used by Cashen to fit jet plume IR data and has also improved the agreement between rocket plume IR data and theory at NWC. None of the other eddy viscosity models in the program fit Cashen's data. The Stowell-Smoot correlations listed in Table 1 have also been used at NWC. The entire AeroChem program is listed with full, clear instructions for its use in Ref. 12.

Mikatarian⁶ has recently modified the AeroChem model to incorporate a turbulent kinetic energy (TKE) model. We feel this program needs further study to explain its large differences from the other models shown in Figure 22. One should also note the latest AeroChem model (Ref. 51) which was developed too late to be fully examined prior to this writing.

2.7.2 The REP-1 Plume Model

The Rocket Propulsion Establishment (RPE) has been involved in the development of increasingly sophisticated plume models during the past several years. The first of these models, the REP-1 plume computer program (Ref. 67), uses a finite difference scheme to solve the problem of an initially parallel, axisymmetric turbulent free jet.⁷ Chemical reaction rates are modeled as described in this section (2.7). Solid particle reactions can be modeled and a range of particle sizes can be included. Non-unity and non-equal Prandtl and Schmidt numbers are allowed. A constant axial pressure gradient can be input to the program. For matching the program to the output of an inviscid plume calculation, it would be desirable to modify the pressure gradient coding to allow a variable gradient.

The unique feature of the REP-1 model is in the modeling of the eddy viscosity coefficient. A two-equation turbulent kinetic energy model is used. That is to say, in addition to the standard equations of conservation solved for the other plume models, two additional partial differential equations are solved for the turbulent properties of the flow. These properties are then used to determine the eddy viscosity coefficient. The two variables chosen are the turbulent kinetic energy, $k = 1/2(u'^2 + v'^2 + w'^2)$, and $W = k/\ell^2$, where ℓ is the characteristic length scale of the turbulence and W represents the square of the characteristic frequency of the energy-containing eddies.

The transport equations are:

⁶ Private communication, August 1973, R. R. Mikatarian, Lockheed Missile and Space Corp. (LMSC), Huntsville, Alabama. Also *8th JANNAF Plume Technology meeting*, July 1974.

⁷ The program documentation is included in Naval Weapons Center Reg. 451-150-73, September 1973.

Turbulent kinetic energy

$$\rho u \frac{\partial k}{\partial x} + \rho v \frac{\partial k}{\partial r} = \frac{1}{r} \frac{\partial}{\partial r} \left[\frac{r\mu}{\sigma_k} \frac{\partial k}{\partial r} \right] + \mu \left(\frac{\partial u}{\partial r} \right)^2 - C_D \rho k W^{1/2}$$

Square of characteristic frequency

$$\rho u \frac{\partial W}{\partial x} + \rho v \frac{\partial W}{\partial r} = \frac{1}{r} \frac{\partial}{\partial r} \left(\frac{r\mu}{\sigma_w} \frac{\partial W}{\partial r} \right) + C_1 \mu \left(\frac{\partial u}{\partial r} \right)^2 - C_2 \rho W W^{1/2} + C_3 \frac{W}{k} \mu \left(\frac{\partial u}{\partial r} \right)^2$$

where the nomenclature follows Ref. 67. Thus, there are two additional equations added to the conservation equations which must be solved simultaneously to define the plume.

The local eddy viscosity coefficient, μ , is then recovered using the equation

$$\mu = \rho k / W^{1/2}$$

and the length scale of turbulence, l , from the definition of W , is

$$l = (k/W)^{1/2}$$

The model is readily extended to consider other statistical properties of the turbulence. For example, the mean square fluctuation of temperature and several species concentrations can be generated by the program on input request. Thus, the program generates eddy viscosity, turbulent scale and turbulent intensities from basic equations. The turbulent properties are necessary for computations of plume-induced noise (Ref. 2) or plume radar cross section (Ref. 69 through 73). The model uses the chemical reaction rate data of Ref. 68. The model is based on the work of Spalding (Ref. 74 through 77).

A modification to REP-1, known as REPSI, has recently been announced.⁸ REPSI computes the static pressure field from the radial and longitudinal momentum equations. Results of one calculation and data are shown in Figure 23.

Another new RPE program, BAFL, uses an elliptic iterative solution for non-equilibrium chemistry. Because of the iterative solution, the program has a long run-time. Its use has been limited to solving the problem of base recirculation with chemical kinetics (see Section 2.4 for equilibrium base solutions). Combination of BAFL and REP has shown good correlation with both static and flight data.

⁸ Combustion Heat and Mass Transfer, Ltd., *The Rocket Exhaust Plume Program REPSI*, by Akshai K. Runchal, CHAM/631/1, April 1974.

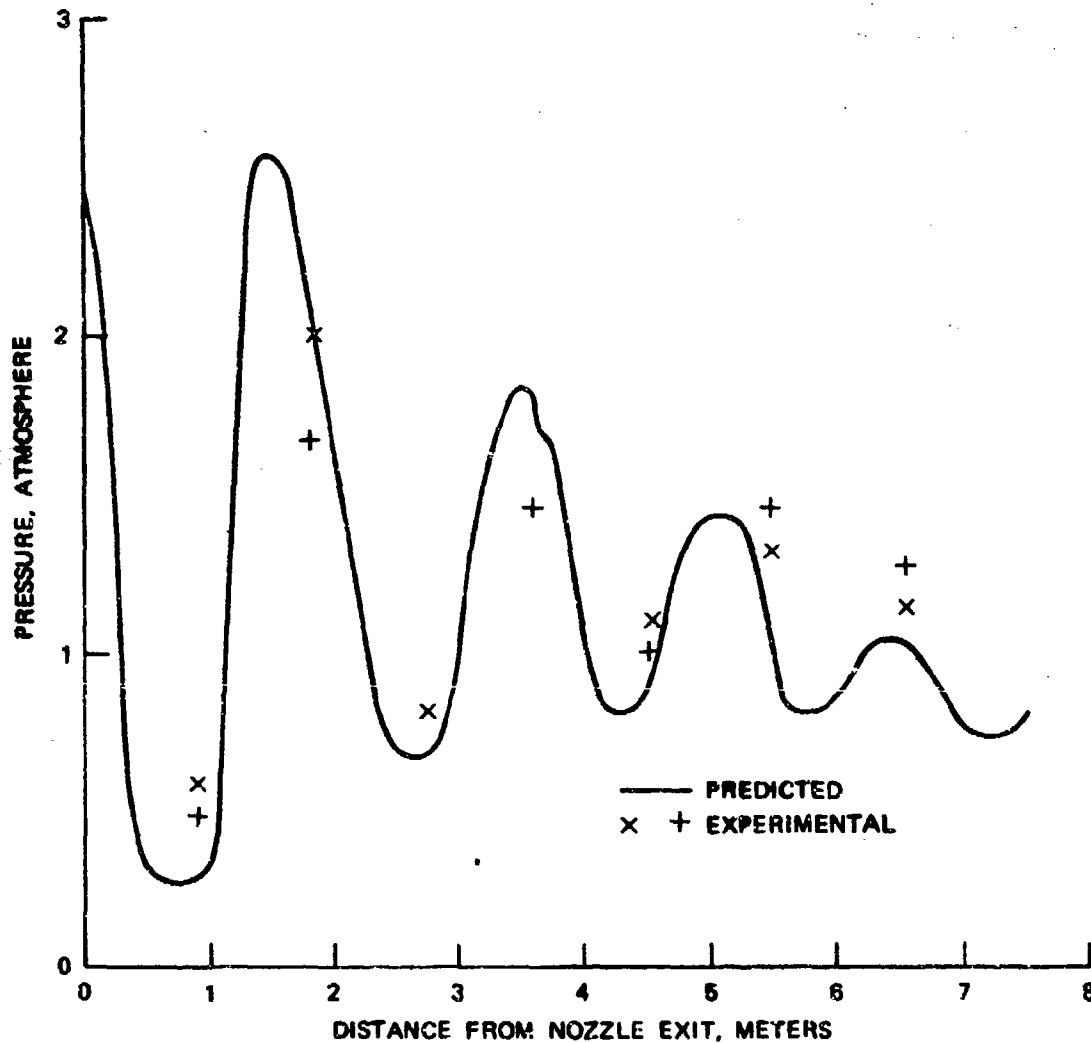
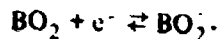


FIGURE 23. Comparison of Experimental and Computer Predicted (REPSI) Centerline Pressure for an Underexpanded Rocket Exhaust.

2.8 PREDICTION OF THE EFFECTS OF ATTENUATION-REDUCING ADDITIVES

A number of compounds capable of reducing the electron density (and thereby RF attenuation) of rocket exhaust plumes have been identified. Compounds of molybdenum, boron, tungsten, vanadium, cobalt, tin, chromium, iron, and copper have all been shown to reduce attenuation in controlled tests. Experimental work done on the problem prior to 1967 was summarized in Ref. 78. More recent measurements on the same, and other additives, are reviewed in Section 4.5. These include several simulated flight tests and a limited number of in-flight measurements.

Until the introduction of theoretical mechanisms for additive effects by Jensen (Ref. 79 and 80) and Pergament (Ref. 81), predictions of additive effectiveness were based entirely on analysis of empirical data. Fleischer, et al., (Ref. 82) postulated a simple mechanism for boron additives which involved the chemical reaction



By assuming an electron affinity of 3.5 eV for the BO_2 radical (80 Kcal/mole), the effects of boron additives have been calculated using the NWC equilibrium thermochemistry radar attenuation computer program (Ref. 83, program described in Section 2.6.2). Data and theory are compared in Figure 24. More comparisons of data and theory for boron should be made to substantiate this simple model and to compare it with the more complete mechanisms described by Jensen (Ref. 80) and given by reactions [7] through [9] on the following page.

Jensen proposed the following quantitative mechanisms and equilibrium constants for electron suppression by molybdenum, tungsten, and boron additives (Ref. 80, 84). Indicated reaction rates for molybdenum were proposed by Pergament (Ref. 14) for incorporation in the AeroChem plume computer program (Section 2.7.1), but are not needed for the equilibrium models of equations 13 through 15.

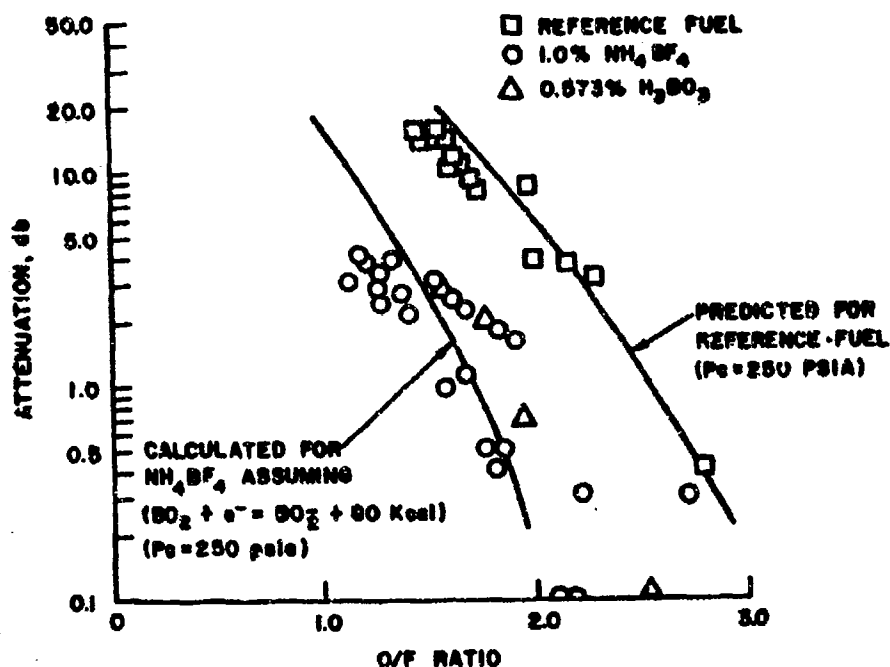


FIGURE 24. Data and Theory for Attenuation Suppression by Boron Compounds (Ref. 83).



$$\text{Rate} = 6 \times 10^{-11} \exp(-1000/RT)$$

$$K_1 = 3.6 \exp(3500/T)$$



$$\text{Rate} = 3 \times 10^{-9}$$

$$K_2 = 24 \exp(500/T)$$



$$\text{Rate} = 1.3 \times 10^{-10} \exp(-4000/RT)$$

$$K_3 = 0.85 \exp(10,400/T)$$



$$K_4 = 4.0 \exp(2900/T)$$



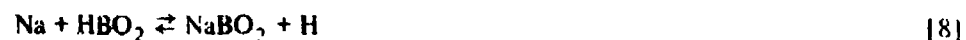
$$K_5 = 25 \exp(1300/T)$$



$$K_6 = 0.87 \exp(5700/T)$$



$$K_7 = 37 \exp(-2500/T)$$



$$K_8 = 12 \exp(-3000/T)$$



$$K_9 = 1500 \exp(-10,000/T)$$

The possible ways in which additives can reduce electron concentrations, as described by Calcote and Kurzius in Ref. 85, include (1) electron attachment, (2) compound formation by alkali metals (potassium being the principle source of electrons), (3) suppression of hydrocarbon chemi-ionization by removal of chemi-ion precursors (including CH radicals and oxygen atoms), (4) suppression of plume afterburning by removal of radicals, and (5) acceleration of electron decay by replacement of slowly-combining atomic ions by rapidly-combining molecular ions.

NWC TP 5319, Part 1

Molybdenum, tungsten, and boron reduce electron concentration by mechanisms 1 and 2. Molybdenum and tungsten also appear to operate by mechanism 3. The possibility that both of these additives operate through mechanism 4, as well cannot be ruled out (Ref. 80), especially since apparant changes in afterburning plume appearance have been noted to accompany electron suppression (Ref. 78).

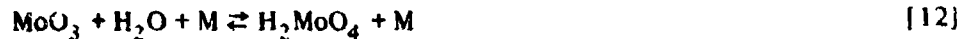
A scheme by which molybdenum may operate by mechanism 4 was proposed by Jensen (Ref. 84) but does not give results comparable to data:



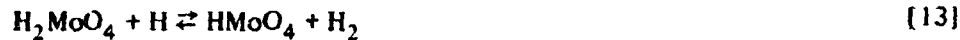
$$\text{Rate coefficient} \sim 10^{-28} \text{ at } 2,000^\circ\text{K}$$



$$\text{Rate coefficient} \sim 0.5 \exp(30,000/T)$$



$$\text{Rate coefficient} \sim 1.4 \times 10^{-23} \exp(26,000/T)$$



$$\text{Rate coefficient} \sim 0.02 \exp(-1700/T)$$

More recently, Jensen and Jones⁹ have obtained experimental verification for the schemes (where M represents Mo or W)



$$r_{\text{Mo}} = 1.1 \times 10^{-10} \exp(-1400/T)$$

$$r_{\text{W}} = 1.1 \times 10^{-10} \exp(-1000/T)$$



$$r_{\text{Mo}} = 1 \times 10^{-11}$$

$$r_{\text{W}} = 1 \times 10^{-10}$$



$$r_{\text{Mo}} = 1.4 \times 10^{-10} \exp(-300/T)$$

$$r_{\text{W}} = 3.3 \times 10^{-10} \exp(-1000/T)$$

⁹ Jensen, D. E., and G. A. Jones, *Mass Spectrometric Tracer and Photometric Studies of Catalyzed Radical Recombination in Flames*. Preprint (Proceedings Royal Society). 15 July 1974.

Considering the other ionization reactions which occur in a rocket exhaust



$$K_{14} = 10.3 \exp(-2100/T)$$



$$K_{17} = 180 \exp(-7600/T)$$

and further assuming that

$$[K^+] \cong [Cl^-] + [HMoO_4^-] + [MoO_3^-], [KCl] + [KHM_oO_4] \cong [K]_c$$

and

$$[H_2MoO_4] \cong [Mo]_c$$

where the subscript c represents total concentration of the element combined, ionized, or free in the plume, Jensen (Ref. 80) has generated the following expression for calculating electron suppression by molybdenum:

$$\frac{[e^-]_a}{[e^-]_o} = \left(1 + \frac{K_1 [Mo]_c}{K_{14} [HCl]}\right)^{-1/2} \left(1 + \frac{K_2 [Mo]_c}{K_{17} [HCl]} + \frac{K_2 K_3 [Mo]_c [H]}{K_{17} [HCl] [H_2O]}\right)^{-1/2} \quad (13)$$

where the subscripts a and o signify the presence and absence of additive, respectively.

Table 2 shows some results of applying Eq. 13 to typical rocket exhaust conditions. Similar computations for tungsten (Ref. 80) indicated somewhat less effectiveness.

Pergament (Ref. 80) developed the similar expression given by Eq. 14 for calculating electron suppression by molybdenum. (The notation has been changed from that of Pergament to make it consistent with Jensen's.)

$$\frac{[e^-]_a}{[e^-]_o} = \left(1 + \frac{K_2 [Mo]_c}{[H] (1 + (pK_{18} [H_2O])^{-1})} \frac{[H]}{([H] + K_{17} [HCl])} \left(1 + \frac{K_3 [H]}{[H_2O]}\right)\right)^{-1} \quad (14)$$

NWC TP 5319, Part 1

TABLE 2. Reduction of Plume Electron Concentrations by Molybdenum.

[Mo] _c	Temperature, °K	[e ⁻] _a /[e ⁻] _o Equation 13				Equation 15 with	
		[H] = 3 × 10 ⁻²	[H] = 1 × 10 ⁻²	[H] = 3 × 10 ⁻³	[H] = 1 × 10 ⁻³	K ₂	K ₂ (mod)
0.004	2600	0.75	0.86	0.90	0.92	0.96	0.98
	2300	0.60	0.75	0.85	0.88	0.94	0.96
	2000	0.38	0.56	0.72	0.80	0.91	0.95
	1700	0.16	0.29	0.46	0.60	0.84	0.81
	1400	0.051	0.088	0.16	0.25	0.68	0.56
	1100	0.0066	0.011	0.021	0.036	0.39	0.21
0.001	2600	0.92	0.96	0.97	0.98		
	2300	0.84	0.92	0.96	0.97		
	2000	0.66	0.82	0.91	0.94		
	1700	0.38	0.55	0.74	0.85		
	1400	0.12	0.20	0.34	0.51		
	1100	0.018	0.031	0.056	0.09		

Note: [Mo]_c and [H] are expressed as mole fractions
[HCl]_c = 0.15; [H₂O] = 0.20

The major difference between Eq. 13 and 14 is the inclusion in Eq. 14 of the reaction.



$$K_{21} = 7.1 \times 10^{-5} \exp(26,200/T) \text{atm}^{-1}$$

In an earlier paper (Ref. 79), Jensen had given the simpler Eq. 15 to calculate electron suppression by molybdenum. The effects of reactions [17], [18], and [19]

$$\frac{[e^-]_a}{[e^-]_o} = \left[1 + \frac{K_2 [\text{Mo}]_c}{K_{17} [\text{HCl}]} \right]^{-1/2} \quad (15)$$

which are also included in this mechanism, cancel out because they are assumed to be unaffected by the presence of molybdenum. In developing Eq. 15, Jensen had assumed a different value for the equilibrium constant K₂:

$$K_2(\text{mod}) = 3.8 \exp(4000/T)$$

The results of using Eq. 15 with both values of K₂ are included in Table 2. It should be noted that changes in [H] have no direct effect on Eq. 15. Substitution of K₂(mod) for K₂ in Eq. 13 has no significant effect on the results of calculations.

Equation 15 is the second term in Eq. 13 and represents the electron reduction stemming from the formation of HMoO₄⁻. The formation of MoO₃ is the predominant contributor to electron reduction at temperatures below 2100°K. Since this is the

NWC TP 5319, Part 1

region in which molybdenum is predicted to be most effective, it is clear that Eq. 15 will not adequately predict additive effectiveness. This is unfortunate since the equation is so simple and easy to use.

The term $K_{17}[\text{HCl}]/[\text{H}]$ which appears in both Eq. 13 and 14 equals $[\text{Cl}^-]/[\text{e}^-]$: the relative concentration of chlorine ions to free electrons. In his calculations, Jensen fixed the values of $[\text{H}]$ and $[\text{HCl}]$. On the other hand, Pergament (Ref. 81), using Eq. 14, examined molybdenum suppression of free electrons while keeping $[\text{Cl}^-]/[\text{e}^-]$ constant. Equation 14 also includes a pressure effect in the term p . By expressing $[\text{Mo}]_c$ in terms of mass fraction, Y_{Mo} , Pergament set

$$[\text{Mo}]_c = \frac{W}{W_{\text{Mo}}} (Y_{\text{Mo}})_p \left(1 - \frac{W_\infty [\text{N}_2]}{W [\text{N}_2]_\infty} \right)$$

where W represents molecular weight and the subscripts ∞ and p stand respectively for values in free stream and propellant. (Values in the plume have no subscript.) This is a convenient method for relating dilution of Mo in the plume to diffusion of ambient air into the plume. Typical results from Ref. 81 are given in Table 3.

In addition to using Eq. 14 to predict electron suppression effectiveness at various temperatures, Pergament (Ref. 81, 14) has also used the equation for calculating attenuation reductions in entire plumes. In general, observed attenuation reductions by Mo are greater than those calculated by the equilibrium techniques given by Eq. 13 and 14. Figure 25 is a typical comparison of data and theory. For the limited comparisons that have been made, calculated values are somewhat closer to measurements at higher altitudes. Actually, data are so scattered, as shown in Section 4.5, that there is no basis for accurately critiquing the theory.

TABLE 3. Calculated Reduction in Electron Concentrations from Equation 14 for $S_o = X_{\text{Cl}^-}/X_{\text{e}^-} = 100$.

Temperature, °K	Pressure, atm						
	$X_{\text{N}_2} = 0.1$			$X_{\text{N}_2} = 0.6$			
	0.12	0.37	1.0	0.12	0.37	1.0	
	$(Y_{\text{Mo}})_p = 0.01$						
1500	0.23	0.23	0.23	0.68	0.67	0.67	} $[\text{e}^-]_a/[\text{e}^-]_o$
2000	0.78	0.69	0.65	0.95	0.93	0.92	
2500	0.98	0.95	0.92	0.99	0.98	0.98	
	$(Y_{\text{Mo}})_p = 0.03$						
1500	0.092	0.091	0.091	0.41	0.41	0.41	} $[\text{e}^-]_a/[\text{e}^-]_o$
2000	0.55	0.43	0.39	0.89	0.84	0.81	
2500	0.95	0.89	0.80	0.98	0.97	0.96	

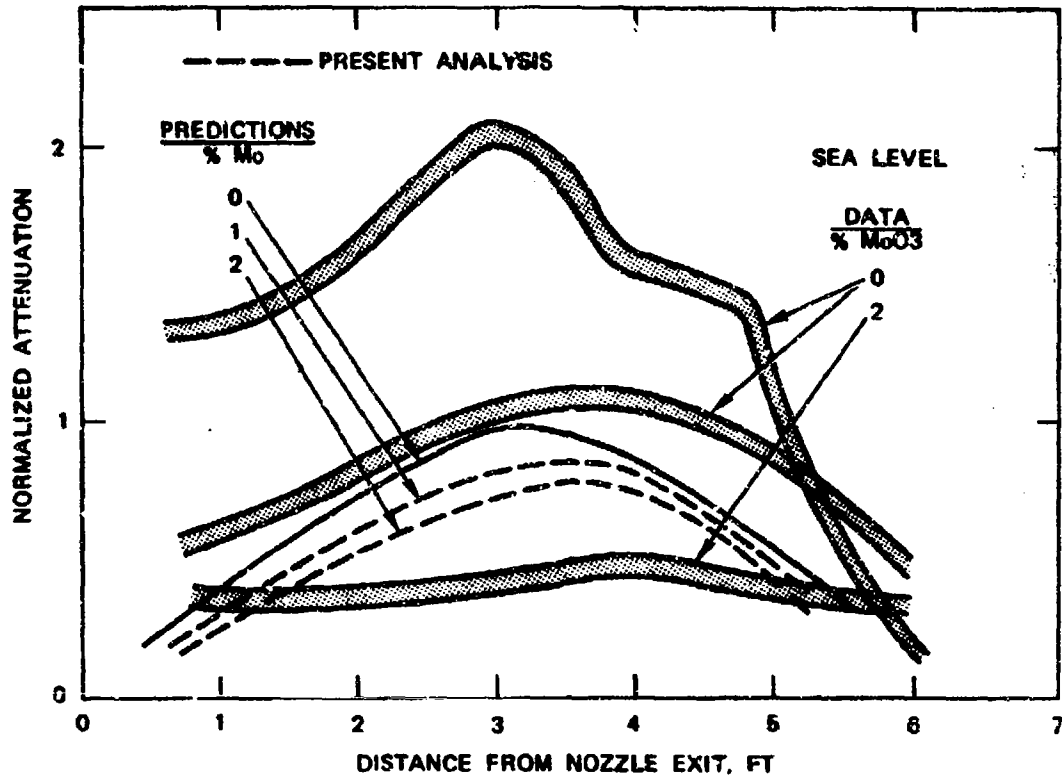


FIGURE 25. Comparison of Measured and Predicted Suppression of Attenuation for a 88/12 Propellant (Ref. 81).

In his latest studies, Pergament (Ref. 14) incorporated the reaction rates shown previously for reactions [1] to [3] for molybdenum in the AeroChem plume computer program (Section 2.7.1). While the results do not vary substantially from those of the equilibrium model of Eq. 14, they permit examination of the influence of the turbulent mixing model on Mo effectiveness. Results of these calculations are compared with data in Figure 26. Pergament showed that an eddy viscosity factor (α) has a major influence on the calculation of additive effectiveness. This occurs because changes in α affect the distribution of species and temperature in the plume.

More study will be required to correct this technique to a useful predictive tool. It is suggested that combinations of the mixing coefficients of Stowell and Smoot (as given in Table 1) with the AeroChem model (as described in Section 2.7.1 and including the molybdenum reactions) should be studied for a number of plume conditions which have been tested. Without such additional study, the theoretical techniques will probably underpredict additive effectiveness, probably due more to uncertainties in plume mixing models than to inadequacy of the chemical models for

NWC TP 5319, Part I

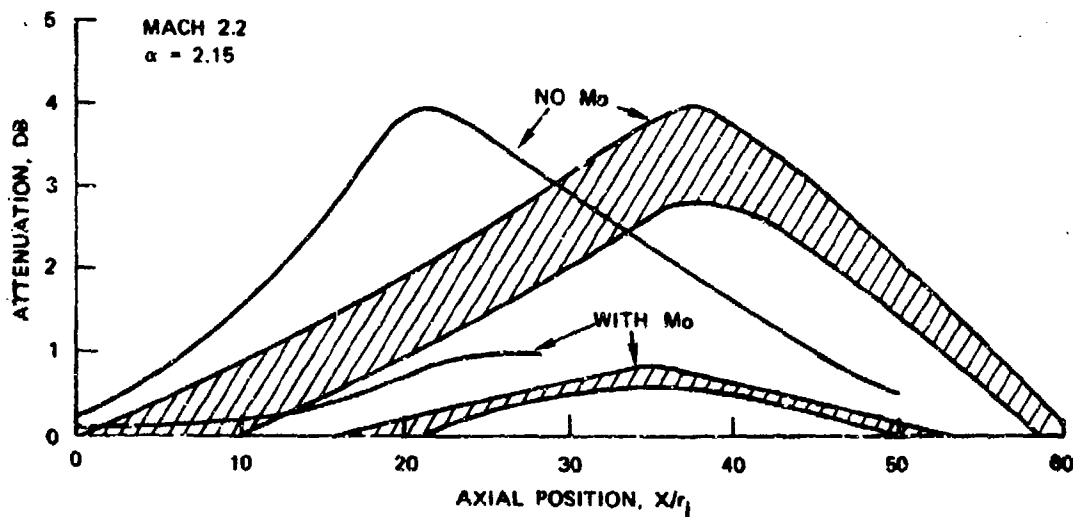
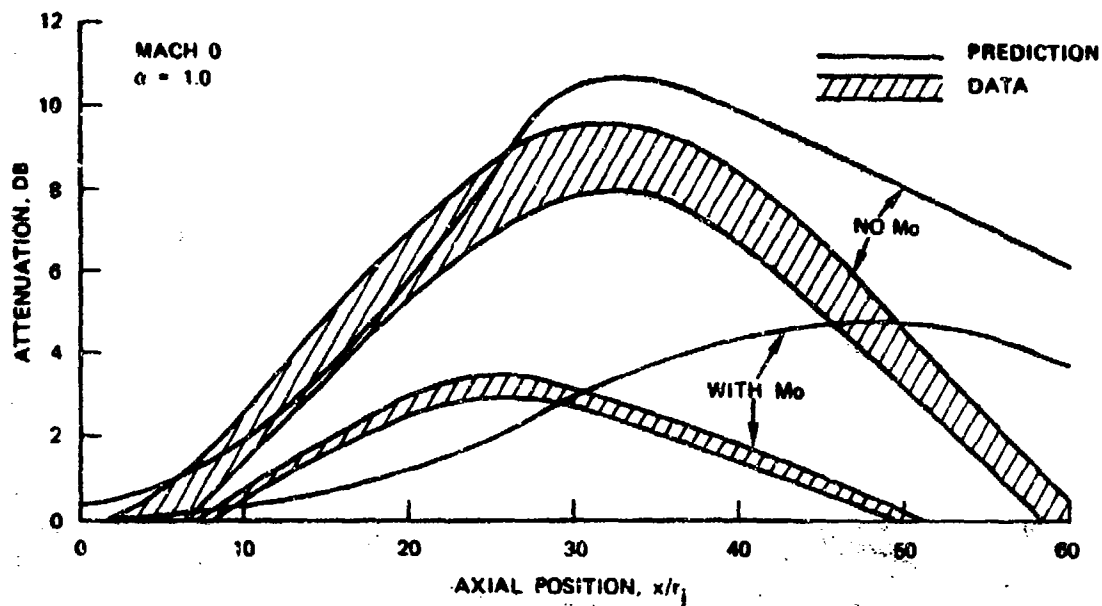


FIGURE 26. Effect of Molybdenum on Attenuation of 87/10 Composite Propellant Containing 1% $KClO_4$. Additive is 1% MoO_3 , simulated altitude 36,000 ft. (Ref. 14)

electron suppression. Therefore, unless the reader is prepared to pursue such a study, it is recommended at this time that predictions of additive effectiveness might as well be based on the crude empirical conclusions drawn in Section 4.5.

3.0 RF INTERACTION MODELS

In order to perform RF interaction calculations, the spacial distribution of electron density and electron collision frequency in the plume must be obtained from one of the plume computations described in the previous section (2.0). Of the programs generally available, only the NWC and BYU programs generate line-of-sight attenuation for any antenna orientation, transverse or diagonal. The AeroChem model generates only transverse line-of-sight attenuation (across the plume) for each specified axial output location. In general, for RF interaction calculations it is probably most useful to output the results of each plume model as an output grid of the following variables: x, y, electron density, collision frequency, pressure, density, and temperature, where the last three variables are of general interest rather than for RF calculations. The output grid can then be used for line-of-sight attenuation calculations by the method given in Appendix A. In addition, output of turbulent scale and electron density fluctuation intensity are necessary output from the REP programs (Section 2.7.2) for later calculation of plume-induced noise or RF cross section. (With any plume program other than REP-I or AeroChem TKE, the user must generate turbulent properties according to some set of assumptions (Ref. 2).)

The interaction models discussed in this section are all approximate techniques. Although Hasserjian and Clark (Ref. 86 and 87) developed a sophisticated model of RF interactions, which has been made available to government agencies on request, its use appears too cumbersome for the scale of problems encountered in tactical missile plumes and it should probably be reserved for problems of the scope of the Saturn plume, for which it was developed.

In the following subsections, interactions are subdivided into the types:

1. Line-of-sight attenuation
2. Diagonal refraction
3. Diagonal diffraction
4. Dispersion of focused beams in transverse attenuation measurements (transverse refraction)
5. Pulse distortion

A computer program for RF noise calculations is described in Part 2 of this publication (Ref. 2).

NWC TP 5319, Part 1

As will be seen in Section 3.1, the concept of electron collision frequency, ν , is important to all RF interactions with plumes. The numerical value of ν is equal to the number of collisions per second encountered by an average single electron in a plasma. For electron-neutral collisions (which predominate in a rocket plume)

$$\nu = n Q \left(\frac{8kT}{m_e} \right)^{1/2} \quad (16)$$

The following variables are used in this section.

- α = attenuation coefficient in dB/cm
- β = phase shift coefficient in radians per meter
- c = velocity of light in vacuum (2.9978×10^{10} cm/sec)
- ω = RF frequency in radians/sec = $2\pi \times$ Hz
- ω_p = plasma frequency = $\sqrt{\frac{4\pi n e^2}{m_e}} = 5.64(10^4) \sqrt{n_e}$ radians/sec
- ν = electron collision frequency
- Q = electron collision cross section for momentum transfer
- n = gas particle density, particles/cm³
- n_e = electron density, electrons/cm³
- m_e = electronic mass ($9.1085(10^{-28})$ gram)
- v_e = electron velocity = $5.21(10^5) T^{1/2}$ cm/sec
- T = temperature, °K
- k = Boltzmann constant = 1.3805×10^{-16} erg/deg

Approximate expressions have been published (Ref. 88) for electron-electron (Q_{ee}) and electron-ion cross section (Q_{ei})

$$Q_{ee} = 2.1 \times 10^{-10} T^{-2} \ln \left[\frac{1.24 \times 10^7 T^{3/2}}{n_e} \right] (\text{mks})$$

$$Q_{ei} = 1.25 \times 10^{-10} T^{-2} \ln \left[\frac{1.54 \times 10^{14} T^3}{n_e} \right] (\text{mks})$$

However, because of the very low concentration of electrons and ions in rocket exhausts the contribution of these two terms will be small and can usually be neglected.

Electron-neutral collision cross section values used for RF interference calculations at NWC are given in Table 4. The use of these values in Eq. 16 will result in small errors since the value of Q actually varies with electron energy and hence with

NWC TP 5319, Part I

TABLE 4. Collision Cross Sections for 0.3 eV Electrons (~3000°K) With Various Species.

Species	Cross section, m ²	Species	Cross section, m ²
LiF ^a	6.9 x 10 ⁻¹⁸	HCl ^a	2.0 x 10 ⁻¹⁹
LiCl ^a	6.0 x 10 ^{-18b}	H	1.4 x 10 ⁻¹⁹
LiBr ^a	5.0 x 10 ^{-18b}	H ₂	1.4 x 10 ⁻¹⁹
AlCl ^a	4.0 x 10 ^{-18b}	CO	1.2 x 10 ⁻¹⁹
HF ^a	6.0 x 10 ⁻¹⁹	CO ₂	1.1 x 10 ⁻¹⁹
H ₂ O ^a	5.0 x 10 ⁻¹⁹	HBr	9.0 x 10 ⁻²⁰
HCN	4.0 x 10 ⁻¹⁹	N ₂	8.5 x 10 ⁻²⁰
AlCl ₃ ^a	3.4 x 10 ⁻¹⁹	O ₂	6.0 x 10 ⁻²⁰
AlF ₃ ^a	3.4 x 10 ^{-19b}	N ₂ O	5.6 x 10 ⁻²⁰
NH ₃	3.0 x 10 ⁻¹⁹	CH ₄	2.8 x 10 ⁻²⁰

Note: A cross section of 1.0 x 10⁻¹⁹ square meter is assumed for most species not in Table 4 or present in concentrations less than 1 mole %.

^a For polar molecules, $Q = 4.74 \times 10^{-20} (D^2/E)$ square meter, where D = dipole moment Debye units, and E = electron energy (eV).

^b Assumed value.

temperature. More accurate calculations require inclusion of this variation. Altshuler, Moe, and Molmud (Ref. 89) have used an expression

$$Q = C v_e^n$$

where v_e is the electron velocity and n may be ±2, 1, or 0, and C is an arbitrary constant. In the REP-1 computer program (Section 2.7.2) the general expression

$$Q = C v_e^n + B \tag{17}$$

is used where both C and B are constants.

Generally these expressions for collision cross section include the effects of inelastic electron collisions in which the electron collision causes an energy state change in the atom or molecule struck. Altshuler (Ref. 90) has shown that $Q = 5.9 v_e^{-2}$ (cgs units) for water vapor. A list of electron-neutral cross sections used in the AeroChem plume program (Ref. 12) is given in Table 5 in the format of Eq. 17.

NWC TP 5319, Part 1

TABLE 5. Collision Cross Section, Q, as Function of Electron Velocity.

Species	Q, cm ²
CO	$2.08 (10^{-23}) v_e^a + 2.46 (10^{-16})$
CO ₂	$4.7 (10^{-8}) v_e^{-1}$
H ₂ O	$5.9 v_e^{-2}$
HCl	$1.85 v_e^{-2}$
N ₂	$3.29 (10^{-23}) v_e$
H ₂	$1.45 (10^{-23}) v_e + 8.9 (10^{-16})$

^a Electron velocity, $v_e = 6.21 (10^5) T^{1/2}$ cm/sec

3.1 LINE-OF-SIGHT ATTENUATION CALCULATIONS

Line-of-sight attenuation calculations are based on computing the absorption of a single RF ray as it passes through the plume. Along the ray path, the plume is assumed to absorb as a series of homogeneous plasma slabs normal to the ray. The calculation is discussed in Ref. 91, 92, and 93.

The attenuation α (or energy absorbed) per unit path length is given by

$$\alpha = 0.08686 \left(\frac{\omega}{c} \right) \left[-\frac{(1-A)}{2} + \frac{1}{2} \sqrt{(1-A)^2 + A^2 \left(\frac{\nu}{\omega} \right)^2} \right]^{1/2} \text{ dB/cm} \quad (18)$$

where $A = \omega_p^2 / (\nu^2 + \omega^2)$. Equation 19 can be substituted for Eq. 18.

$$\alpha \cong 0.461 \frac{n_e}{\nu} \left(\left(\frac{\omega}{\nu} \right)^2 + 1 \right)^{-1} \quad (19)$$

However, Eq. 19 is valid only under the condition that

$$\omega_p^2 / (\nu^2 + \omega^2) \leq 0.1$$

and

$$\left[\omega_p^2 / (\omega^2 + \nu^2) \right] \left(\frac{\nu}{\omega} \right) \leq 0.85$$

NWC TP 5319, Part 1

The phase shift coefficient, β , is given by Eq. 20.

$$\beta = \frac{1}{\sqrt{2}} \frac{\omega}{c} \left[(1 - A) + \sqrt{(1 - A)^2 + A^2 \left(\frac{\nu}{\omega}\right)^2} \right]^{1/2} \text{ radians/meter} \quad (20)$$

The total phase shift through a length d of homogeneous plasma is given by

$$\theta = (\beta - \beta_0) d$$

where

$$\beta_0 = \frac{\omega}{c}$$

The terms α and β are the real and imaginary parts, respectively, of the complex propagation constant γ which defines the electric field of the propagating ray where

$$\bar{E} = \bar{E}_0 e^{-\gamma x} e^{-i\omega t} = \bar{E}_0 e^{-x(\alpha + i\beta)} e^{-i\omega t}$$

and

$$\gamma = \alpha + i\beta \quad (21)$$

Under certain conditions the predicted line-of-sight attenuation is a reasonably good estimate of measurable values. These conditions include focused-beam transverse attenuation with intersection of plume and beam axes (Ref. 94) for a beam half-power radius no more than one-fourth the plume radius. Predictions of diagonal attenuation by the line-of-sight method have been reasonably good for plumes of composite propellants containing less than 5% aluminum. Such plumes have a maximum predicted electron density of less than 10^{10} electrons/cm³ and show a ratio of measured maximum diagonal attenuation to measured maximum transverse attenuation of between 7 and 10. Almost all line-of-sight predictions of attenuation show this same ratio, e.g.,

$$(\text{diagonal atten})_{\max} / (\text{transverse atten})_{\max} \cong 10 \text{ (predicted)}$$

Figure 27 shows measured values of the ratio for a wide range of composite propellants. The measured ratios range from 10 to 0.7. The following sections of this publication describe computations which can bring predicted attenuation values closer in line with measured values.

Appendix A describes a computer program which will compute line-of-sight attenuation for any plume for which α , from Eq. 18 is specified for a number of x, y points. In addition, this program will compute linearly interpolated values of the gradient of the refractive index at the same points. A modification of the computer program (A-II) also computes ray bending due to changes in refractive index.

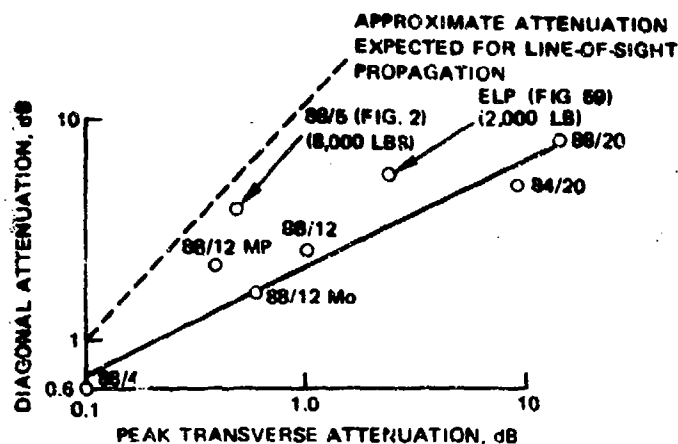


FIGURE 27. Comparison of Diagonal and Transverse Attenuation for 1,000-Pound Thrust Motors (Except as Noted). Numbers indicate % solids/% al. (Ref. 1).

Figure 28 shows predicted transverse attenuation and electron density using the NWC model (Section 2.6.2) for composite propellants with 85 and 88% solids (ammonium perchlorate plus aluminum) and 2 to 20% aluminum. Figure 29 shows the calculated chamber, exit plane and maximum afterburning plume temperatures for the same propellants. One might use these as a rough guide to attenuation prediction. Using the same model, calculated diagonal attenuation ranged between 8.5 and 10 times the transverse values.

Figure 30 is a nomograph for sea level static line-of-sight X-band attenuation calculations for aluminized composite propellants developed at NWC from similar calculations some years ago. To use the nomograph, one connects, with a straight line, the percent Al (line 1) with percent ammonium perchlorate (line 2). The intercept on line 3 is connected by straight line to the motor thrust level on line 4. The projection of that straight line to line 5 and thence from line 5 through the appropriate aspect angle on line 6 will give predicted diagonal attenuation on line 7. Curve 6 would have to be modified for other antenna positions. This nomograph can be used to estimate inputs for the diffraction model described in Section 3.3 and Appendix B (program B-1). The nomograph is set up only for an antenna located 3 exit radii from the nozzle centerline (assuming optimum sea level expansion). Although antenna location has a major effect on calculated line-of-sight attenuation, the effect on ray diffraction is less severe and reasonable estimates can probably be obtained from Figure 30 for most operational antenna positions, if equilibrium chemistry applies to the particular plume.

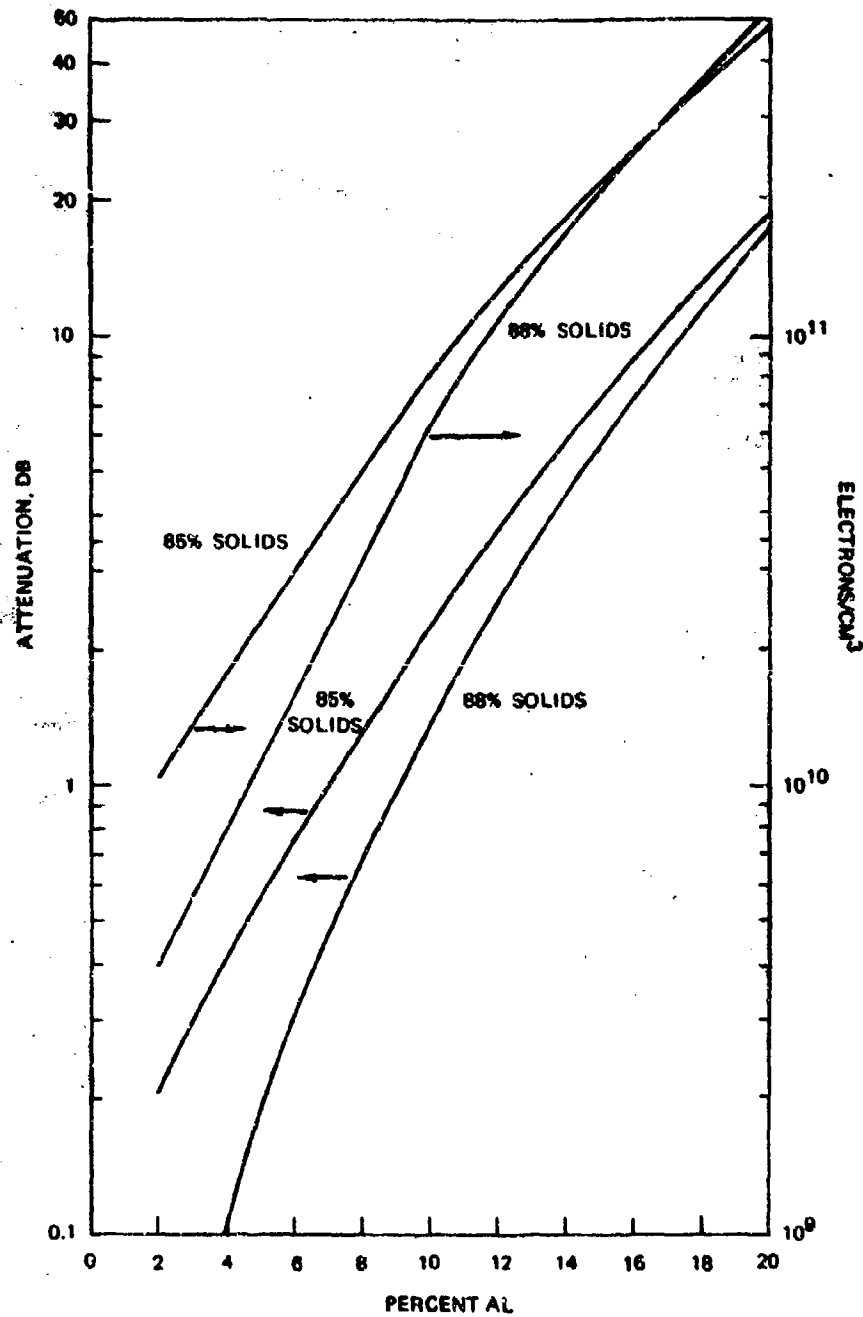


FIGURE 28. Peak Calculated Transverse X-Band Attenuation and Electron Density for Composite Propellants (1,000 psia Chamber, Sea-Level, 1,000-Pound Thrust, Equilibrium Thermo-Chemistry, 120 ppm Na, 40 ppm K).

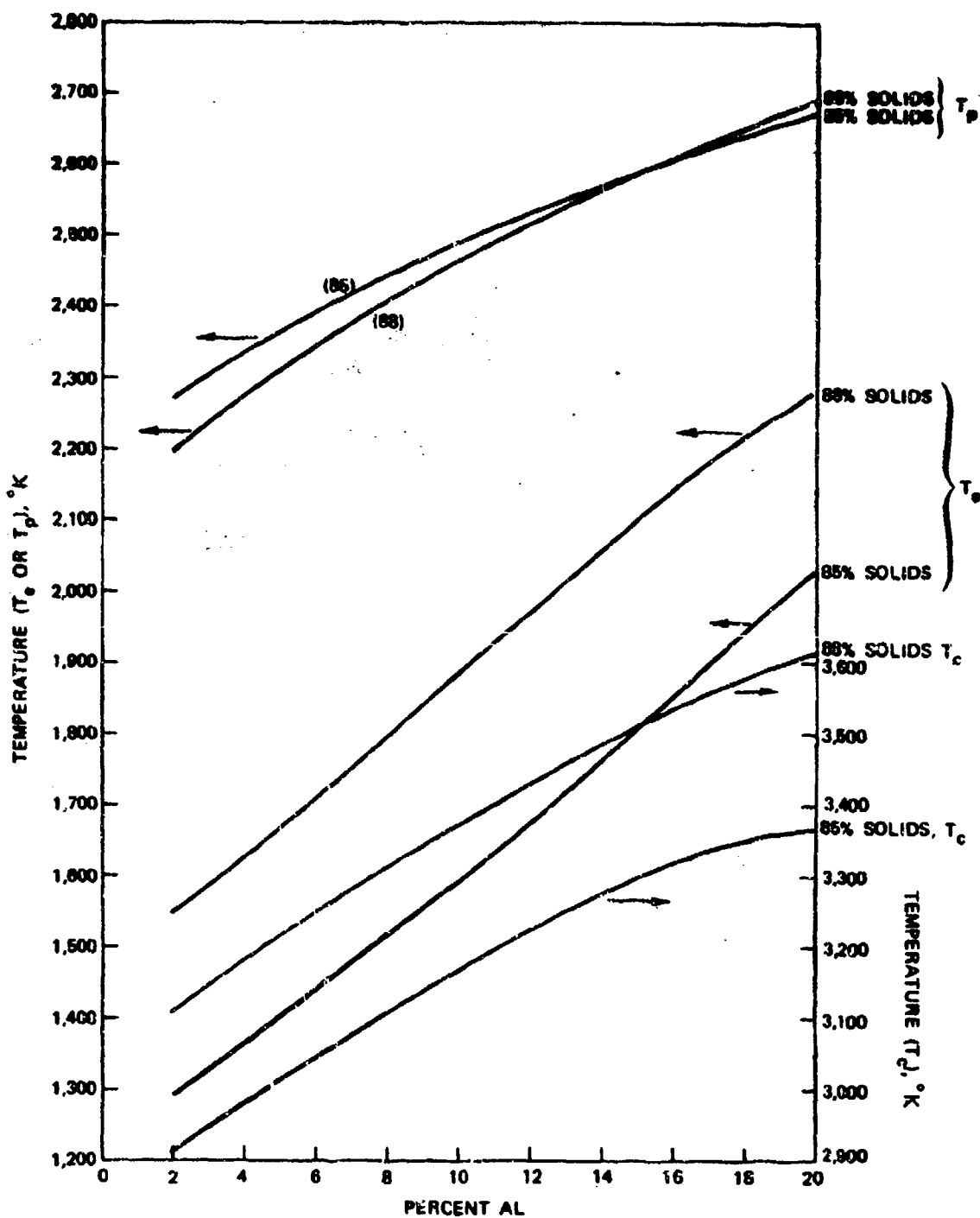


FIGURE 29. Calculated (Equilibrium) Chamber (T_c), Exit (T_p) and Maximum Plume Temperatures (T_j) for Composite Propellants With Same Conditions as Figure 27.

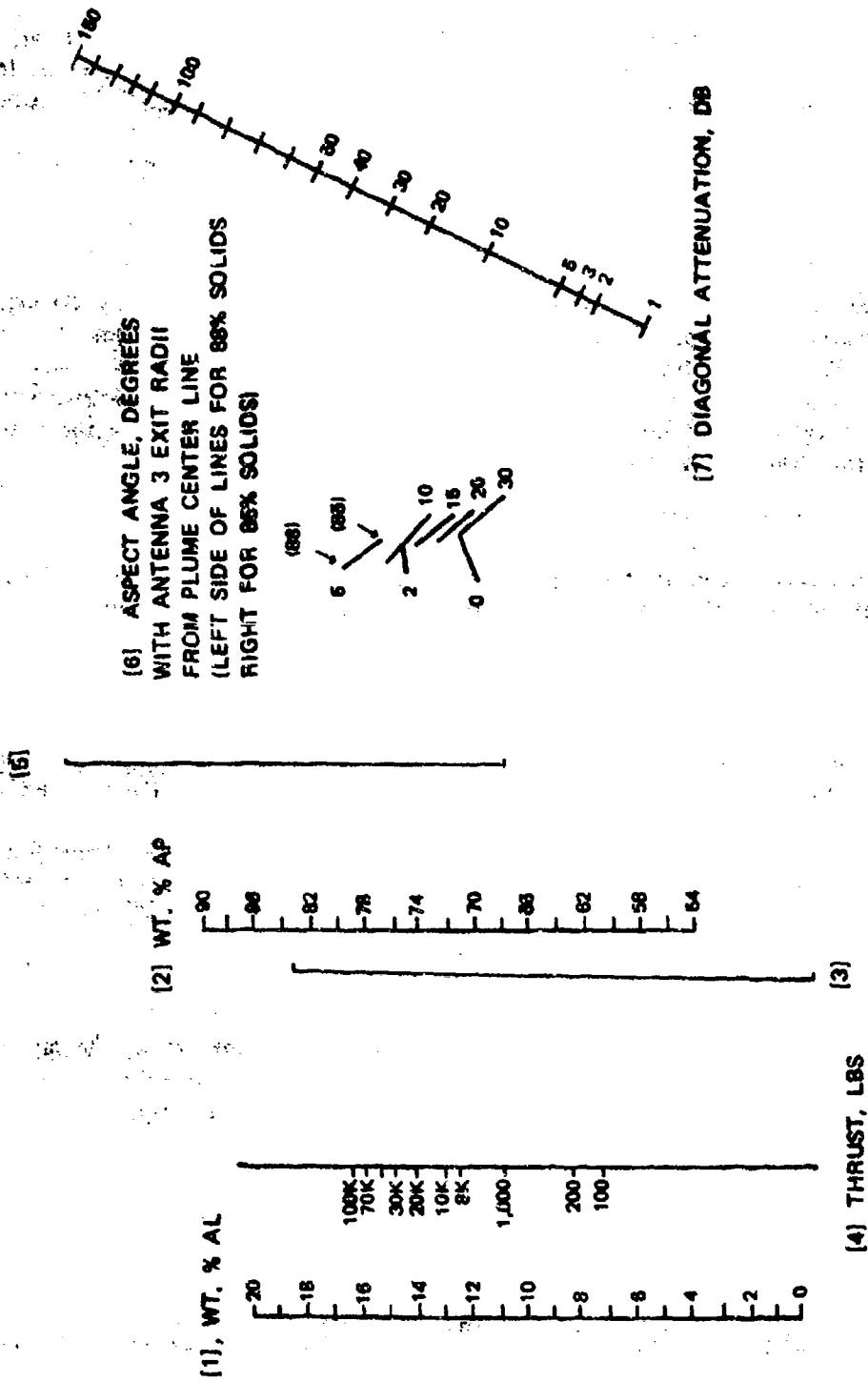


FIGURE 30. Line-of-Sight X-Band Attenuation Nomograph for Composite Propellants.

3.2 DIAGONAL REFRACTION

The refractive index of a medium is given by $n = c/v$, where v is the velocity of electromagnetic radiation in the medium and c is its velocity in a vacuum. In an absorbing medium the index of refraction is complex: $\underline{n} = n(1 + ik)$. The complex refractive index \underline{n} is related to the propagation constant

$$\gamma = \alpha + i\beta \quad (21)$$

since $\alpha = \frac{\omega}{c}nk$ and $\beta = \frac{\omega n}{c}$, so $n = \frac{\beta c}{\omega} + \frac{i\alpha c}{\omega}$

The complex nature of the refractive index affects the path of the ray through an absorbing medium and since Poynting's vector oscillates in such a medium, the energy path cannot be deduced from this vector. This leads to computations of considerable complexity. Epstein (Ref. 95) has shown that if absorption over one wavelength is not appreciable, then the complex law of diffraction deviates negligibly from the ordinary Snell's law for absorbing media

$$n_1 \sin \theta_1 = n_2 \sin \theta_2 \quad (22)$$

where the subscripts refer to the media on either side of a boundary crossed by the radiation. In this case, the index of refraction for each medium is given by

$$n_i = c\beta_i/\omega \quad (23)$$

The angles θ_i are defined as the angles between a ray and the normal to the boundary surface at which refraction (ray bending) occurs. When $\sin \theta_2$ (i.e., $n_1 \sin \theta_1/n_2$) is greater than unity, a reflection is predicted at the boundary between the two media.

In an inhomogeneous medium, such as a rocket plume, the refractive index varies continuously with position and the boundary for refraction is not necessarily clearly defined. The basic equation for refraction in such a medium (Ref. 96) is

$$\frac{d\bar{t}}{d\sigma} = \frac{\nabla n \cdot \bar{u}}{n} \bar{u} \quad (24)$$

where \bar{t} is the unit vector in the ray direction, σ is an arc length along the ray, ∇n is the gradient of refractive index (in the direction of fastest change of n), \bar{u} is a unit vector perpendicular to \bar{t} and lying in the plane of \bar{t} and ∇n (\bar{u} is tangent to the wave front). These vectors are shown in Figure 31.

Equating magnitudes in Eq. 24 gives

$$\left| \frac{d\bar{t}}{d\sigma} \right| = \frac{|\nabla n| \sin \gamma}{n} \quad (25)$$

where γ is the angle between \bar{t} and ∇n . $\left| \frac{d\bar{t}}{d\sigma} \right|$ is the curvature of the ray so R denotes the radius of curvature and $\frac{1}{R} = \frac{|\nabla n| \sin \gamma}{n}$.

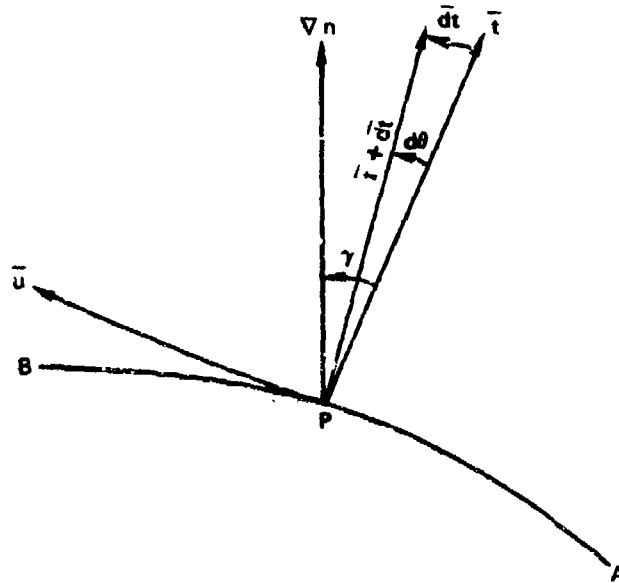


FIGURE 31. Vector Diagram for Continuous Refraction.

For very oblique ray angles, $n \cong \sin \gamma \cong 1$ so that $\frac{1}{R} \cong |\nabla n|$ and the ray will be concave downward where n increases into the plume (i.e., ∇n points downward) and the ray will be concave upward where ∇n points upward. Both of these effects are predicted at appropriate positions in plume by the model in Appendix A. Cashen has also developed a refraction model based on the preceding development by Kerr (Ref. 97).

Equation 23 can be written in a different form as

$$\frac{dn}{ds} = \nabla n \cdot \bar{t} \quad (26)$$

Combining Eq. 24 and 26 gives

$$\frac{d(n\bar{t})}{ds} = \nabla n \quad (27)$$

Equation 26 is subject to a number of manipulations. For example, if we let \bar{j} be a unit vector in the ∇n direction and assume that ∇n is constant in direction, we can show that

$$\frac{d}{ds} (n\bar{j} \times \bar{t}) = 0$$

resulting in

$$\frac{d}{d\sigma} (n \sin \gamma) = 0 \quad \text{or } n \sin \gamma = \text{constant}$$

which is the simple form of Snell's law, identical to Eq. 22 for a single refraction.

One possible method for calculating diagonal refraction through a plume is to define a number of contours of constant refractive index; apportion constant, linearly averaged values of refractive index to the volumes bordering the contours, and allow refraction to occur at the boundaries defined by the contours in accordance with Snell's law. The rays are assumed to travel in straight lines between contours. This was done in Ref. 98, which demonstrates that a very large number of contours may be necessary to overcome the fact that the contours are just a simplifying artifice. In actuality, refraction is occurring continuously along the ray (Eq. 24 and 26).

For example, suppose that the plume is divided into 100 contours. It is possible to trace the ray through the plume and calculate the refractions (up to 200) which will occur as the ray first enters and finally leaves the plume. Alternatively, it would be convenient to examine $n \sin \gamma$ or n or a similar variable for invariance as it moves between contours. The ray could then be assumed to travel linearly between refractions for a distance which is based on the physics of the situation rather than on arbitrary spacing of contours.

A diagonal refraction computer program (A-II), which we developed more recently, is included in Appendix A. This program is based on the solution of Eq. 25 assuming ∇n is normal to the plume axis throughout the plume and computes both the bending and attenuation of a ray. The program is much simpler than that described in Ref. 98, and is not limited to use with the NWC plume program.

The refractive index in a vacuum is unity. Since the phase shift coefficient is lower in a warm plasma than in free space, the refractive index in a plume, given by Eq. 23, will be less than unity. This is opposite from the normal dielectric for which n is greater than unity. In the normal field of a typical afterburning plume the refractive index decreases from unity as the ray enters the plume; toward the core where the electron density decreases, n begins to increase. The order is reversed as the ray passes through the centerline of the plume and moves outward again.

Diagonal refraction is further complicated since the plume, as seen by an arbitrary entering ray, is three-dimensional and co-planarity of ∇n , \vec{l} and the plume axis (two-dimensionality) is a very special case. The solutions described in Ref. 98 and Appendix A are for the two-dimensional case only. Hence, they only provide a *feel* for refraction by a plume but not a complete ray-trace solution. The results of several two-dimensional refraction calculations are shown in Figures 32 and 33. It can be clearly seen that very oblique entering rays are refracted in the direction of increasing

NWC TP 5319, Part 1

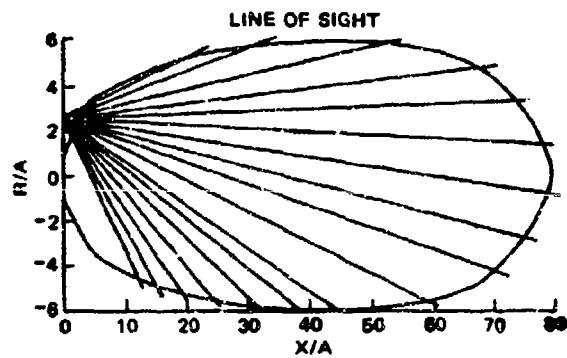
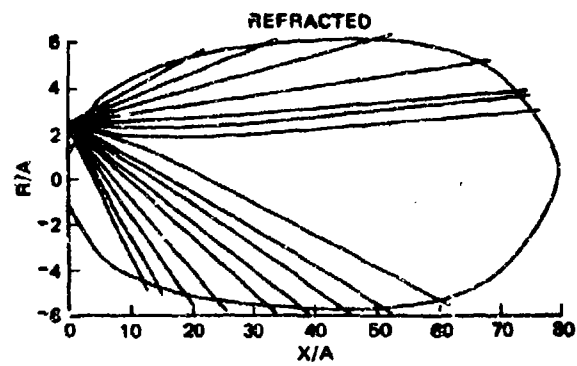


FIGURE 32. Comparison of Line-of-Sight and Refracted Ray Calculation for 12% Al/88% Solids Propellant (Ref. 87).

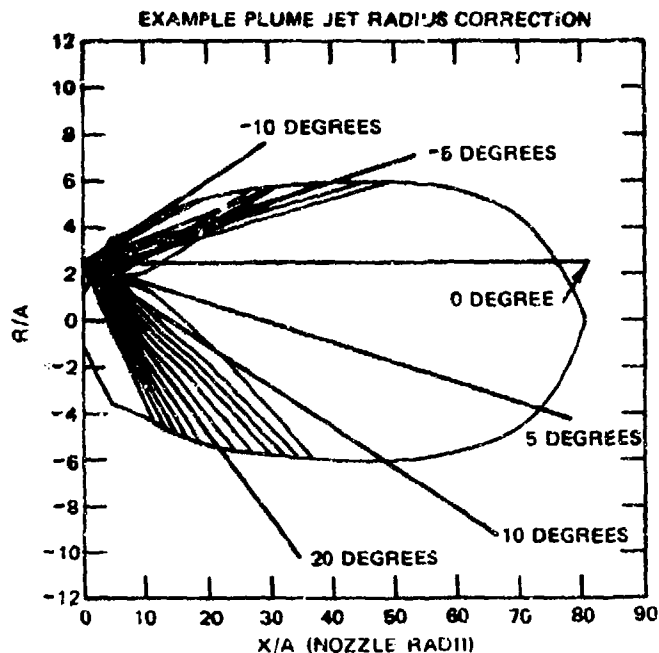


FIGURE 33. Refracted Ray Calculation for 20% Al/88% Solid Propellant (Ref. 87). Reference angles are projected beyond plume outline.

n so strongly that they seem to almost glance off the plume. The comparison with a line-of-sight propagation calculation shows strikingly how much the refracted rays can diverge from their original paths.

Evidence from diagonal attenuation measurements (Ref. 1 and 99) indicates that diffraction is far more important than refraction in determining the ultimate destination of RF radiation through plumes. However, the combined effects of diffraction and refraction are likely to give more accurate predictions of signal loss than diffraction calculations alone. A computer program, (B-II) utilizing this combination is described in Appendix B.

3.3 DIAGONAL DIFFRACTION

Simple computer programs for calculating diffraction of microwave radiation by afterburning tactical missile plumes are given in Appendix B. One of these programs (B-I) has reproduced experimental diagonal attenuation data fairly well (Figure 34). Further substantiation of a diffraction mechanism was presented in Ref. 1, which showed very close agreement between plume attenuation measured for a 0.2% potassium seeded, 20% aluminized rocket motor and the diffraction pattern of an aluminum cylinder (Figure 35). Lower potassium and/or aluminum loadings of the rocket propellant result in similar radiation patterns, but with reduced signal loss.

NWC TP 5319, Part 1

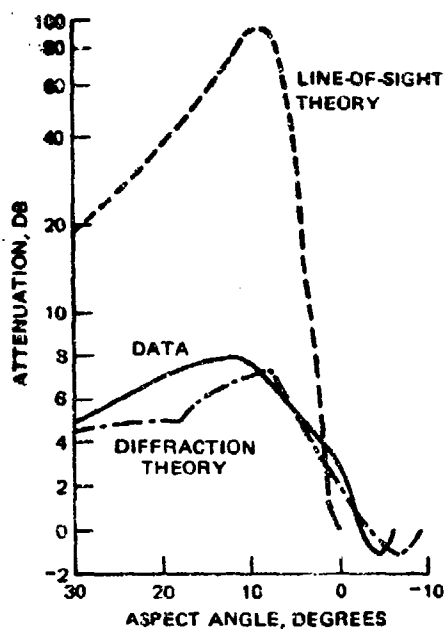


FIGURE 34. Comparison of Attenuation Data, Line-of-Sight Calculation and Diffraction Calculation for 20% Al/88% Solids Propellant.

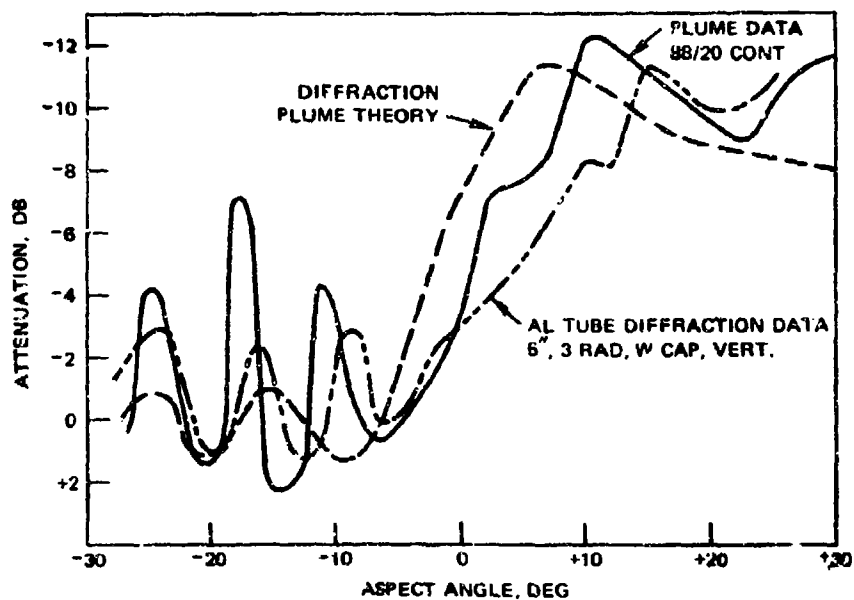


FIGURE 35. Comparison of X-Band RF Attenuation by 20% Al/88% Solids (With 2,000 ppm Potassium) Rocket Motor Plume, Diffraction by 5-Inch-Diameter Aluminum Cylinder and Prediction by Model B-II. (Cylinder data are shifted 5 degrees to left to account for nonsimilarity of antenna locations.)

There is no question that the line-of-sight model has been inadequate for predicting diagonal attenuation in many cases. A comparison of the diffraction and line-of-sight models with measurements is contained in Figure 34.

Since accurate diffraction calculations for an axisymmetric plume, such as that shown in Figure 36, are extremely complex (Ref. 86, 87, 100, and 101), we have developed a simple model based on the theory of line source diffraction by semi-infinite wedges and strips (Ref. 102-111). Figure 37 shows the way the plume of Figure 36 is modeled for calculating diffraction by the programs in Appendix B. One-dimensional diffracting edges are shown by the heavy solid and dashed lines which form the boundaries of the shaded surfaces.

The area labeled B is modeled by a strip extending to infinity in the positive and negative y directions. Radiation power in the shadow and *direct radiation* regions of this strip is calculated by the Fresnel diffraction method of Jenkins and White (Ref. 102). A brief description of Fresnel diffraction follows.

For the arrangement of radiation source S, diffracting strip D, and observation point P, shown in Figure 38, the quantity

$$I = |A(V_1) + A(V_2)|^2 \quad (28)$$

is defined as the ratio of the signal intensity at P in the presence of the obstacle D to the intensity in the absence of the obstacle, where

$$A(V) = \frac{1}{\sqrt{2}} \left[\int_0^V \exp\left(\frac{iu^2}{2}\right) du - \frac{1}{2}(1+i) \right] \quad (29)$$

and

$$V_{1,2} \cong \psi_{1,2} (2a/\lambda)^{1/2}$$

or more exactly,

$$V_{1,2} = a \tan \psi_{1,2} \sqrt{\frac{1(a+b)}{ab\lambda}}$$

where λ is the wavelength of radiation in the same units used for linear dimensions.

The integral in Eq. 29 is the Fresnel integral for which tables have been published (Ref. 102). The form of the Fresnel integral solution is shown by the Cornu spiral in Figure 39. The integral can be evaluated by noting the values of V along each leg of the spiral and determining the corresponding values of C and S [the real and imaginary parts of A(V)]. Then $A(V) = 0.707(C + iS)$.

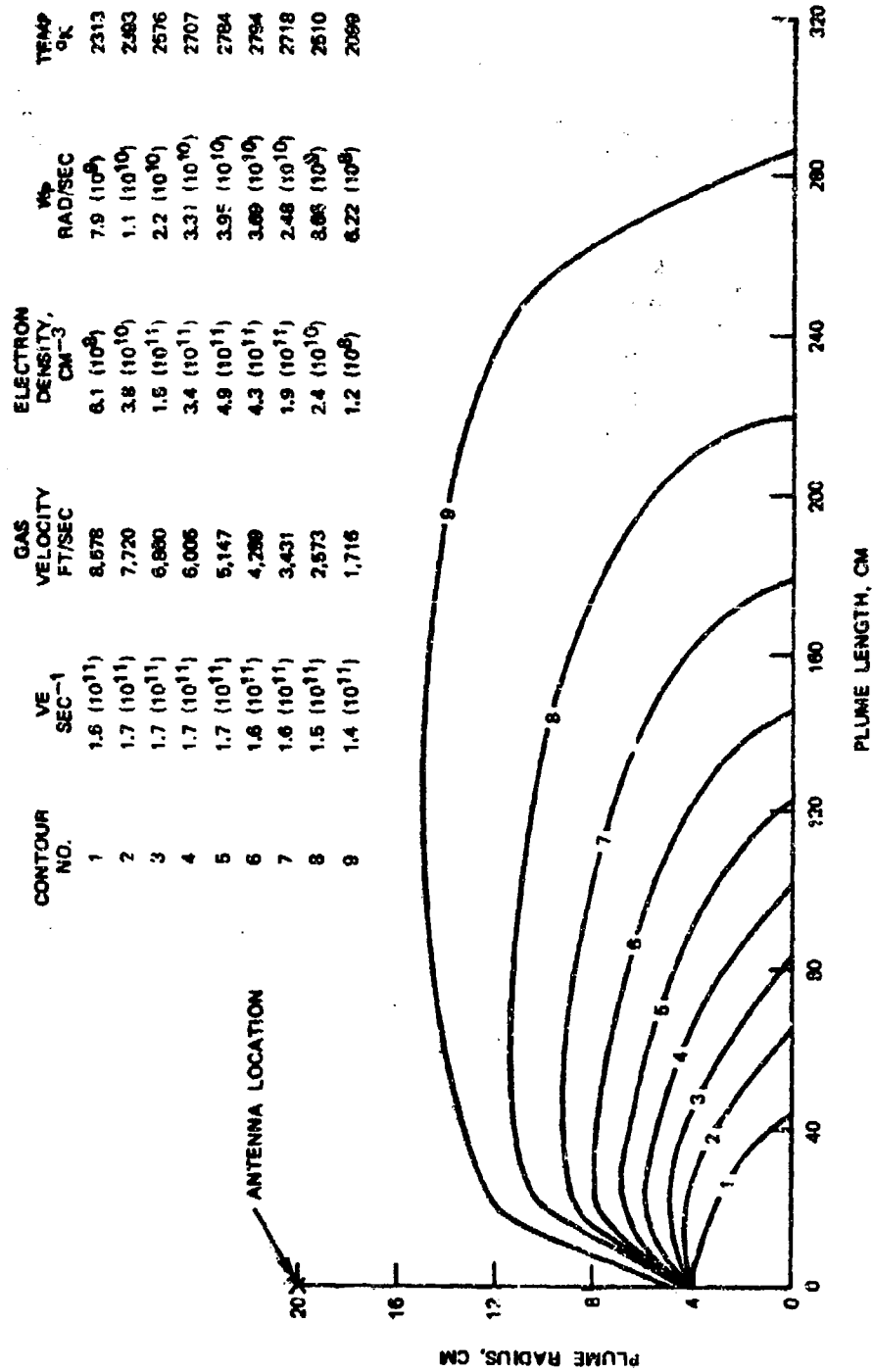


FIGURE 36. Calculated Properties of 88/20 Propellant (Static Sea Level).

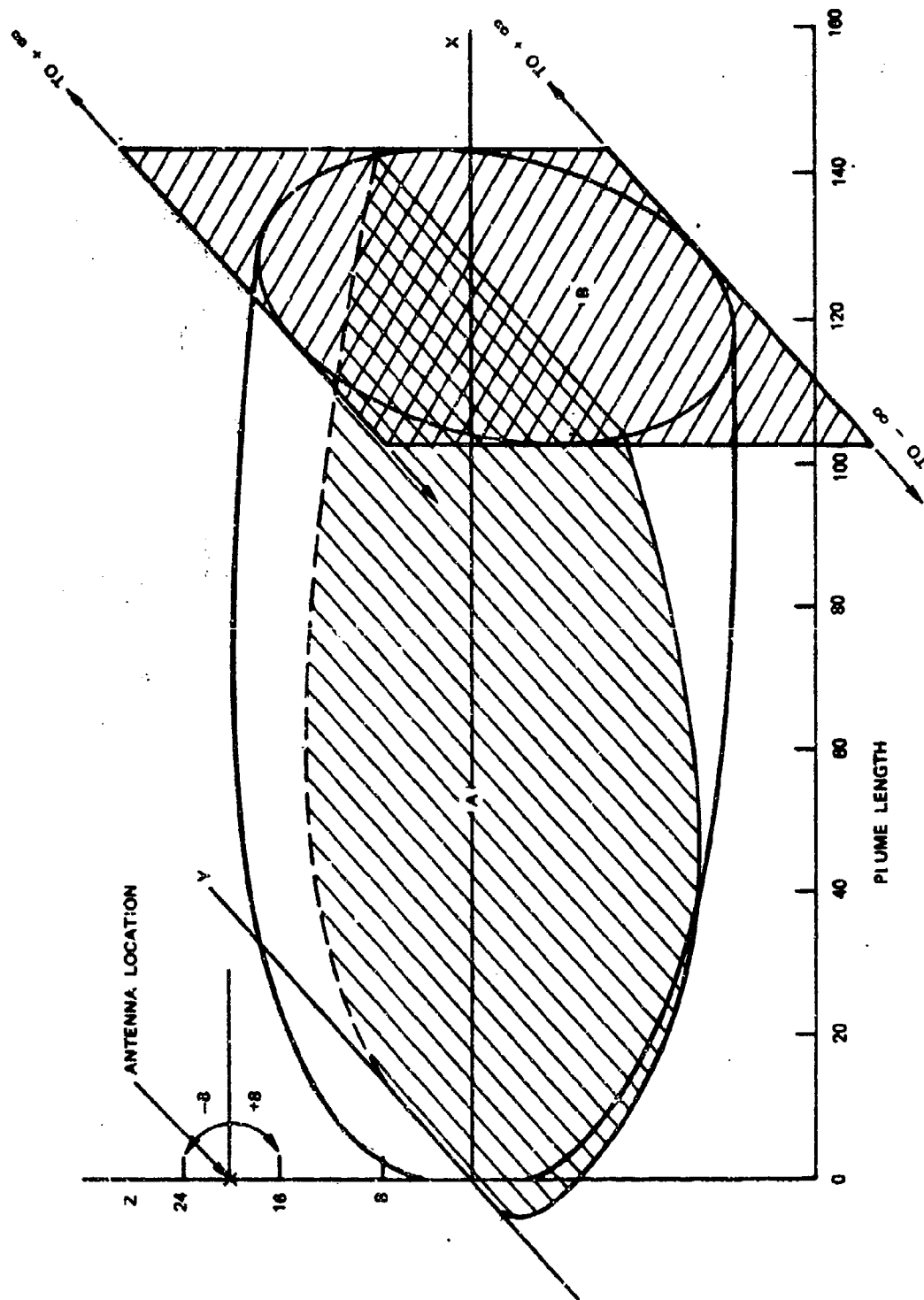


FIGURE 37. Plume Model for Diffraction Calculation.

NWC TP 5319, Part 1

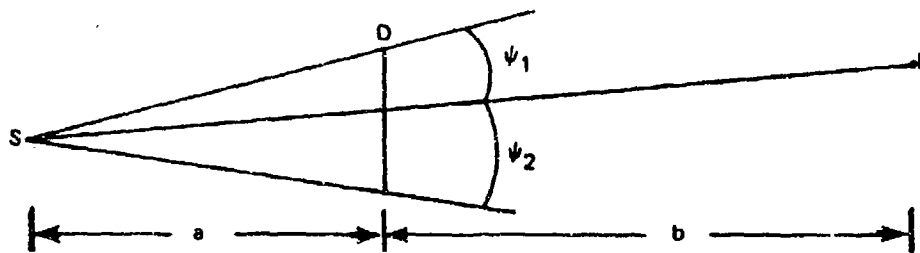


FIGURE 38. Schematic Drawing of Geometry for Diffraction by a Strip.

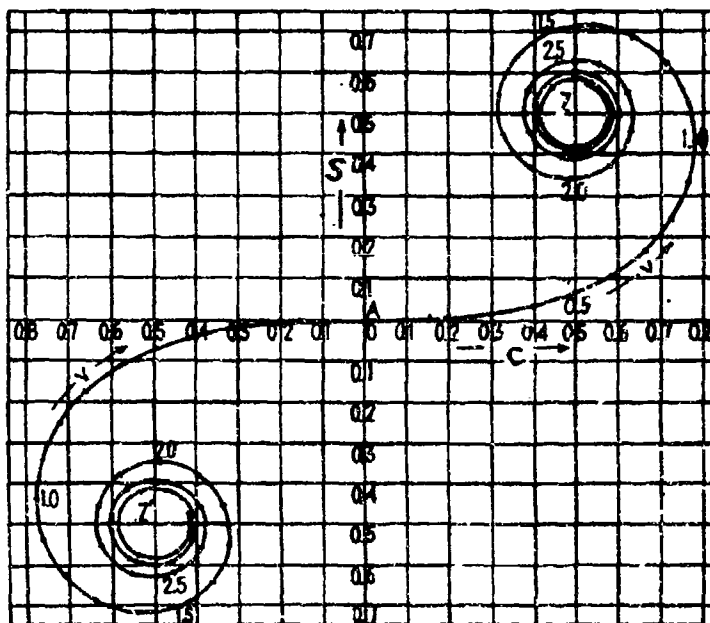


FIGURE 39. Cornu's Spiral, a Plot of the Fresnel Integrals.

For diffraction by a strip, the length of the vector drawn between V_1 on the upper spiral, and V_2 on the lower defines the intensity of radiation received at P. For diffraction by a single straight edge (semi-infinite wedge), the vector length between V_1 and the origin defines the intensity at P.

The preceding method is the one used in computer programs B-I and B-II of Appendix B to compute diffraction by the plane B in Figure 37. The vertical distance from the plume centerline to the upper edge of the plane B is the length HTA (defined in Figure 40), which is located at a distance DIST from the nozzle exit. DIST

INPUT VARIABLES FOR THIS PLUME WERE:
 THRUST, HTA, ATTN, DIST, AL, WAVEL, SHIFT, HTI, ANTE, ATMAX
 10000.0 16. -40. 125. 20. 3. 6. 4. 3. 93

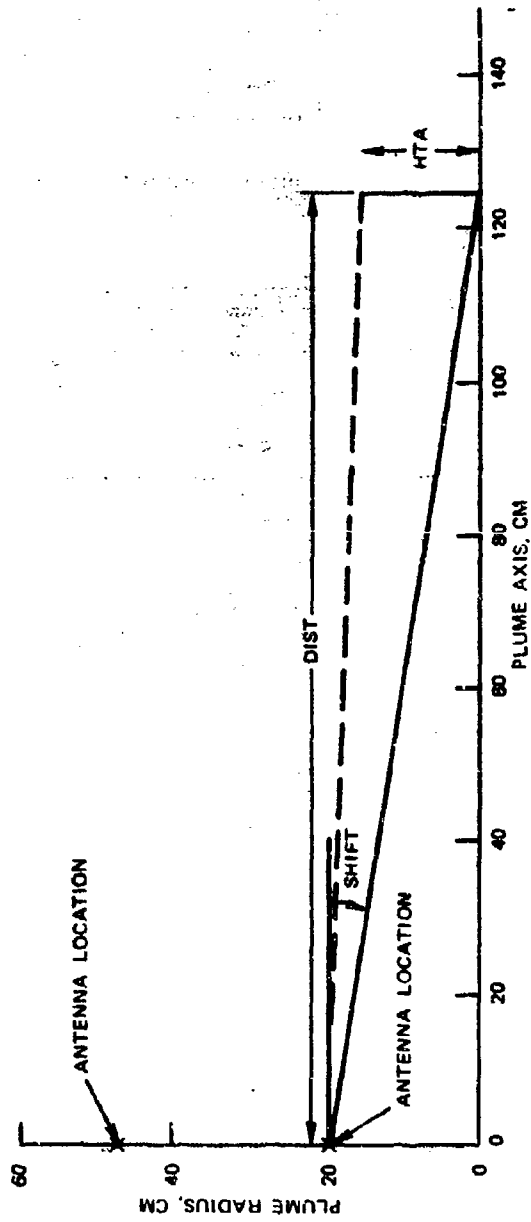


FIGURE 40. Plume Geometry for Diffraction Calculation.

NWC TP 5319, Part 1

in program B-I is defined as the x coordinate of the intersection of the line-of-sight ray of maximum attenuation with the plume axis. HTA in program B-I is defined by the intersection of the line-of-sight ray suffering 3 dB attenuation with the vertical line drawn at x = DIST. This forms the location of the first diffracted ray [A(V₁)]. The diffracting strip width extends to -HTA in the negative z direction also. This method of locating the effective "diffracting strip" is unsophisticated; possible improvements are discussed in conjunction with program B-II in Appendix B.

The line-of-sight method is also used to calculate, for the plume of Figure 36, the attenuation of the ray which would intersect the bottom of the strip -HTA. This attenuation is entered into the calculation of A(V₂). When the ray passing below the plane B is attenuated by 20 dB or more, the diffraction, for all practical purposes, is identical to that for a semi-infinite wedge (e.g., A(V₂) = 0).

In addition to the energy diffracted by the plane B, the energy diffracted around the cigar-shaped body of the plume must also be added in the shadow region. This is done by treating the sides of the plane A as diffracting edges and summing the energy diffracted by planes A and B with that which passes through the plume according to the line-of-sight calculation. This calculational method will always give attenuation values lower than those calculated by the line-of-sight method alone. In the case of high electron density plumes, the line-of-sight contribution is negligible.

In order to improve the fit of computer program B-I to existing data, it was necessary to make a few empirical corrections to the program. One of these was the selection, described above, of the 3-dB ray as the diffracted ray. A second correction, described in Appendix B, is the modification of calculated signal loss by the multiplication factor

$$\frac{1}{9} \cdot \log(ATMAX) \cdot \log(THRUST)$$

This factor ratios the maximum calculated line-of-sight attenuation for the plume (ATMAX) to a value of 1,000 dB and the motor thrust to a 1,000-lb thrust level.

We believe this factor comes about as the result of ignoring the effect of refraction on the propagation of the diffracted ray. Examination of Figures 32 and 33 shows that some refracted rays are bent so strongly that at the location on the edge of the "electrical plume" where such rays would be diffracted, they appear to have originated at some point in the nozzle exit plane much closer to the nozzle axis than the actual antenna. This is an effect which will not scale independently of plume dimensions or of electron density and so may help account for the correction factor.

The B-I diffraction model was developed to fit data using the NWC plume model (Section 2.6.2) to generate plume properties. The effect of using this diffraction model with several other equilibrium plume models as well, is shown in Figure 41. Several comparisons of the diffraction model with data are shown in Figure 42.

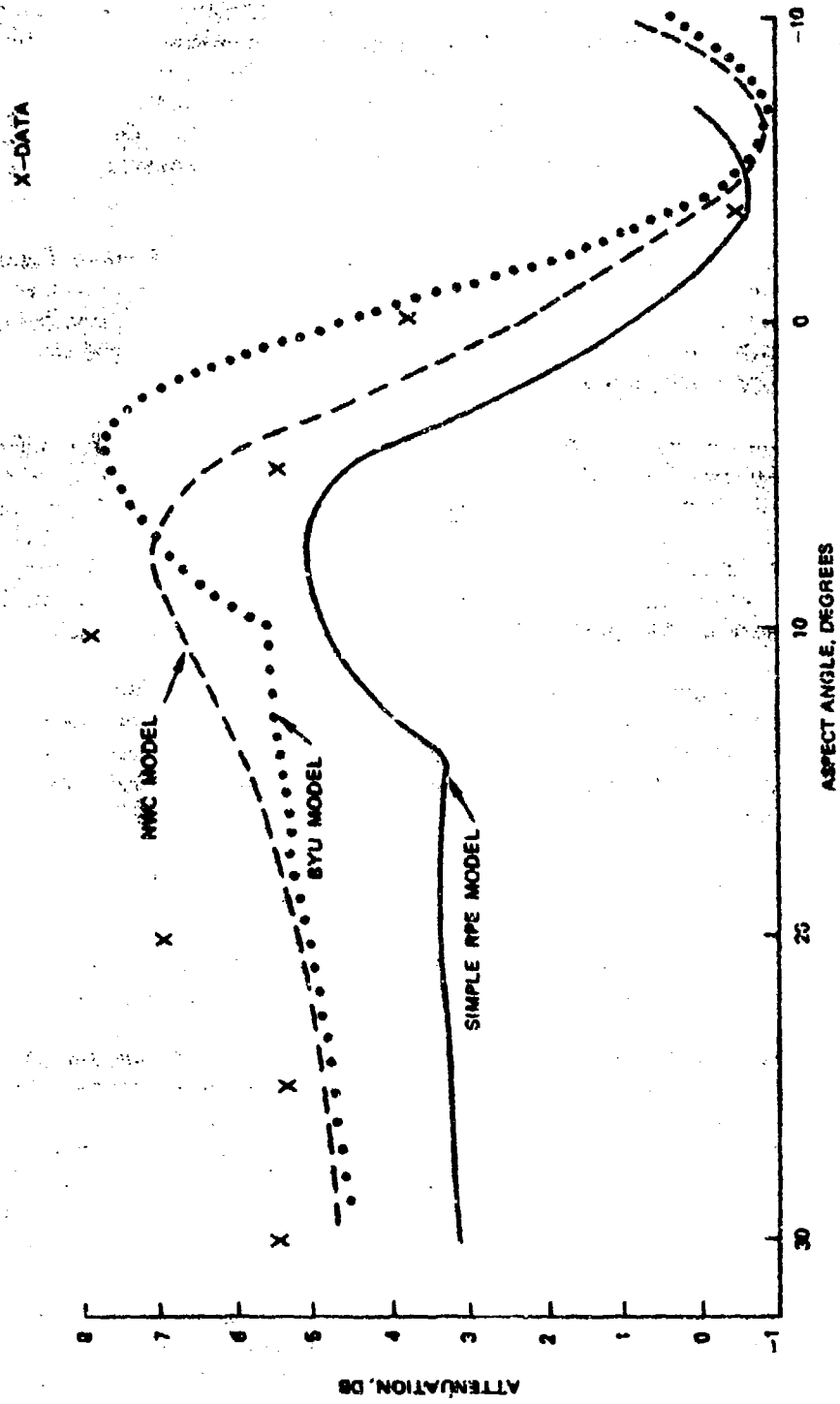


FIGURE 41. Comparison of BYU, NWC, and Simple RPE Plume Models Used for Diagonal Diffraction Calculations for 88/20 Composite Aluminized Propellant.

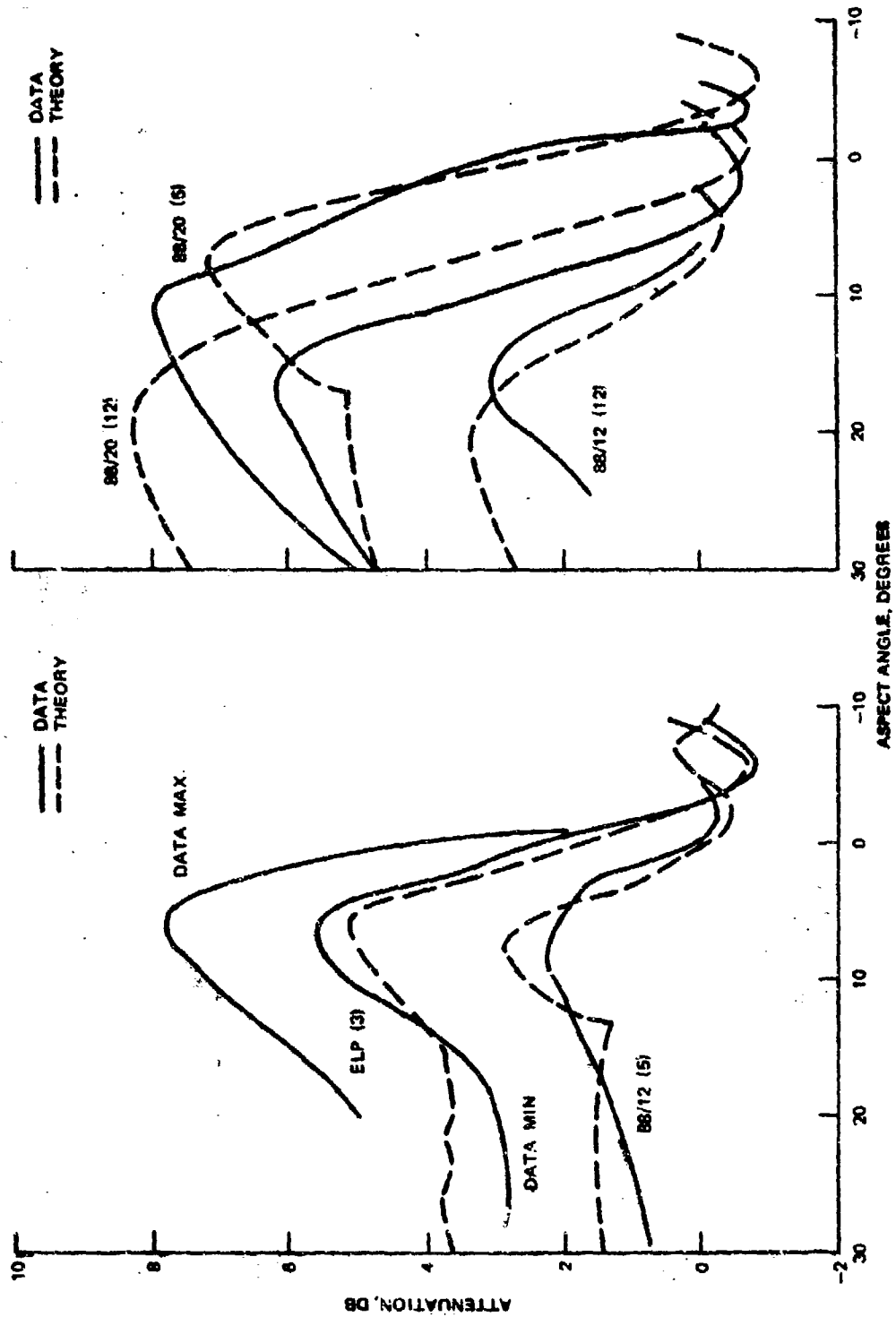


FIGURE 42. Comparison of Data and Diffraction Theory.

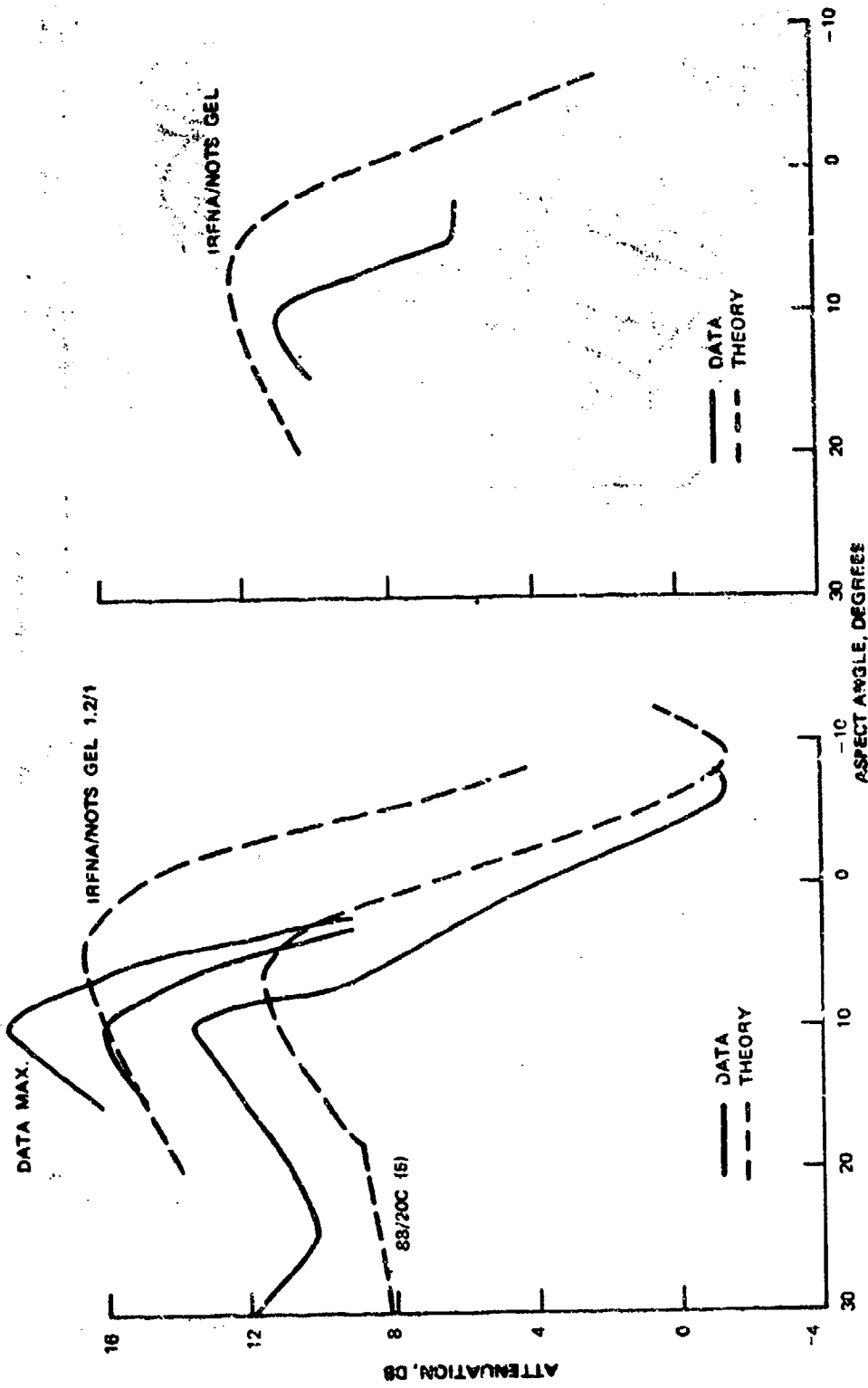


FIGURE 42. (Contd.)

NWC TP 5319, Part 1

In a recent paper, Webb (Ref. 112) used the B-1 diffraction model for data correlation on large motors. Very good agreement was obtained, however, several of the computer program input variables had to be redefined as follows:

1. SHIFT - Figure 43
2. DIST - The maximum length of the predicted 0.01 dB/cm contour divided by a factor of 4
3. HTA - The maximum radius of the 0.01 dB/cm contour

In addition, Webb used a correction factor for mass flow which is similar in effect to the term $1/3 \log(\text{THRUST})$ shown earlier. This term was not used in Webb's version of the program.

Webb's formulation can be used when the ray of maximum predicted line-of-sight attenuation does not cross the plane axis, a situation for which the original model of Appendix B-1 fails.

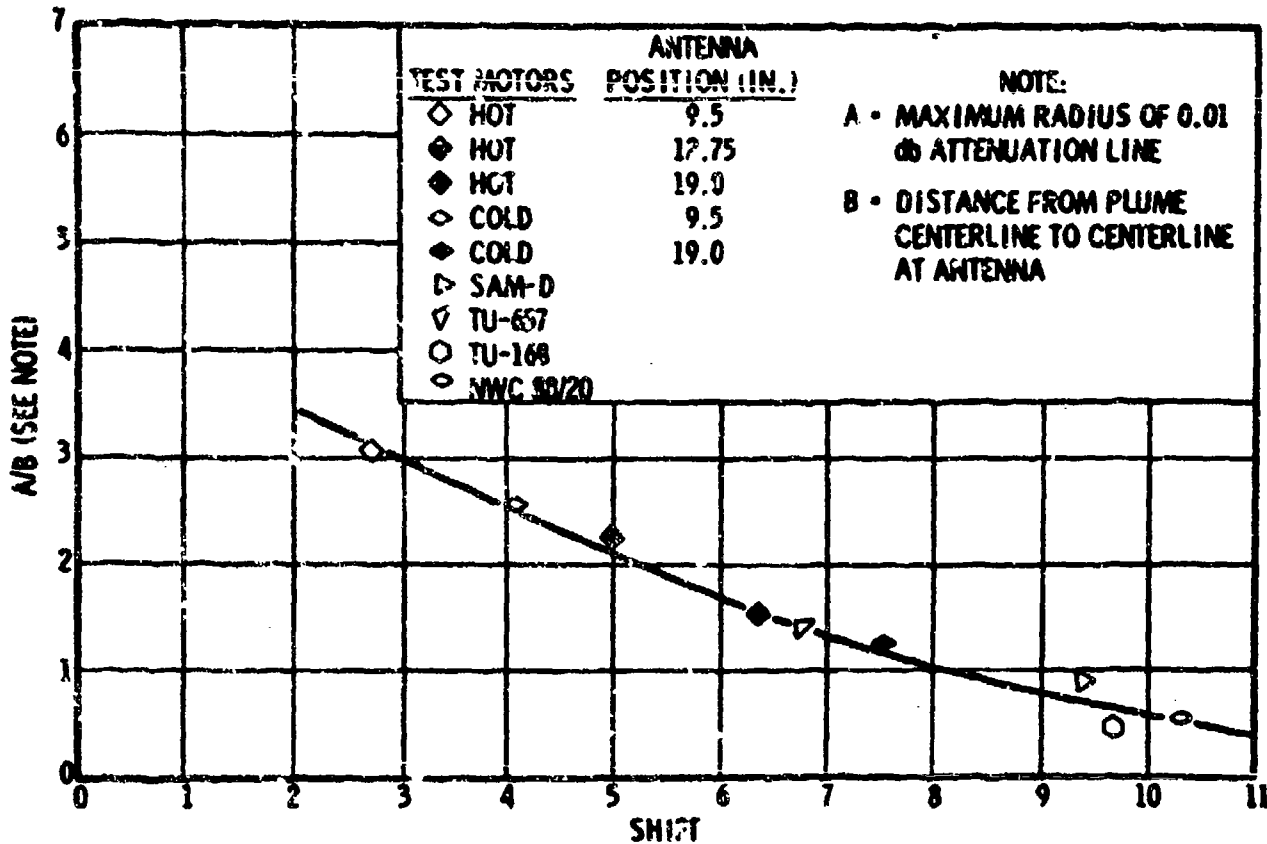


FIGURE 43. Correction Factor (Shift) for Diffraction Prediction Model Modifications by Webb.

NWC TP 5319, Part 1

One additional feature of the diffraction computer programs of Appendix B is the inclusion of a subroutine (FUZZ) which can be used to treat "fuzzy edges" of the plane A (Figure 37) by the technique of Walters and Wai (Ref. 111). Use of FUZZ permits one to linearly vary the opacity of the plume from zero at the edge to infinity at some internal surface. Nonlinear methods are also described in Ref. 111. Although the subroutine is rarely used, it is activated by a variable called "BEEF" which is the half-width of "fuzz" in cm (e.g., the distance between the 0-dB and 3-dB points or between 3-dB and infinite attenuation points). As currently coded, inclusion of BEEF = 0.01 in the B-I program effectively deactivates FUZZ and the subroutine reverts to the standard Fresnel calculation.

Diffraction computer program B-II differs from B-I in that some of the input parameters are derived from the ray trace (refraction) calculations given by program A-II. None of the *fudge factors* associated with B-I are contained in B-II.

3.4 DISPERSION OF FOCUSED MICROWAVE BEAMS IN TRANSVERSE ATTENUATION MEASUREMENTS

Focused microwave radiation is frequently used in radar attenuation studies on rocket exhaust plumes. The focused beam technique does not simulate operational attenuation problems but it does enable an investigator to diagnose the plasma properties of the plume. This in turn can be related to operational problems.

Several experimental arrangements have been used for focused beam diagnostics in which the plume and beam axes are perpendicular. The most complex involve simultaneously moving the beam horizontally and vertically through the horizontal rocket exhaust plume (Ref. 113). Simpler techniques involve moving the beam horizontally through the exhaust while beam and plume axes intersect (Ref. 114) or measuring at a single position in the exhaust, again with intersecting axes (Ref. 115).

The simplest analytical approach to the problem is to assume that all radiation is concentrated in a "line" or ray that intersects the plume. If the path length of the plume (d) and attenuation per unit length (α) can be specified, this calculation yields attenuation (AT) as the product of d and the average value of α , i.e., ($\bar{\alpha}$), or more precisely

$$AT = \int_0^d \alpha(s) ds = \bar{\alpha} d \quad (30)$$

This approach is reasonable if the plume diameter is much greater than the beam diameter.

NWC TP 5319, Part 1

In the second approach, described by Weston (Ref. 113), the beam is assumed to have a finite extent. The focused radiation in space is assumed to follow a Bessel function distribution (Figure 44), which actually resembles the measured spacial distribution. Equation 30 is then integrated over the entire volume of the beam. The plume and beam axes need not intersect. In practice, the problem is treated by summing a large number of rays and allotting to each ray the energy apportioned by the distribution in Figure 44, and the signal loss calculated by Eq. 30. The attenuation coefficient (α) is assumed to be radially invariant. In the work of Hedman and Smoot (Ref. 116), radial variation of α is considered.

In the more sophisticated approach described in Ref. 94, the previous work is expanded to include the effect of the plasma phase shift coefficient on refraction by the plume and on interference phenomena that can affect the signal strength at the receiver. Radial variations of attenuation and phase shift coefficients in a rocket exhaust plume are included.

The interaction of a focused transverse microwave beam with a plume is shown in Figure 45, which shows a beam larger than the plume. The effect of refraction by a homogeneous plume on a single ray is shown in Figure 46. The effects of refraction are to (1) change path length and direction of radiation in the plume and from the plume to the receiver; this changes the calculated signal loss by attenuation and by phase shift, (2) change location of signal in receiver pattern, and (3) shunt some of the refracted radiation out of the receiver main lobe pattern completely.

The details of the refraction calculation can be studied in the computer program listed in Ref. 94. Conceptually, the calculation is very simple. Complexities arise because it is necessary to provide logical decisions for all unusual ray behavior to avoid failure of a computing run.

The general discussion of refraction in Section 3.2 has a bearing on this section. Consider Eq. 27

$$\frac{d(\vec{n})}{d\sigma} = \nabla n \quad (27)$$

For the assumption of radial variation of refractive index, n , ∇n is always in a radial direction from a fixed center. Let \vec{P} be the position vector of a point of the ray referred to the center as origin. Since \vec{P} and ∇n are parallel, the vector product of Eq. 27 by \vec{P} yields

$$\vec{P} \times \frac{d}{d\sigma} (\vec{n}) = 0$$

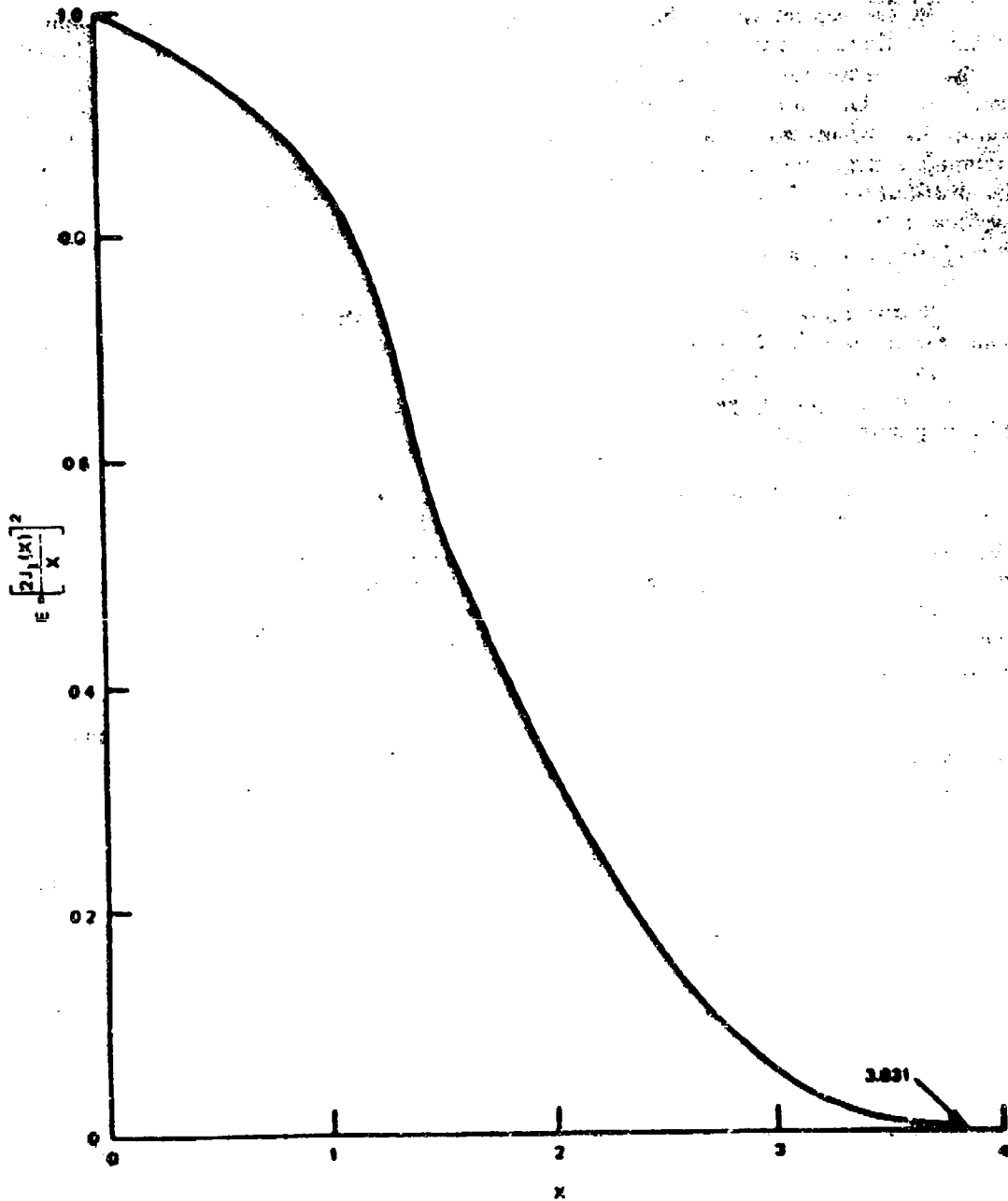


FIGURE 44. Focused Microwave Beam Energy Distribution ($x = 3.831 \tau/R$, see Fig. 45).

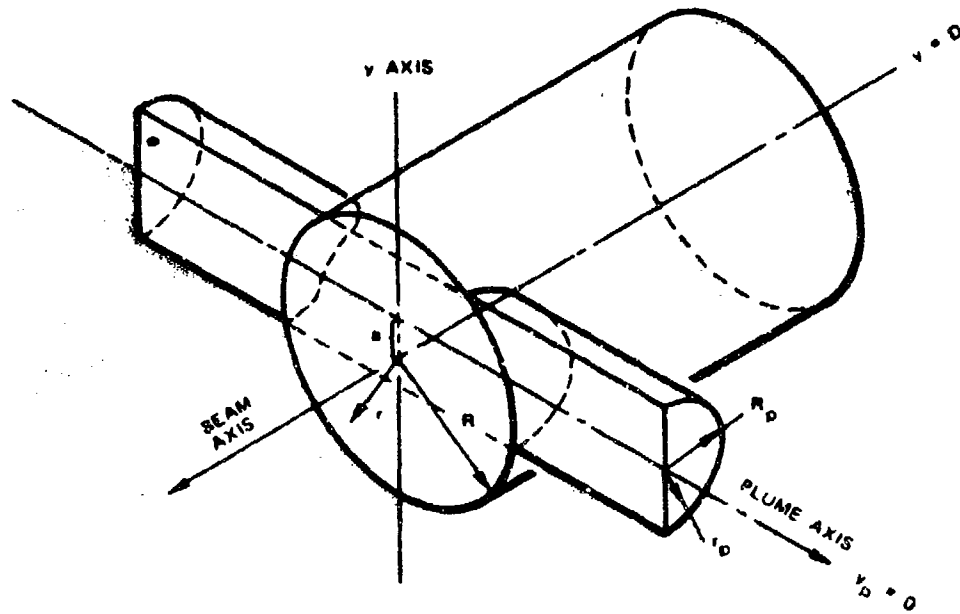


FIGURE 45. Model of the Intersection of the Plume and the Microwave Beam.

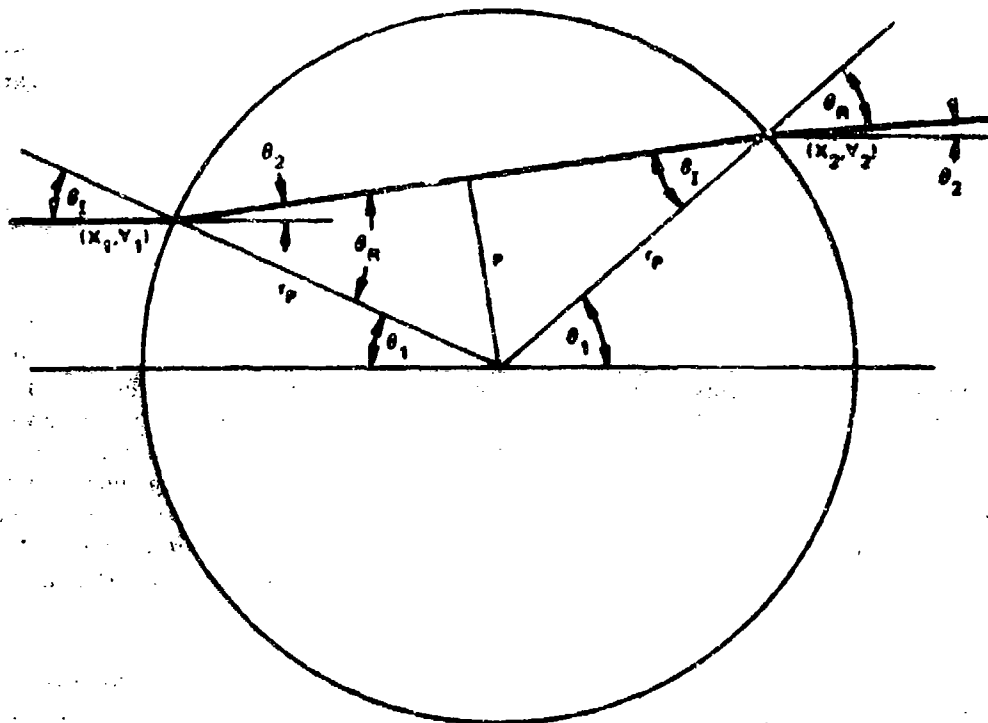


FIGURE 46. Model of Interaction of Ray With Refracting Plasma Cylinder.

Now since

$$\frac{d}{d\sigma} (\bar{P} \times n\bar{t}) = \frac{d\bar{P}}{d\sigma} \times n\bar{t} + \bar{P} \times \frac{d}{d\sigma} (n\bar{t})$$

and $\frac{d\bar{P}}{d\sigma}$ is tangent to the ray and hence parallel to $n\bar{t}$

$$\bar{P} \times \frac{d}{d\sigma} (n\bar{t}) = \frac{d}{d\sigma} (\bar{P} \times n\bar{t})$$

and Eq. 27 becomes

$$\frac{d}{d\sigma} (\bar{P} \times n\bar{t}) = 0$$

and

$$\frac{d}{d\sigma} (|\bar{P}| n \sin \gamma) = 0$$

where γ is the angle between \bar{P} (and hence ∇n) and the direction of the ray, \bar{t} . Thus $|\bar{P}| n \sin \gamma$ is a constant along any ray. This is the generalization of Snell's law to the case of a radially-directed refractive index gradient.

The energy in a focused microwave beam has been reported to vary as a first order Bessel function of the first kind (Eq. 31). This is shown graphically in Figure 44. For an experimental arrangement

$$E = \left[\frac{2J_1(x)}{x} \right]^2 \quad (31)$$

with conical horns, $x = 2\pi r \ell / \lambda$, where r is the radius of a chosen point for which the energy density is to be calculated, ℓ is the ratio of lens radius to lens focal length, and λ is the microwave wavelength. At $x = 3.831$, $E = 0$ and $r = 1.52\lambda$. This defines the radius of the first energy minimum, or the effective beam radius at the region of focus. This first diffraction disc contains 85.9% of the radiated energy. If the receiving antenna has identical characteristics, in the absence of refraction, 99.5% of the received energy comes from the first diffraction disc. Several test cases were calculated with additional discs of the Bessel function. These resulted, even when including refraction, in only slight differences over the first disc calculation. Therefore, for economy and simplicity, only the first diffraction disc has been included in the computer program of Ref. 94.

The model described in Ref. 94 was inspired by an earlier inability to correlate large amounts of attenuation data. At that time, we had hoped to publish recommended values of transverse attenuation (in dB/1,000-lb thrust units) for those propellants

which had been measured. However, when the data were examined from firings on diverse thrust levels, it was found that when reduced to the common units, the smaller motors of identical propellant generally gave higher attenuation values. Theoretical line-of-sight predictive techniques, when adjusted to duplicate measured attenuation for high thrust levels, would predict values too low at lower thrusts.

The study described in Ref. 94 was intended to develop a tool which would remedy such discrepancies. As indicated in Figure 47, it appears that this goal was achieved. Figure 47 compares experimental transverse attenuation data from firings of three motor sizes containing identical propellant (Ref. 117), with the results of the model developed in Ref. 94. The refraction model agrees with the data far better than the simpler attenuation model. In using the model, a beam radius of 0.05 meter and beam focal length of 1.0 meter were assumed. The plume parameters were obtained from Ref. 118 and are shown in Table 6.

The results of additional calculations given in Ref. 94 indicate that phase shift interference does not appear to be important to received power calculations for most rocket plumes, although the literature indicates that there are plasma regions ($n_e > 10^{12}/\text{cm}^3$) in which it must be considered (Ref. 119). This refraction model indicates why scaling laws, which fail to account for refraction (beam spreading), are unable to correlate the extensive data on focused transverse plume RF attenuation.

3.5 PULSE DISTORTION BY A ROCKET EXHAUST PLUME

A rocket exhaust degrades a microwave beam that passes near or through it. A continuous wave passing through an exhaust will suffer attenuation, a phase shift and will be amplitude- and phase-modulated. A pulsed wave form will be further degraded because the plume is a dispersive medium and will effect each of the spectral components of the pulse differently. This distortion causes the pulses to smear into each other, giving the possibility that a space may be interpreted as a mark or vice versa (Ref. 120). If this happens, the error rates may increase in the received signal and thus degrade the information being transmitted (Ref. 120).

For this analysis, the exhaust plume is considered "loss-less" with the only degradation due to the non-linear phase distortion.

Pulse distortion by a plasma is generally treated by Elliott's method (Ref. 120-123). Elliott's parameter:

$$a = 2/(\pi\sqrt{\pi c}) \cdot \frac{1}{f^{3/2}} \sqrt{\int_{S_1}^{S_2} \frac{f_p^2}{n^3} dS} \quad (32)$$

is related to distortion of a pulse form as shown in Figure 48.

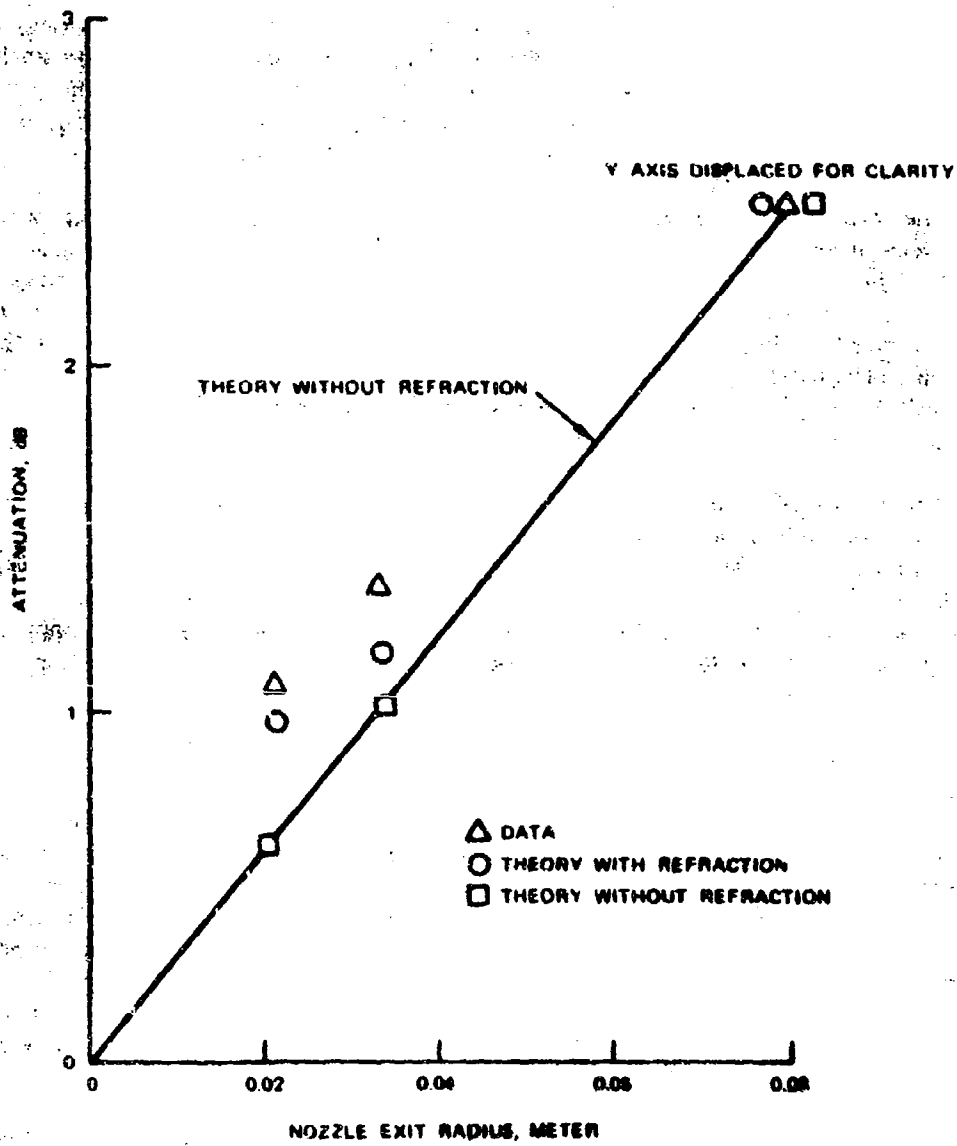


FIGURE 47. Comparison of Attenuation Data With Theoretical Results Both With and Without Refraction. Calculations are for conditions of Table 6.

NWC TP 5319, Part 1

TABLE 6. Plume Parameters for Comparison with Experiment.^a

Plume contour no.	Relative contour radius	Contour radii for plume A, meter ^b	Contour radii for plume B, meter ^b	Contour radii for plume C, meter ^b	Electron density, N _e ^c cm ⁻³
1	1.0	0.035	0.055	0.128	1.3 (10)
2	0.85	0.03	0.047	0.109	2.6 (10)
3	0.76	0.027	0.042	0.097	5.2 (10)
4	0.7	0.024	0.038	0.090	6.5 (10)
5	0.6	0.021	0.033	0.077	7.8 (10)
6	0.42	0.015	0.023	0.054	7.8 (10)
7	0.3	0.01	0.016	0.038	6.5 (10)
8	0.15	0.005	0.008	0.019	5.2 (10)

Note: Numbers in parentheses represent exponents of 10, i.e., (10) = (10¹⁰). Results of calculations are compared with data in Figure 47.

^a 9.5 GHz radiation frequency assumed with 1-meter focal length and 0.05-meter beam radius.

^b Corresponding exit radii (Figure 47) for the three plumes are: A = 0.02 meter, B = 0.035 meter, and C = 0.078 meter.

^c Collision frequency = 2.5×10^{11} sec⁻¹.

NWC TP 5319, Part 1

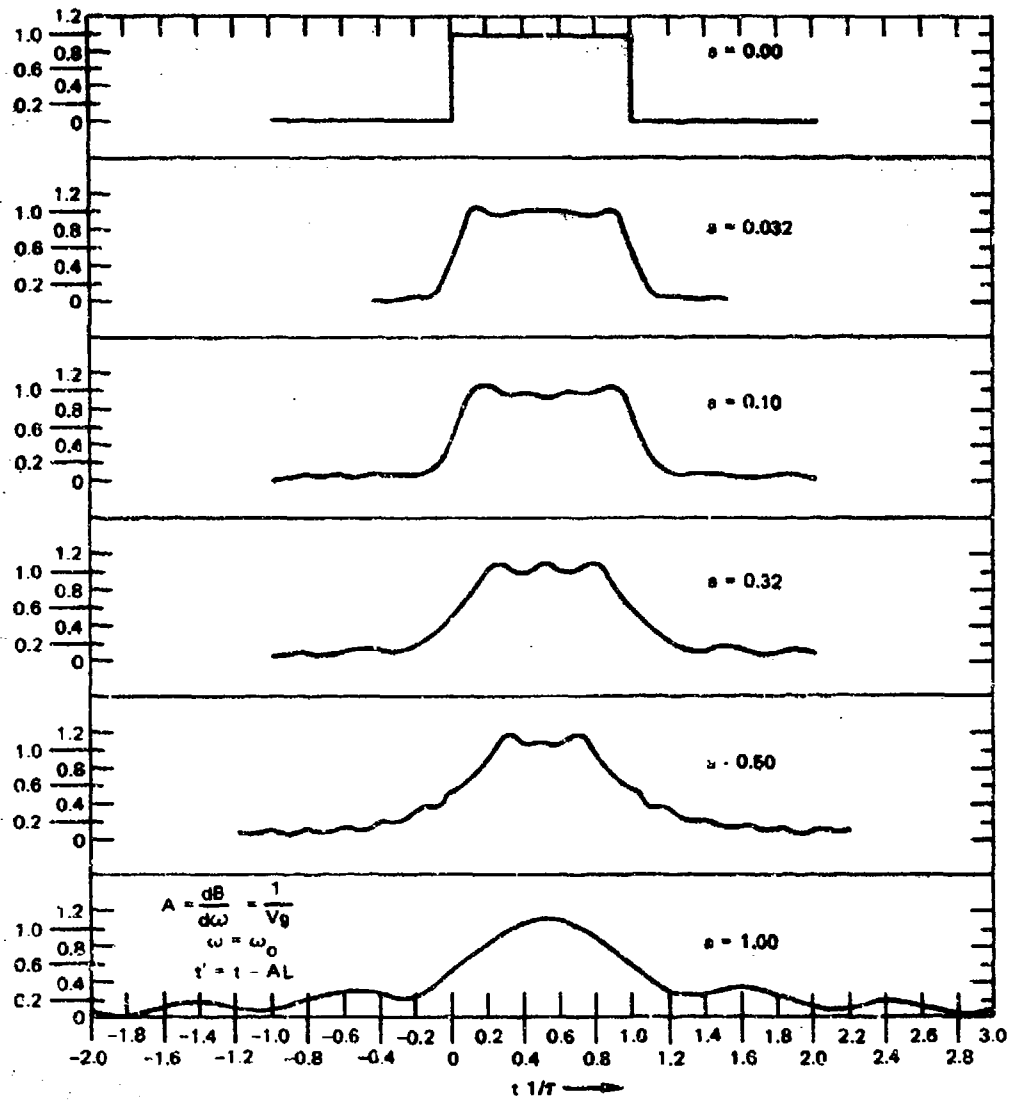


FIGURE 48. Pulse Shape Distortion Due to Dispersion in a Rocket Exhaust.

NWC TP 5319, Part 1

Breil (Ref. 123) has prepared a simple computer program for calculating pulse distortion by a rocket exhaust plume. Communications experts warn that values of "a" as low as 0.1 can indicate a serious level of communication pulse distortion. Breil has shown that for conditions at which equation 19 applies (Ref. 124), Elliott's parameter can be rewritten as:

$$a = \frac{0.088}{Tf^{3/2}} \left[\nu \left(\frac{\omega^2 + \nu^2}{\nu^2} \right) A \right]^{1/2} \quad (33)$$

In these equations the variables are defined as follows:

- T = pulse duration, sec
- c = speed of light, cm/sec
- n = index of refraction of plasma
- f = carrier frequency, Hz
- f_p = plasma frequency = $56,000\sqrt{n_e}$
- n_e = electron density, cm^{-3}
- ν = electron collision frequency, sec^{-1}
- $\omega = 2\pi f$
- A = attenuation over the path $S_2 - S_1$, db

For a numerical calculation of Elliott's parameter, consider an exhaust plume with the following parameters:

- $\nu = 1.9 \times 10^{11} \text{ sec}^{-1}$
- $\omega_p = 2.6 \times 10^{10} \text{ radian/sec}$
- $\omega = 2\pi f = 6.28 \times 10^{10} \text{ radian/sec}$
- $n_e = 2.15 \times 10^{11} \text{ electron/cm}^3$
- $T = 1 \times 10^{-9} \text{ sec} = 0.001 \text{ } \mu\text{sec}$
- attenuation (predicted) = 50 dB

$$a = \frac{0.088}{1 \times 10^{-9} \sqrt{10^{10}}^3} \left[1.9 \times 10^{11} \frac{(6.28 \times 10^{10})^2 + (1.9 \times 10^{11})^2}{(1.9 \times 10^{11})^2} 50 \right]^{1/2}$$

$$a = 0.29$$

This large value for "a" may have a serious effect on the quality of the information being transmitted, depending on the specific modulation scheme employed (Ref. 120).

The above analysis is only strictly valid for the underdense plume where $\omega_p/\omega > \omega$. A more general formulation of the problem is needed to determine the pulse distortion for an overdense exhaust plume. Given a value of "A", the following computer program predicts the resulting waveform.

NWC TP 5319, Part 1

Computer Program to Predict the Pulse Shape Given A (Elliott's Parameter).

```

10 READ, A
11 PRINT, A
20 XX = 0
21 14 CONTINUE
30 Y1 = ERFF((XX + 1)/A)
40 Y2 = ERFF((XX - 1)/A)
50 CALL FRENEL(((XX + 1)/A) +2, C1, S1)
60 CALL FRENEL(((XX - 1)/A) +2, C2, S2)
70 PULSE = .5*SQRT((Y1 - Y2) +2 + (C1 - S1 - C2 + S2) +2)
71 XX2 = XX/2
72 PRINT 21, PULSE, XX2
80 XX = XX + .1
90 IF(XX - 2.1)14, 14, 15
92 21 FORMAT(2F20.5)
100 15 END
170 FUNCTION ERFF(Y)
180 DIMENSION A(7)
190 A(1) = 1.
191 A(2) = 70.5230784E - 3
192 A(3) = 42.2820123E - 3
193 A(4) = 9.2705272E - 3
194 A(5) = 1.520143E - 4
195 A(6) = 2.765672E - 4
196 A(7) = 4.30638E - 5
210 YY = ABS(Y)
220 IF(YY - 6.0) 1, 10, 10
230 10 ERFF = 1.
240 GO TO 2
250 1 IF(YY - .00001) 12, 12, 6
260 12ERFF = 2.*YY/1.7725
270 GO TO2
280 6 SDFO = 0.
290 DO $ I = 1, 7
300 5 SDFQ = SDFO + (A(I)) * (YY**(I - 1))
310 ERFF = - (SDFQ**(- 16) - 1.)
320 2 ERFF = SIGN(ERFF, Y)
321 ZZ = ERFF
330 RETURN
340 END
600 SUBROUTINE FRENEL (X, C, S)
610 SV = X
620 X = ABS(X)
630 F = (1. + .926*X)/(2. + 1.792*X + 3.104*X+2)
640 G = 1./(2. + 4.142*X + 3.492*X+2 + 6.67*X+3)
650 U = 3.14159*X+2/2.
660 C = .5 + F*SIN(U) - G*COS(U)
670 S = .5 - F*COS(U) - G*SIN(U)
680 IF(SV) 3, 4, 4
690 3 C = - C
700 4 S = - S
710 4 RETURN
720 END
READY

```

4.0 PLUME-RF ATTENUATION DATA SUMMARY

Large amounts of radar attenuation data for a variety of rocket motor plumes have been generated over the past decade. Table 7 outlines the major variables which have been studied in the tests.

TABLE 7. Variables in Plume-RF Attenuation Tests.

-
- A. Test Characteristics
1. Microwave (RF) equipment
 - a. Focused beam (curved or Fresnel lenses)
 - b. Unfocused beam (standard open antennas)
 - c. Single- or multiple-frequency
 2. Orientation of test
 3. Dynamics of tests
 - a. Static
 - (1) Sea level
 - (2) Simulated altitude
 - (3) Inert atmosphere effects (e.g., N₂ shroud)
 - (4) Special effects (e.g., flameholders, torch, air injection)
 - b. Dynamic (flowing free stream)
 - (1) Wind tunnel simulation
 - (2) Flight test
 - (3) Inferences from flight data on missile evaluation tests
- B. Motor Characteristics
1. Chamber pressure
 2. Expansion ratio
 3. Propellant composition
 - a. Solids level
 - b. Aluminum level
 - c. Alkali metal impurity level
 - d. Suppressant additives
 4. Thrust level
-

The following paragraphs generalize about the variables listed in Table 7.

Test Characteristics

1. Microwave (RF) Equipment. Focused beams are generally limited to short path lengths between antennas and hence to transverse orientations (with a few exceptions). It is very important that the beam diameter be considerably

NWC TP 5319, Part 1

smaller than the plume or complicated analysis will be required to extract meaningful data from the tests (Section 3.4).

Unfocused beams do not give easily analyzable data except for those cases where plume-RF interactions are so weak that line-of-sight approximations can be applied. Unfocused beams are generally used for diagonal tests.

Multiple frequency tests have the advantage that electron density and electron collision frequency can both be inferred directly from measurements and further that any inconsistencies due to beam size can usually be spotted.

2. Orientation of Test. Although the diagonal orientation (RF "beam" at an oblique angle to the plume axis) simulates missile in-flight system geometry, it is generally used only for static tests (or naturally for flight tests). Since in this static case no other test variables, other than orientation, actually resemble an operating missile system, the diagonal orientation is only useful to evaluate electromagnetic interaction models for already well characterized plumes.

Transverse tests with focused beams provide a diagnostic tool for evaluating predictions of electron density distribution. Transverse measurements can be made for all dynamic situations (except flight test); however, it is usually impossible to traverse (longitudinal travel) a sufficient length of plume in a wind tunnel flight simulation. Transverse measurements have also been made while moving the plume in a second dimension, normal to the beam axis, to measure attenuation off the plume axis; very fine collimation of the RF beam is required for sensible results in such measurements.

3. Dynamics of Tests. Attenuation measurements on static plumes have been used to evaluate the simplest plume models. After verification of transverse predictions, a comparison of diagonal measurements and predictions can be used to evaluate diagonal interaction models. The plumes of missiles in flight are so different from static plumes that a static test really may not provide much information about the attenuation properties of an in-flight plume. Special static tests have explored the use of flameholders (Ref. 125, 126, 127, and 128) to cause increased plume afterburning, but the results did not fully simulate the more dramatic effects noted in flight plumes. Early tests to demonstrate the importance of afterburning with air were performed in which static plumes exhausted into inert atmospheres or were shrouded with nitrogen (Ref. 129). Tests at reduced ambient pressure (simulated altitude) have shown differences from static sea level results (generally higher attenuation at reduced pressures), but it is not known how much was a pressure effect, and how much the result of inadequately focused beams. Theory does predict rate-dependent chemical effects at reduced plume pressure which result in increased electron density.

Dynamic plume tests, with a co-flowing free stream, provide the closest simulation of an in-flight missile. Wind tunnel restrict the placement of the antenna and can cause undesirable shock reflection effects. The best measurements are limited to transverse focused-beam attenuation studies of electron density distribution. Only in actual flight tests can one obtain all the variables and then it can be very difficult to monitor them sufficiently well to obtain useful signal loss data.

Motor Characteristics

Motor characteristics have been shown to have a significant effect on attenuation measured in tests of all the types described above. The type of propellant can strongly affect the pattern of afterburning in the plume and hence the attenuation. Attenuation increases with increasing aluminum level for all propellant classes. For rubber-base composite propellants, increasing the solids (oxidizer) level seems generally to decrease attenuation. For all propellants, attenuation increases approximately as the square root of the concentration of potassium or sodium impurities, and approximately as the square root of thrust level. Increasing chamber pressure seems to decrease attenuation. Underexpanded exhaust plumes have a pronounced shock structure which can cause high attenuation levels near the nozzle exit. When these act as ignition sites for afterburning, plume attenuation may increase significantly with decreasing expansion ratio. Overexpansion does not appear to significantly alter the attenuation observed for optimum expansion conditions.

4.1 STATIC TRANSVERSE ATTENUATION DATA

The Thiokol Chemical Company IR&D programs sponsored an extensive review of transverse attenuation data obtained from static motor firings. These data are presented in Appendix C in more detail than has been previously published in Ref. 61 and 130. The Lockheed Propulsion Company summarized their radar attenuation data obtained between 1963 and 1969 in Ref. 131. Pertinent data come from sources more numerous than we could review completely. Whenever possible, prior reviews have been used.

Some measured effects of simulated altitude and motor scale on transverse attenuation are shown in Figure 49. The data were scaled by dividing both attenuation and distance from the nozzle exit by the square root of motor thrust. Although this is not a perfect scaling law, it does describe the relationship inherent in equilibrium plume models. Discrepancies could easily be due to experimental uncertainties; too large microwave beams for the smaller motor plumes or an inadequate scaling concept. Seen in this light, the agreement is remarkably good, since in every case peak attenuation is within a factor of two, and locations of attenuation peaks are within reasonable agreement. (See Ref. 130 for comparison parameters.)

NWC TP 5319, Part 1

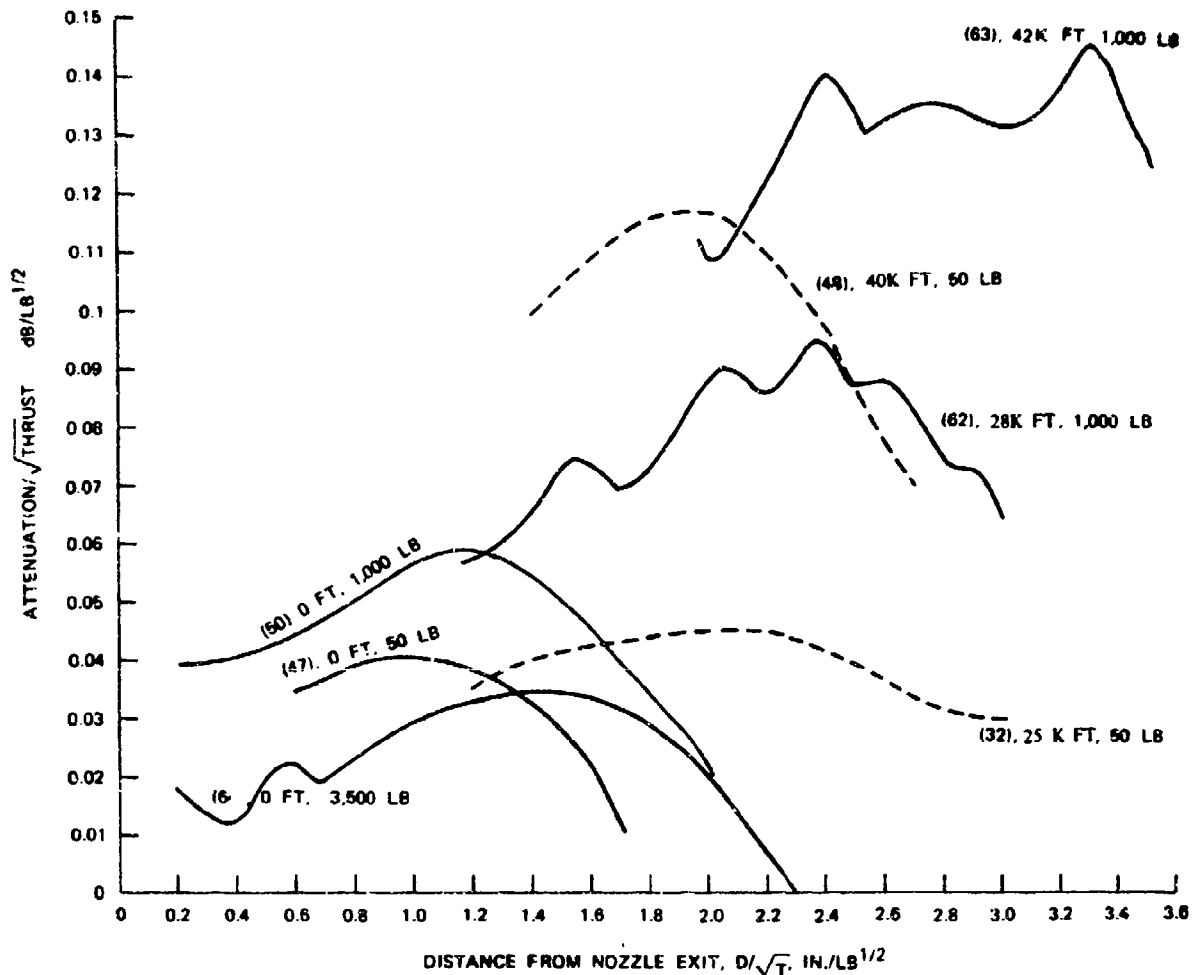


FIGURE 49. X-Band Transverse Attenuation Data for Static Plumes of 88/12 Composite Propellant Scaled by $(\text{Thrust})^{1/2}$. Numbers in parentheses indicate data source in Appendix C; numbers following represent test altitude in thousands of feet and motor thrust in pounds.

Many additional simulated altitude measurements have been made at the Naval Research Laboratory (NRL) (Ref. 132). Although most of these remain unpublished, some can be traced reasonably well through the JANNAF Radar Attenuation, Plume-Signal Interference, and Plume Technology Meeting Bulletins (Ref. 13 through 15, 18, 21, and 22 of Ref. 1). These simulated altitude studies attempted to determine which propellants would produce serious attenuation in flight by looking at the effect of external static pressure alone. In a gross way, the technique seems to work since "bad actors" spotted in reduced pressure tests (but not in sea level tests) did in fact give serious flight attenuation. The technique is less useful for determining the altitude sensitivity of in-flight attenuation because so many other effects influence the plume in flight.

NWC TP 5319, Part 1

Breil and Victor (Ref. 125) attempted to reproduce worst-case flight attenuation effects by inserting flameholders into the plume within 6 inches of the nozzle exit. ATJ graphite flameholders, backed by stainless steel, failed before attenuation data could be obtained (except in the case of Propellant "C") because of the severe oxidizing and corrosive conditions. Later repetition of the tests with cylindrical tungsten flameholders gave the data shown in Figure 50. It was hoped that flow stagnation behind the flameholders would create conditions similar to base recirculation and combustion induced in flight and simulated flight tests on some propellants. There is a resemblance between 88/12 flameholder data (Figure 50) and simulated flight data (Figure 51) (also see Section 4.3). For ELP and Propellant C the flameholder tests failed to reproduce the very large increases in attenuation observed in both simulated and actual flight. It should be noted that tungsten has been demonstrated to be an effective electron suppressing additive and eroded tungsten may have reduced attenuation in the flameholder tests.

There is no evidence that composite propellants experience very large attenuation increases at flight conditions. Although it has been shown that reduced atmospheric pressure increases attenuation (Figure 49), the addition of free stream velocity has countered this increase in all known tests (compare Figures 49, 51, 52, and 53). The only reasonable explanation for this behavior is that the exhaust gases of composite propellants are already so hot that complete afterburning of the gases occurs in the atmosphere without the addition of extra heat from base recirculation or shock stagnation. If this is the case, the failure of the flameholder tests to cause large attenuation increases, except directly downstream of the flameholder, is understandable. However, the absence of a significant effect with ELP and Propellant C is contrary to both flight and simulated flight data.

4.2 STATIC DIAGONAL ATTENUATION DATA

There are fewer data from diagonal attenuation measurements than from transverse. Primary reasons are the additional space and instrumentation required for diagonal measurements. Because of the complexities of diagonal RF propagation through and near an exhaust plume, diagonal attenuation measurements do not give much information about plume electron density or collision frequency distributions. Furthermore, since plume properties can vary drastically with flight conditions, the diagonal data obtained in static tests may have little relation to flight data obtained with the same measurement geometry.

The value of static diagonal measurements lies in their use to confirm diagonal prediction models. The following logical steps are involved:

1. Static transverse attenuation data are used to confirm the static plume model.
2. Dynamic (wind tunnel) transverse attenuation data are used to confirm the in-flight plume model.

NWC TP 5319, Part 1

$$P = \frac{\text{PEAK ATTEN. (FB)}}{\text{PEAK ATTEN. (OPT)}}$$

$$A = \frac{\int \text{ATTEN. (FB)}}{\int \text{ATTEN. (OPT)}}$$

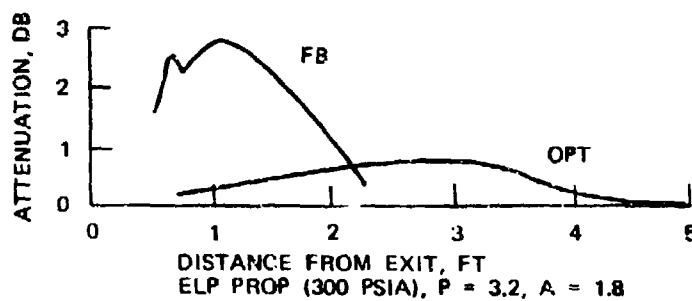
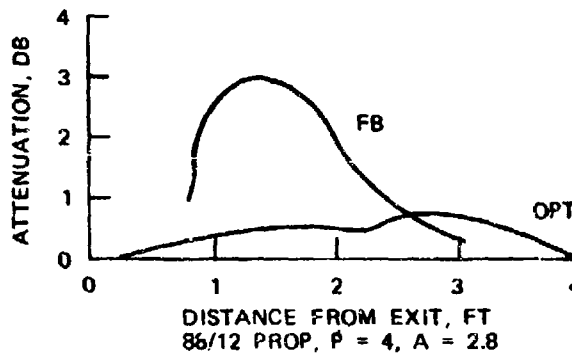
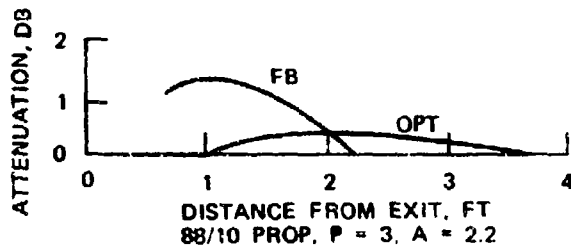


FIGURE 50. Effect of Flameholders on Plume K-Band (35 GHz) Attenuation.

NWC TP 5319, Part 1

$$P = \frac{\text{PEAK ATTEN. (FB)}}{\text{PEAK ATTEN. (OPT)}}$$

$$A = \frac{\int \text{ATTEN. (FB)}}{\int \text{ATTEN. (OPT)}}$$

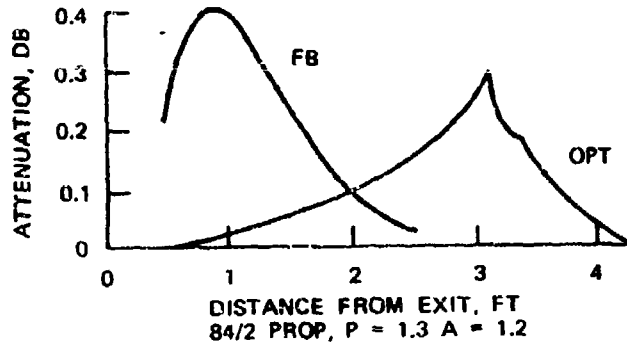
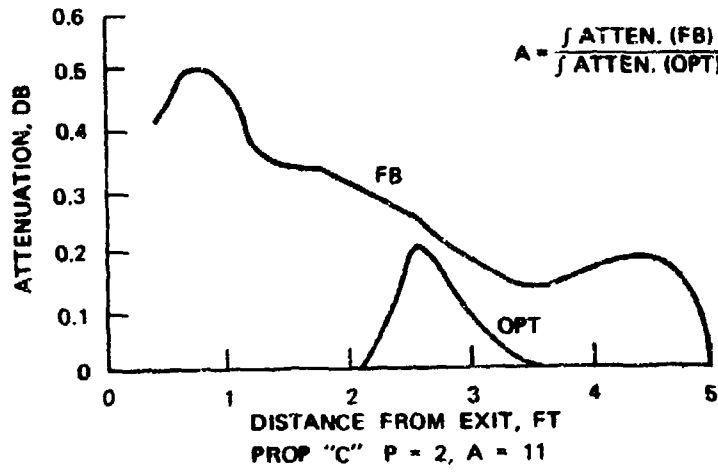


FIGURE 50. (Contd.)

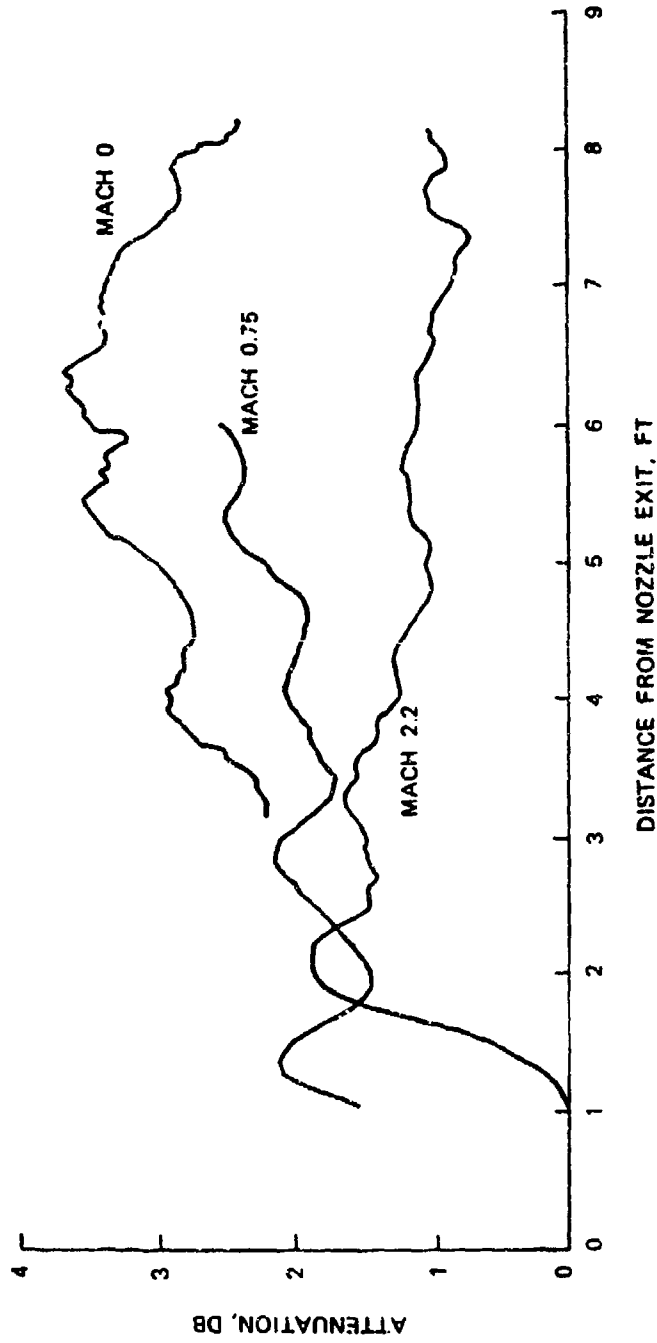


FIGURE 51. Simulated Flight Data, 88/12 Propellant, 28,000-Ft Simulated Altitude Effect on Mach Number on Attenuation, X-Band (Ref. 146, OAL).

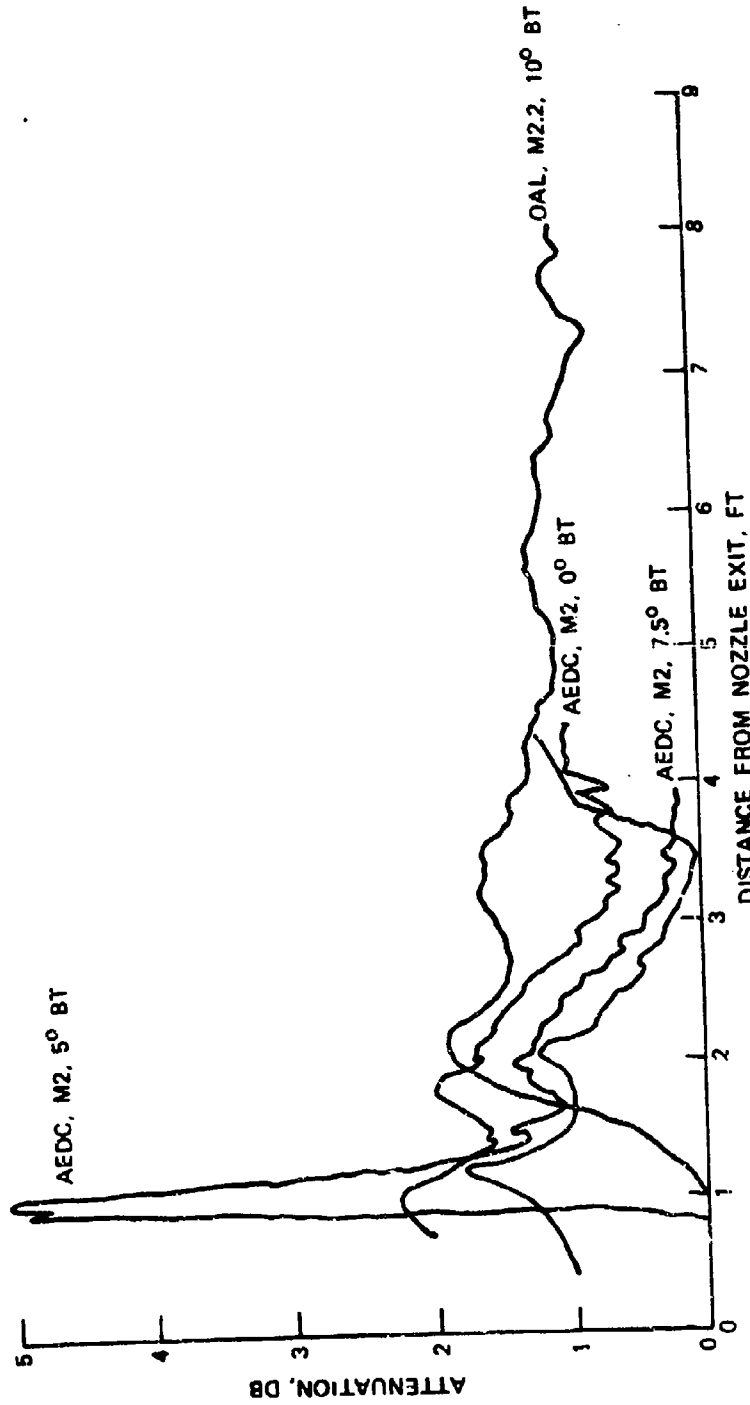


FIGURE 52. Simulated Flight Data, 88/12 Propellant, 28,000 to 30,000-Ft Simulated Altitude, Effect of Boat-Tail and Facility (OAL - X-Band; AEDC - K-Band) (Ref. 146, 147).

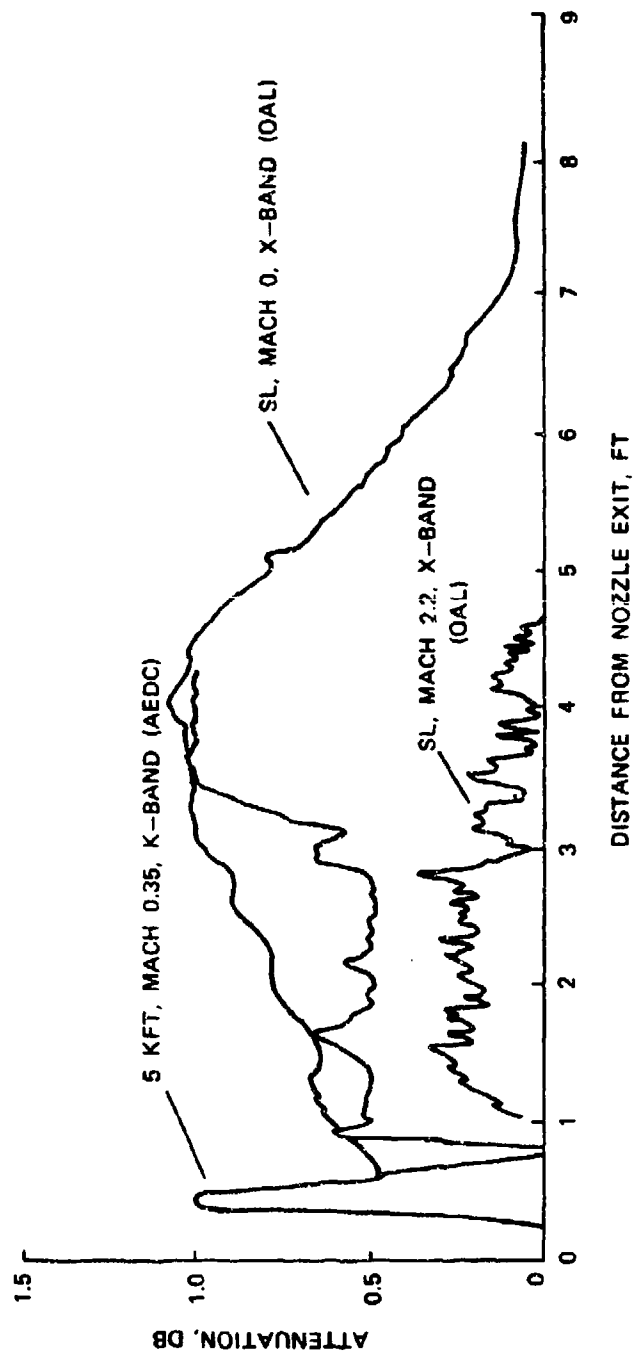


FIGURE 53. Simulated Flight Data, 88/12 Propellant, Low Altitude, Effect of Velocity (Ref. 146, 147).

3. Static diagonal attenuation data are used to confirm the diagonal propagation model for the already confirmed static plume.
4. The diagonal propagation model is used to extrapolate the dynamic model to a flight situation.

Static diagonal data are valuable only from this analytical standpoint, and then only if enough data are obtained to characterize the plume over a wide range of aspect angles. Ideally, the motor should be rotated in the RF field so that a continuous variation of attenuation with angle can be measured. Good measurements have also been obtained with multiple receiving antennas spaced at angles in the field. However, data from continuous angle measurements show that the use of multiple receiving antennas is likely to greatly decrease the value of a measurement since so much information, valuable for assessment of propagation models, will be missing.

Although diagonal attenuation data have been reported numerous times, the only attempt at a consistent study is described in Ref. 133.

The data in Figure 54 show the effect of varying propellant composition on diagonal attenuation for one antenna orientation. The motors were rotated during firing so that a continuous trace of attenuation versus aspect angle was obtained. Figure 27 compared peak values of diagonal and transverse attenuation for a number of motor firings.

The relationship for the straight line in Figure 27 is given by the equation.

$$\log D = 0.517 \log T + 0.363 \quad (32)$$

where

D = peak diagonal attenuation, dB
 T = peak transverse attenuation

It would be unwise to attach too much significance to Eq. 32; it is only an empirical relationship which has been derived from data on fairly small motors.

Additional diagonal attenuation data were shown in Figures 34 and 42 (Section 3.3) where they are compared with calculated values.

The results of extensive measurements of transverse and diagonal attenuation of the composite modified double base (CMDDB) Propellant ELP are shown in Figure 55. This propellant and the Propellant FDS are discussed further in the following sections.

Measured diffraction by an aluminum cylinder (similar in size to an exhaust plume) was compared with diagonal attenuation data in Figure 35. On the basis of that comparison, it seems safe to say that such diffraction by a "perfect conductor" sets an upper limit to diagonal attenuation. This could be a useful relationship for estimating in-flight attenuation.

NWC TP 5319, Part 1

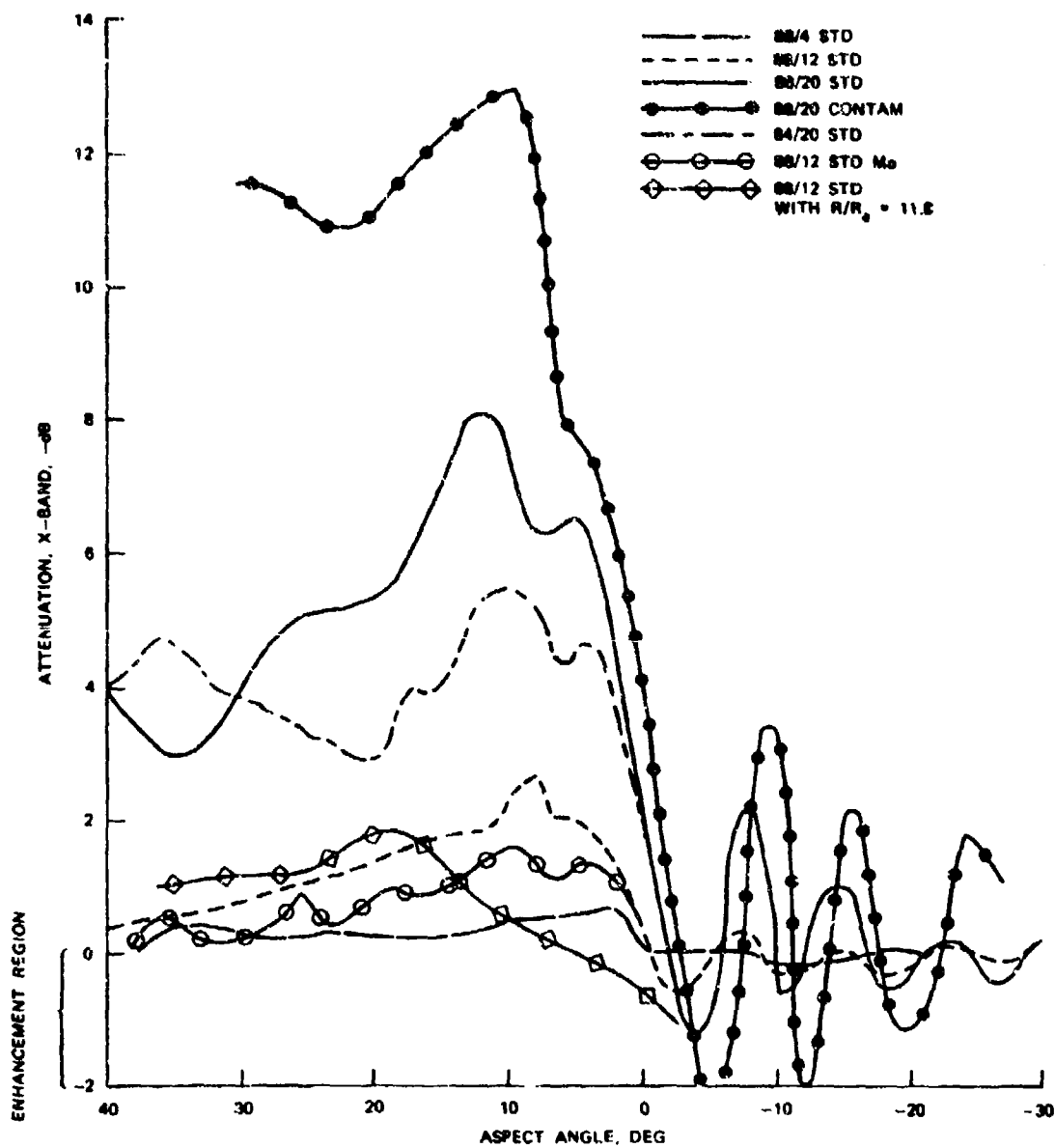
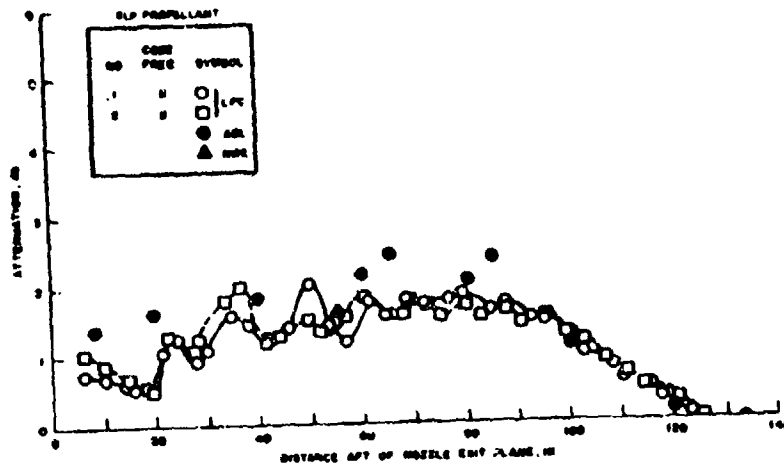
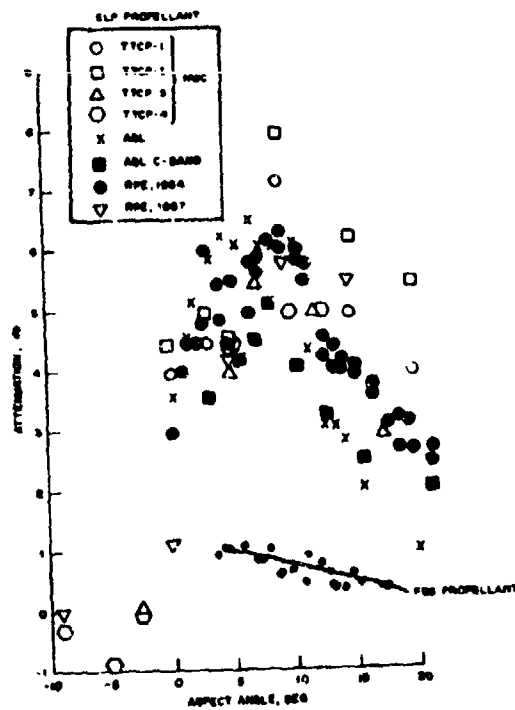


FIGURE 54. Composite Propellant Sea-Level Static Firing Diagonal X-Band Attenuation Data for 1,000-Pound-Thrust Motors With Transmitting Antenna at Exit Plane 5 Exit Radii from Nozzle Centerline ($R/R_e = 5$) (Ref. 000).

NWC TP 5319, Part 1



(a) Transverse Attenuation



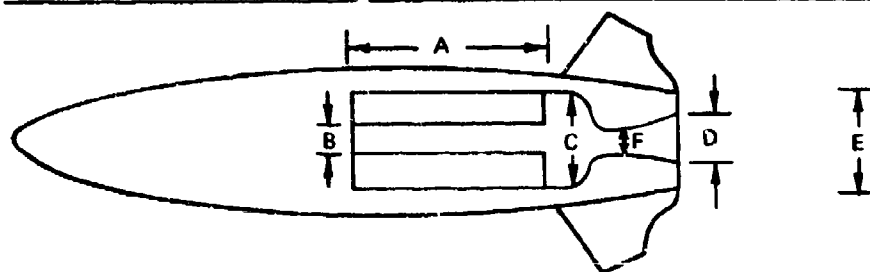
(b) Diagonal Attenuation

FIGURE 55. Transverse and Diagonal Attenuation Data on ELP Propellant and Diagonal Data for Propellant FDS.

4.3 DYNAMIC TRANSVERSE ATTENUATION DATA

The Navy has sponsored five major studies of plume attenuation with wind tunnel simulation of the free stream (Ref. 134, 135, 136, 14, 126, and 137). The Air Force co-sponsored the study of Ref. 136. In all cases, the goal was to obtain information to assist in developing or evaluating in-flight plume attenuation models. None of the studies was conclusive, in that flaws in planning or execution created effects with unknown influences on the data. The first tests (dimensions in Table 8) were limited mostly to the Propellant ELP, an Al-Mg containing composite modified

TABLE 8. Dimensions of Components for Figures 56 and 57.



Dimension	OPC, in.	TPC, in.	FPC, in.
A	4.5	7.5	15.0
B	1.5	1.8	4.8
C	2.5	4.5	8.4
D	1.655	2.628	5.476
E	4.954	7.868	11.72
F	0.712	1.132	2.355
Base ratios (D/E)			
	OPC/OPC ^a	0.334	
	OPC/TPC	0.210	
	TPC/TPC	0.334	
	TPC/FPC	0.224	
	FPC/FPC	0.467	

Note: All boat tails were angled at 3.88 degrees, all $\epsilon = 5.404$, all $P_c \sim 250$ psia.

^a The designation OPC/TPC refers to an OPC motor (ABCDF) in a TPC missile (E), etc.

NWC TP 5319, Part 1

double base (C MDB) propellant, which is not typical of present high-energy solid-rocket propellants. The studies of Ref. 135 and 136 utilized composite solid propellants with 12 or 20% aluminum (some containing molybdenum or MoO_3 additive for attenuation suppression).

The study of Ref. 14 used concentric air and rocket nozzles and 87/10 composite propellant (see Ref. 134). The rocket nozzle was contoured to minimize the effect of shocks and base mixing which have major effects on in-flight attenuation. This was intended to make possible reasonable comparisons with the many plume-mixing models which ignore shock structure and base recirculation. Unfortunately, the beam width (X-band) appears to have been too large for the plume and the meaning of the data may be ambiguous. Beam width corrections applied to the data brought reasonable agreement with calculated values. Some of the data from Ref. 14 were compared with theory in Figure 26.

The fifth test series demonstrated base-induced afterburning quite strikingly for several propellants in small rocket motors.

From the dynamic test data available on the first three test series, selected excerpts are presented in Figures 51 through 53 and 56 through 59. It would be nice if one could discern certain trends from these figures which would permit easy extrapolation of static data to flight, or from one flight condition to another. Unfortunately, the differences in behavior of the two propellants shown seem to be qualitative, thus obviating analogies between them. For the 88/12 composite propellant, the two sets of independently obtained data are so dissimilar that comparisons of numerical values tell us nothing. We do know that the normal shock is the major effect seen in the AEDC data and that any significant afterburning (if it occurred) was downstream of the observed positions in the plume.

The Ordnance Aerophysics Laboratory (OAL) data on ELP propellant show some interesting behavior (Figures 56 and 57). The attenuation increases with altitude for all data at a given velocity. Varying the base ratio has a significant effect on attenuation. The only "strange" datum is that for the TPC/FPC motor/"missile body" pair. Offhand one would expect this largest base/nozzle ratio to give attenuation values about two or three times the OPC/TPC pair. The actual measured values are comparable to the OPC/OPC data. The implications of this would seem to be that the base effect is more complicated than one of base ratio alone, and probably involves scale as well. There is also the unhappy possibility that the larger FPC system created "scale" effects in the wind tunnel which completely hid the plume/flow effects being sought.

Therefore, the best one can do for predicting flight plume effects is to use models to match dynamic data which seem most consistent and extrapolate to the flight case.

* A SEA LEVEL STATIC FIRING (K-BAND) FOR THE SAME SIZE MOTOR IS INCLUDED FOR COMPARISON.

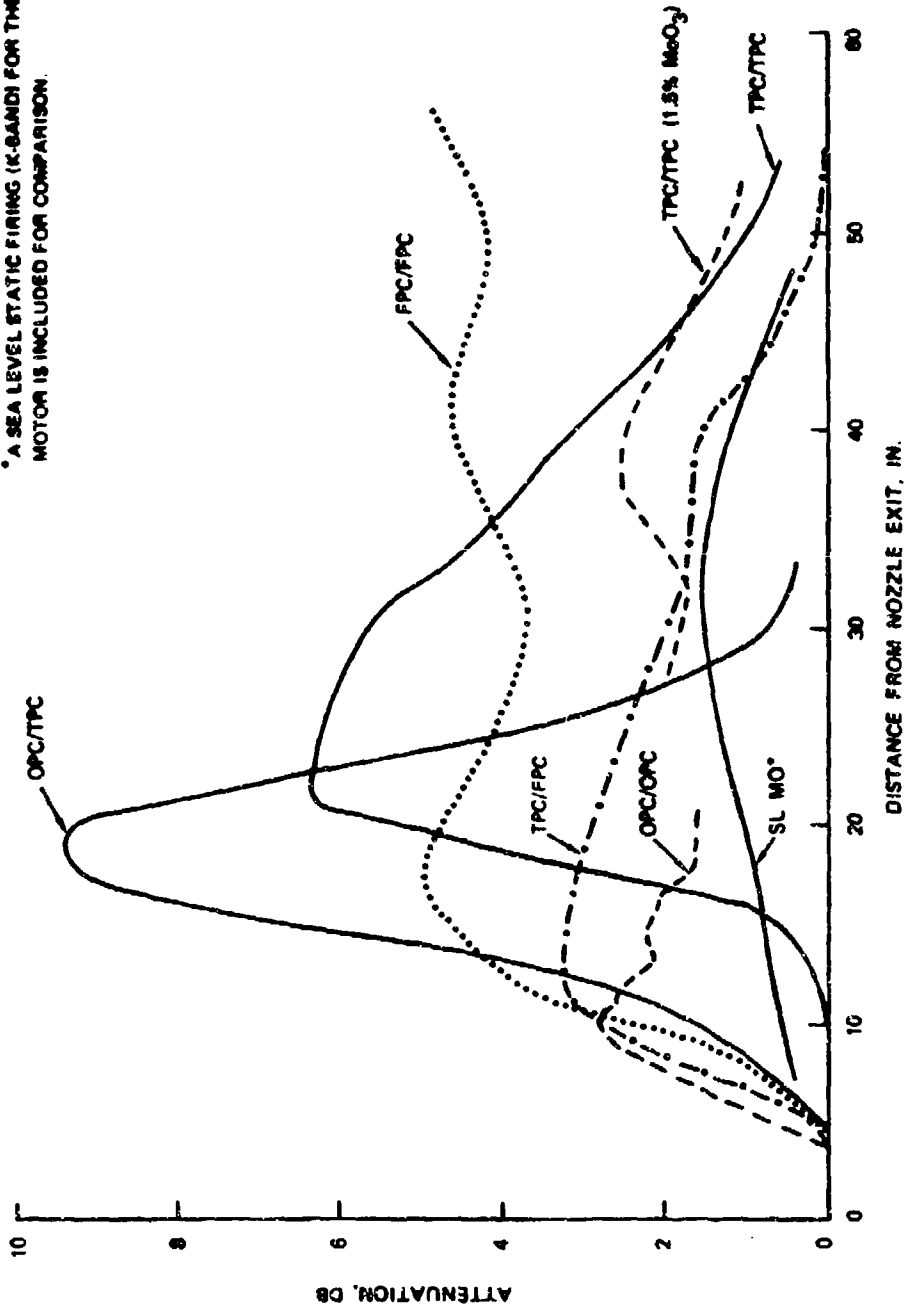


FIGURE 56. Simulated Flight Data, ELP Propellant, 28,000-Ft Simulated Altitude, Mach 2.2, X-Band. Effect of varying motor and "missile" size (Ref. 134). See Table 8.

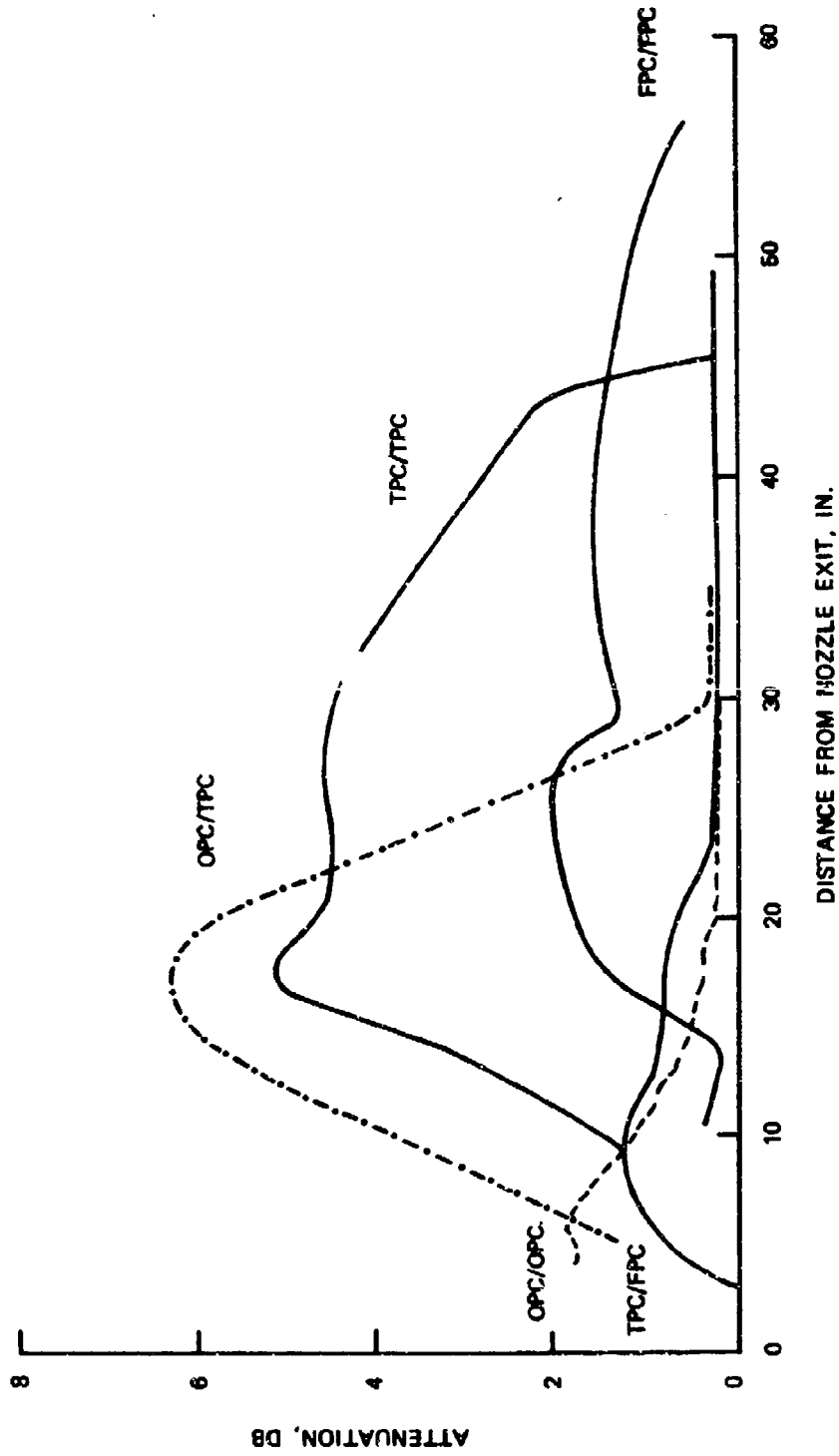


FIGURE 57. Simulated Flight Data, ELP Propellant, 450-Ft Simulated Altitude, Mach 2.2, X-Band. Effect of varying motor and "missile" size (Ref. 134). See Table 8.

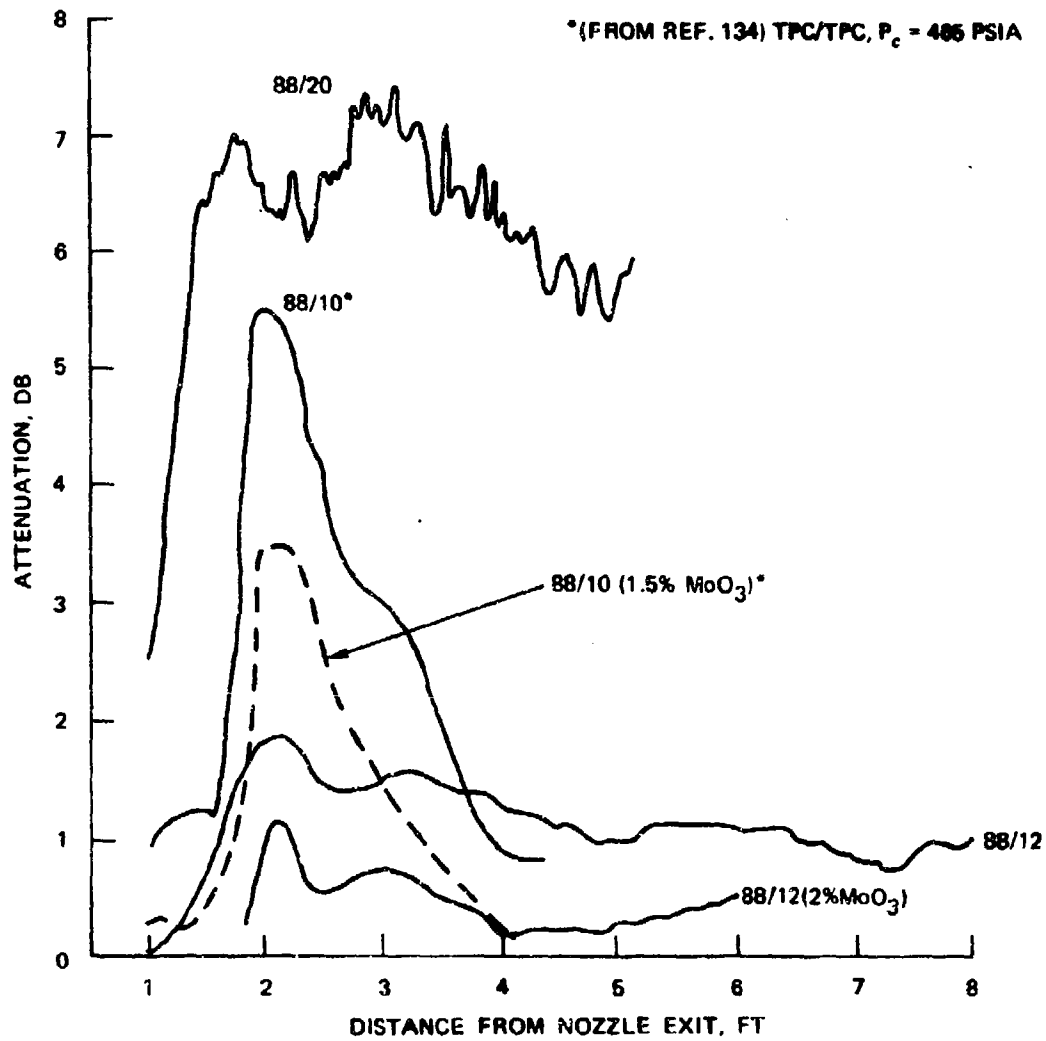


FIGURE 58. Simulated Flight Data OAL Tests, Composite Propellants, 28,000-Ft Simulated Altitude, Mach 2.2, Effect of Propellant Composition (Ref. 135).

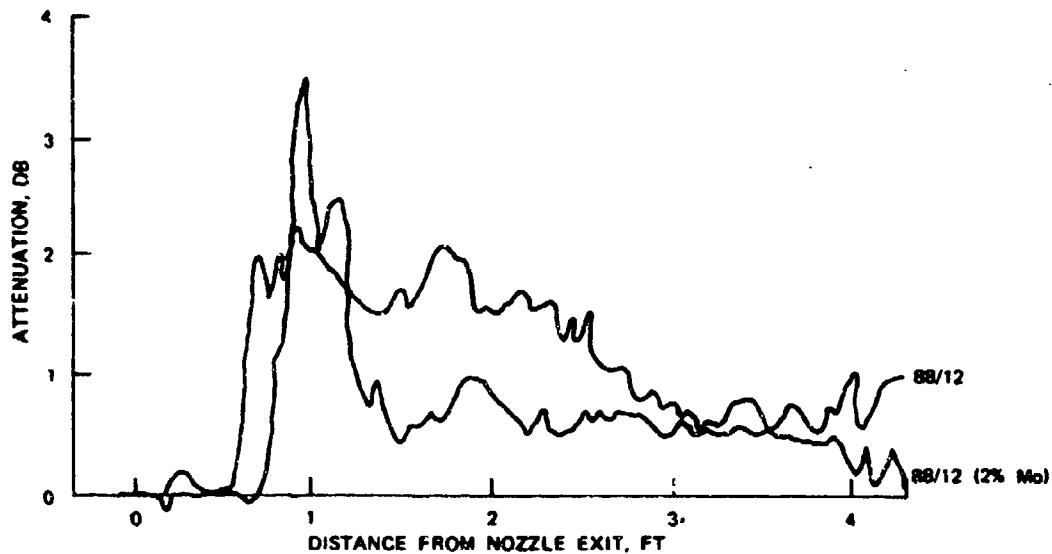


FIGURE 59. Simulated Flight Data, 88/12 Propellant, 29,000-Ft Simulated Altitude, Effect of Attenuation Suppressing Additive (Ref. 136).

The fifth series of simulated flight tests made at OAL (Ref. 126 and 137) on six propellants are summarized in Figure 60. Only the tests which gave the largest attenuation are shown. (Three different motors were tested for each propellant and the peak attenuation occurred at the maximum free stream velocity in all cases except one, Propellant E). Propellant E was unusual in that it contained 3% potassium sulphate. Knowing this, the relatively low attenuation shown in Figure 60 for Propellant E is an indication that full afterburning did not occur.

Cinema photographs of the tests show that afterburning attached to the missile base occurred for Propellants G, F, and C only for those tests summarized in Figure 60. For the other tests, on these and the other three propellants, attached base burning either did not occur or occurred only intermittently at ignition or during tailoff.

Attached base burning was observed only during tailoff in the AEDC tests at Mach 2.0 (Ref. 136). Unfortunately, the microwave equipment was not in a position to measure attenuation during the phenomenon.

Propellant C used in flameholder tests (Figure 50) and Propellant C discussed here are believed to have been of the same composition. All simulated altitude tests on Propellants C through H gave values of attenuation below the sensitivity of the measurement system (0.01 to 0.05 dB) (Ref. 126 and 34) and were not indicative of the potential in-flight attenuation problems. These simulated flight tests and in-flight measurements on the same propellants are discussed more fully in the next two sections.

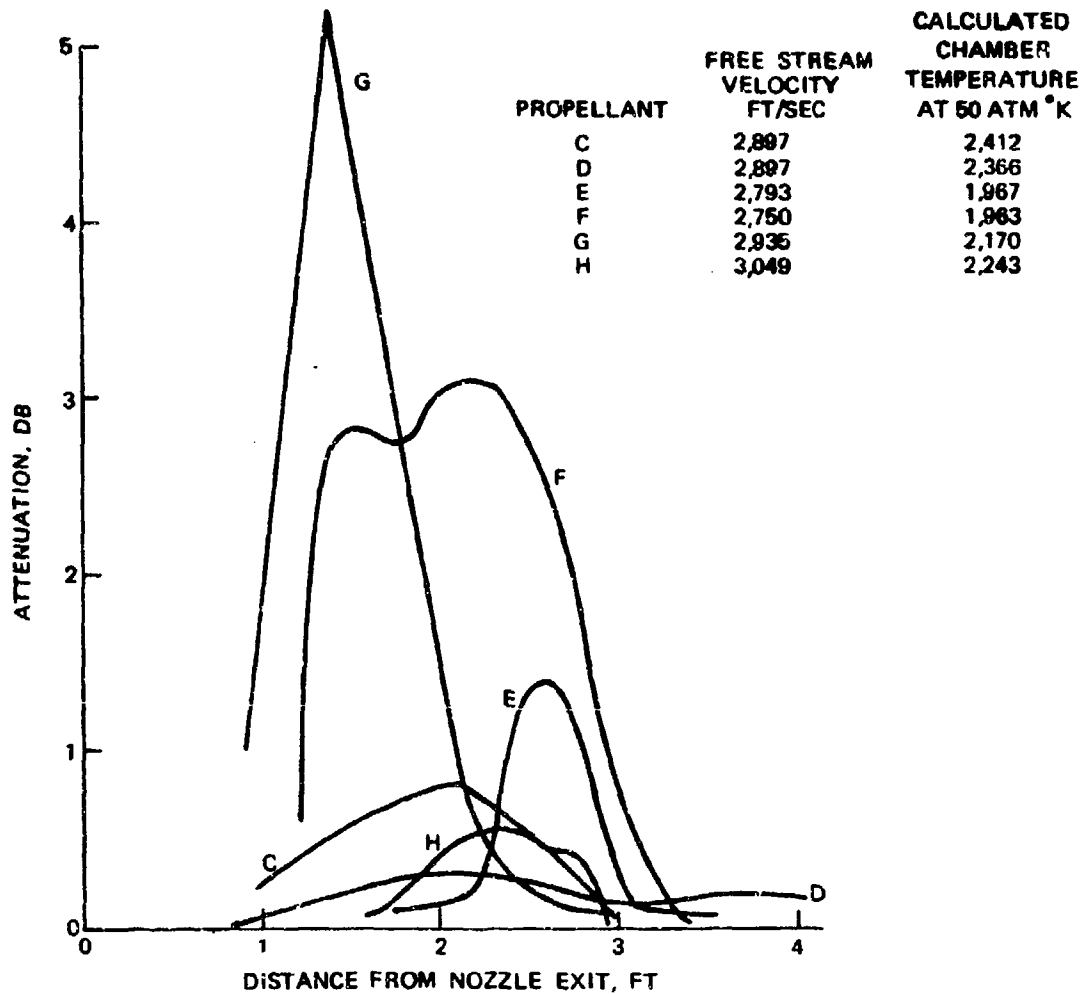


FIGURE 60. Simulated Flight Data for Six Propellants (50-Pound Thrust, 33,000 to 38,000-Ft Simulated Altitude).

4.4 IN-FLIGHT ATTENUATION DATA

Extensive in-flight attenuation data reported by Poehler (Ref. 138, 139, 140, and 141) were obtained from strategic or space vehicle launchings. Since these data are for RF transmission through plumes at higher altitudes than are of interest in tactical missiles, they will not be discussed in this report.

In-flight attenuation data were examined by Smoot in a 1970 report (Ref. 34). It was hoped that enough good flight data might be available for evaluation of models then existing—or to serve as a guide to the improvement of the models. It was also hoped that *piggy-back* techniques would become obvious by which more flight attenuation data could be obtained from tactical missile system flight tests. It soon

became clear that existing prediction models were not adequate to explain the data. However, by examining the data, improvisations and improvements to the models have been made.

Unfortunately too, *piggy-back* testing is disliked by systems development people because it can interfere with their objectives and schedules. It is also rare that one can add sufficient instrumentation in a piggy-back to obtain enough data for full analysis of flight attenuation. Figure 61 is an example of data from a well-instrumented attenuation flight test. Four such figures may be constructed from data in this one flight: for two different RF frequencies and two different receiver sites. Rotation of the missile during flight (1 rps) provided positive and negative aspect angle data and data out of the antenna/nozzle axis plane. Such data are helpful for confirming diagonal propagation models.

In-flight attenuation data (for positive aspect angles, i.e., "through the plume") for the propellants of Figure 60 are summarized in Figure 62. The order of attenuation is grossly different for the simulated flight and flight data except that D and H had the lowest attenuation in both test series. Propellants C and D were identical in composition except for the addition of 1% lead chromate to Propellant D as an electron suppressant. This is discussed further in Section 4.5.

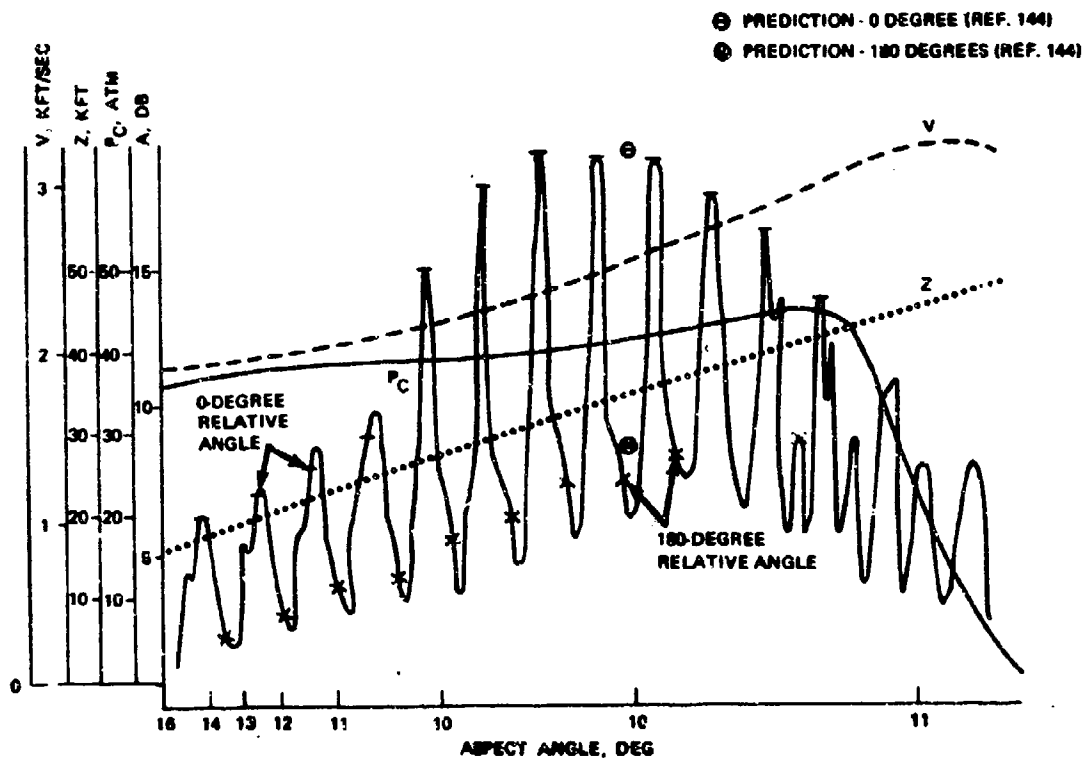


FIGURE 61. In-Flight Attenuation for Propellant C (Rolling Missile).

NWC TP 5319, Part 1

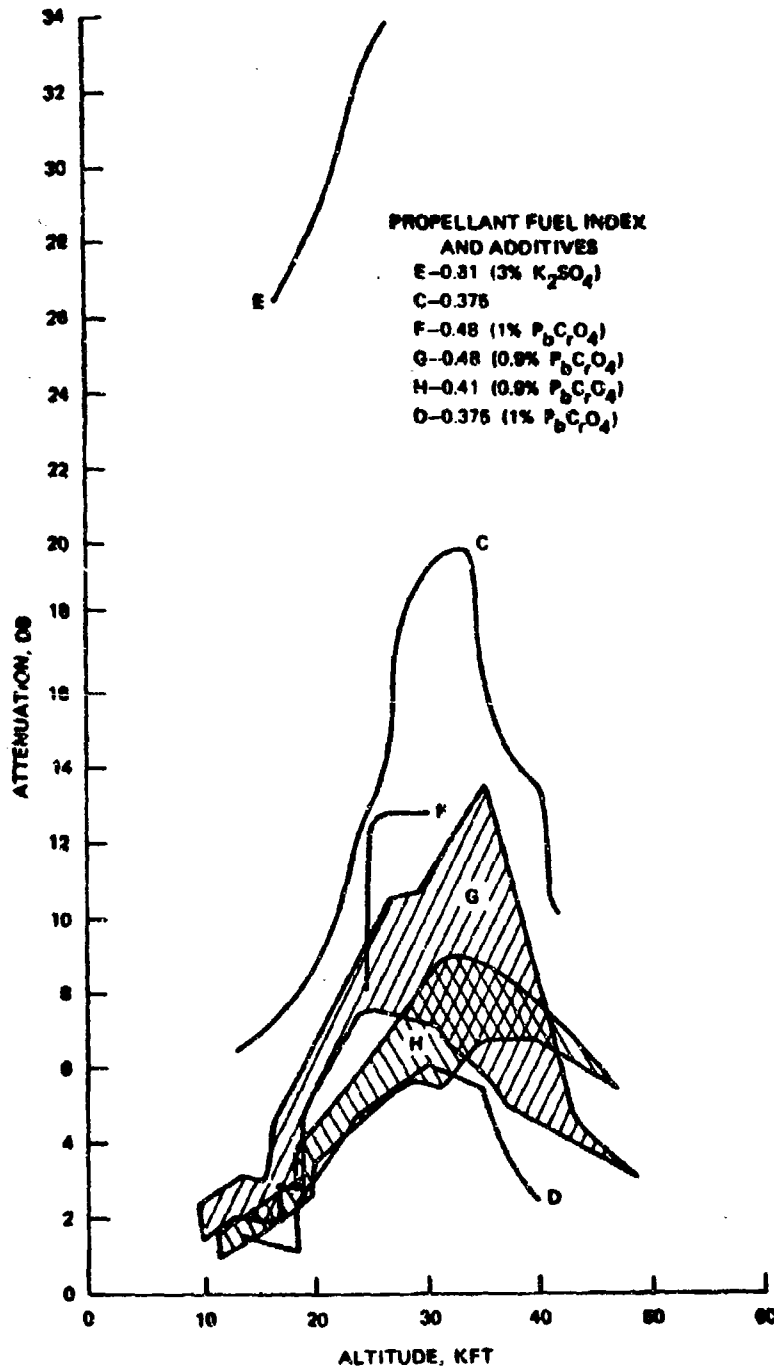


FIGURE 62. Flight Attenuation Data for Propellant of Figure 60 (Section 4.3). Aspect angle range from 2 degrees at 10,000 ft to 10 degrees at 35,000 ft and above.

NWC TP 5319, Part 1

All of these propellants had impurity levels of 170-345 ppm sodium and 50-75 ppm potassium. Missile nozzle/base diameter ratios were small, 0.32, indicating a large base and likelihood of significant base recirculation. Photographs of the missile flights show onset of vigorous afterburning attached to the base at flight Mach numbers of 2.1 to 2.3 (which occurred in the altitude regime of 19,000 to 25,000 feet). Altitude is believed to be of minor importance to the onset of afterburning, provided only that sufficient air is present to support afterburning. (The Terrier missile observations (Ref. 128 and 142) show the same velocity dependence for the initiation of afterburning.)

The data and the appearance of full base burning during tailoff in AEDC tests (Ref. 136) noted in Section 4.3 adds credibility to the suggestion that there may be some critical combinations of the variables (1) free stream velocity, (2) base/nozzle diameter ratio, (3) boat-tail angle, (4) exhaust gas velocity, (5) exhaust gas temperature, and (6) exhaust gas fuel index, and species and reaction rates required for ignition in the base region. All of these variables (except the reaction rates) enter into the equilibrium base recirculation model (Section 2.4). However, since combination of that model with an aft-plume calculation has only recently been developed, little evidence has yet been developed to prove the adequacy of the model. A new non-equilibrium base recirculation model was mentioned in Section 2.7.2.

Pergament (Ref. 143), Victor (unpublished), and Smoot (Ref. 34) have calculated plume properties for some of the Propellants C through H. Victor and Smoot's equilibrium calculations gave electron densities much lower than those necessary to explain the data seen with full base burning. Pergament's non-equilibrium calculations (without base effects) predicted peak afterburning plume temperatures much lower than the equilibrium models (1,800 versus 2,100°K). However, because of the rate coefficients in the calculation, Pergament predicted much higher electron densities (6×10^{11} versus 8×10^{10}). Pergament's predicted electron densities are of the order required to explain the simulated flight data of Figure 60. These electron densities, when applied to full-scale diagonal line-of-sight attenuation calculations, lead to predictions of the order of several hundred decibels. Victor and Breil used a simple diffraction model (Ref. 144) to calculate propagation "through" Pergament's plumes (propellants C and H) and obtained agreement to within 2 dB of the flight data at aspect angles of ± 0 degrees (see circles in Figure 61).

Flight data from the Terrier missile and two experimental rocket test vehicles (RTV) are shown in Figure 63. The experimental propellants are examined more fully in Section 4.5. The Terrier double-base propellant failed to attenuate RF signals in static tests (much like the propellants C through H). The propellants in RTV-1 and -2 (ELP and FDS, respectively) are described in Section 4.5. Static sea-level attenuation data on ELP and FDS were shown in Figure 55; simulated flight data on ELP were shown in Figures 56 and 57.

Simulated flight tests on FDS propellant gave constant attenuation of about 0.1 dB along the entire plume except for peaks of about 1 to 2 dB at ignition and 0.4 to 0.6 dB at tailoff.

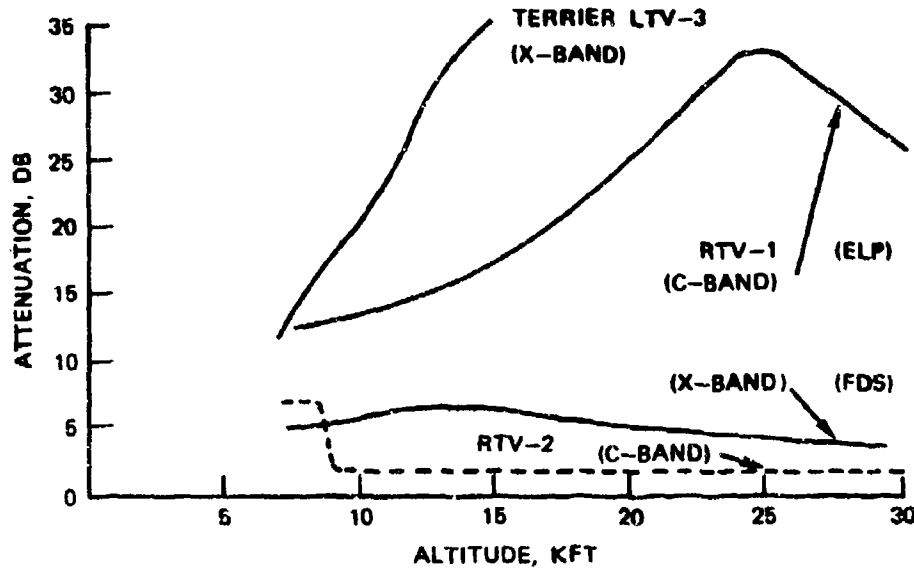


FIGURE 63. Flight Attenuation Data.

4.5 RF ATTENUATION SUPPRESSING ADDITIVE DATA

Additive data obtained prior to 1967, which were reviewed in Ref. 78, are summarized in Figure 64. Unfortunately, more recently published data, although covering additional additive substances and test conditions, have not decreased the uncertainties concerning the quantitative effectiveness of molybdenum, the effect of propellant aluminum content (through its effect on plume temperature) or the relationships between attenuation suppression at test conditions and in operational flights.

Smoot and Hedman (Ref. 145) summarized the results of four additive studies:

1. Selected additives at weight percentages of one or two can reduce peak attenuation by factors of 2 to 6. Optimum additive concentrations have not been established, but will probably be close to 1%.
2. Compounds containing molybdenum seemed to be the most effective additives. Molybdenum metal was recommended as the best additive for rubber-based composite propellants.
3. Reducing alkali metal impurity content of the propellant is a very effective way to reduce attenuation. Attenuation varies about as the square root of potassium concentration for all test conditions.

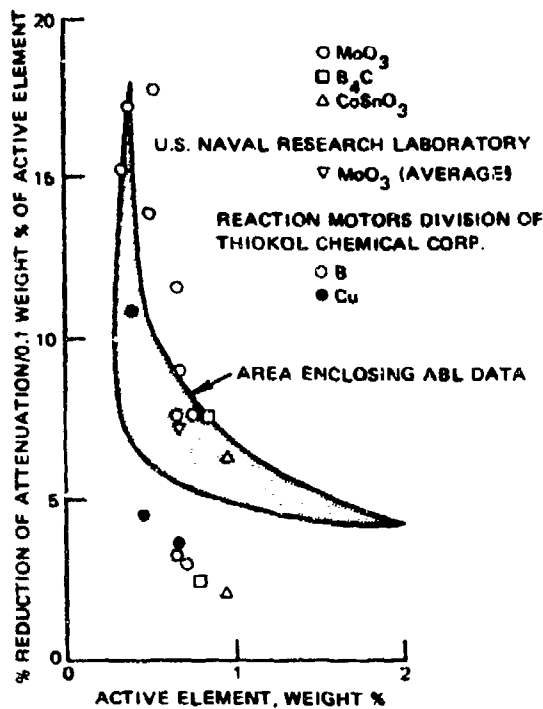


FIGURE 64. Comparison of the Results of Different Additive Studies (Ref. 78).

4. Attenuation reductions greater than 90% are possible by using ammonium perchlorate with reduced potassium in conjunction with an effective additive like molybdenum.

Myers, Jenks, and Hartsock (Ref. 146 and 31) continued the Hercules additive study program and measured the effectiveness of a number of additives in tests which included simulated flight conditions.

At NWC, Harp (Ref. 83) performed the boron additive studies shown in Figure 24. Under NWC sponsorship, wind tunnel tests at AEDC (Ref. 136) demonstrated the effectiveness of molybdenum at simulated flight conditions.

Altman, Thompson, and Sukanek at the Air Force Rocket Propulsion Laboratory (Ref. 147) measured the effect of a number of additives at concentrations of 1 and 3% on diagonal attenuation with composite propellants containing 7, 12, 16, and 20% aluminum.

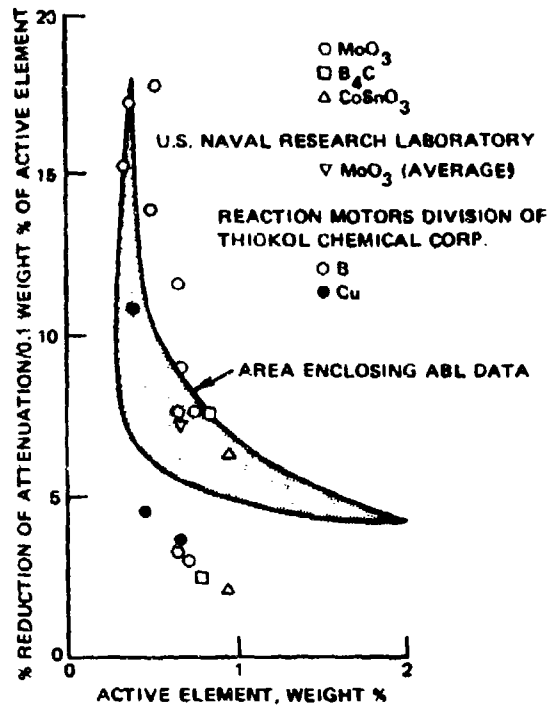


FIGURE 64. Comparison of the Results of Different Additive Studies (Ref. 78).

4. Attenuation reductions greater than 90% are possible by using ammonium perchlorate with reduced potassium in conjunction with an effective additive like molybdenum.

Myers, Jenks, and Hartsock (Ref. 146 and 31) continued the Hercules additive study program and measured the effectiveness of a number of additives in tests which included simulated flight conditions.

At NWC, Harp (Ref. 83) performed the boron additive studies shown in Figure 24. Under NWC sponsorship, wind tunnel tests at AEDC (Ref. 136) demonstrated the effectiveness of molybdenum at simulated flight conditions.

Altman, Thompson, and Sukanek at the Air Force Rocket Propulsion Laboratory (Ref. 147) measured the effect of a number of additives at concentrations of 1 and 3% on diagonal attenuation with composite propellants containing 7, 12, 16, and 20% aluminum.

NWC TP 5319, Part 1

In tests of static sea level diagonal attenuation and noise, Fuller and Williams at the Lockheed Propulsion Company measured the effect of molybdenum addition on diagonal attenuation by motor plumes containing 12% aluminum and both standard (STD) and reduced levels of potassium (MP) (Ref. 133).

All of the transverse additive data obtained on molybdenum additives (including Mo, MoO₃ and MoS₂) are summarized in Figure 65. Diagonal data from Ref. 133 are included also; however, those from Ref. 147 are left out for reasons shown later in this section. The shaded area from Figure 64 is included in Figure 65 for purposes of comparison. The heavy solid line represents the upper possible limit of additive effectiveness (i.e., 100% reduction of attenuation). The two lighter solid lines represent

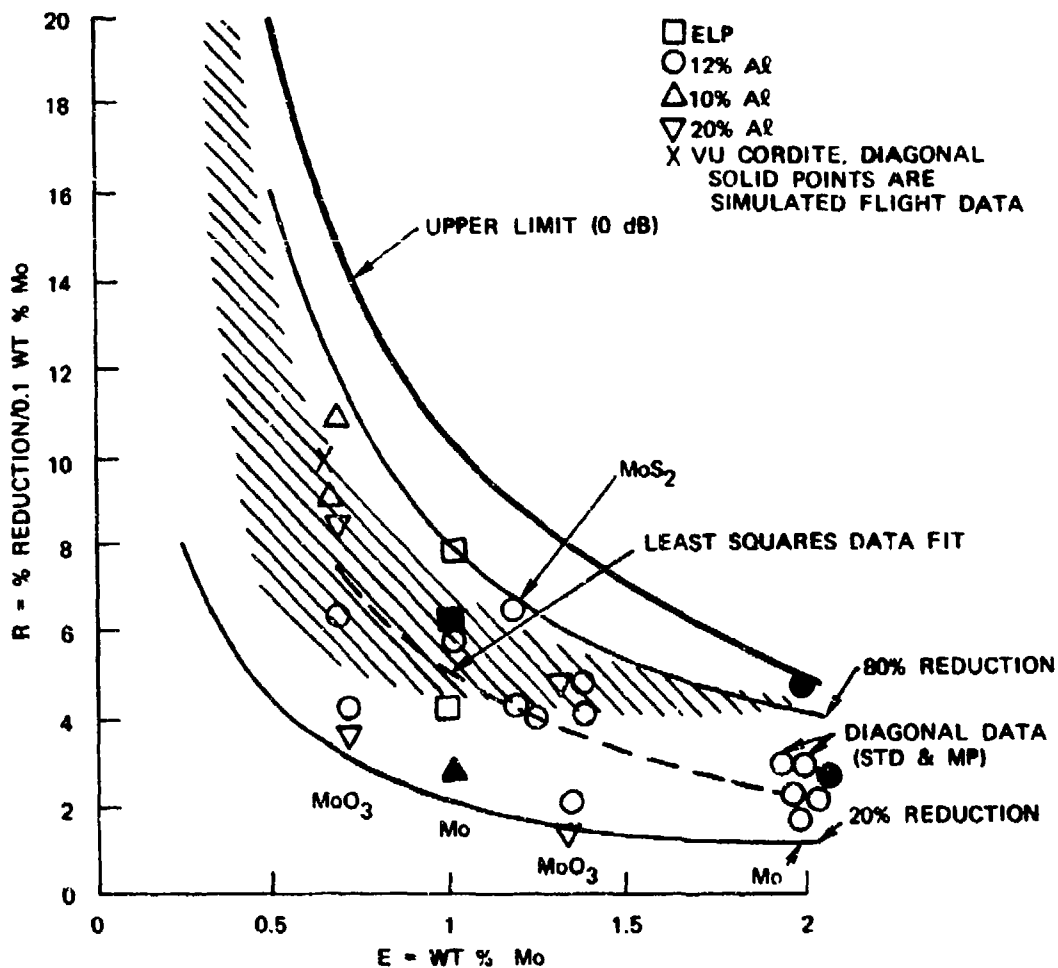


FIGURE 65. Summary of Molybdenum Attenuation Suppressing Effectiveness.

80 and 20% attenuation reduction, corresponding to the apparent upper and lower limits of the data. The dashed line represents a least squares fit of all the data to a quadratic equation:

$$R = 12.3 - 9.1E + 2.2E^2 \quad (33)$$

The equation is about the same, whether fit to all the data points or only to the mean values, at each of the indicated weight percentages of elemental molybdenum. When fit to the means, the quadratic curve is statistically significant. However, because of the scatter of individual data points, the quadratic curve is statistically insignificant when compared to the best *linear* fit to all the points ($R = 8.9 - 3.2E$). The linear curve would seem to imply an optimum mean-effectiveness of 60% at 1.25 weight percent Mo and reduced effectiveness at both higher and lower weight percentages.

Altman, Thompson, and Sukanek (Ref. 147) showed an apparent dependence of attenuation reduction by Mo on the aluminum content of the propellant in diagonal tests. Both 1 and 3% of Mo and other additives were studied. The results for molybdenum and boron additives are summarized in Figure 66. The greatly reduced effectiveness of Mo at high aluminum content might be thought to be due to the mode of RF propagation in the plume (see Section 3.3) rather than to a lack of electron reduction. At least, this might seem reasonable in light of the apparent insensitivity of the transverse data in Figure 65 to aluminum content if it were not for the nearly constant effectiveness of boron suppression for all aluminum concentrations. At first glance this is in agreement with the models of Section 2.8 which predict reduced Mo additive effectiveness and increased boron effectiveness at the higher temperatures which accompany increased aluminum content in a propellant. This conclusion cannot be made very strongly because diagonal attenuation is not directly proportional to electron concentration (transverse attenuation is), but the results do provide some substantiation of the equilibrium models of Section 2.8.

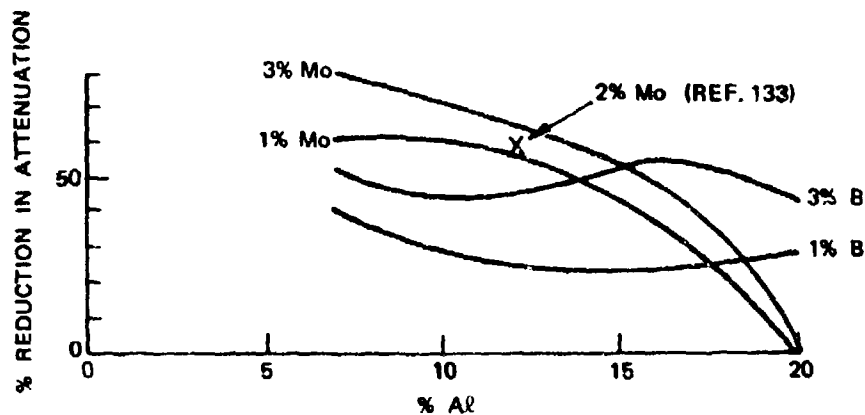


FIGURE 66. Effect of Propellant Aluminum Content on the Effect of Molybdenum and Boron for Suppressing Attenuation at Diagonal Orientations (Ref. 147).

NWC TP 5319, Part 1

Diagonal tests on 20,000-lb thrust motors performed at NWC and United Technology Center (unpublished) show the effect of 1% molybdenum additive, by implication only, since no control was run with the 13% aluminum propellant which contained the additive. However, propellants with 10 and 12% aluminum gave higher attenuation than the 13% aluminum propellant with 1% Mo (Figure 67).

Much of the additive data from references 145 and 147 are summarized in Figure 68. There seem to be trends in the data, but the scatter is too large to make definitive quantitative statements about additive effectiveness. Other data from the same references, but which have not been shown here, show inconsistent dependences on simulated altitude and on RF frequency. Unpublished data from small motor diagonal measurements (30-degree aspect angle) at UTC are included as circled symbols in Figure 68. These data as well as the diagonal data from Ref. 14 show some dependence of attenuation suppression on Mo concentrations.

In summary, the conclusions of Smoot and Hedman, cited earlier in this section, still seem to be true. In addition, Mo additive effectiveness has not shown a definite dependence on any test variables and seems to be generally capable of reducing attenuation by 50% regardless of its concentration. The exceptions to this have been noted. The dependence of Mo effectiveness on aluminum content shown by Figure 66 is unsubstantiated by transverse tests and should be studied further. On the basis of these data, obtained under controlled conditions, there is no evidence to contradict the theoretical mechanisms discussed in Section 2.8.

Very limited flight data are available on additive effectiveness. Only the results shown in Figures 62 and 63 were found. Figure 69 shows the results of propellant tailoring efforts to improve the attenuation properties of the CMDB Propellant ELP. The final propellant selected, FDS was compared, in flight, with ELP in Figure 63 (Ref. 1 and 34). Propellant composition data are shown in Table 9. Additional flight data comparisons shown in Figure 70 for a lead chromate additive were also reported in Ref. 34. These flight data (Propellants C and D) were discussed in Section 4.4 and shown somewhat differently in Figure 62.

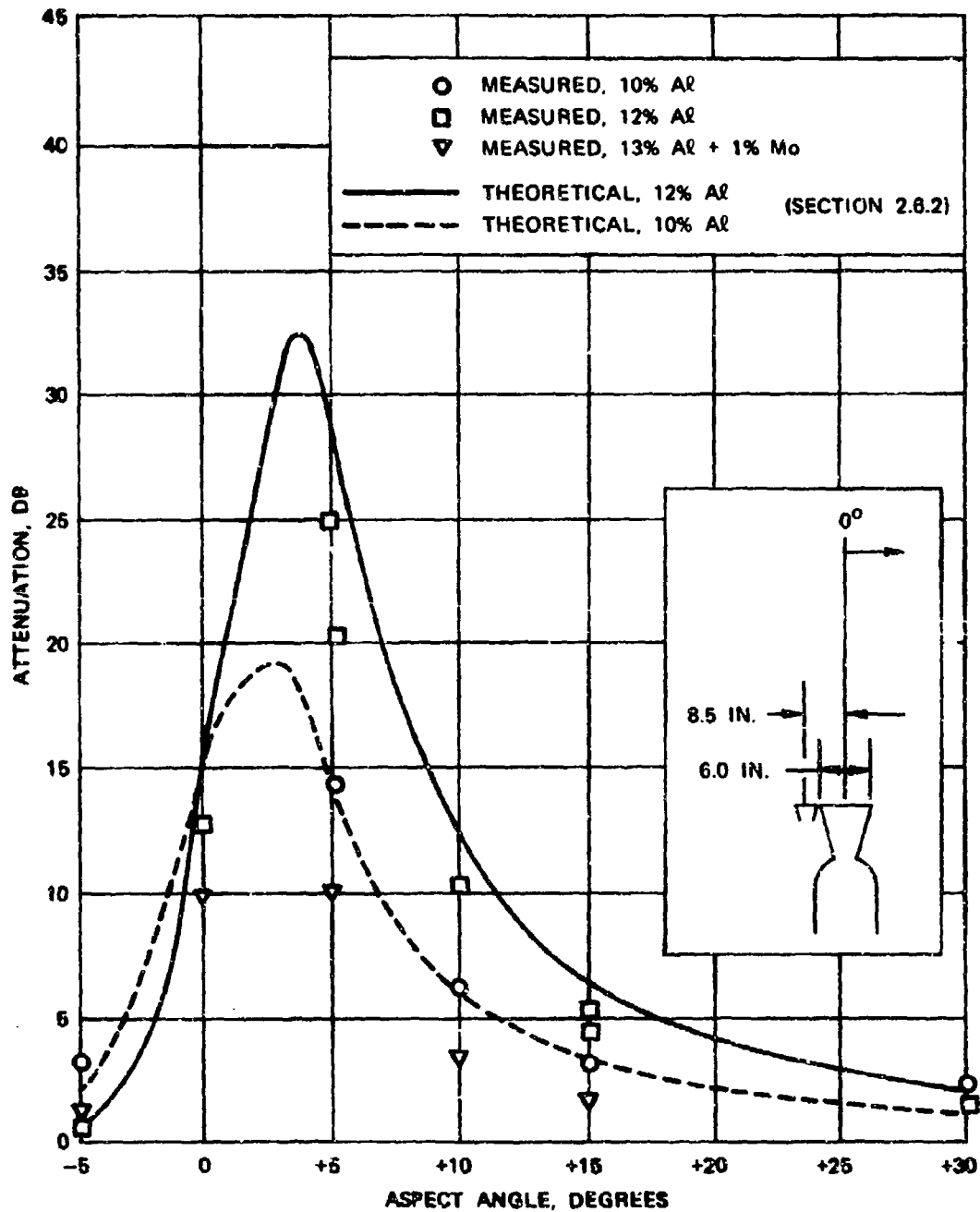


FIGURE 67. Diagonal Attenuation Suppression by Molybdenum, 20,000-Pound-Thrust Motors.

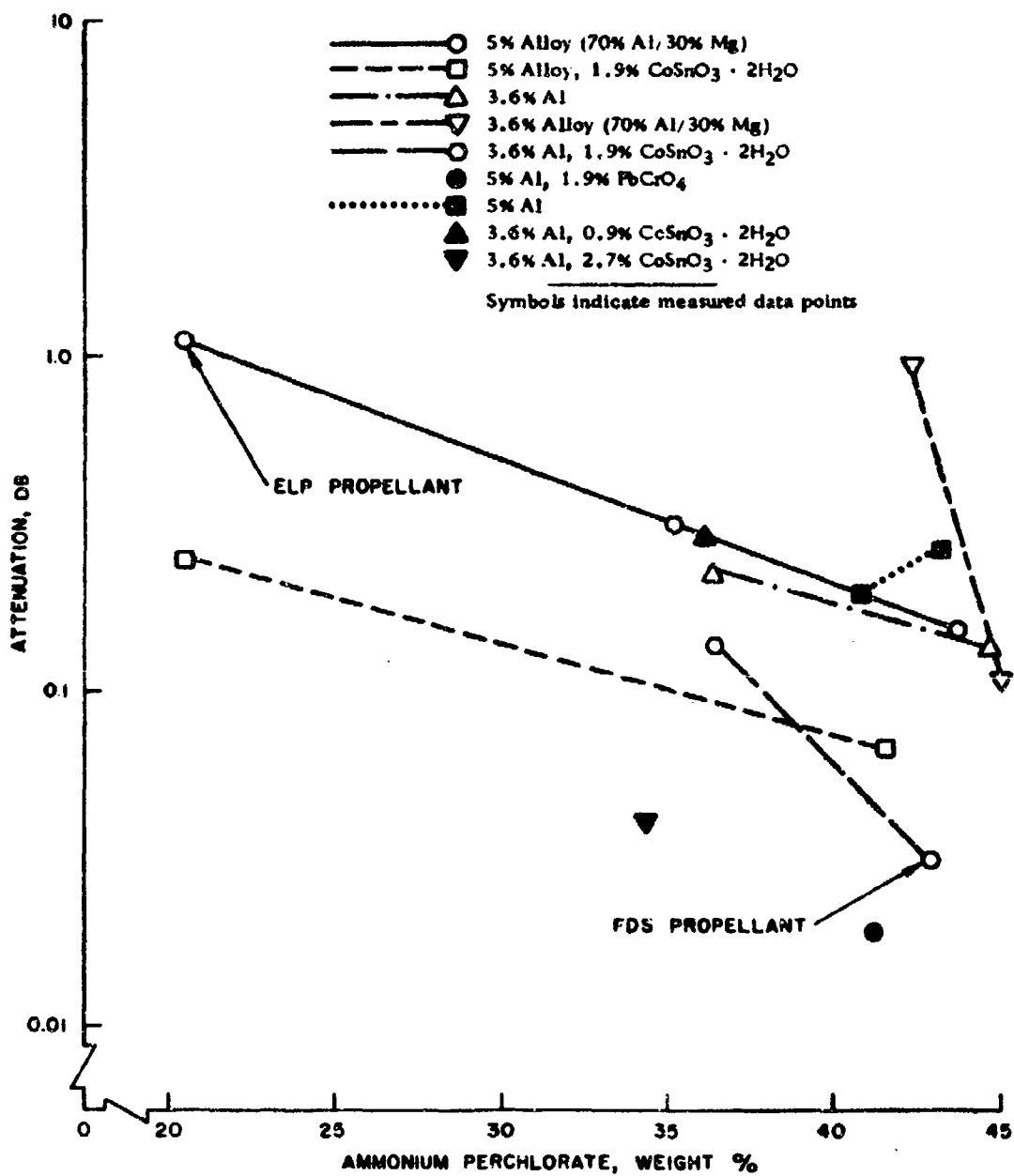


FIGURE 59. Summary of ABL Study of CMDB Propellants (Simulated Altitude: 50,000 Ft; X-Band Radiation).

NWC TP 5319, Part 1

TABLE 9. Propellant Composition Data.^a

Constituent	RTV-1 ELP	RTV-2 FDS
Aluminium	3.5	3.6
Magnesium	1.5	...
Ammonium perchlorate	20.2	42.7
Resorcinol	1.1	1.4
Nitrodiphenylamine	1.0	1.0
Nitrocellulose	28.8	15.9
Nitroglycerine	37.2	26.8
Triacetin	6.7	6.7
Hydrated cobalt stannate	...	1.9
Calculated fuel index	0.4	0.16

^a Missile flight test from Figure 63.

PROPELLANT INGREDIENTS	C %	D %
AMMONIUM PERCHLORATE	75	75
POLYURETHANE	24	23
TiO ₂	1	1
Pb ₃ O ₄	1	1

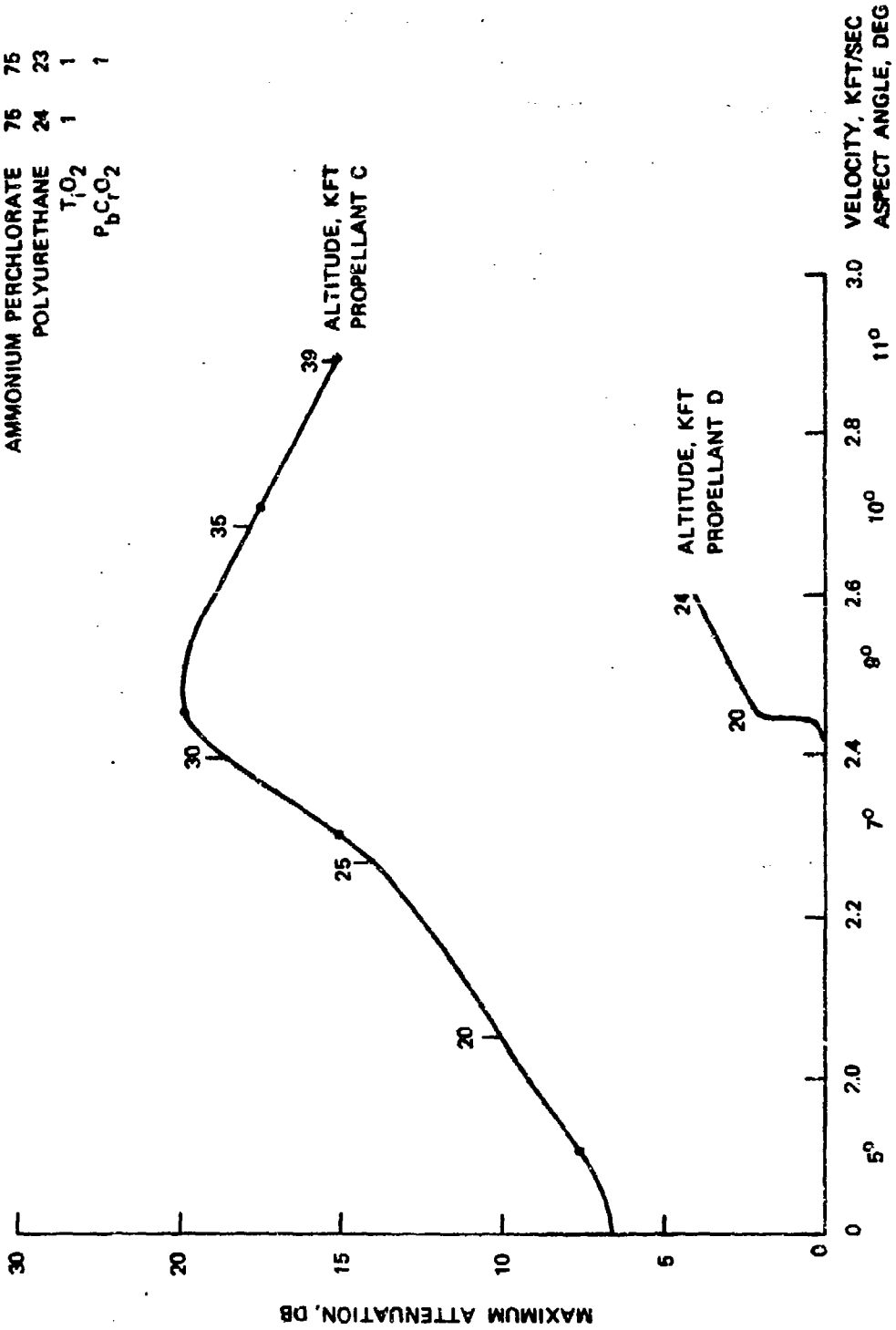


FIGURE 70. Effect of Lead Chromate Additive on In-Flight Attenuation.

5.0 PROBLEM SOLVING

Prior to the budget cut which ended this study prematurely, 15 sample problems were being prepared for inclusion in this section. A six-month effort was planned for solution of these problems including the use of techniques and computer programs (and any necessary adaptations or modifications) which we had at the Naval Weapons Center. We had no intention of acquiring or developing new programs if the effort showed that existing techniques were inadequate. The objective of the effort was to verify the adequacy of the existing models (both plume flow field and electromagnetic interaction models) for the prediction of attenuation at the following conditions:

1. Static sea level firings, transverse and diagonal attenuation
2. Static sea level firings, effect of molybdenum additive
3. Static firings at simulated altitudes
4. Wind tunnel tests, transverse attenuation
5. Flight tests, diagonal attenuation

In order to check the validity of the calculations, only cases for which data exist were selected. The selected problems, including four different propellants in the problem matrix, are summarized in Table 10. It was felt that these probably represent a reasonable spectrum of the propellant types responsible for serious attenuation in low- to moderate-altitude flight. For all four of these propellants, free electron formation is due mainly to ionization of alkali metal impurities. This ionization is greatly enhanced by the high temperatures due to afterburning of fuel-rich exhaust gases with air.

Although all four of these propellants have fuel-rich exhausts, there are differences in the factors influencing afterburning. In particular, Propellant C is calculated to have a very cool exhaust and has been shown to afterburn only at conditions of supersonic flight (greater than Mach 2.2), with a large ratio of base to nozzle exit radius. (The original Terrier sustainer propellant behaved similarly.) Simulated flight tests with the 88/12 and 88/20 composite propellants have not demonstrated that flight effects have a significant effect on afterburning or attenuation. If anything, for these propellants the dynamic free stream seems to reduce downstream afterburning compared with data at static conditions. The Propellant ELP also afterburns at all test conditions. However, the presence of a large base/nozzle ratio seems to increase afterburning and attenuation dramatically, but no clear relationship has been shown between the measured levels of attenuation for the variety of test conditions. If a calculational technique can reasonably predict the behavior of these 15 plumes, then it can be assumed to be sufficiently general for use on unmeasured systems.

When our funding problems became apparent, it was obviously necessary to reduce the scope of the study. A number of calculations had been made previously for static test conditions (albeit unsystematically). Some which correspond to cases in

NWC TP 5319, Part 1

TABLE 10. Study Matrix for Attenuation Data/Model Comparisons.^a

Propellant conditions	Plume models				EM models				Source	
	2.6.4	2.4 ^b	2.7.1	2.6.2 ^c	Transverse	3.1	3.2	3.3	Data	Calculations
A. ELP										
1. Flight	①	⊙	✓	✓	⊙	⊙	⊙	⊙	Fig. 63	
2. Simulated flight										
a. OPC/OPC	②	⊙	✓	✓	⊙	✓	✓	✓	Fig. 56	Fig. 71
b. OPC/TPC	③	⊙	✓	✓	⊙	✓	✓	✓	Fig. 56	Fig. 71
c. TPC/FPC	④	⊙	✓	✓	⊙	✓	✓	✓	Fig. 56	Fig. 71
3. Sea-level static			✓	✓	✓	✓	✓	✓	Fig. 42, 55	Fig. 42
4. 29 Kft static			✓	✓	✓				Appendix C, test no. 87	
5. 48 Kft static			✓	✓	✓				Appendix C, test no. 87	
B. Propellant C										
1. Flight	⑤	⊙	⊙	⊙	⊙	⊙	⊙	⊙	Fig. 61	Fig. 61
2. Sea-level static			✓	✓	✓				Ref. 34	
C. 88/12										
1. Simulated flight	⑥	⊙	✓	✓	⊙				Fig. 51, 52, 58, 59	Fig. 71
2. Sea-level static			✓	✓	✓	✓	✓	✓	Fig. 42, 51	Fig. 42
3. 25 Kft static			✓	✓	✓				Appendix C, test no. 32	
4. Sea-level 2% Mo			✓	✓	✓	✓	✓	✓	Fig. 66	
D. 88/20										
1. Sea-level static			✓	✓	✓	✓	✓	✓	Fig. 42	Fig. 42
2. 25 Kft static			✓	✓	✓				Appendix C, test no. 33	

^a Computations actually performed are circled.

^b 2.4 (Base model) is part of BYU program (2.6.4).

^c 2.6.2 (NWC model) is used to obtain input for the AeroChem model (2.7.1).

Table 10 appear in figures earlier in this report. The corresponding figure numbers are shown in the last column of Table 10. Therefore it was felt that the scope of the study could be reduced to those problems in Table 10 which represent flight or simulated flight conditions (see plumes numbered 1 through 6 in the first column of the table). These plumes had not been calculated previously. This change reduces the value and generality of the study.

Dr. L. D. Smoot was engaged to use the complete BYU low-altitude flight plume computer program to compute plume properties and line-of-sight attenuation for these six cases. This was much less costly than adapting the program (which needed some changes) for use at NWC.

NWC TP 5319, Part 1

5.1 USE OF THE BYU PLUME MODEL

The results of Dr. Smoot's calculations for cases 1 through 6 are summarized in Appendix D. The technique used has three components: (1) base recirculation (Section 2.4), (2) internal and external method of characteristics (MOC from Ref. 32) and (3) the aft-plume calculation with equilibrium chemistry (Section 2.6.4).

The base recirculation calculation (1) provides input to the MOC calculation (2). Both (1) and (2) provide the inputs for the aft-plume calculation (3), which is matched to the fluctuating pressures and velocities of the MOC flow field. Attenuation was then calculated using the predicted equilibrium electron density and collision frequency distributions (Section 3.0). Curves of calculated transverse attenuation for cases 1 through 4 and 6 are shown in Figure 71. Figures appearing earlier in this report in which related data can be found are referenced in the figure as well as in the next to last column of Table 10. The calculated results for case 5 were two orders of magnitude lower than the data (Figure 61, Propellant C) and hence are not included. Earlier work (Ref. 143) indicated that chemical kinetics must be included in the plume model to explain the high measured attenuation values for Propellant C. This case is explored further in Section 5.2.

For the Propellant ELP (cases 2, 3 and 4), the predicted values of attenuation in Figure 71 correspond to plumes about twice as long as those measured in simulated flight tests. This could be explained either by too low a mixing coefficient or by condensing effects in the wind tunnel flow field. Otherwise, there is a rough correspondence between the measured and calculated data. The calculations clearly show the effect of a large base/nozzle ratio. Since equilibrium chemical effects are independent of plume size, the effect of increasing the eddy viscosity in the BYU aft-plume model can be simulated by compressing the X axis in Figure 71. If this is done, cases 2 and 3 both show some agreement with data. The data corresponding to case 4 (TPC/FPC) are lower than one would expect intuitively. One would expect the TPC/FPC attenuation to be greater than that for TPC/TPC (due to the base effect), but Figure 56 shows that is not so. Strangely, the prediction for case 4 (when X is scaled by a factor of 2) agrees very well with data for TPC/TPC rather than TPC/FPC.

The BYU calculation for case 6 (88/12 composite propellant) is quantitatively quite good. The predicted level of attenuation in Figure 71 is quite close to the measured value shown in Figure 52. The BYU prediction does not indicate the relative attenuation peak which is measured near the exit, but instead predicts attenuation which is still increasing 10 feet from the nozzle exit. The measured peak may be due to ionization in the normal shock, or to persistence of high electron concentrations from the base recirculated region. Neither of these effects is calculated by the BYU model. An error inadvertently crept into the definition of case 6. The propellant contained 76% ammonium perchlorate, not 66% as indicated in Table 1 of Appendix D. When the composition is normalized to a basis of 100%, the effect on the calculation is to make the composition 87/13 instead of 88/12 (solids/aluminum). A crude correction, based on Figure 28, would lower the attenuation curve in Figure 71 for case 6 by about 28%.

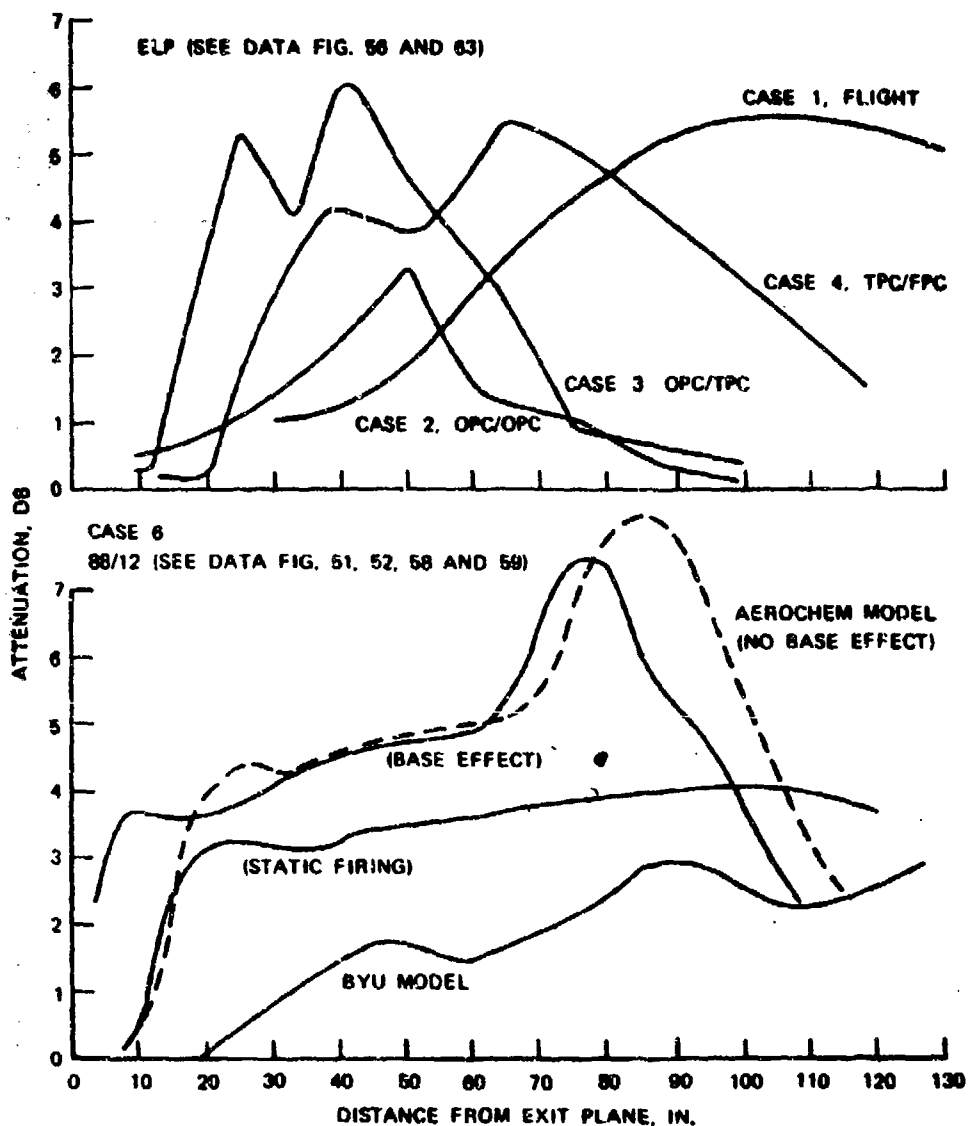


FIGURE 71. Results of Plume Transverse Attenuation Calculations for Dynamic Conditions Using BYU Model (Section 2.6.4).

Several calculations for case 6 made with the AeroChem model are also shown in Figure 71. These are described in Section 5.2.

The case 1 calculations must be compared with diagonal in-flight attenuation data (Figure 63) since there have been no corresponding transverse attenuation measurements. To do this we used the electromagnetic interaction computer programs of Appendices A and B (A-I, line-of-sight; A-II, ray trace; and B-II, diffraction based

on ray tracing), as described therein. The predicted variation of attenuation with aspect angle for the three calculations is shown in Figure 72. The measured data for this case are about 50% higher than the values predicted using diffraction model B-II. Using a reduced plume length (corresponding to a higher mixing coefficient as indicated earlier in this section) did not change the calculations substantially. Figure 72 shows a similarity of curve shapes for data and the B-II calculation. This may be misleading since the data were taken over a range of altitudes. No really firm conclusions can be drawn from this comparison for case 1 because the diagonal attenuation (as calculated by diffraction techniques) is so insensitive to specific details of the plume flow field for large plumes.

Equilibrium plume models other than BYU might have been used for these calculations. However, the other models lack the base recirculation and MOC calculations as well as the special mixing correlation for a dynamic free stream. Therefore one would expect that, in a qualitative sense, the shortcomings would appear in the other equilibrium models as well.

Failure of the equilibrium chemistry assumption for some cases was anticipated in the planning of the study. The AeroChem plume program with non-equilibrium chemistry (Section 2.7.1) was to be run for all cases for comparison. Economic realities intervened here too, and in the end we were limited to chemical kinetic analysis of only that case for which the equilibrium model has always been inadequate, Propellant C, case 5.

5.2 USE OF THE AEROCHEM PLUME MODEL

In the use of a plume model with non-equilibrium chemistry, it is very important that accurate values are chosen for species concentrations at the starting line of the computation. This is not a problem for major species such as CO_2 , H_2O , HCl , H_2 or CO , which remain near equilibrium and vary little between the chamber and the nozzle. However, it is very important for the H , O and OH radicals which trigger and sustain plume afterburning. This often demands that a kinetic nozzle expansion program be used instead of the more common equilibrium calculations.

Draper (Ref. 148) has pointed out that the two body reactions tend to remain in equilibrium but that the three body reactions (reactions [2] and [5] of Section 2.7), which involve most re-combinations of the radicals and of free electrons, remain below the rates necessary for equilibrium. Thus, the plume can build up an excess of free radicals and free electrons at downstream locations. The radicals can drive combustion even at temperatures below the equilibrium temperature (and we note as in Figure 22 that non-equilibrium plumes are generally calculated to be cooler than equilibrium). The build-up of free electrons can cause attenuation far greater than would be predicted for an equilibrium plume even at higher temperatures (Ref. 143 and 144).

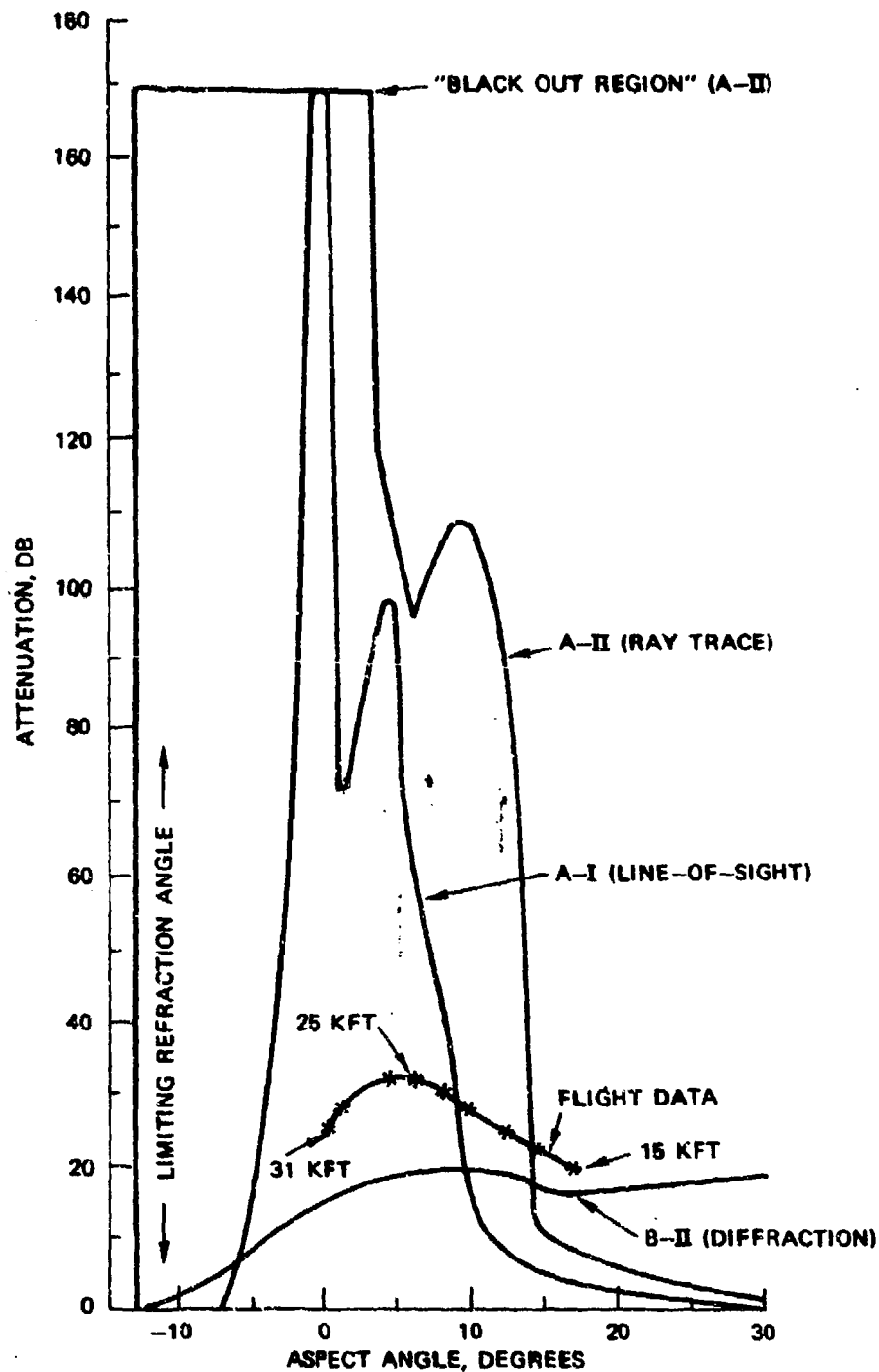


FIGURE 72. C-Band Attenuation Calculations for ELP Propellant In-Flight at 25,000-Ft Altitude. (Flight data are shown for the altitude range 15,000 to 31,000 ft.)

NWC TP 5319, Part 1

The AeroChem model (Section 2.7.1) is generally used with a homogeneous start line. For such a case, one need only specify the temperature, velocity and species concentrations of the exhaust jet (which apply from the centerline to the jet boundary) and of the free stream air (which apply outside of the boundary). These conditions apply prior to the start of any mixing. There are conditions when the program must be started with initial inhomogeneities. These are allowed for in the AeroChem program. The condition occurs most frequently if the program stops prior to completion of a desired run; output cards defining an inhomogeneous restart can be re-entered and the run continued. In the same way, inhomogeneous starting conditions can be used for inhomogeneous nozzle exit conditions or to start a plume calculation when mixing has already started, as is the case for an in-flight aft-plume with base recirculation. The procedure for specifying an inhomogeneous start (other than the self-contained restart) is not described in Ref. 12 but can be obtained either from the authors of that report or this one.

The procedure used to set up the AeroChem program for case 5 involved using the base conditions derived from the BYU model (Section 2.4), which generates species concentrations only at the stagnation condition (region 7 of Figure 3) at the base. In order to find the species in the mixing region surrounding the base, the NWC SUPPEP program (Section 2.6.2) was used with the assumption that the velocity in the recirculation region equals zero. It was then assumed that these species concentrations pass through the trailing shock without change (Figure 73). This gives high free radical concentrations at the start of the aft-plume. The starting aft-plume pressure and

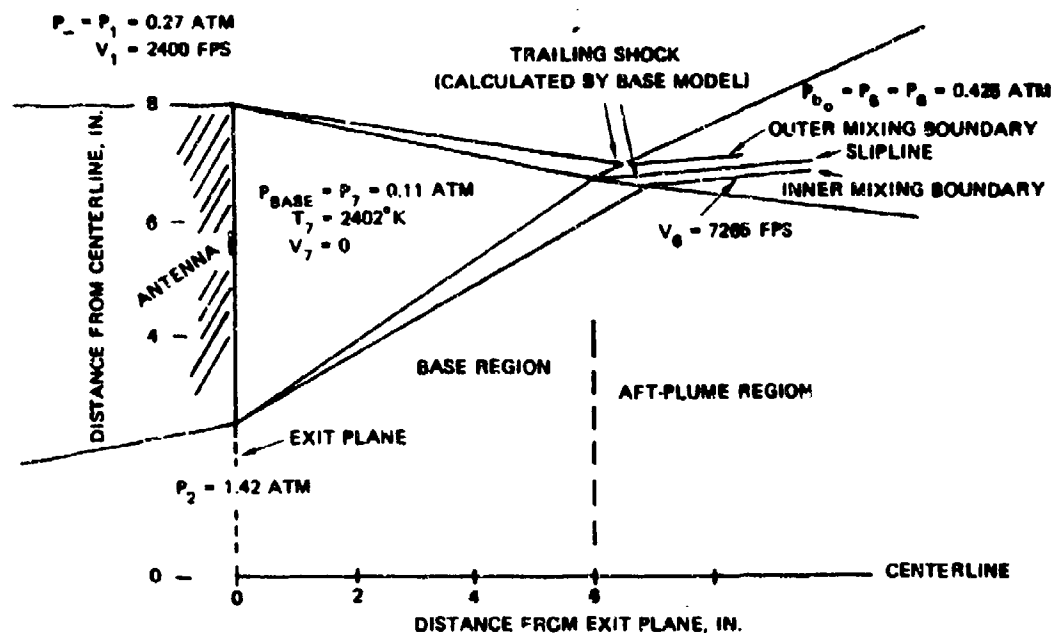


FIGURE 73. Calculated Base Region Conditions for Propellant C, Case 5.

NWC TP 5319, Part 1

temperatures were assumed to be those corresponding to equilibrium at the supersonic conditions just behind the trailing shock. Although these aft-plume temperatures can be calculated with the BYU base program (Section 2.4, Option 1 - Complete Plume), we found it less expensive and easier to use the BYU model, Option 4 - Base Region Only to define the base region and the start and pressure of the trailing shock, and then use the NWC SUPPEP model to calculate equilibrium temperatures behind the shock.

Ideally, the trailing shock pressure, P_{b_0} , of Figure 73 should be taken as the starting pressure of the AeroChem calculation. This pressure is then allowed to taper exponentially to ambient pressure (P_∞) using Eq. 8. The constant c in Eq. 8 is chosen so that $c(10 \cdot r_{b_0}) = 1$, where r_{b_0} is the radius to the slipline at the start of the aft-plume. However, a gross error may be made when one assumes that the trailing shock pressure applies across the entire jet at the start of the aft-plume. A MOC or stream-tube calculation is required to determine the actual pressure distribution. Typical results are shown in Figure 15. Since the parallel flow non-equilibrium plume program (AeroChem or REP-1) is unable to handle a radial pressure gradient, the only other assumption possible is that the free stream pressure applies throughout the aft-plume region. Since we were unable to obtain economical solutions with the AeroChem program for the varying pressure assumption, all of the following results are for a constant pressure plume ($P = P_\infty = 0.27$ atm). The variable pressure run cost almost \$200 for the first two feet of plume. The chemical reactions used for Propellant C are shown in Table 11.

TABLE 11. Propellant C (Case 5) Chemical Reactions and Rates Used in AeroChem Program.^a

REACTIONS BEING CONSIDERED	K _r = A · EXP(B/RT) / T ⁿ		
	A	N	9
1 O + O + M = O2 + M	1.000-29	1.0	.0
2 O + H + M = OH + M	1.000-29	1.0	.0
3 H + H + M = H2 + M	5.000-29	1.0	.0
4 H + OH + M = H2O + M	2.000-28	1.0	.0
5 C ₂ + O + M = CO2 + M	1.000-29	1.0	-484.0
6 OH + H2 + M = H2O + H	3.600-11	.0	-5167.0
7 O + H2 + M = OH + H	2.900-11	.0	-9399.0
8 H + O2 + M = OH + O	3.700-10	.0	-15692.0
9 CC + OH + M = CO2 + H	9.000-13	.0	-1073.0
10 OH + OH + M = H2O + O	1.000-11	.0	-775.0
11 H + Cl2 + M = HCl + Cl	7.000-10	.0	-2981.0
12 Cl + H2 + M = HCl + H	4.000-11	.0	-4372.0
13 H2C + Cl + M = HCl + OH	5.000-11	.0	-14878.0
14 OH + Cl + M = HCl + O	3.000-11	.0	-4968.0
15 K + HCl + M = KCl + H	6.000-10	.0	-4968.0
16 H + Cl + M = HCl + M	4.000-26	2.0	.0
17 Cl + Cl + M = Cl2 + M	3.000-29	1.0	.0
18 K + Cl + M = KCl + M	2.000-28	1.0	.0
19 K+ + E- + M = K + M	2.000-22	1.5	.0
20 K+ + Cl- + M = K + Cl	1.000-08	.5	.0
21 Cl + E- + M = Cl- + M	3.000-30	.0	.0
22 HCl + E- + M = Cl- + H	1.000-08	.0	-15872.0
23 H+ + O2 + M = OH + OH	1.600-10	.0	-70400.0
24 CO2 + O + M = CO + O2	3.200-09	.0	-54150.0

^a See Section 5.2.

(MOLECULE-ML-SEC UNITS)

NWC TP 5319, Part 1

Figure 74 shows the X-band transverse attenuation calculated by the AeroChem program for the propellant C constant pressure flight plume. Experimental wind tunnel data (Propellants C and F) from Figure 60 are also shown for comparison. These data have been scaled by multiplying the measured attenuation and the longitudinal axis by the ratio of the throat diameters for the flight case/wind tunnel case (6.834). Since we have no experience in scaling a flight plume, we cannot tell if this simple method should scale the non-equilibrium calculation. In the wind tunnel tests (Figure 60) there was no attempt to scale the base/nozzle ratio of the model to the flight missile ratio. The wind tunnel model base/nozzle exit diameter ratio was over twice as large as that for the missile: 6.5 compared to 3.0. The wind tunnel model base diameter was 5 inches. Comparison of Figures 60 and 62 shows a failure of scaling comparisons between flight data and wind tunnel data. It is possible that this may be due to non-reproducibility of the wind tunnel tests which did show considerable data scatter. In that case the attenuation levels of the wind tunnel tests would not be expected to scale in a predictable way. However, it is obvious in Figure 74 that the longitudinal axis relationship (i.e., position of peak attenuation) scales as the nozzle ratio.

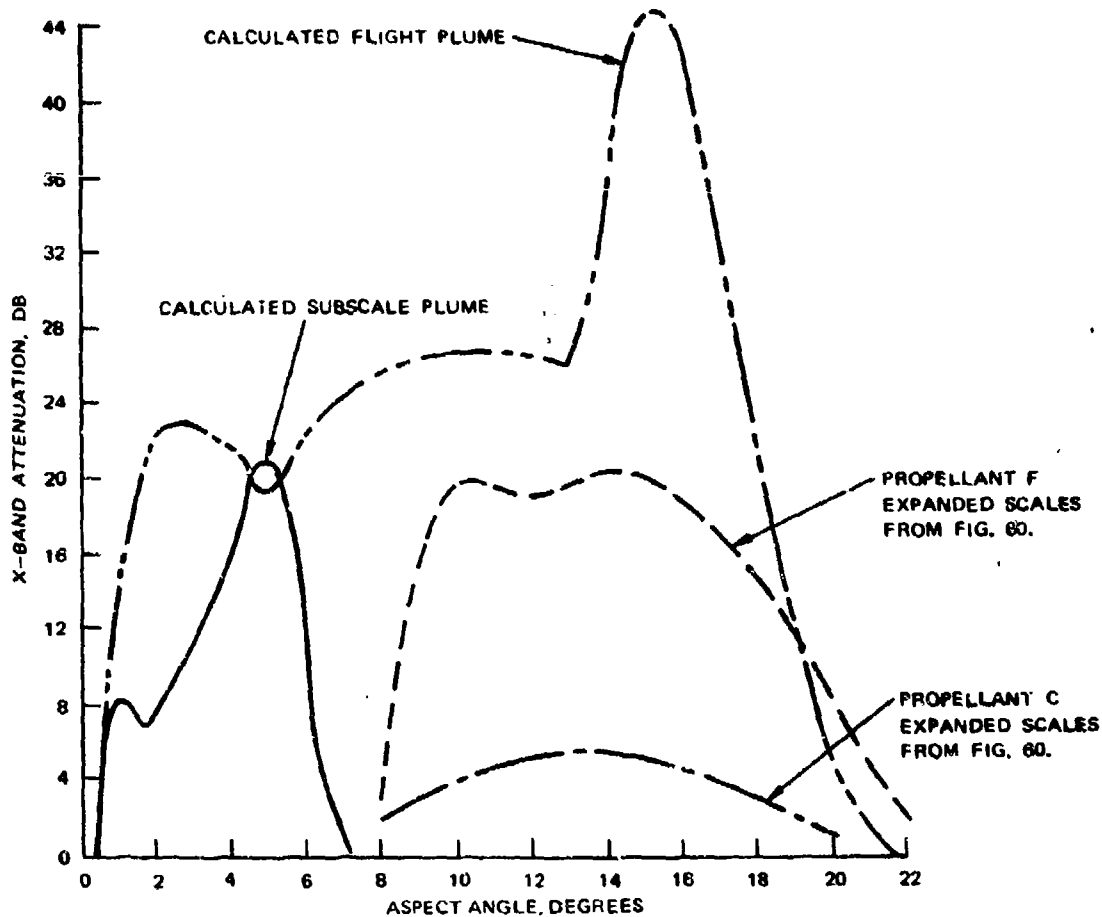


FIGURE 74. Calculated Transverse X-Band Attenuation for Propellant C.

NWC TP 5319, Part 1

To further study this scaling, the AeroChem plume program was rerun for Propellant C with a 5-inch base diameter and with the nozzle exit diameter also reduced by the same 0.32:1 scale. This was not a simulation of the wind tunnel experiment; such a simulation would have required more work than our resources allowed. It was just a way of determining if the afterburning could occur with shorter free radical residence times. The calculated transverse attenuation for this case (subscale plume) is also shown in Figure 74.

The plume length for the two calculations does scale as the ratio of base (and nozzle exit) diameters, however calculated peak attenuation for the smaller model is reduced by a factor of only 0.47 rather than by the diameter ratio (0.32). The initial attenuation peaks (21 and 8 dB) do scale as the diameter ratios. Detailed examination of the AeroChem output showed that the difference in attenuation by the two plumes is due entirely to a higher level of electron density and an effectively wider electrical plume for the subscale plume. The calculated temperature and electron density profiles for the flight and subscale plumes are shown respectively in Figures 75 and 76. It is interesting that the smaller plume is cooler, yet has a higher average electron density. Except for the difference in base and nozzle dimensions, all other factors in the two calculations were identical. From this comparison we believe that more detailed analysis of the wind tunnel plumes will be required to investigate scaling effects. We also feel that although the afterburning is rate limited to some extent, it is not the major factor affecting the electron density level for this propellant. Therefore, the electron level scales more linearly than the afterburning chemistry.

Diagonal attenuation calculations for the plume of Figure 75 were made using the line-of-sight (A-I) and ray trace (A-II) computer programs of Appendix A. The results are compared in Figure 77 with the results of the calculation for the same system reported in Ref. 143. The difference in angle dependence between the present calculation and that of Ref. 143 is due to the addition of the base effect to the present plume.

The results of programs A-I and A-II were used to define input for diffraction programs B-I and B-II, respectively, of Appendix B. The results of the diffraction calculations are shown in Figure 78. Two points from the flight data (Figure 61) are included for comparison. The inputs used for programs B-I and B-II are listed below.

B-I Input

THRUST	HTA	ATTEN	DIST	AL	WAVEL	SHIFT	HT1	ANTE	ATMAX
4000.	30.	-50.	161.	14.5	7.3	5.0	30.	0.	1000.

B-II Input

HTA	ATTEN	EFAT	DIST	AL	WAVEL	ESHIF	HT1	ANTE	HT2	ATH
40.	-45.	19.	160.	14.5	7.3	5.5	30.	0.	27.	37.

NWC TP 5319, Part 1

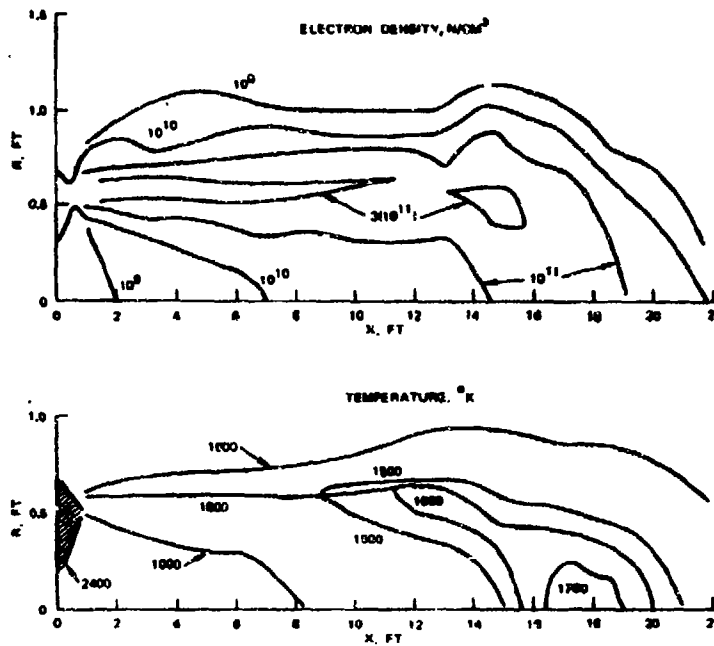


FIGURE 75. Calculated Plume Temperatures and Electron Density Profile for Propellant C.

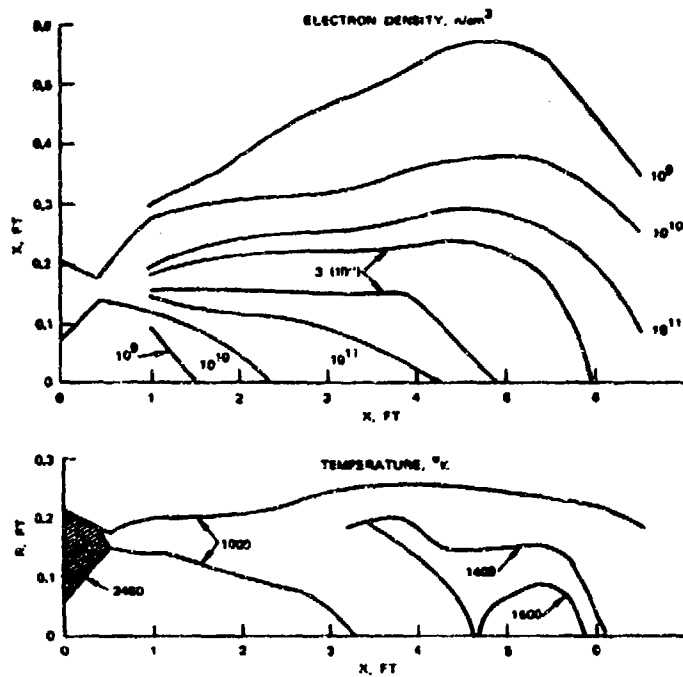


FIGURE 76. Calculated Plume Temperature and Electron Density Profile for Propellant C Plume With 5-inch Base Diameter.

NWC TP 5319, Part 1

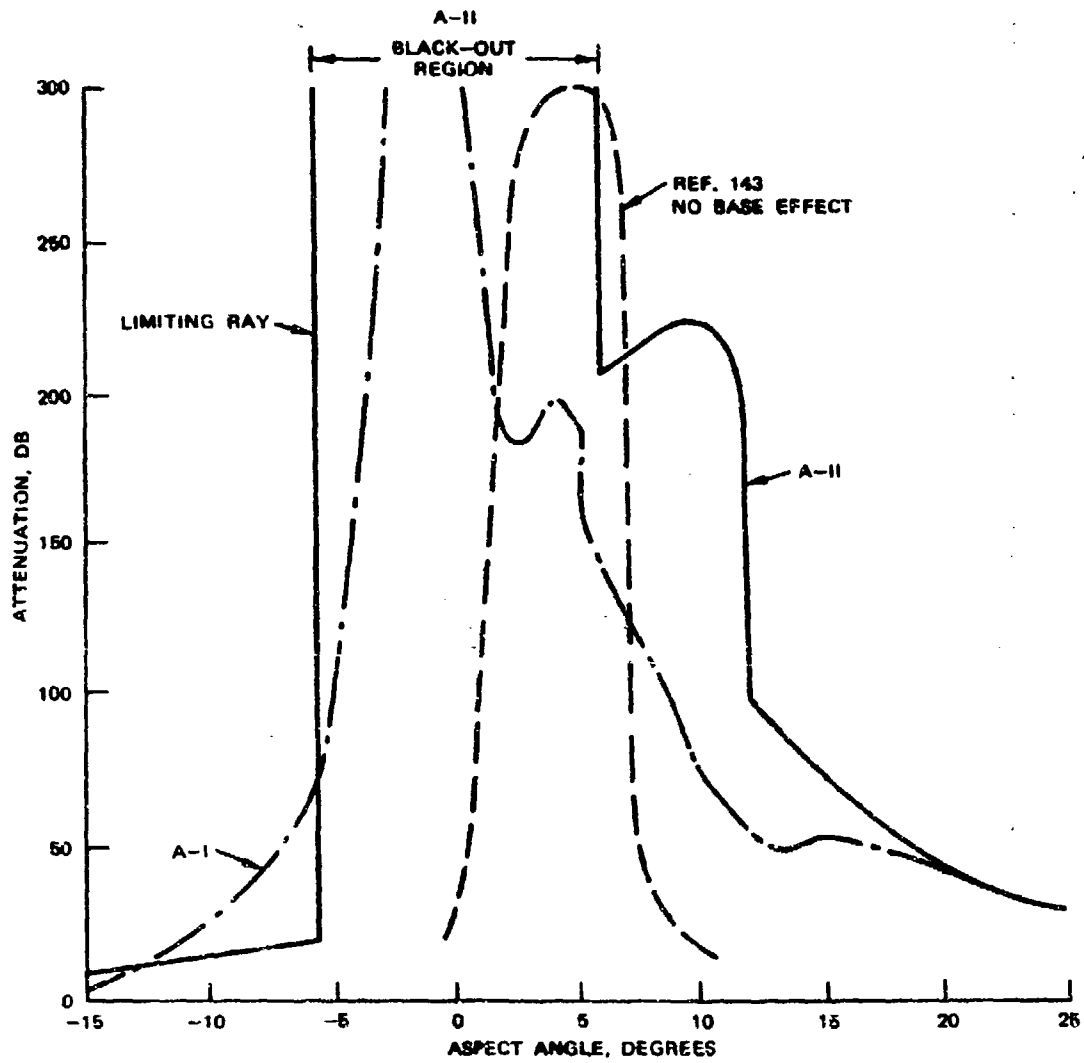


FIGURE 77. Calculated Propellant C In-Flight Attenuation by Line-of-Sight (A-I), Ray Trace (A-II) and AeroChem Line-of-Sight (Ref. 143).

NWC TP 5319, Part 1

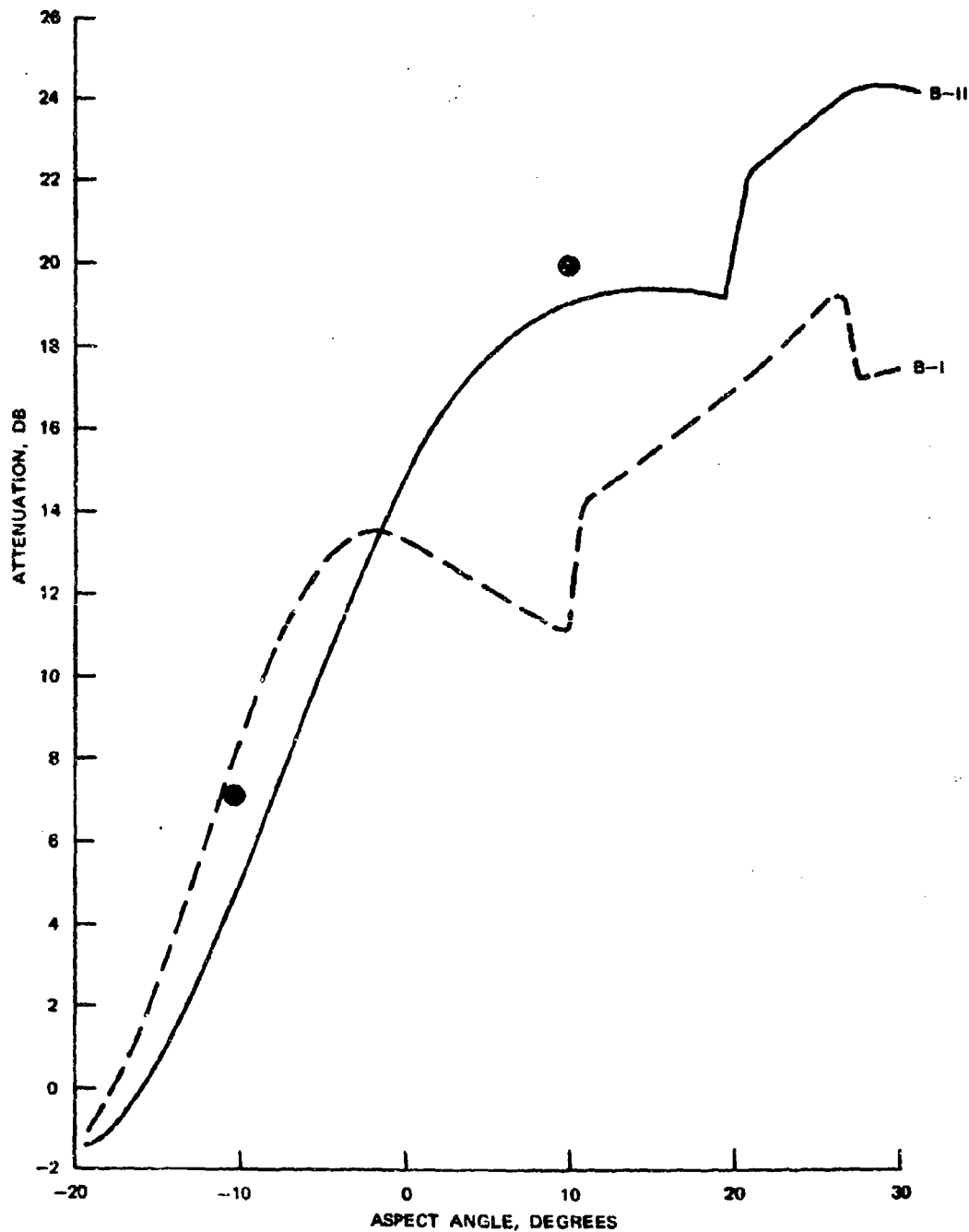


FIGURE 78. Calculated Attenuation of Propellant C In-Flight Due to Diffraction. Data from Figure 61 (●) are included for comparison.

NWC TP 5319, Part 1

The variables SHIFT, DIST and HTA in the B-I program were defined in the manner of Webb (Ref. 112) as indicated in Section 3.3. The information required to generate these variables is part of the output of programs A-I or A-II. The variable ATMAX was chosen as 1000 in order to cancel its effect in the B-I program and insure compatibility with Webb's modifications.

The B-II program was run assuming that the plume edges are linearly varying in electron density. The results of using these input assumptions are in excellent agreement with both positive and negative aspect angle flight data. This is probably fortuitous considering the coarseness of model B-II.

While this report was in the final review stage, an opportunity occurred to briefly examine case 6 with the AeroChem program. The BYU base recirculation program was run for the correct composition (88/12 solids/aluminum). The result was coupled with the AeroChem program in the same manner as for case 5. The resulting K-band attenuation prediction is labeled "base effect" in the lower half of Figure 71. Case 6 was also run without the base effect (also shown in Figure 71). In both of these runs all core region chemical species were assumed to be in equilibrium at the start line of the AeroChem calculation. Two additional runs were made assuming elevated concentrations of core region free radical and ionic species at the start line. The run which included an afterburning base resulted in an attenuation curve nearly identical to the base effect curve in Figure 71. The other run, for which a non-afterburning base recirculation region was assumed, gave a very similar result to the "no base" curve in Figure 71 except that the slight peak 2 feet from the exit plane was not predicted. An AeroChem attenuation prediction for a static firing at 5 psia ambient pressure is also shown in Figure 71.

The results of the calculations on case 6 leave much to be desired. By assuming a reacting base recirculation region it is possible to predict the attenuation peak which is measured about one foot from the nozzle exit. However, the resulting elevated radical concentrations lead to more predicted downstream combustion than the data support. The downstream prediction is nearly the same whether the radicals originate in the base region, core region or both. In fact, even changing exit plane radical concentrations by two orders of magnitude has no significant effect on the total plume calculation. A small part of the difference might be explained by using the dispersion technique of Section 3.4. The same technique should be used for all transverse calculations on small plumes when fine details are being investigated. The data related to case 6 are also unsatisfying because the AEDC measurement section was only 4 feet long. Some of the OAL data indicate persistence of moderate attenuation levels.

It would be worthwhile to thoroughly examine the reaction rate set used for these calculations. Changes in some of the recombination reactions or reaction rates would change the predicted attenuation. As things now stand, the equilibrium model appears to be a better predictor for some regions of composite propellant plumes than does the non-equilibrium model.

NWC TP 5319, Part 1

5.3 CONCLUDING REMARKS ON PROBLEM SOLVING

It should be the first order of business, when this report is used to evaluate a future operational missile problem, to compute the other sample problems in Table 10, particularly those which resemble the operational situation. Only in this way can the general utility intended for this report be guaranteed.

Other considerations are:

1. For the solution of plume-signal-interference problems, the author suggests that Figure 1 of this report and Ref. 4 be consulted carefully for the guidance they offer.
2. Hasty evaluations based on equilibrium chemical assumptions or on Figure 30 should be viewed and presented with caution.
3. The refraction model, A-II, is only a two-dimensional representation of a three-dimensional phenomenon; its true physical utility does not extend beyond defining input for the diffraction program B-II or for its listing of axially symmetric refractive index values based on mean plume properties. In practice, A-II is used as a Monte-Carlo technique with the density of input rays corresponding to the antenna pattern. Some ray trace paths may be fraught with error because of excessively large refractive index gradients, but these rays can be neglected if a large enough sample is taken. Such erroneous rays are indicated in the program output. An iterative technique to reduce bending angles would eliminate this problem.
4. The diffraction models of Appendix B are gross approximations and could be improved by modifications based on comparisons with data. Program B-II, in particular, warrants a more sophisticated treatment of some of the basic assumptions and probably a complete revamping.
5. Improved plume models should be used if and when they are available.
6. Use Appendix C as a guide to existing static attenuation data.
7. New attenuation test measurements should be carefully planned in view of the related operational problem and the difficulties that can occur in relating test data to other test or operational conditions. Will the planned test yield new and useful information?
8. The results of sample problems in this section indicate that even the results of sophisticated calculations must be suspect without good experimental verification. Always bear in mind that the calculation represents an average of microscopic spatial and temporal fluctuations and it is by no means certain that the plume calculations provide proper or consistent averages.

NWC TP 5319, Part 1

REFERENCES

1. Victor, A. C., and S. H. Breil. "A Decade of Rocket Plume Signal Interference Research (U)," *JANNAF 7th Plume Technology Meeting*, June 1973. (CPIA Publication no. 234, publication CONFIDENTIAL.)
2. Naval Weapons Center. *Plume-Signal Interference. Part 2. Plume-Induced Noise (U)*, by A. C. Victor. China Lake, Calif., NWC, May 1972. (NWC TP 5319, Part 2, publication CONFIDENTIAL.)
3. Martin Marietta. *Plume Technology Handbook*. Prepared on Contract AF F04611-73-C-0074 for the JANNAF Plume Technology Working Group. (Chapter 2. *Flow Fields*, by Milt Hetrick, is complete; other chapters in progress.)
4. Chemical Propulsion Information Agency. *Recommended Guidelines for Determining Flight Radar Attenuation*, by JANNAF Plume Technology Working Group, January 1971. (CPIA Publication no. 205.)
5. AeroChem Research Laboratories. *Prediction of Radar Attenuation in Typical Solid Propellant Rocket Exhausts (U)*, by H. S. Pergament, July 1965. (TP-116A, publication CONFIDENTIAL.)
6. ———. *Radar Attenuation in the Exhaust Plume of the Phoenix Missile (U)*, by H. S. Pergament, September 1965. (TP-116, publication CONFIDENTIAL.)
7. ———. *Radar Interference in the Exhaust Plume of the Condor Weapons System (U)*, by H. S. Pergament, September 1965. (TP-121, publication CONFIDENTIAL.)
8. Naval Weapons Center. *Microwave Interference Characteristics of a Solid Rocket Motor Exhaust (U)*, by A. C. Victor. China Lake, Calif., NWC, October 1968. (NWC TP 4199, publication CONFIDENTIAL.)
9. Smoot, L. D., and D. L. Underwood. "Prediction of Microwave Attenuation Characteristics of Rocket Exhausts," *J SPACECRAFT*, 3, No. 3. Pp. 302-309, March 1966.
10. Chemical Propulsion Information Agency. *4th ICRPG Plume-Signal Interference Symposium, 28-29 June 1966 (U)*, September 1966. (CPIA Publication no. 115, publication CONFIDENTIAL.)
11. Abramovich, G. N. *Theory of Turbulent Jets*. Cambridge, Mass., MIT Press, 1963.
12. Air Force Rocket Propulsion Laboratory. *A Fast Computer Program for Non-equilibrium Rocket Plume Predictions*, by R. R. Mikatarian, C. J. Kan, and H. S. Pergament. AeroChem Research Laboratories, August 1972. (AFRPL-TL-72-94.)

NWC TP 5319, Part 1

13. Naval Weapons Center. *Development and Evaluation of a Flight Attenuation Model. Final Report*, by L. D. Smoot, J. M. Simonsen, and P. O. Hedman. Brigham Young University, Utah. China Lake, Calif., NWC, November 1971. (NWC TP 5048.)
14. Hercules, Inc. *ABL Annual Research and Exploratory Development Report-1972. Volume I* (U). December 1972. Pp. 1-98. (A04022-101-07-004, DCN-N-26-12, publication CONFIDENTIAL.) Also see "Mach Disk Location in Jets in Co-flowing Air Streams," by F. I. Buckley. *AIAA Journal*, 13, (1975), p. 106.
15. Edelman, R. B., and G. Weilerstein. "A Solution of the Inviscid-Viscid Equations with Applications to Bonded and Unbonded Multicomponent, Reacting Flows," *AIAA 7th Aerospace Sciences Meeting*, New York, January 1969. (Paper 69-83.)
16. Libby, P. A. "Theoretical Analysis of Turbulent Mixing of Reactive Gases with Application to Supersonic Combustion of Hydrogen," *ARS J*, 32, (1962), p. 388.
17. National Aeronautics and Space Administration. *Free Turbulent Shear Flows. Volume I. Conference Proceedings*. NASA Langley Research Center, 1973. (NASA SP-321.)
18. Aerospace Corporation. *Proceedings of the Rocket Plume Phenomena Specialists Meeting. Volumes I and II* (U). 1 October 1968. (TOR-020(S4960-10, publication CONFIDENTIAL.)
19. Kliegel, J. R. "Ga Particle Nozzle Flows," *9th Symposium on Combustion*, Combustion Institute (1963).
20. Carlson, D. J., and R. F. Hoglund. "Particle Drag and Heat Transfer in Rocket Nozzles," *AIAA Journal*, 2, (1964), p. 1980.
21. Cruise, D. R. "Notes on the Rapid Computation of Chemical Equilibria," *J PHYS CHEM*, 68, (1964), p. 3797.
22. Interagency Chemical Rocket Propulsion Group. *ODE: ICRPG One-Dimensional Equilibrium Nozzle Analysis Computer Program*, published by Dynamic Science, July 1968.
23. Selph, C. *Thermochemical Program*, Rocket Propulsion Laboratory, Edwards Air Force Base, California.
24. Air Force Rocket Propulsion Laboratory. *Plume Contamination Effects Prediction - The CONTAM Program*, by R. J. Hoffman, W. D. English, R. G. Oeding and W. T. Webber. McDonnell Douglas Astronautics Co., December 1971. (AFRPL-TR-71-109); also see *The CONTAM Program - Version II*, August 1973 (AFRPL-TR-73-46).

NWC TP 5319, Part 1

25. Lockheed Propulsion Company. *Investigation of High Performance Solid Propellants with Favorable Attenuation Characteristics: Mechanisms Which Cause Radar Attenuation (U)*, by L. D. Smoot. January 1967. (LPC Report no. 756-F, publication CONFIDENTIAL.)
26. United Technology Corp. *Dynamics of Two-Phase Flowing Rocket Nozzles*, by M. Gilbert, R. Dunlap, C. T. Crowe, P. G. Willoughby, H. Wolff and M. Rogers. 1963 (UTC-2005-Q19.)
27. Interagency Chemical Rocket Propulsion Group. *ODK: ICRPG One-Dimensional Kinetic Nozzle Analysis Computer Program*, published by Dynamic Science, July 1968.
28. ———. *TDK: ICRPG Two-Dimensional Kinetic Nozzle Analysis Computer Program*, published by Dynamic Science, July 1968.
29. ———. *TDE: ICRPG Two-Dimensional Equilibrium Nozzle Analysis Computer Program*, published by Dynamic Science, July 1968.
30. ———. *TBL: ICRPG Turbulent Boundary Layer Nozzle Analysis Computer Program*, published by Dynamic Science, July 1965.
31. Myers, R. B. "Effect of Plume Signal Interference Specifications on Propulsion Tailoring Techniques (U)," *JANNAF 7th Solid Propellant Combustion Conference*, February 1971. (CPIA Publication no. 204, publication CONFIDENTIAL.)
32. Naval Weapons Center. *Development and Evaluation of an Improved Aft-Plume Model*, by L. D. Smoot, J. M. Simonsen and G. A. Williams. Brigham Young University, Utah. China Lake, Calif., NWC, November 1973. (NWC TP 5521.)
33. Lee, R. S., and W. W. Balwanz. "Ignition Points in a Rocket Exhaust," *JANNAF 5th Plume-Signal Interference Conference*, May 1969. (CPIA Publication no. 186.)
34. Brigham Young University. *Review and Analysis of Flight Data for Radar Attenuation Caused by Rocket Exhausts (U)*, by L. D. Smoot, P. O. Berrett, B. R. Potter, and J. M. Simonsen. Provo, Utah, BYU, February 1970. (BYU-010-F, publication CONFIDENTIAL.)
35. Beheim, M. A., J. L. Klann and R. A. Yeager. *Jet Effects on Annular Base Pressure and Temperature in a Supersonic Stream*. 1962. (NASA Technical Report R-125.)
36. ———. *Flows in the Base Region of Axisymmetric and Two-Dimensional Regions*. 1961. (NASA Technical Report R-77.)

NWC TP 5319, Part 1

37. Dixon, R. J., M. J. Richardson and R. H. Page. "Turbulent Base Flow on an Axisymmetric Body with a Single Exhaust Jet," *AIAA Fluid and Plasma Dynamics Conference*. June 1969. (Paper no. 69-650.)
38. Hedman, P. O., L. D. Smoot and J. M. Simonsen. "A Theoretical Model and Parametric Predictions of the Flow in the Base Region of a Rocket Powered Supersonic Missile," *JANNAF 6th Plume Technology Meeting*, April 1971. (CPIA Publication no. 209.)
39. U.S. Army Missile Command. *Analysis of the Axisymmetric Base-Pressure Problem and Base-Temperature Problem with Supersonic Interacting Freestream-Nozzle Flows Based on the Flow Model of Korst, et al. Part I. A Computer Program and Representative Results for Cylindrical Afterbodies*, by A. L. Addy. July 1969. (RD-TR-69-12.)
40. Baughman, L. E., and F. D. Kochenderfer. *Jet Effects on Base Pressure of Control Afterbodies at Mach 1.91 and 3.12*. August 1957. (NASA RME57E06.)
41. Love, E. S., C. E. Grigsby, L. T. Lee and M. J. Woodling. *Experimental and Theoretical Studies of Axisymmetric Free Jets*, 1959. (NASA TR R-6.)
42. Lewis, C. H., and D. J. Carlson, "Normal Shock Location in Underexpanded Gas and Gas-Particle Jets," *AIAA Journal*, 2, (1964), p. 776.
43. Eastman, D. W., and L. P. Radtke. "Location of the Normal Shock Wave in the Exhaust Plume of a Jet," *AIAA Journal*, 4, (1966), p. 918.
44. Wilcox, D. E., A. A. Weir, J. A. Nicholls and R. Dunlap. "Location of Mach Discs and Diamonds in Supersonic Air Tests," *J AERONAUTICAL SCIENCES*, 24, (1957), p. 150.
45. Bauer, A. B. "Normal Shock Location of Underexpanded Gas-Particle Jets," *AIAA Journal*, 3, (1965), p. 1187.
46. Buckley, F. T., and R. B. Myers. "Studies of Solid Rocket Exhaust Afterburning with a Finite Difference Equilibrium Chemistry Model," *JANNAF 6th Plume Technology Meeting*, April 1971. (CPIA Publication no. 209.)
47. Air Force Rocket Propulsion Laboratory. *A Study of Wind Tunnel Simulation of High Altitude Rocket Plumes*, by J. S. Draper and J. P. Moran. Aerodyne Research, Burlington, Mass., February 1973. (AFRPL-TR-72111.)
48. ———. *Predicted Plume Radar Characteristics for Various Air Launched Missiles (U)*, by W. J. Rothschild and D. J. Stanford. August 1973. (AFRPL-TR-72-122, publication CONFIDENTIAL.)

NWC TP 5319, Part 1

49. Rocket Propulsion Establishment. *A Simple Model of Radio Scattering in Rocket Exhaust Jets*, by H. Williams. August 1966. (RPE Technical Report no. 66/11.)
50. Dynamic Science. *Mixing and Combustion in a Fuel Rich Moderate Altitude Exhaust Plume*, by R. J. Hoffman and J. N. Levine. May 1967. (SN-93-3.)
51. Kelly, J. T. "Low/Mid-Altitude Two-Phase Plume Computational Technique Including Mixing and Nonequilibrium Chemistry," *JANNAF 7th Plume Technology Meeting*, June 1973. (CPIA Publication no. 234); also see "AeroChem Under-expanded Rocket Plume Program, Parts I and II," by J. T. Kelly and H. S. Pergament. November 1973. (AFRPL-TR-73-000.) and November 1974. (AFRPL-TR-74-59.)
52. Prozan, R. J. *Development of a Method-of-Characteristics Solution for Supersonic Flow of an Ideal, Frozen or Equilibrium Reacting Gas Mixture*. Lockheed Missiles and Space Company, Huntsville, Alabama, April 1966. (LMSC-HREC A782535.)
53. Smith, S. D., and A. W. Ratliff. *Rocket Exhaust Plume Computer Program Improvement. Vol. 1 - Final Report, User's Manual, Variable O/F Ratio Method of Characteristics Program for Nozzle and Plume Analysis*. Lockheed Missiles and Space Company, Huntsville, Alabama, June 1971. (LMSC-HREC D1662220-1, HREC-77611.)
54. Butler, H. W. *User's Manual, Description of a Digital Computer Program for Nozzle and Plume Analysis by the Method of Characteristics*. Lockheed Missiles and Space Company, Huntsville, Alabama, December 1966. (LMSC/HREC A783573, TM 54/20-108.)
55. Dynamic Science. *Gas Dynamics and Thermochemistry of Rocket Nozzle and Exhaust Plume Flows - Real Gas, Method of Characteristics Computer Program*, by R. J. Hoffman. August 1965. (DSC-TR-101.)
56. Stowell, D. E., and L. D. Smoot. *Master of Science Thesis*. Brigham Young University, Utah, May 1973. Also see "Summary of Recent Turbulent Mixing Measurements and Analysis," *JANNAF 7th Plume Technology Meeting*, June 1973. (CPIA Publication no. 234) or *AIAA/SAE 9th Propulsion Conference*, Las Vegas, Nevada, 5 November 1973. (Paper no. 73-1194) and *JANNAF 8th Plume Technology Meeting*, September 1974. (CPIA Publication no. 257.)
57. Naval Weapons Center. *A Computer Program for the Calculation of Microwave Attenuation in a Rocket Exhaust (U)* by R. W. Buecher and A. C. Victor. China Lake, Calif., NWC, October 1967. (NWC TP 4377, publication CONFIDENTIAL.)
58. ———. *An Analytical Approach to the Turbulent Mixing of Coaxial Jets*, by A. C. Victor and R. W. Buecher. China Lake, Calif., NWC, October 1966. (NWC TP 4070.)

NWC TP 5319, Part 1

59. McCarten, R. M. "Comparison of Experimental Data with Two Analytical Plume Prediction Techniques," *JANNAF 6th Plume Technology Meeting*, April 1971. (CPIA Publication no. 209.)
60. Donaldson, C. P., and K. E. Gray. "Theoretical and Experimental Investigation of the Compressible Free Mixing of Two Dissimilar Gases," *AIAA Aerothermochemistry of Turbulent Flows Conference*, December 1965. (AIAA Paper 65-822.)
61. Webb, J. K., and L. D. Smoot. "Comparison of Rocket Exhaust Plume Microwave Attenuation Prediction Models," *JANNAF 7th Plume Technology Meeting*, June 1973. (CPIA Publication no. 234.)
62. Buckley, F. T., and G. M. Williams. "The Prediction of Turbulent Mixing in Moderately Underexpanded Exhaust Plumes; Bulletin of the First Meeting," *TTCP/D-5 Plume Technology Working Group*, Naval Weapons Center, March 1972. (NWC Reg. 4535-100-72.)
63. Smoot, L. D. "Review and Analysis of Flight Attenuation Data (U)," *JANNAF 6th Plume Technology Meeting*, March 1972. (CPIA Publication no. 209, publication CONFIDENTIAL.)
64. Tuffs, L. W., and L. D. Smoot. "A Turbulent Mixing Coefficient Correlation for Coaxial Jets With and Without Secondary Flows," *J SPACECRAFT ROCKETS*, 8, (1971), p. 1183.
65. Arnold Air Force Station. *Free Turbulent Mixing: A Critical Evaluation of Theory and Experiment*, by D. T. Harsha. February 1971. (AEDC-TR-71-36.)
66. Moretti, G. A. "New Technique for the Numerical Analysis of Non-Equilibrium Flows," *AIAA Journal*, 3, (1965), p. 223.
67. Wilson, A. S. "Modeling of Chemically-Reacting Turbulent Plumes," *JANNAF 7th Plume Technology Meeting*, June 1973. (CPIA Publication no. 234.)
68. Rocket Propulsion Establishment. *Gas-Phase Reaction Rate Coefficients for Rocketry Applications*, by D. E. Jensen and G. A. Jones. October 1971. (RPE Technical Report no. 71/9.)
69. Naval Weapons Center. *A Theoretical Study of Rocket Exhaust Plume Radar Reflectivity (U)*, by S. H. Breil and A. C. Victor. China Lake, Calif., NWC, August 1968. (NWC TP 4320, publication CONFIDENTIAL.)
70. AeroChem Research Laboratories. *Radar Cross Section of Turbulent Rocket Exhaust Plumes. Final Report. Vol. I and II (U)*, by H. S. Pergement. Princeton, N. J., January 1970. (AeroChem TP-228, publication CONFIDENTIAL.)

NWC TP 5319, Part 1

71. Air Force Rocket Propulsion Laboratory. *Radar Reflectivity of Turbulent Rocket Exhaust Plumes (U)*, by H. S. Pergament, S. Birnbaum and R. R. Mikatarian. AeroChem Research Laboratories, Princeton, N. J., December 1967. (AFRPL-TR-67-251, DDC AD-338 832, publication CONFIDENTIAL.)
72. Draper, J. S., P. O. Jarvinen and T. D. Conley. "Analysis of Radar Return from Turbulent High Altitude Rocket Exhaust Plumes," *AIAA Journal*, 8, (September 1970), p. 1568.
73. Air Force Rocket Propulsion Laboratory. *A Computer Program to Predict Radar Cross Section of Rocket Exhaust Plumes*, by H. S. Pergament and R. J. Wasneski. AeroChem Research Laboratories, Princeton, N. J., August 1969. (AFRPL-TR-69-182.)
74. Patankar, S. V., and D. B. Spalding. *Heat and Mass Transfer in Boundary Layers*, 2nd ed. London, England, Intertext Books, 1970.
75. Spalding, D. B., Imperial College, Department of Mechanical Engineering, 1970. (Report BBL/TN/A/35.)
76. ———. Imperial College, Department of Mechanical Engineering, 1969. (Report EF/TN/A/16.)
77. ———. "A Two Equation Model of Turbulence," *VDI FORSCHUNGSHEFT*, 5, (1972), p. 549.
78. Naval Weapons Center. *Low Radar Attenuation Propellants - Principles of Formulation (U)*, by A. C. Victor. China Lake, Calif., NWC, June 1967. (NWC TP 4311, publication CONFIDENTIAL.)
79. Jensen, D. E. "Chemistry of Ionization in Rocket Exhaust Plumes (U)," *Proceedings of Rocket Plume Phenomena Specialists Meeting*, AeroSpace Corp., 1 October 1968. (TOR-0200(S4960-10, Vol. I); or AeroChem TP-173. (publication CONFIDENTIAL.)
80. ———. "Chemical Controls on Electro Magnetic Properties of Rocket Exhaust Plumes (U)," *JANNAF 6th Plume Technology Meeting*, April 1971. (CPIA Publication no. 209, publication CONFIDENTIAL.)
81. Pergament, H. S. "Prediction of the Effects of Molybdenum Additives on Rocket Exhaust Plume Electron Concentrations (U)," *Bulletin of TTCP Plume Technology Working Group Meeting*. China Lake, Calif., NWC, March 1972. (NWC Reg. 4535-100-72); or AeroChem, November 1971. (TP-271 and Addendum, publication CONFIDENTIAL.)

82. Fleischer, D., V. J. Siminski and W. R. Kineyko. "The Effects of Additives on Microwave Attenuation in Rocket Plumes at Simulated Altitude Conditions (U)," *4th ICRPG Plume-Signal Interference Symposium*, September 1966. (CPIA Publication no. 115, publication CONFIDENTIAL.)
83. Breil, S. H., A. C. Victor and D. L. Harp. "Radar Attenuation Measurements on Liquid and Slurry Propellants (U)," *JANNAF 5th Plume-Signal Interference Conference*, May 1969. (CPIA Publication no. 186, publication CONFIDENTIAL.)
84. Jensen, D. E. "Free Radicals and Secondary Combustion in Rocket Exhaust Plumes," *Bulletin of TTCP Plume Technology Working Group Meeting*. Naval Weapons Center, China Lake, Calif., March 1972. (NWC Reg. 4535-100-72.)
85. Calcote, H. F., and S. C. Kurzius. "Mechanisms by Which Chemical Additives Alleviate Radar Interference Effects in Rocket Exhausts (U)," *4th ICRPG Plume-Signal Interference Symposium*, September 1966. (CPIA Publication no. 115, publication CONFIDENTIAL.)
86. Hasserjian, G., and G. A. Clark. "Interaction of Electromagnetic Waves With the Exhaust Flame of Launch Vehicles," in *Proceedings of the Third Symposium on the Plasma Sheath, Vol. III*, May 1967, Air Force Cambridge Research Laboratories. (AFCRL-67-0280, Vol. III.)
87. Boeing Company. *Saturn Plume Effects on Radio Transmission, Computer Program, AS2229*, by G. A. Clark and G. Hasserjian. (Code Ident No. 81205, Number D5-111418-4/5/6.)
88. Krzycki, L. J., H. M. Larsen and W. M. Byrne, Jr. "Magneto Hydrodynamic Power Generation from a Supersonic Rocket Exhaust," *Physico-chemical Diagnostics of Plasmas*, Evanston, Ill., Northwestern University Press, 1963.
89. Space Technology Laboratories. *The Electromagnetics of the Rocket Exhaust (U)*, by S. Altshuler, M. M. Moe, and P. Molmud. June 1958. (GM-TR-0165-00397.)
90. Altshuler, S. *PHYS REV*, 107, (1957), p. 114.
91. Naval Ordnance Test Station. *Radar Attenuation Characteristics of Propellant Exhaust Gases (U)*, by A. C. Victor, D. L. Harp and H. M. Larsen. China Lake, Calif., NOTS, May 1967. (NOTS TP 3892, publication CONFIDENTIAL.)
92. ———. *A Solution of the Complex Dielectric Equations for Rocket Exhaust Microwave Interferometry*, by L. J. Krzycki and C. H. Turner. China Lake, Calif., NOTS, January 1964. (NOTS TP 3332.)
93. Naval Research Laboratory. *Interaction Between Electromagnetic Waves and Flames. Part 6. Theoretical Plots of Absorption, Phase Shift and Reflection*, by W. W. Balwanz. Washington, D.C., September 1959. (NRL Report 5388.)

NWC TP 5319, Part 1

94. Naval Weapons Center. *Interaction of Focused Microwave Radiation with a Rocket Exhaust*, by A. C. Victor and J. C. Mantz. China Lake, Calif., NWC, February 1972. (NWC TP 5119.)
95. Epstein, P. S. "Geometrical Optics in Absorbing Media," *PROC NAS*, 16, (1930), p. 37.
96. Kerr, D. G. *Propagation of Short Radio Waves*, New York, McGraw Hill, 1951.
97. Cashen, J. F., G. Kimura and R. R. Gold. "Prediction of Attenuation and Multipath in Underdense Rocket Plumes," in *Proceedings of the Rocket Plume Phenomena Specialists Meeting*, AeroSpace Corporation, October 1968. (TOR-0200(S4960.10.))
98. Naval Weapons Center. *Computer Program for Calculating RF Refraction*, by R. G. LaCombe. China Lake, Calif., NWC, December 1970. (NWC Reg. 4535-65-71.)
99. Lockheed Propulsion Company. *The Influence of Aspect Angle and Antenna Pattern on X-Band AM/PM Noise and Attenuation (U)*, by W. F. Fuller and J. W. Williams. June 1970. (LPC Report No. 366-F, publication CONFIDENTIAL.)
100. Lockheed Missile and Space Division. *General Research in Diffraction Theory. Vol. 1 and 2*, by N. A. Logan. December 1959. (LMSD 288089 and 288088; DDC AD-241228 and AD-243182.)
101. Air Force Cambridge Research Laboratories. *Numerical Investigation of Electromagnetic Scattering and Diffraction by Convex Objects*, by N. A. Logan. December 1965. (AFRCL-66-153.)
102. Jenkins, F. A., and H. E. White. *Fundamentals of Optics*. 3rd ed. New York, McGraw Hill, 1957.
103. Born, M., and E. Wolf. *Principles of Optics*. 3rd ed. Pergamon Press, 1965.
104. Sommerfeld, A. *Optics*, Academic Press, 1967.
105. Aerospace Corporation. *Diffraction by Rocket Exhausts*, by K. E. Golden, E. C. Taylor and F. A. Vicente. May 1967. (Aerospace Report No. TR-1001(2220-10)-5.)
106. Vicente, F. A., E. C. Taylor and R. W. Phelps. "Analysis of Flame Effects on Measured Electromagnetic Propagation Data," *J SPACECRAFT*, 4, (August 1967), p. 1069.
107. Golden, K. E., E. C. Taylor and F. A. Vicente. "Diffraction by Rocket Exhausts," *IEEE Transactions, Antennas and Propagation*, September 1968, p. 614.

NWC TP 5319, Part 1

108. Cashen, J. F., J. G. Seubold and R. R. Gold. "Voyager-RADVS-Exhaust Plume Interference," in *Proceedings of the 5th Space Congress*, Cape Kennedy, December 1968.
109. Naval Weapons Center. *Preliminary Report on Radar Diffraction Calculations for Highly Absorbent Rocket Exhausts (U)*, by A. C. Victor. China Lake, Calif., NWC, June 1970. (NWC Reg. 4535-211-70, publication CONFIDENTIAL.)
110. Ufimtev, P. Ia. J TECH PHYS (USSR), 27, (1957), p. 1708 and 28, (1958), p. 2386.
111. Walters, L. C., and J. R. Wait. *Computation of a Modified Fresnel Integral Arising in the Theory of Diffraction by a Variable Screen*, 1964. (NBS Technical Note no. 224.)
112. Webb, J. K. "Exhaust Plume Radar Attenuation Measurements on 15K to 45K Thrust Motors (U)," *JANNAF 8th Plume Technology Meeting*, 23-25 July 1974. (CPIA Publication no. 257, publication CONFIDENTIAL.)
113. Naval Research Laboratory. *Estimating the Diameter of the Plasma in a Propulsion Motor Plume*, by J. P. Weston. Washington, D.C., NRL, 22 May 1969. (NRL Report 6872.)
114. Chemical Propulsion Information Agency. "Experimental and Analytical Studies of Microwave Attenuation and Modulation by Rocket Exhaust Plumes (U)," by A. C. Victor, D. L. Harp and H. M. Larsen, *4th ICRPG Plume-Signal Interference Symposium*, 28-29 June 1966, September 1966. (CPIA Publication no. 115, publication CONFIDENTIAL.)
115. Naval Weapons Center. *Radar Attenuation Characteristics of Propellant Exhaust Gases (U)*, by A. C. Victor, D. L. Harp and H. M. Larsen. China Lake, Calif., NOTS, May 1967. (NOTS TP 3892 (NAVWEPS Report 8791), publication CONFIDENTIAL.)
116. Lockheed Propulsion Company. *Influences of the Flight Environment and Propellant Additive Form on Radar Interference Caused by Rocket Motor Exhausts (U)*, by P. O. Hedman and L. D. Smoot. Redlands, Calif., LPC, February 1969. (LPC Report No. 915-F, publication CONFIDENTIAL.)
117. Ordnance Aerophysics Laboratory. *Radio Frequency Attenuation of Solid Propellant Rocket Motors, in the Blowdown Facility, for the Naval Air Systems Command (U)*, by J. D. Means. Daingerfield, Texas, OAL, December 1968. (OAL Report 701-6, publication CONFIDENTIAL.)
118. AeroChem Research Laboratories. *Radio Frequency Modulation in Turbulent Rocket Exhaust Plume (U)*, by R. R. Mikatarian. Princeton, N. J., July 1969. (AeroChem TP-212, publication CONFIDENTIAL.)

NWC TP 5319, Part 1

119. Heald, M. A., and C. B. Warton. *Plasma Diagnostics with Microwaves*. New York, John Wiley and Sons, 1965. Pp. 150-154.
120. Marquedant, R., C. M. Knop and H. Hodara. "Performance of Digital Signals Through Plasmas," *IEEE Transactions on Communication Systems*, March 1964. (Vol. CS-12, Number 1.)
121. Lockheed Aircraft Corporation. *Calculations of Ground-Space Propagation Effects*, by V. A. Counter and E. P. Riedel. Sunnyvale, Calif., May 1958. (LMSD 2461.)
122. Elliott, R. S. "Pulse Waveform Degradation Due to Dispersion in Waveguides," *IRE Transactions on Microwave Theory and Techniques*, October 1957. Pp. 254-257. (Vol. MTT-5.)
123. Naval Weapons Center. *Pulse Distortion by a Rocket Exhaust Plume*, by S. H. Breil. China Lake, Calif., NWC, 11 December 1972. (NWC Reg. 4535-065-73.)
124. AeroChem Research Laboratories. *Radar Attenuation in Advanced Propellant Systems (U)*, by H. F. Calcote, H. S. Pergament and H. Silla. Princeton, N. J., December 1964. (AeroChem TP-106, publication CONFIDENTIAL.)
125. Breil, S. H., and A. C. Victor. "A Technique for Simulating Flight Attenuation at Sea Level Static Conditions (U)," *JANNAF 6th Plume Technology Meeting*, April 1971. (CPIA Publication no. 209, publication CONFIDENTIAL.)
126. Naval Research Laboratory. *Simulation Testing on Propellants (U)*, by W. W. Balwanz. Washington, D.C., 8 October 1968. (NRL Report 5110-244, publication CONFIDENTIAL.)
127. Royal Aircraft Establishment. *X-Band Radio Attenuation and Modulation Measurements on a 17-Inch Solid Propellant Rocket Motor (U)*, by L. A. Kerridge. Westcott, England, September 1955. (Tech. Note RPD-126, publication CONFIDENTIAL.) (Activity name changed to Rocket Propulsion Establishment)
128. Bureau of Ordnance, Department of the Navy. *Radar Signal Attenuation in Terrier Missiles Due to Sustainer Afterburning*, by A. Graps. Washington, D.C., September 1958. (NAVORD Report 6477.)
129. Rohm and Haas. *Radar Attenuation by Solid Propellant Rocket Exhaust (U)*, by W. A. Wood. September 1965. (Report No. S-78, publication CONFIDENTIAL.)
130. Webb, J. K., and L. D. Smeot. "Comparison of Rocket Exhaust Plume Microwave Attenuation Models," *Bulletin of TTCP Plume Technology Working Group Meeting*, Naval Weapons Center, China Lake, Calif., March 1972. (NWC Reg. 4535-100-72.)

NWC TP 5319, Part 1

131. Lockheed Propulsion Company. *Exhaust Plume Microwave Interference Data Summary* (U). Redlands, Calif., LPC, September 1969. (LPC Doc. No. 4218-6-4965, publication CONFIDENTIAL.)
132. Balwanz, W. W., and J. R. Boller. "Properties of Plumes from Small Motors Using Poseidon Type Propellants (U)," *JANNAF 5th Plume-Signal Interference Conference*, May 1969. (CPIA Publication no. 186, publication CONFIDENTIAL.)
133. Lockheed Propulsion Company. *The Influence of Aspect Angle and Antenna Pattern on X-Band AM/PM Noise and Attenuation* (U), by W. F. Fuller and J. W. Williams. Redlands, Calif., LPC, June 1968. (LPC Report No. 366-F, publication CONFIDENTIAL.)
134. Hercules, Inc. *Plume Interference Investigations* (U), (ABL Test Summary for OAL 701-6), by R. B. Myers and R. D. Hartsock. July 1970. (ABL-TR-70-26, publication CONFIDENTIAL.)
135. Hedman, P.O., L. S. Smoot and H. Simonsen. "Effect of Flight Environment on Exhaust Plume Radar Attenuation (U)," *JANNAF 5th Plume-Signal Interference Conference*, May 1969. (CPIA Publication no. 186, publication CONFIDENTIAL.)
136. Arnold Engineering Development Center. *Attenuation of Microwaves Transmitted Through the Exhaust Plumes of Solid Propellant Rocket Motors Operating in a Simulated Flight Environment of Mach Numbers 0.38, 2.0 and 3.0*, by C. R. Darlington, L. R. Bahr and J. A. Sprouse. ARO, Inc., February 1972. (AEDC-TR-71-259.)
137. Ordnance Aero Physics Laboratory. *Microwave Attenuation Characteristics of Solid Propellant Rocket Exhaust Plumes for the Naval Air Systems Command* (U), by J. D. Means. 14 August 1968. (OAL Report 746, Vol. I, publication CONFIDENTIAL.)
138. Air Force Eastern Test Range. *Rocket Exhaust Plume Interference Problems, Current Status* (U), by H. A. Poehler. July 1969. (ETR-TR-69-4, Vol. I, publication CONFIDENTIAL.)
139. ———. *Rocket Exhaust Signal Attenuation and Degradation, Final Report, Vol. I*, by H. A. Poehler. July 1969. (ETR-TR-8.)
140. ———. *Rocket Exhaust Signal Attenuation and Degradation, Final Report, Vol. II*, by H. A. Poehler. July 1969. (ETR-TR-69-4, Vol. II.) (Collection of unclassified AFETR rocket exhaust signal attenuation and degradation reports)
141. Poehler, H. A. "Attenuation Predictions from Exhaust Plume Models," *J SPACE-CRAFT*, 6, No. 9 (September 1969), p. 1057.

NWC TP 5319, Part 1

142. Applied Physics Laboratory/Johns Hopkins University. *In-Flight Flame Attenuation Measurements on the Terrier II STV-5*, by H. D. Zink, Jr. Silver Spring, Maryland, August 1955. (APL/JHU CF-2417.)
143. AeroChem Research Laboratory. *Radar Attenuation Calculations and Comparisons with Flight Data for Solid Propellant Rocket Exhaust Plumes* (U), by R. R. Mikatarian and H. S. Pergament. October 1968. (AeroChem TP-185, publication CONFIDENTIAL.)
144. Naval Weapons Center. *Speculations on the Radar Attenuation Observed During Two Flight Tests* (U), by A. C. Victor and S. H. Breil. China Lake, Calif., NWC, 1969. (NWC Reg. 4535-198-69, publication CONFIDENTIAL.)
145. Smoot, L. D., and P. O. Hedman. "Recent Research on Propellant Additives as Electron Suppressants (U)," *JANNAF 5th Plume-Signal Interference Conference*, May 1969. (CPIA Publication no. 186, publication CONFIDENTIAL.)
146. Hercules, Inc. *Allegany Ballistics Laboratory Annual Supporting Research Reports* (U). (publications CONFIDENTIAL.)
- | | |
|------------------------------|------------------------------|
| February 1965 (ABL/X-134) | December 1969 (ABL-TR-69-29) |
| February 1967 (ABL-TR-67-2) | December 1970 (ABL-TR-70-41) |
| February 1968 (ABL-TR-68-4) | December 1971 (ABL-TR-71) |
| December 1968 (ABL-TR-68-38) | December 1972 (DNC-N-26-12) |
147. Air Force Rocket Propulsion Laboratory. *Radar Attenuation Measurements of Selected Solid Propellant and the Effect of Additives*, by L. G. Altman, S. B. Thompson, and P. C. Sukanels. May 1973. (AFRPL TR-73-29.)
148. Air Force Rocket Propulsion Laboratory. *The Rocket Exhaust Plume Radar Cross Section at Low Altitudes* (U), by J. S. Draper, et al. Aerodyne Research, Inc., Burlington, Mass., June 1974. (AFRPL-TR-74-12, publication SECRET.)

NWC TP 5319, Part 1

Appendix A

(b)(4)

NWC TP 5319, Part 1

(b)(4)

NWC TP 5319, Part 1

(b)(4)

(b)(4)

NWC TP 5319, Part 1

(b)(4)

NWC TP 5319. Part 1

(b)(4)

NWC TP 5319, Par 1

(b)(4)

NWC TP 5319, Part 1

(b)(4)

NWC TP 5319, Part 1

Appendix B

DIAGONAL DIFFRACTION COMPUTER PROGRAMS

This appendix presents two computer programs for predicting microwave diffraction by rocket exhaust plumes. The program B-I is designed for use with output from a line-of-sight attenuation program (A-I) and contains corrections (fudge factors) to adjust it for scale effects (see Section 3.3). Program B-II is intended for use with output from a ray trace attenuation program (A-II). B-II has no "fudge" factors and uses the ray at the limiting refracted angle (Figure A-2) as the diffracted ray. Results of programs B-I and B-II are compared in Figure B-1 for the plume discussed in Figure A-1. Another comparison is shown in Figure 78.

Diffraction Program B-I

1. Run a diagonal line of sight attenuation calculation (A-I) for the plume of interest. Note the following parameters:

- a. Maximum diagonal attenuation (ATMAX), dB
- b. Aspect angle of maximum attenuation (SHIFT), degrees (see Section 3.3)
- c. Attenuation at an aspect angle twice the size of the angle in b, (ATTEN), dB
- d. Aspect angle of ray attenuated by 3 dB, degrees

2. Set up a scale drawing of the plume as in Figure 40 (main text). Locate the antenna.

- a. Draw a line at the angle obtained in 1.b to intersect the plume axis (SHIFT), or determine shift from Figure 43.
- b. Draw a line (dashed) from the antenna at the aspect angle of 3-dB attenuation (determined in 1.d).
- c. The perpendicular line (heavy) from the intersection of the first line (formed by the angle SHIFT) to the second line (3-dB projection) is the half-width of the diffracting edge axis called "HTA" in the program.

3. Input to the program is entered in the following order. There are 10 input variables.

THRUST, lbs	- motor thrust
HTA, cm	- half-widths of equivalent diffraction strip for plane B (see Figures 37 and 40, or Section 3.3.)
ATTEN, dB	- (negative number); predicted attenuation at aspect angle of $2 \times$ SHIFT. No need to ever make it larger than -20.

NWC TP 5319, Part 1

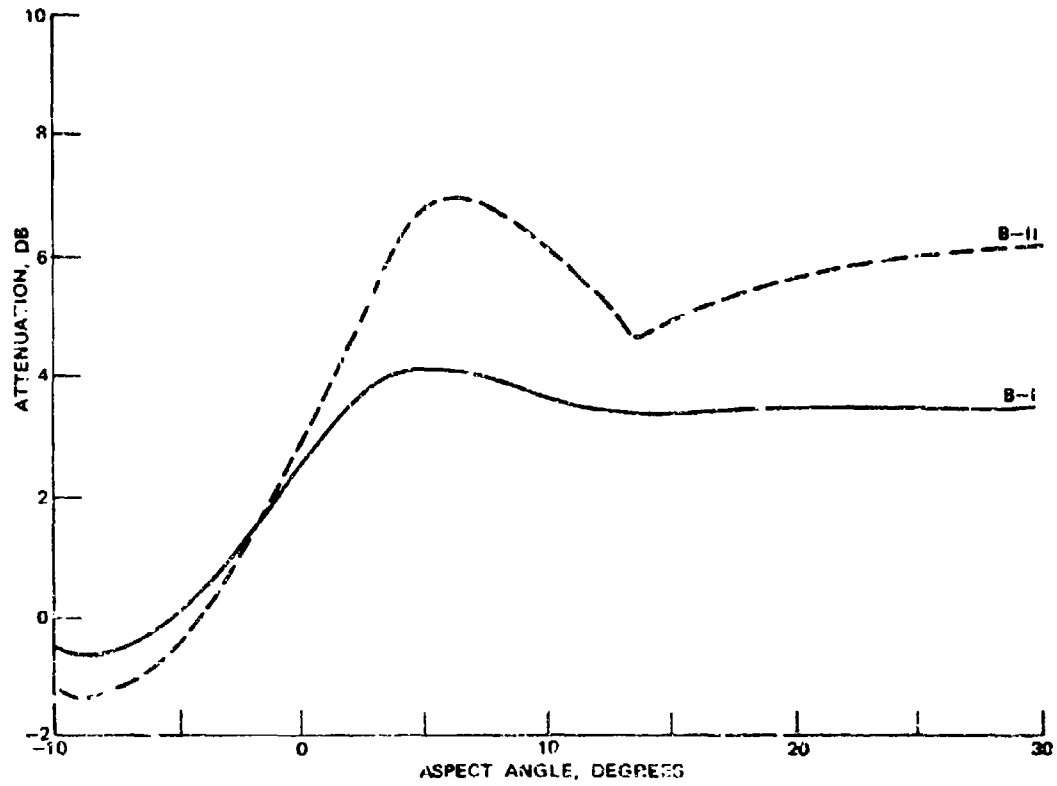


FIGURE B-1. Comparison of Diffraction Computer Programs B-I and B-II.

NWC TP 5319, Part 1

DIST, cm - distance along x axis from exit plane to HTA (See Figures 37 and 40, or Section 3.3.)

AL, cm - distance from plume axis to antenna location along z axis.

WAVEL, cm - wavelength of radiation (X-band = 3 cm).

SHIFT, degrees - angle defined in Figures 40 or 43. This is equivalent to the shift from an axially mounted transmitting antenna.

HT1, cm - nozzle exit radius.

ANTE, cm - effective radius (in y direction) of exit plane antenna.

ATMAX, dB - (positive number); maximum diagonal attenuation predicted by SUPEP, occurs at aspect angle SHIFT.

Input format is (8F10.0). User instructions for program B-I follow.

LISTING OF DIFFRACTION COMPUTER PROGRAM B-I WITH SAMPLE INPUT

```

*PUN 412000.145321070050.4514.1.100/3 . 41452 1245 . DIFFRACTION B-I
-FCR.I .MAIN
*****DIFFRACTION PROGRAM B-I
LVDEF
10 READ 9000,THRUST,HTA,ATTEN,DTST,AL,WAVEL,SHIFT,HT1,ANTE,ATMAX
PRINT 9010
DELTA=1.0
X1=0.
K2=DTST
X3=2.*DIST
HT2=HTA
HT3=0.
THEM=30.
ANG=THEM
THETA=ANG-SHIFT
DTSTA=DTST
HW=ATAN(HTA/DTSTA)
HW=ABS(HW)
BEE1=.01
REE=ATAN(BEE1/DTSTA)
REE=ABS(REE)
SPECT=BEE1
DO 90 I=1,50
THETA=.01745*THETA
B=100000.
FI2=HW-THETA
FI2=SIN(FI2)
FI1=HW+THETA
FI1=SIN(FI1)
TAP=(2.*(B+DIST)/E/DTSTA/WAVEL)

```

NWC TP 5319, Part 1

```

TAP=ABS(TAP)
FAC=DTSTA*SQRT(TAP)
BEEP=FAC*BEE
BEEPT=1./BEEP
V1=FAC*F11
V2=FAC*F12
CALL FRENEL(V1,CZ,SZ)
AV1R=.707*(CZ-.5)
AV1I=.707*(CZ+.5)
CALL FRENEL(V2,C6,S6)
AV2R=.707*(C6-.5)*(10.)*(ATTEN/13.)
AV2I=.707*(C6+.5)*(10.)*(ATTEN/10.)
CRUD=AV1I+AV2I
CRUDD=CRUD**2
CLUD=AV1R+AV2R
CLUDD=CLUD**2
STRAY=CLUDD+CRUD)
THETA=THETA/.01745
ANG=THETA+SHIFT
ANGLE=ANG
ANG=.01745*ANG
BETA=1.571-ANG
CAY=AL/COS(BETA)
CAY=ABS(CAY)
Y=AL*TAN(BETA)
X=ABS(X)
HWY=ANG/.01745
HY=SHIFT+HW/.01745
TRY=SHIFT-HW/.01745
IF (HWY-HY) 20,20,30
20 HWY=HW
FFA1=FFRAY
CAY=DTSTA
IF (HWY-TRY) 60,60,40
30 CALL EX2(X,HT,X1,X2,X3,HFL,HT2,HT3)
HAT=HT-ANTE
HAY=ASIN(HAT/CAY)
HAY=ABS(HAY)
40 TOT=(2.+(B+CAY)/3/CAY/WAVEL)
TOT=ABS(TOT)
FACE=CAY*SOPT(TOT)
SBEE=ATAN(SBEE/CAY)
SBEE=ABS(SBEE)
SBEEP=FACE*SBEE
SBEEPT=1./SBEEP
V3=FACE*HAY
CALL FU27(VT,SBEEPT,C1,S1)
AV3R=.707*(C1-.5)
AV3I=.707*(C1+.5)
G=2.*AV3R

```

NWC TP 5319, Part 1

```

3SQ=3*3
CA=AV3I*2.
3ASQ=3A*3A
R1=CSQ+CASQ
FFA1=FFRAT*31
IF(MHY-HY)50,50,EC
50 HAPY=HW/.01745
FFA1=R1*(ANGLE-TRY)/2./HAPY+FFRAT*(HY-ANELE)/2./HAPY
60 DIF1=.43439*ALOG(FFA1)
ATFAC=.43439*ALOG(ATMAX)/2.
ATFAC=.43439*ATFAC*ALOG(T4RUST)/3.
DIF1=DIF1*ATFAC
ANG=ANG/.01745
HW=HW/.01745
IF(LV-50)80,70,71
70 LV=0
90 PRINT 9070,ANG,DIF1
THETA=THETA-DELTHE
LV=LV+1
HW=.01745*HW
90 CONTINUE
GO TO 10
9080 FORMAT(8F10.0)
*010 FORMAT(*1PREDICTED ATTENUATION ASSUMING DIFFRACTION EM// * ROCKIT E
1X4AUST PLUME USING FTN PROGRAM ATFIN COMPILED ON DIFFRA.*/ ** ASP
2ECT ANGLE ATTENUATION*/
9020 FORMAT(1X,2F12.2)
END
*FOR,I ,FRENEL
SUBROUTINE FRENEL (X,C,S)
SV=X
X=ABS(X)
F=(1.+ .926*X)/(2.+1.792*X+3.138*X**2)
G=1./(2.+4.142*X+3.492*X**2+E.67*X**3)
U=3.14159*X**2/2.
C=.5+F*SIN(U)-G*COS(U)
S=.5-F*COS(U)-G*SIN(U)
IF(SV)10,20,20
13 C=-C
S=-S
20 RETURN
END
*FOR,I ,FUZZ
SUBROUTINE FUZZ(ZC,E,FREAL,FIM)
Z2=Z0+1./B
Z1=Z0-1./B
Z2SQ=.5*3.1416*(Z2**2)
Z1SQ=.5*3.1416*(Z1**2)
CALL FRENEL (Z2,C2,S2)
CALL FRENEL (Z1,C1,S1)

```

NWC TP 5319, Part 1

```

REAL=-.5*(C2*CL)-.5*B*73*(C2-CL)+.5*(3/3.1415)*(SIN(7152)-
1 SIN(7150))+.5
REAL=REAL-.5
REAL=-REAL
FIM=.5*(S2+S1)-.5*B*Z0*(S1-S2)+.5*(3/3.1415)*(COS(2257)-COS(2150))
1 -.5
FIM=FIM+.5
RETURN
END
#FOR,I ,EX2
SUBROUTINE EX2(X,HT,X1,V2,K3,HT1,HT2,HT3)
A=HT1
C=(X2-X3)/(X1-X2)
C=(C*(HT1-HT2)-(HT2-HT3))/(C*(X1**2-X2**2)-(X2**2-X3**2))
B=(HT2-A-C*X2**2)/X2
HT=A+B*X+C*X**2
RETURN
END
#MAP,IN
#YOT
300.      8.9      -25.      83.      10.      3.      7.      2.
C.        53.
#FIN
#FIN

```

DIFFRACTION COMPUTER PROGRAM 1-1 SAMPLE OUTPUT

PREDICTED ATTENUATION ASSUMING DIFFRACTION BY
ROCKET EXHAUST PLUME USING FTN PROGRAM ATTFIN COMPILED ON DIFFRA.

ASPECT ANGLE	ATTENUATION
30.00	-3.29
29.00	-3.29
28.00	-3.29
27.00	-3.30
26.00	-3.32
25.00	-3.33
24.00	-3.33
23.00	-3.33
22.00	-3.34
21.00	-3.34
20.00	-3.35
19.00	-3.36
18.00	-3.35
17.00	-3.34
16.00	-3.33

NWC TP 5319, Part 1

15.00	-3.32
14.00	-3.31
13.00	-3.09
12.00	-3.25
11.00	-3.41
10.00	-3.58
9.00	-3.75
8.00	-3.90
7.00	-4.04
6.00	-4.12
5.00	-4.13
4.00	-4.03
3.00	-3.79
2.00	-3.42
1.00	-2.92
-.00	-2.39
-1.00	-1.97
-2.00	-1.35
-3.00	-.87
-4.00	-.43
-5.00	-.04
-6.00	.27
-7.00	.50
-8.00	.63
-9.00	.64
-10.00	.51
-11.00	.24
-12.00	-.12
-13.00	-.44
-14.00	-.51
-15.00	-.26
-16.00	.11
-17.00	.35

Diffraction Program B-II

This program is best understood by reference to Figure A-2. Its applicability is based on the assumption that the ray bending predicted by computer program A-II defines the effective diffracting edge. The "limiting refraction angle" is also defined as the incident angle of the diffracted ray. Regions of greatest electron density (as evidenced by maximum refractive index gradients) are used to define the x distance from the antenna to the diffracting edge (DIST). Refraction of the limiting ray is assumed to change the effective antenna location (EFAT shown in Figure A-1). At this stage the program is crude and has not been checked extensively. (See problem solution in Section 5.0 of the main text.) However, it is believed that with some exercise, it can become more flexible than program B-I.

If needed changes to the program become apparent to the user, they should be made.

1. Run a diagonal ray-trace attenuation calculation (A-II) for the plume of interest. Note the following parameters:

- a. Limiting angle of refracted ray (HW), degrees
- b. Aspect angle, zeta, of first ray crossing the plume axis, reconvergent angle (ESHIF), degrees
- c. Attenuation at an angle equal to $(2 \times \text{ESHIF})$ ATTEN, dB
- d. Y axis intercept of limiting refracted ray (EFAT), cm
- e. Value of x after limiting ray undergoes major angle changes (DIST), cm
- f. Value of y after limiting ray undergoes major angle changes (HTA), cm
- g. Value of y where attenuation coefficient $\alpha = \frac{\tan(2 \times \text{ESHIF})}{0.3 \times \text{HTA}}$, at x = DIST, HT2, cm
- h. Value of y where attenuation coefficient $\alpha = \frac{\tan(2 \times \text{ESHIF})}{\text{HTA}}$, at x = DIST, ATH, cm

2. Input to the program is entered in the following order:

HTA, cm	see 1f.
ATTEN, dB	see 1c. (always input as a negative number or zero)
EFAT, cm	see 1d.
DIST, cm	see 1e.
AL, cm	distance from plume axis to antenna location on y axis
WAVEL, cm	wavelength of radiation (X-band = 3 cm)
ESHIF, deg	see 1b.
HT1, cm	nozzle exit radius

NWC TP 5319, Part 1

ANTE, cm effective radius of exit plane antenna
 HT2, cm see 1g.)
 ATH, cm see 1h.) These variables affect use of subroutine FUZZ

Input format is (8F10.0). User instructions for program B-II follow.

LISTING OF DIFFRACTION COMPUTER PROGRAM B-II WITH SAMPLE INPUT

```

*RUN *12011,145021070050,4514112,1,10070 . / ICF OR 7302
*FOR,IS            MAIN
C*****DIFFRACTION PROGRAM B-II
LV=50
10 READ 9000,HT,ATTEN,EFAT,DIST,AL,WAVEL,ESHIF,HT1,ANTE,HT2,ATH
PRINT 9010,HTA,ATTEN,EFAT,DIST,AL,WAVEL,ESHIF,HT1,ANTE,HT2,ATH
DELTHE=1.0
X1=0.
X2=DIST
X3=2.*DIST
HT3=0.
THEMIN=30.
ANG=THEMIN
IF (ESHIF-ANG) 110,110,100
100 SHIFT=ATAN(EFAT/DIST)
GO TO 120
110 SHIFT=ESHIF
120 THETA=ANG-SHIFT
DISTA=DIST
HW=ATAN(HTA/DISTA)
HW=ABS(HW)
BEET=.01
BEE=ATAN(BEET/DISTA)
BEE=ABS(BEE)
SBEE=BEE
DO 90 I=1,50
THETA=.01745*THETA
B=100000.
FI2=HW-THETA
FI2=SIN(FI2)
FI1=HW+THETA
FI1=SIN(FI1)
TAP=(2.*(B+DISTA)/B/DISTA/WAVEL)
TAP=ABS(TAP)
FAC=DISTA*SQRT(TAP)
BEEP=FAC*BEE
BEEPI=1./BEEP
V1=FAC*FI1
V2=FAC*FI2
CALL FRFNEL(V1,CZ,SZ)
    
```

NWC TP 5819, Part 1

```

AV1R=.707*(CZ-.5)
AV1I=.707*(SZ-.5)
CALL FRENEL(VZ,CW,SW)
AV2R=.707*(CW-.5)*(10.)*(ATTEN/10.)
AV2I=.707*(SW-.5)*(10.)*(ATTEN/10.)
CRUD=AV1I+AV2I
CRUDD=CRUD**2
CLUD=AV1R+AV2R
CLUDD=CLUD**2
FFRAT=CLUDD+CRUDD
THETA=THETA/.01745
ANG=THETA+SHIFT
ANGLE=ANG
ANG=.01745*ANG
BETA=1.571-ANG
CAY=AL/COS(BETA)
CAY=ABS(CAY)
X=AL*TAN(BETA)
X=ABS(X)
WHY=ANG/.01745
HY=SHIFT+HW/.01745
TRY=SHIFT-HW/.01745

```

```

IF(WHY-HY)20,20,30
20 HAY=HW
   FFAI=FFRAT
   CAY=0.1STA
   IF(WHY-TRY)60,60,40
30 CALL EX2(X,HT,X1,X2,X3,HT1,HT2,HT3)
   HAT=HT-ANTE
   HAY=ASIN(HAT/CAY)
   HAY=ABS(HAY)
40 TOT=(2.+(B+CAY)/B/CAY/WAVEL)
   TOT=ABS(TOT)
   FACE=CAY*SQRT(TOT)
   BEEF = ABS(HT2 - ATH)
   SBEE = ATAN(BEEF/CAY)
   SREE = ABS(SBEE)
   SREEF=FACE*SBEE
   SREEF I=1./SREEF
   V3=FACE*HAY
   CALL FUZZ(V3,SBEEFI,C1,S1)
   AV3R=.707*(C1-.5)
   AV3I=.707*(S1-.5)
   G=2.+AV3R
   GSQ=G*G
   GA=AV3I*2.

```

NWC TP 5319, Part 1

```

GASQ=GA*GA
P1=GSB+GASQ
FFA1=FFRAT*P1
IF (WHY-HY) 50, 50, 60
50 HAPY=HW/.01745
   FFA1=B1*(ANGLE-TRY)/2./HAPY+FFRAT*(HY-ANGLE)/2./HAPY
60 DIF1=4.3439*ALOG(FFA1)
   ANG=ANG/.01745
   HW=HW/.01745
   IF (LV-S0180, 70, 70)
70 LV=0
80 PRINT 9020, ANG, DIF1
   THETA=THETA-DEL THE
   LV=LV+1
   HW=.01745*HW
90 CONTINUE
   GO TO 10
9000 FORMAT(8F10.0)
9010 FORMAT ('IHTA= ', 1PE10.3/ ' ATTN=' , E10.3/ ' EFAT=' , E10.3/ ' DIST='
1 ' , E10.3/ ' AL=' ', E10.3/ ' WAVFL=' , E10.3/ ' ESHIF=' , E10.3/ ' HT1=' ',
2 E10.3/ ' ANTE=' , E10.3/ ' HY2=' ', F10.3/ ' ATHE=' , E10.3/ ' ' PREDICTE
3D ATTENUATION ASSUMING DIFFRACTION BY ' ' ROCKET EXHAUST PLUME USIN
4G FTN PROGRAM ATFIN COMPILED ON DIFFRA. ' ' ' ' ASPECT ANGLE ATTEMU
5ATION ' ')
9020 FORMAT(1X, 2F12.2)
   END
*FOR, IS      FRENEL
SUBROUTINE FRENFL (X, C, S)
SV=X
X=ABS(X)
F=(1.+ .926*X)/(2.+1.792*X+3.109*X**2)
G=1./(2.+4.142*X+3.492*X**2+6.67*X**3)
U=3.14159*X**2/2.
C=.5+F*SIN(U)-G*COS(U)
S=.5-F*COS(U)-G*SIN(U)
IF (SV) 10, 20, 20
10 C=-C
   S=-S
20 RETURN
   END
*FOR, TS      FUZZ
SUBROUTINE FUZZ(Z0, B, FREAL, FIM)
Z2=Z0+1./B
Z1=Z0-1./B
Z2SQ=.5*3.1416*(Z2**2)
Z1SQ=.5*3.1416*(Z1**2)
CALL FRENFL (Z2, C2, S2)
CALL FRENFL (Z1, C1, S1)
FREAL=-.5*(C2+C1)-.5*B*70*(C2-C1)+.5*(8/3.1416)*(SIN(Z2SQ)-

```

NWC TP 5319, Part 1

```

1 SIN(Z1S0))+.5
FREAL=FRFAL-.5
FREAL=-FREAL
FIM=.5*(S2+S1)-.5*B*Z0*(S1-S2)+.5*(B/3.1416)*(COS(Z2S0)-COS(Z1S0))
1 -.5
FIM=FIM+.5
RETURN
END
#FOR,JS      FX2
SURROUTINE FX2(X,HT,X1,X2,X3,HT1,HT2,HT3)
A=HT1
C=(X2-X3)/(X1-X2)
B=(C*(HT1-HT2)-(HT2-HT3))/(C*(X1**2-X2**2)-(X2**2-X3**2))
HT=A+B*X+C*X**2
RETURN
END
#XGT
4.3      -23.      9.08      48.      10.      3.      9.08      2.
0.
#FIN
#FIN

```

DIFFRACTION COMPUTER PROGRAM B-II SAMPLE OUTPUT

```

HT1= 4.300+00
ATTEN= -2.300+01
CFAT= 3.200+00
CFRT= 4.200+01
ALF= 1.000+01
WAVELE= 7.000+00
SCHISE= 3.200+00
HT1E= 2.000+00
ANT1E= 0.200
HT2E= 4.000+00
ATHE= 5.300+00

```

DEDUCTED ATTENUATION ACCOUNTING DIFFRACTION BY
ROCKET EXHAUST PLUME USING FIN PROGRAM ATTEN COMPILED ON DIFFRA.

ASPECT ANGLE	ATTENUATION
37.70	-5.33
29.00	-5.07
22.00	-5.34
27.00	-5.39

NWC TP 5319, Part 1

25.00	-5.34
25.00	-5.79
24.00	-5.73
23.00	-5.87
22.00	-5.51
21.00	-5.54
20.00	-5.47
19.00	-5.38
18.00	-5.29
17.00	-5.15
16.00	-5.01
15.00	-4.93
14.00	-4.82
13.00	-4.71
12.00	-5.31
11.00	-5.77
10.00	-5.11
9.00	-5.47
8.00	-5.75
7.00	-5.89
6.00	-5.35
5.00	-6.59
4.00	-5.35
3.00	-5.22
2.00	-4.77
1.00	-3.54
-1.00	-2.72
-2.00	-1.04
-3.00	-1.21
-4.00	-0.55
	.04

NWC TP 5319, Part 1

Appendix C

TRANSVERSE ATTENUATION DATA

by

Keith Webb
Thiokol Chemical Corporation

The following information was supplied by the Thiokol Chemical Corporation, Wasatch Division. It had been accumulated and studied in the work which led to publication of References 61 and 130. It is the most complete compendium of static transverse attenuation data in existence.

TABLE I. TRANSVERSE, STATIC DATA MATRIX

Identification Number Reference for Data Propellant Al/Solids (1) Impurity Level, ppm K/Na	1		2		3		4		5		6	
	1	1	1	1	1	1	1	1	1	1	1	1
	6/88	80/125	6/88	80/125	6/88	80/125	6/84	80/125	6/84	80/125	6/84	80/125
Altitude, ft	23K											
Chamber Pressure, psi (2)	494	773	773	773	1000	1000	467	467	467	467	1133	1133
Throat Radius, inches	.177	.169	.169	.169	.151	.151	.168	.168	.168	.168	.136	.136
Expansion Ratio	8.8	7.9	7.9	7.9	15	15	7.5	7.5	7.5	7.5	11.4	11.4
Thrust, lbf. approx.	100	100	100	100	100	100	100	100	100	100	100	100
Radial Frequency, GHz	9	9	9	9	9	9	9	9	9	9	9	9
Maximum Attenuation, db	.21	.155	.155	.155	.25	.25	.48	.48	.48	.48	.51	.51
Location Max. Attenuation, in.	19	23	23	23	23	23	21	21	21	21	22	22
Chamber Temperature, °K	3187.8	3223.7	3223.7	3223.7	3243.3	3243.3	2930.5	2930.5	2930.5	2930.5	2930.5	2930.5
Pressure Ambient, psi	5.74	5.66	5.66	5.66	5.81	5.81	5.62	5.62	5.62	5.62	6.11	6.11
Expansion Ratio Opt.	11.24	15.79	15.79	15.79	18.8	18.8	10.12	10.12	10.12	10.12	18.35	18.35
Nozzle Exit Radius Opt., in.	.593	.670	.670	.670	.655	.655	.534	.534	.534	.534	.583	.583
Temperature Ambient, °K	300	300	300	300	300	300	300	300	300	300	300	300
Exit Velocity, ft/sec (3)	8420.8	8717.6	8717.6	8717.6	8956.1	8956.1	8189.2	8189.2	8189.2	8189.2	8636.8	8636.8

Model Predictions Presented

NWC
LPC
AeroChem
Hercules

NOTES

- (1) See propellant table for complete formulation
- (2) At maximum attenuation conditions
- (3) At optimum conditions
- (4) See table for AeroChem prediction conditions
- (5) Reference for prediction
- (6) Double base propellant - see propellant table for complete formulation

TRANSVERSE J, STATIC DATA MATRIX

	7	8	9	10	11	12
Identification Number	1	1	1	1	1	1
Reference for Data	6/84	12/88	12/88	12/88	12/88	12/86
Propellant Al/Solids(1)	80/125	80/125	80/125	80/125	80/125	80/125
Impurity Level, ppm K/Na						
Altitude, ft	23K	23K	23K	23K	23K	23K
Chamber Pressure, psi(2)	1133	553	553	988	988	781
Throat Radius, inches	.136	.174	.174	.139	.139	.150
Expansion Ratio	11.4	7.0	7.0	11.0	11.0	9.5
Thrust, lbf, approx.	100	100	100	100	100	100
Radar Frequency, GHz	13	9	15	9	16	9
Maximum Attenuation, db	.415	.7	.63	.55	.62	1.05
Location Max. Attenuation, in.	24	17	15	18	18	19
Chamber Temperature, °K	296.21	3370.8	3370.8	3423.7	3423.7	3282.7
Pressure Ambient, psi	6.11	6.33	6.33	6.62	6.62	6.05
Expansion Ratio Opt.	18.35	12.12	12.13	18.09	18.09	15.51
Nozzle Exit Radius Opt., In.	.583	.606	.606	.591	.591	.589
Temperature Ambient, °K	300	300	300	300	300	300
Exit Velocity, ft/sec(3)	8636.8	8569.3	8589.3	8963.0	8963.0	8807.4

Model Predictions Presented

NWC	2(5)	2	2	2	2	2
LPC			3	3		
AeroChem						
Hercules						

TRANSVERSE, STATIC DATA MATRIX

	13	14	15	16	17	18
Identification Number	1	1	1	1	1	1
Reference for Data	12/86	12/86	18/88	18/88	18/88	18/88
Propellant Al/Solids (1)	80/125	80/125	80/125	80/125	80/125	80/125
Impurity Level, ppm K/Na	23K	23K	23K	23K	23K	23K
Altitude, ft	781	781	572	572	572	964
Chamber Pressure, psi(2)	.150	.15	.169	.169	.169	.186
Throat Radius, inches	9.5	9.5	7.95	7.95	7.95	12.3
Expansion Ratio	100	100	100	100	100	100
Thrust, lbf, approx.	16	32	9	16	32	9
Radar Frequency, GHz	.75	.48	2.8	2.95	1.8	2.7
Maximum Attenuation, db	21	22	18	18	17	20
Location Max. Attenuation, in.	3282.7	3272.7	3522.7	3522.7	3522.7	3577.1
Chamber Temperature, °K	6.06	6.06	5.69	5.69	5.69	6.32
Pressure Ambient, psi	15.51	15.51	14.43	14.43	14.43	19.79
Expansion Ratio Opt.	.589	.589	.640	.640	.640	.603
Nozzle Exit Radius Opt., In.	300	300	300	300	300	300
Temperature Ambient, °K	8807.4	8807.4	8785.5	8785.5	8785.5	9099.2
Exit Velocity, ft/sec(3)						

Model Predictions Presented

NWC	2	2	2	2	2	2
LPC						
AeroChem						
Hercules						

TRANSVERSE, STATIC DATA MATRIX

	19	20	21	22	23	24
Identification Number	1	1	1	1	1	1
Reference for Data	18/88	18/88	18/84	18/84	18/84	18/84
Propellant Al/Solids (1)	80/125	80/125	80/125	80/125	80/125	80/125
Impurity Level, ppm K/Na						
Altitude, ft	23K	23K	23K	23K	23K	23K
Chamber Pressure, psi (2)	964	964	865	865	865	492
Throat Radius, inches	.136	.136	.129	.129	.129	.158
Expansion Ratio	12.3	12.3	12.8	12.8	12.8	8.5
Thrust, lbf, approx.	100	100	100	100	100	100
Radar Frequency, GHz	16	32	9	16	32	9
Maximum Attenuation, db	2.7	.122	2.65	2.3	.95	2.1
Location Max. Attenuation, in	20	19	20	20	20	19
Chamber Temperature, OK	3577.1	3577.1	3256.4	3256.4	3256.4	3213.4
Pressure Ambient, psi	6.32	6.32	5.98	5.98	5.98	6.00
Expansion Ratio Opt.	19.79	19.79	17.55	17.55	17.55	11.52
Nozzle Exit Radius Opt., In.	.603	.603	.538	.538	.538	.535
Temperature Ambient, OK	300	300	300	300	300	300
Exit Velocity, ft/sec(3)	9099.2	9099.2	8981.8	8981.8	8587.4	8587.4

Model Predictions Presented

NWC
LPC
AeroChem
Hercules

2 2 2 2 2 2

TRANSVERSE, STATIC DATA MATRIX

	25	26	27	28	29	30
Identification Number	1	1	4	1	1	1
Reference for Data	18/84	18/84	16/86	12/84	12/84	12/84
Propellant Al/Solids (1)	80/125	80/125	50/180	80/125	80/125	80/125
Impurity Level, ppm K/Na						
Altitude, ft	23K	23K	S.L.	5K	5K	5K
Chamber Pressure, psi (2)	492	492	1998	950	658	1810
Throat Radius, inches	.158	.158	.373	2.25	2.25	2.25
Expansion Ratio	8.5	8.5	20.68	2.59	2.59	6.71
Thrust, lbf, approx.	100	100	1560	21250	14800	45000
Radar Frequency, GHz	16	32	10	9	9	9
Maximum Attenuation, db	2.15	.89	4.36	10.2	9.4	7.1
Location Max. Attenuation, in.	18	18	67	252	216	312
Chamber Temperature, °K	3213.4	3213.4	3518.5	3133.7	3155.7	3161.6
Pressure Ambient, psi	6.00	6.00	14.7	12.5	12.5	12.5
Expansion Ratio Opt.	11.53	11.53	17.14	10.00	7.66	16.1
Nozzle Exit Radius Opt., In.	.535	.535	1.54	7.12	6.23	9.03
Temperature Ambient, °K	300	300	300	300	300	300
Exit Velocity, ft/sec (3)	8587.4	8587.4	8955.2	8379.5	8114.6	8784.3

Model Predictions Presented

NWC	2	2	2	2	2	2
LPC						
AeroChem						
Hercules						

TRANSVERSE, STATIC DATA MATRIX

	31	32	33	34	35	36
Identification Number	1	5	5	5	5	5
Reference for Data	12/84	12/88	20/88	20/88	4/88	20/84
Propellant Al/Solids (1)	80/125	59/171	48/135	48/135	58/145	52/83
Impurity Level, ppm K/Na						
Altitude, ft	5K	25K	25K	25K	25K	25K
Chamber Pressure, psi (2)	1200	1375	1060	1085	1100	1175
Throat Radius, inches	2.25	.091	.091	.091	.091	.091
Expansion Ratio	6.71	9.34	9.34	9.34	9.34	9.34
Thrust, lbf, approx.	29000	50	50	50	50	50
Radar Frequency, CHz	9	10	10	24	10	10
Maximum Attenuation, db	7.3	.69	2.65	1.35	.07	2.5
Location Max. Attenuation, in	240	8-10	8-12	8-10	13-18	9-11
Chamber Temperature, °K	3144.4	3450.4	3609.3	3609.3	3179.6	3260.7
Pressure Ambient, psi	12.5	5.22	5.80	5.80	4.84	5.80
Expansion Ratio Opt.	11.9	28.2	23.4	23.4	22.7	23.3
Nozzle Exit Radius Opt., In.	7.76	.48	.44	.44	.43	.44
Temperature Ambient, °K	300	300	300	300	300	300
Exit Velocity ft/sec (3)	8533.1	9312.0	9248.0	9248.0	8924.5	9181.5

Model Predictions Presented

NWC
LPC
AeroChem
Hercules

2	2	2	2	2	2
3	5	5	5	5	5

NWC TP 5319, Part 1

TRANSVERSE, STATIC DATA MATRIX

	37	38	39	40	41	42
Identification Number	5	5	5	5	5	5
Reference for Data	20/84	12/88	12/88	12/88	12/88	12/88
Propellant Al/Solids (1)	52/83	10/5	10/5	907/167	907/167	8980/184
Impurity Level, ppm K/Na						
Altitude, ft	25K	25K	25K	25K	25K	25K
Chamber Pressure, psi (2)	1043	1200	1200	1150	1155	1095
Throat Radius, inches	.091	.091	.091	.091	.091	.091
Expansion Ratio	9.34	9.34	9.34	9.34	9.34	9.34
Thrust, lbf, approx.	50	50	50	50	50	50
Radar Frequency, GHz	24	24	24	10	24	10
Maximum Attenuation, db	1.8	.075	.05	2.33	1.7	8.85
Location Max. Attenuation, in.	11-13	9-11	11-13	7-9	9-13	8-11
Chamber Temperature, °K	3253.0	3442.9	3439.0	3434.1	3434.5	3433.5
Pressure Ambient, psi	5.709	5.419	5.381	5.091	5.709	5.18
Expansion Ratio Opt.	21.6	25.6	24.9	24.8	22.8	23.6
Nozzle Exit Radius Opt., In.	.42	.46	.45	.45	.43	.44
Temperature Ambient, °K	300	300	300	300	300	300
Exit Velocity ft/sec	9116.8	9241.0	9216.1	9211.7	9147.3	9152.7
Model Predictions Presented	2	2	2	2	2	2
NWC						
LPC						
AeroChem						
Hercules						

TRANSVERSE, STATIC DATA MATRIX

NWC TP 5319, Part 1

	49	50	51	52	53	54
Identification Number	5	6	6	6	6	6
Reference for Data	20/88	12/88	12/84	12/84	12/88	20/88
Propellant Al/Solids (1)	48/135	43/138	40/138	40/138	43/138	38/142
Impurity Level, ppm K/Na						
Altitude, ft	40K	S.L.	S.L.	S.L.	S.L.	S.L.
Chamber Pressure, psi (2)	1115	1040	1075	1075	1040	1270
Throat Radius inches	.091	.4	.4	.4	.4	.4
Expansion Ratio	9.34	9.3	9.3	9.3	9.3	9.3
Thrust, lbf, approx.	50	1000	1000	1000	1000	1000
Radar Frequency, GHz	10	10	10	35	35	10
Maximum Attenuation, db	3.70	1.8	2.25	2.1	1.0	14.5
Location Max. Attenuation, in.	9-12	36-38	45-50	45-50	36-38	34
Chamber Temperature, °K	3614.5	3425.2	3139.8	3139.8	3425.2	3628.0
Pressure Ambient, psi	2.55	14.7	14.7	14.7	14.7	14.7
Expansion Ratio Opt.	46.4	10.2	9.72	9.72	10.2	12.80
Nozzle Exit Radius Opt., In.	.62	1.28	1.25	1.25	1.28	1.43
Temperature Ambient, °K	300	300	300	300	300	300
Exit Velocity ft/sec (3)	9779.4	8453.2	8789.0	8789.0	8453.2	8711.4

Model Predictions Presented

NWC
LPC
AeroChem
Hercules

2 2 2 2 2 2

TRANSVERSE, STATIC DATA MATRIX

Identification Number	55	56	57	58	59	60
Reference for Data	6	6	6	6	6	6
Propellant Al/Solids (1)	20/88	20/84	20/84	20/88	20/88	20/88
Impurity Level, ppm K/Na	38/142	38/142	38/142	373/48	373/48	10/4
Altitude, ft	S.L.	S.L.	S.L.	S.L.	S.L.	S.L.
Chamber Pressure, psi (2)	1270	940	940	1135	1135	855
Throat Radius, inches	.4	.4	.4	.4	.4	.4
Expansion Ratio	9.3	9.3	9.3	9.3	9.3	9.3
Thrust, lbf, approx.	1000	1000	1000	1000	1000	1000
Radar Frequency, GHz	35	10	35	10	35	10
Maximum Attenuation, db	10.6	9.3	5.4	18.6	11.5	2.25
Location Max. Attenuation, in.	34	44-48	44-48	38-45	38-45	50-55
Chamber Temperature, °K	3628.0	3246.1	3246.1	3616.71	3616.71	3586.6
Pressure Ambient, psi	14.7	14.7	14.7	14.7	14.7	14.7
Expansion Ratio Opt.	12.80	9.73	9.73	11.57	11.57	8.98
Nozzle Exit Radius Opt., In.	1.43	1.25	1.25	1.36	1.36	1.20
Temperature Ambient, °K	300	300	300	300	300	300
Exit Velocity ft/sec (3)	8711.4	8387.9	8387.9	8619.1	8619.1	8385.8

Model Predictions Presented

NWC	2	2	2	2	2	2
LPC						
AeroChem						
Hercules						

TRANSVERSE, STATIC DATA MATRIX

	61	62	63	64	65	66
Identification Number	6	7	7	8	9	9
Reference for Data	20/88	12/88	12/88	12/88	18(6)	12
Propellant Al/Solids (1)	10/4	49/75	49/75	50/157	25/157	30/147
Impurity Level, ppm K/Na						
Altitude, ft	S.L.	28K	42K	S.L.	2K	2K
Chamber Pressure, psi (2)	855	1250	1250	1100	2900	2800
Throat Radius, inches	.4	.4	.4	.8	.49	.50
Expansion Ratio	9.3	9.34	9.34	9.3	7.75	7.77
Thrust, lbf, approx.	1000	1000	1000	3500	3300	3300
Radar Frequency, GHz	35	10	10	10	9.3	9.3
Maximum Attenuation, db	1.24	3.72	4.17	2.1	14.4	4.75
Location Max. Attenuation, in.	50-55	77	104	86	84	85
Chamber Temperature, °K	3586.6	3440.9	3440.9	3430.0	3573.5	3383.5
Pressure Ambient, psi	14.7	4.78	2.51	14.7	13.6	13.6
Expansion Ratio Opt.	8.98	27.71	45.73	10.67	24.69	22.45
Nozzle Exit Radius Opt., In.	1.20	2.11	2.71	2.61	2.43	2.37
Temperature Ambient, °K	300	300	300	300	300	300
Exit Velocity ft/sec (3)	8385.8	9296.5	9625.5	8494.2	9178.5	8983.2

Model Predictions Presented

NWC
LPC
AeroChem
Hercules

2 2 2 2 2 2
7 7 7 7 7 7

TRANSVERSE, STATIC DATA MATRIX

	67	68	69	70	71	72
Identification Number	9	9	10	11	11	11
Reference for Data	8	0	5/88	ELP	ELP	ELP
Propellant Al/Solids (1)	34/153	40/163	40/100	19/55	19/55	19/55
Impurity Level, ppm K/Na						
Altitude, ft	2K	2K	S.L.	S.L.	S.L.	S.L.
Chamber Pressure, psi (2)	2900	3600	1150	1000	1000	1000
Throat Radius, inches	.49	.34	1.16	.12	.12	.12
Expansion Ratio	7.58	7.40	4.28	4.0	8.85	13.25
Thrust, lbf, approx.	3300	3300	7500	70	70	70
Radar Frequency, GHz	9.3	9.3	10	9.5	9.5	9.5
Maximum Attenuation, db	4	3.9	.62	.24	.18	.5
Location Max. Attenuation, in	78	188	109	11.5	10	5.3
Chamber Temperature, °K	3164.0	2985.9	3200	3205.2	3205.2	3205.2
Pressure Ambient, spi	13.6	13.6	14.7	14.7	14.7	14.7
Expansion Ratio Opt.	21.58	23.99	10.26	9.33	9.33	9.33
Nozzle Exit Radius Opt., In.	2.28	1.67	3.715	.367	.367	.367
Temperature Ambient, °K	300	300	300	300	300	300
Exit Velocity ft/sec (3)	8756.4	8593.6	8251.5	8142.5	8142.5	8142.5

Model Predictions Presented

NWC
LPC
AeroChem
Hercules

2 2 2 2 2 2

TRANSVERSE, STATIC DATA MATRIX

	73	74	75	76	77	78
Identification Number	11	11	11	11	11	11
Reference for Data	ELP	ELP	ELP	ELP	ELP	ELP
Propellant Al/Solids (1)	19/55	19/55	19/55	19/55	19/55	19/55
Impurity Level, ppm K/Na						
Altitude, ft	S.L.	14K	14K	14K	14K	28K
Chamber Pressure, psi (2)	1000	1000	1000	1000	1000	1000
Throat Radius, inches	.12	.12	.12	.12	.12	.12
Expansion Ratio	21.0	4.0	8.85	13.25	21.0	4.0
Thrust, lbf, approx.	70	70	70	70	70	70
Radar Frequency, GHz	9.5	9.5	9.5	9.5	9.5	9.5
Maximum Attenuation, db	.27	.39	.33	.365	.4	.58
Location Max. Attenuation, in.	6.3	16	12.7	11.4	8.8	19.5
Chamber Temperature, °K	3205.	3205.2	3205.2	3205.2	3205.2	3205.2
Pressure Ambient, psi	14.7	8.63	8.63	8.63	8.63	4.78
Expansion Ratio Opt.	9.33	13.92	13.92	13.92	13.92	21.84
Nozzle Exit Radius Opt., In.	.367	.448	.448	.448	.448	.561
Temperature Ambient, °K	300	300	300	300	300	300
Exit Velocity ft/sec (3)	8142.5	8483.8	8483.8	8483.8	8483.8	8814.1

Model Predictions Presented

NWC	2	2	2	2	2	2
LPC						
AeroChem						
Hercules						

TRANSVERSE, STATIC DATA MATRIX

	79	80	81	82	83	84
Identification Number	11	11	11	11	11	11
Reference for Data (1)	ELP	ELP	ELP	ELP	ELP	ELP
Propellant Al/Solids (1)	19/55	19/55	19/55	19/55	19/55	19/55
Impurity Level, ppm K/Na						
Altitude, ft	28K	28K	28K	45K	45K	45K
Chamber Pressure, psi (2)	1000	1000	1000	1000	1000	1000
Throat Radius, inches	.12	.12	.12	.12	.12	.12
Expansion Ratio	8.85	13.25	21.0	4.0	8.85	13.25
Thrust, lbf, approx.	70	70	70	70	70	70
Radar Frequency, GHz	9.5	9.5	9.5	9.5	9.5	9.5
Maximum Attenuation, db	.48	.51	.41	.49	.22	.28
Location Max. Attenuation, in.	17.4	14.5	13	4.4	4	1
Chamber Temperature, °K	3205.2	3205.2	3205.2	3205.2	3205.2	3205.2
Pressure Ambient, psi	4.78	4.78	4.78	2.15	2.15	2.15
Expansion Ratio Opt.	21.84	21.84	21.84	40.54	40.54	40.54
Nozzle Exit Radius Opt., in.	.561	.561	.561	.764	.764	.764
Temperature Ambient, °K	300	300	300	300	300	300
Exit Velocity ft/sec (3)	8814.1	8814.1	8814.1	9194.9	9194.9	9194.9

Model Predictions Presented

NWC
LPC
AeroChem
Hercules

2

2

2

2

2

2

TRANSVERSE, STATIC DATA MATRIX

Identification Number	85	86	87	88	89	90
Reference for Data	11	13	13	13	12	14
Propellant Al/Solids (1)	ELP	ELP	ELP	ELP	ELP	ELP
Impurity Level, ppm K/Na	19/55	19/55	19/55	19/55	19/55	20/50
Altitude, ft	45K	45K	29K	48K	S.L.	S.L.
Chamber Pressure, psi (2)	1000	235	248	248	260	1050
Throat Radius, inches	.12	.356	.356	.568	1.30	.382
Expansion Ratio	21.0	5.4	5.4	5.4	5.4	2.0
Thrust, lbf, approx.	70	130	130	350	2000	700
Radar Frequency, GHz	9.5	9.3	9.3	9.3	9.57	35
Maximum Attenuation, db	.28	1.15	2.40	4.25	1.9	2.1
Location Max. Attenuation, in.	1	11	28.5	44	61	29
Chamber Temperature, °K	3205.2	3092	3097	3097	3101	3238
Pressure Ambient, psi	2.15	12.4	4.57	1.86	14.7	14.7
Expansion Ratio Opt.	40.54	3.75	8.05	15.81	3.58	9.517
Nozzle Exit Radius Opt., In.	.764	.689	1.01	2.26	2.46	1.19
Temperature Ambient, °K	300	300	300	300	300	300
Exit Velocity ft/sec	9194.9	7046	7950	8545	6985	8177

Model Predictions Presented

- NWC
- LPC
- AeroChem
- Hercules

2 2 2 2 2 2

TRANSVERSE, STATIC DATA MATRIX

	91	92	93	94
Identification Number	14	14	14	7
Reference for Data	ELP	ELP	ELP	ELP
Propellant Al/Solids (1)	20/50	20/50	20/50	9/25
Impurity Level, ppm K/Na				
Altitude, ft	S.L.	S.L.	S.L.	28.5K
Chamber Pressure, psi(2)	1050	1050	1052	250
Throat Radius, inches	.382	.382	.382	.567
Expansion Ratio	4.26	8.87	12.0	5.416
Thrust, lbf, approx.	700	700	700	350
Radar Frequency, GHz	35	35	35	9.3
Maximum Attenuation, db	1.26	1.12	1.09	3.2
Location Max. Attenuation, in.	44	51.5	51.8	52
Chamber Temperature, °K	3238	3238	3238	3112
Pressure Ambient, psi	14.7	14.7	14.7	4.7
Expansion Ratio Opt.	9.617	9.617	9.617	7.912
Nozzle Exit Radius Opt., In.	1.19	1.19	1.19	1.6
Temperature Ambient, °K	300	300	300	300
Exit Velocity ft/sec(3)	8177	8177	8177	7943

Model Predictions Presented

NWC	2	2	2	2
LPC				
AeroChem				
Hercules				

TABLE II
PROPELLANT FORMULATIONS

Identification No.	1, 2, 3	4, 5,	6, 7	8, 9, 10, 11, 32, 38, 39, 40, 41, 42, 43, 47, 48, 50, 53, 62, 63, 64	12, 13, 14	15, 16, 17, 18, 19, 20	21, 22, 23, 24, 25, 26	27	28, 29, 30, 31, 51, 52
Aluminum	6	6	6	12	12	18	18	16	12
Binder, HC	12	16	16	12	14	12	16		16
Ammonium Perchlorate	82	78	78	76	74	70	66	70	72
Binder, HE								14	
Nitrocellulose									
Nitroglycerin									
Triactin									
Magnesium									
Resorcinol									
NLPA									
TEGDN									

TABLE II (Cont.)
PROPELLANT FORMULATIONS

Identification No.	65	66	67	68	69	70 thru 94
Aluminum	20	18	12	8	5	3.4
Binder, HC	12				12	
Ammonium Perchlorate	68	32	33	42	50	83
Binder, HB						
Nitrocellulose		16	16	16	16	28
Nitroglycerin						38.3
Triactin						7.2
Magnesium						1.5
Resorcinol		1.0	1.0	1.0	1	1
NDPA						1
TEGDN	33	33	33	33	33	

NWC TP 5319, Part 1

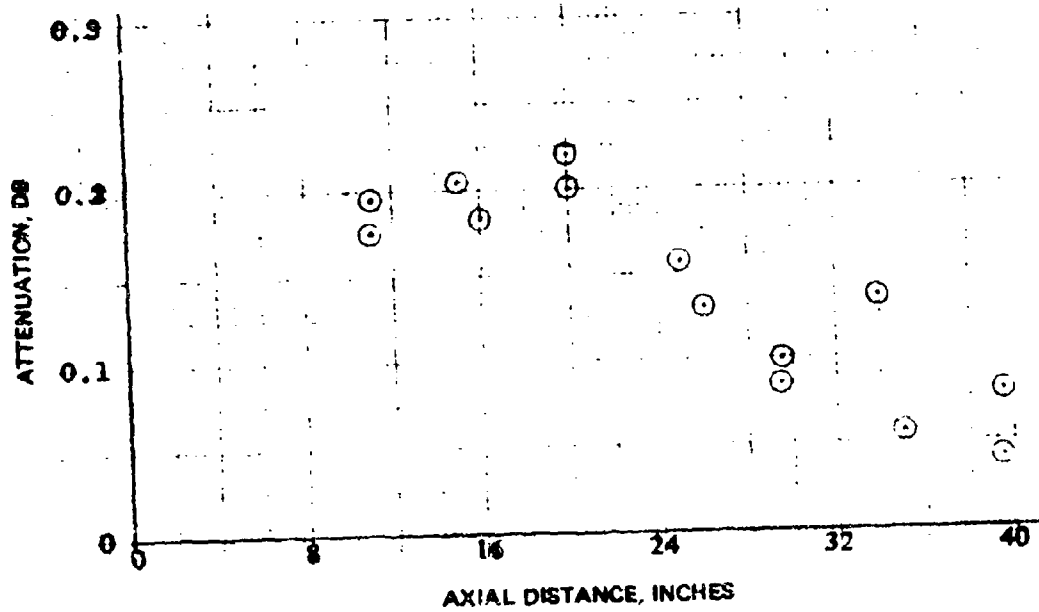
REFERENCES

1. Lund, R. K. and Webb, J. K. "Attenuation Measurements" Work done under Thiokol sponsored IR&D programs and has not been published.
2. Attenuation Prediction made by Thiokol with Naval Weapons Center (NWC) program, reference 7.
3. Attenuation prediction made by Thiokol with Lockheed program, reference 1.
4. Pergament, Harold S. "Radar Cross Section of Turbulent Rocket Exhaust Plumes," AeroChem TP-228, AFRPL TR-69-243, January, 1970.
5. Smoot, L.D., "Investigation of High Performance Solid Propellants with Favorable Attenuation Characteristics: Mechanisms which cause Radar Attenuation," Final Report, Lockheed Propulsion Company, LPC No. 756F, 15 January, 1967.
6. Smoot, L.D., and Williams J. W. "Investigation of Noise and Attenuation Characteristics of High-Performance Solid Propellants," Final Report, Lockheed Propulsion Company, LPC 782F, 15 November 1967.
7. Hedman, P.O. and Smoot, L.D., "Influences of the Flight Environment and Propellant Additive Form on Radar interference Caused by Rocket Motor Exhausts" Final Report, Lockheed Propulsion Company, LPC 915F, 28 February 1969.
8. Smoot, L.D. and Hedman, P.O., "Effect of Propellant Additives and Motor Insulations on Radar Attenuation Caused by Rocket Motor Exhausts," Final Report, Lockheed Propulsion Company, LPC 844F, 15 February 1968.
9. Smoot, L.D. and Seliga, T.J., "Rocket Exhaust Plume Radar Attenuation and Amplitude/Phase Noise", Journal of Spacecraft and Rockets, Vol. 4 No. 6, 774, June 1967.
10. Victor, A.C. "Microwave Interference Characteristics of a Solid Rocket Motor Exhaust," Naval Weapons Center, China Lake, California, NWC TP 4199, October 1968.

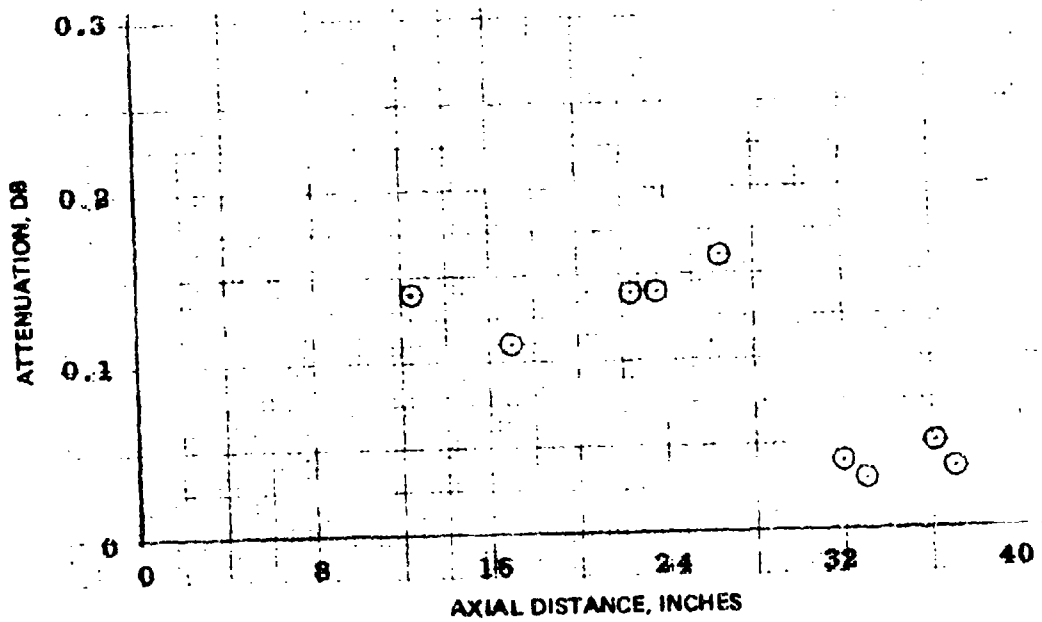
NWC 5319, Part 1

11. Myers, R. B. Hartsock, R. D., Buckley, F. T. and Scott, L. P. "Exhaust Plume Interference Studies," Hercules/Allegany Ballistics Laboratory Quarterly Progress report 68, August 1970.
12. Allegany Ballistics Laboratory. "Radar Attenuation Test of Propellants FDS and ELP Conducted for Triparticle Attenuation Working Group", by J. C. Jenks, ABL Report RES 6417, April 1966.
13. Myers, R. B. and Hartsock, R. D., "Plume Interference Investigations", Hercules/Allegany Ballistics Laboratory, Unclassified Extraction from Classified Document to be Published.
14. Myers, R. B., Hartsock, R.D. and Wilson, W.G., "Exhaust Plume Interference Studies," Hercules/Allegany Ballistics Laboratory Quarterly Progress Report 66, February 1970.

NWC TP 5319, Part 1

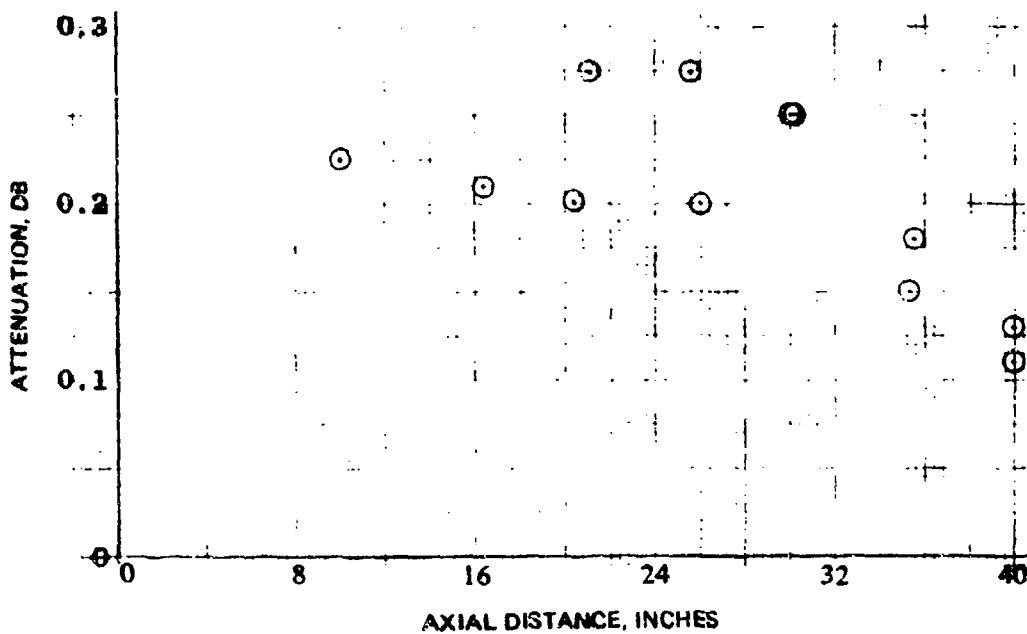


Test No. 1.

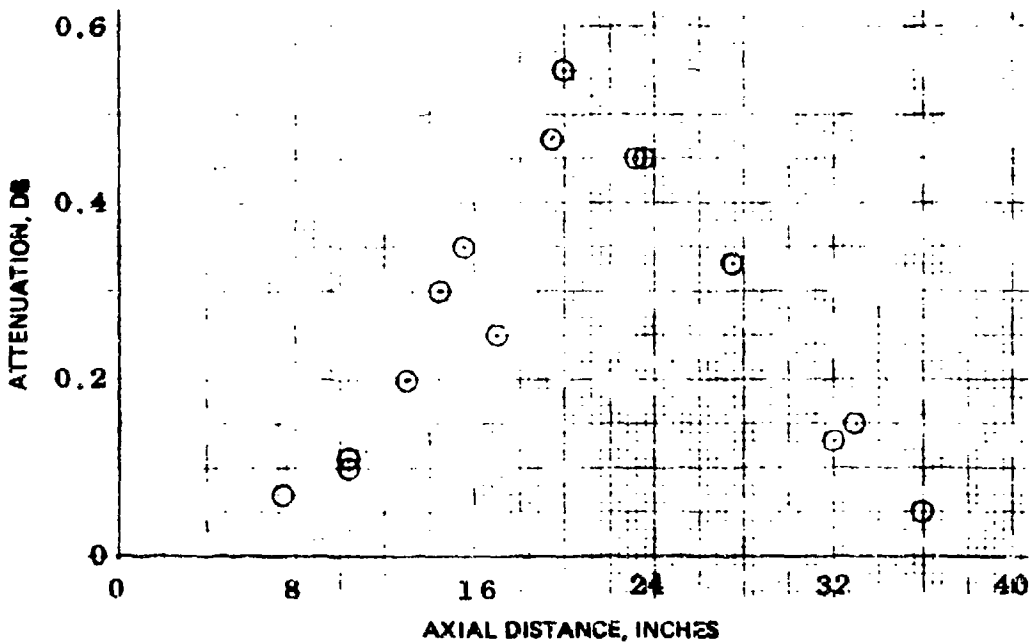


Test No. 2.

NWC TP 5319, Part 1

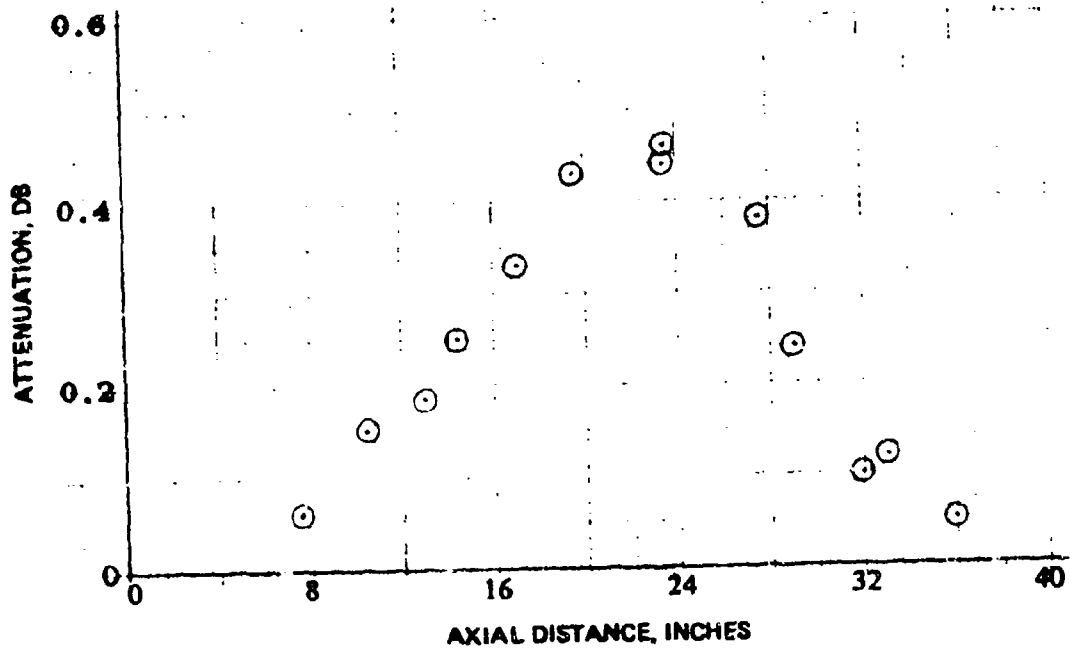


Test No. 3.

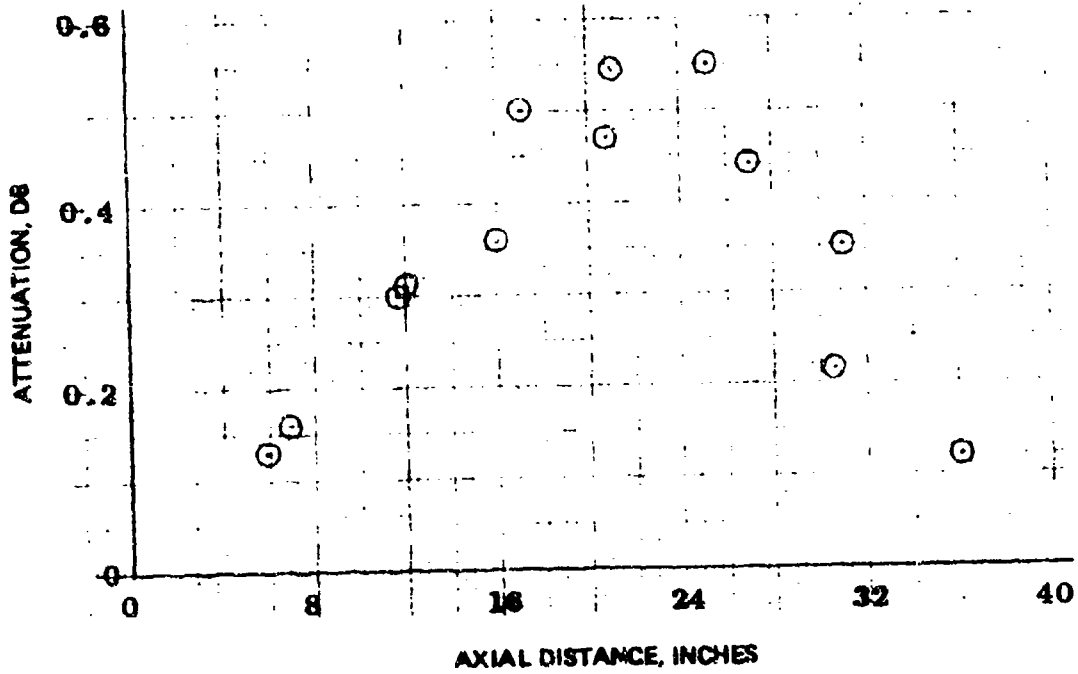


Test No. 4.

NWC TP 5319, Part 1

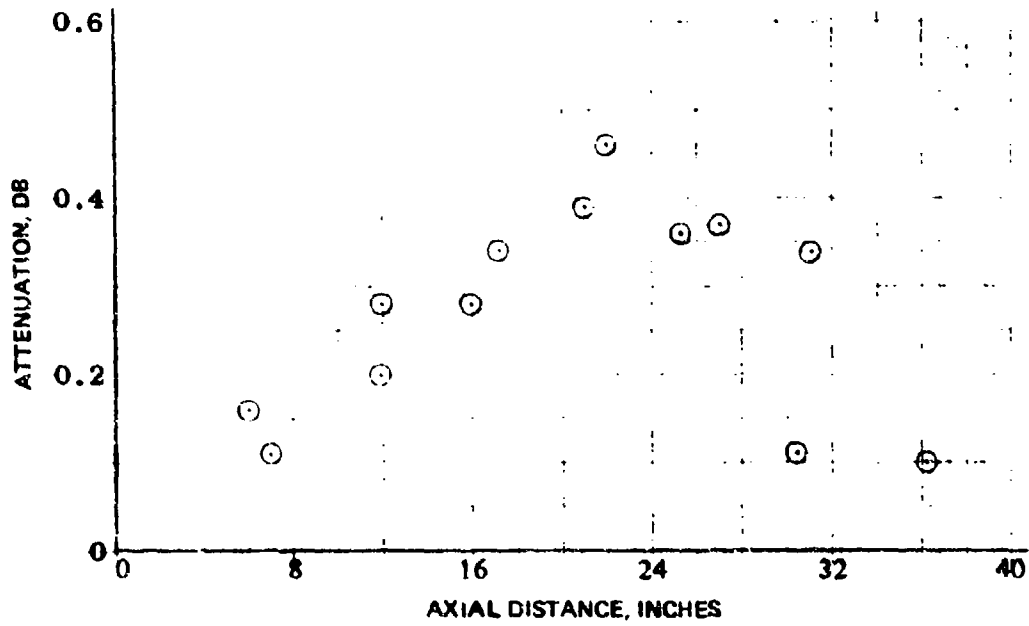


Test No. 5.

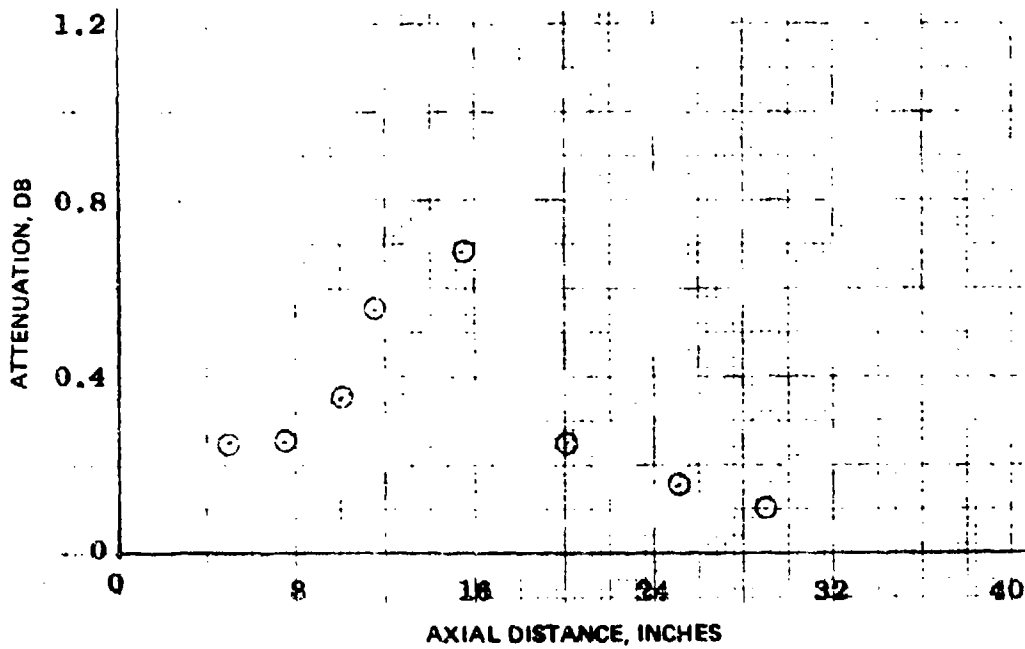


Test No. 6.

NWC TP 5319, Part 1

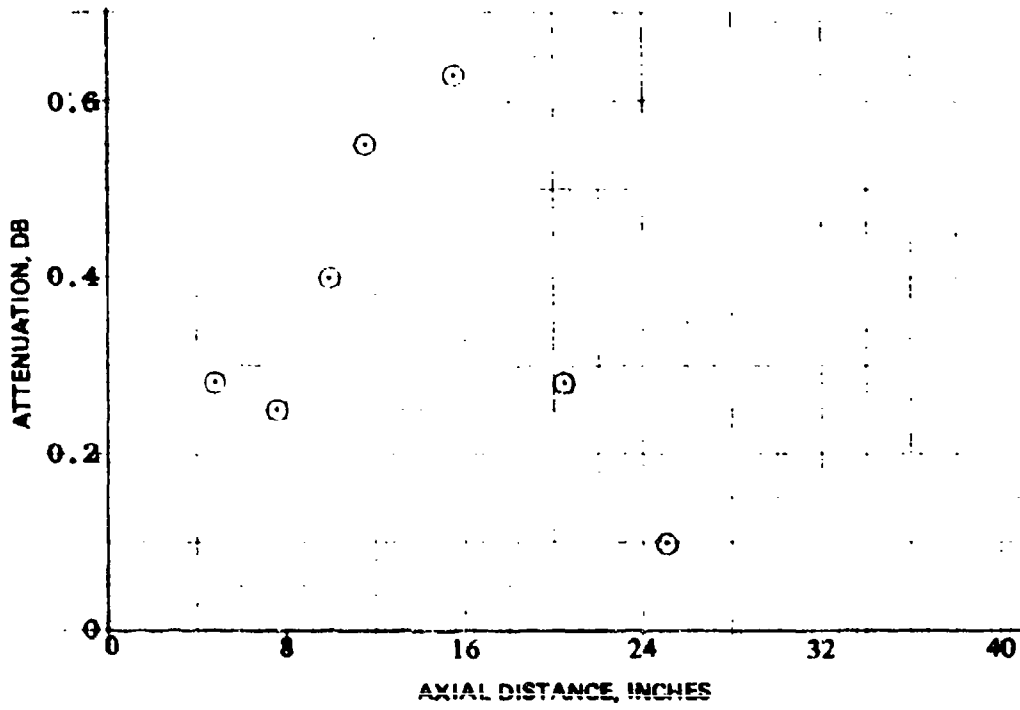


Test No. 7.

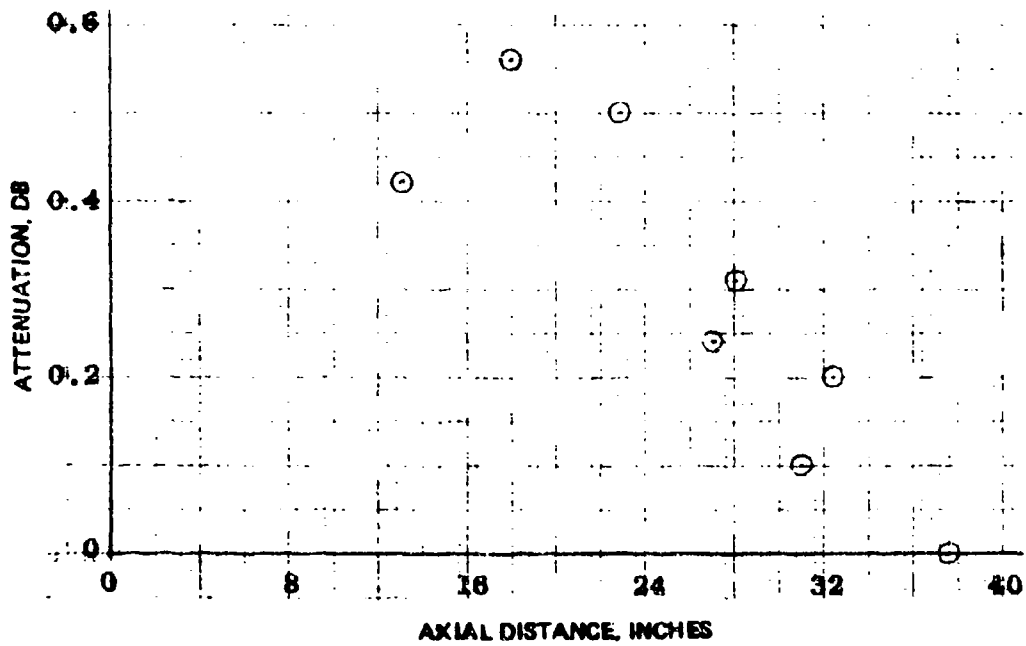


Test No. 8.

NWC TP 5319, Part I

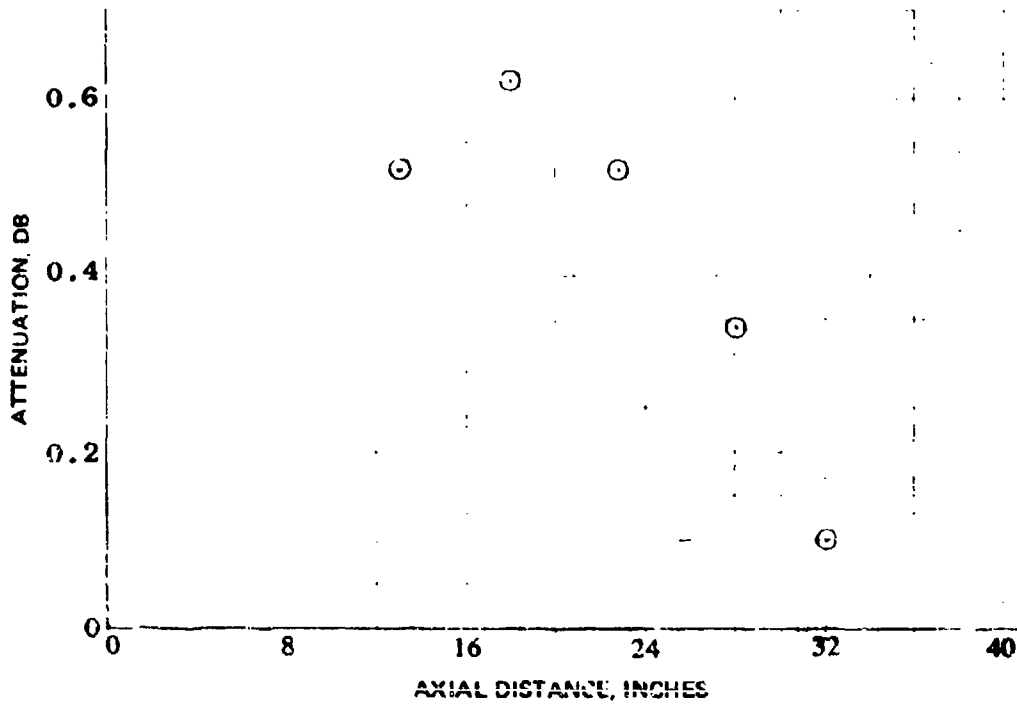


Test No. 9.

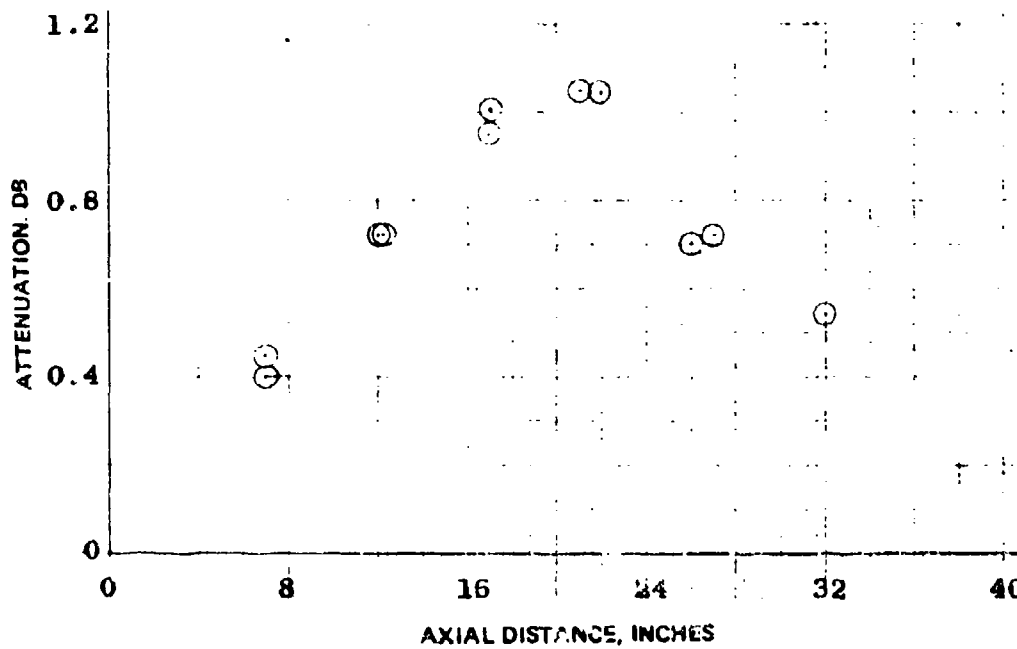


Test No. 10.

NWC TP 5319, Part 1

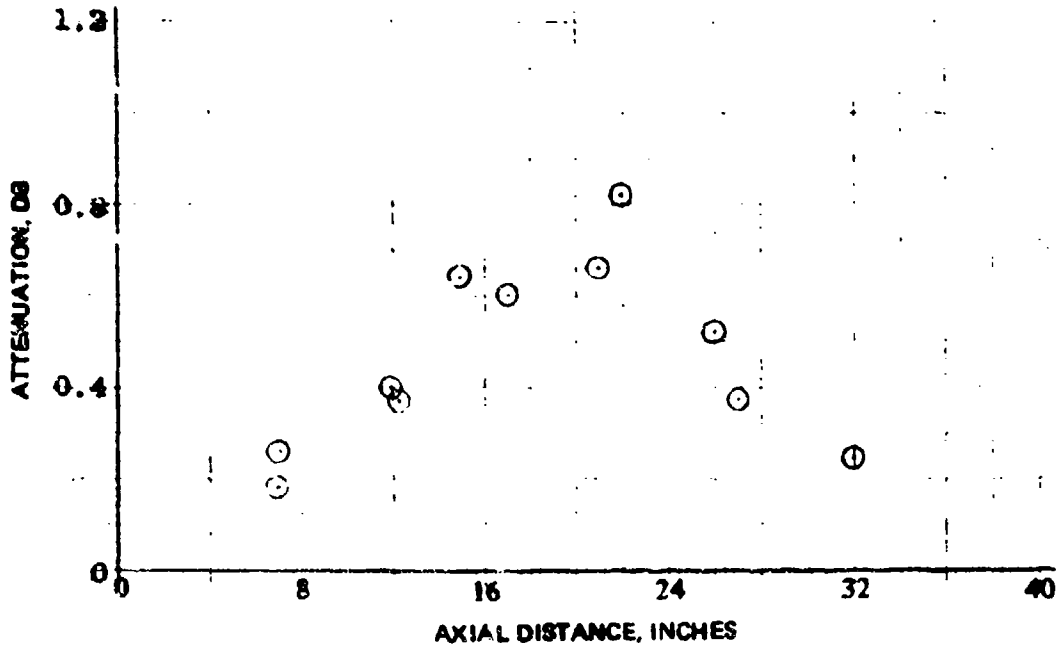


Test No. 11.

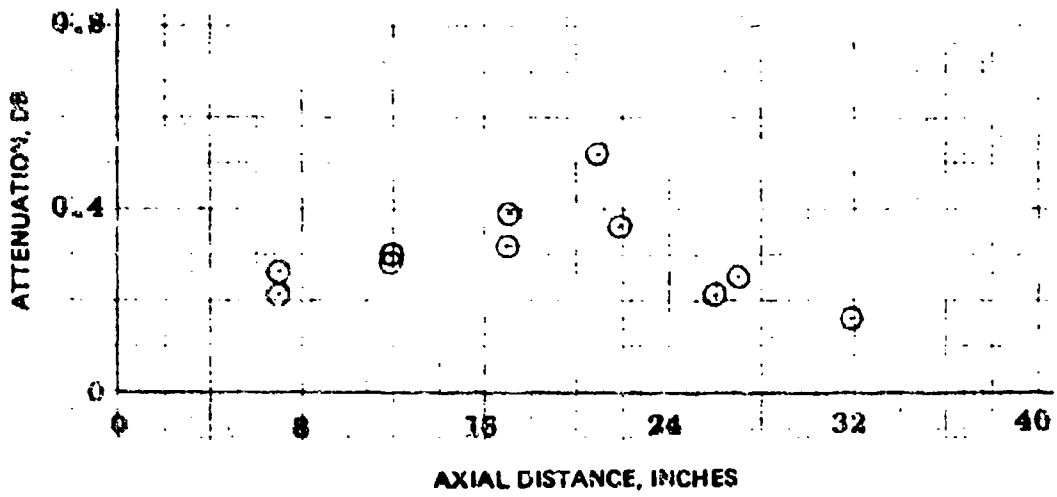


Test No. 12.

NWC TP 5319, Part 1

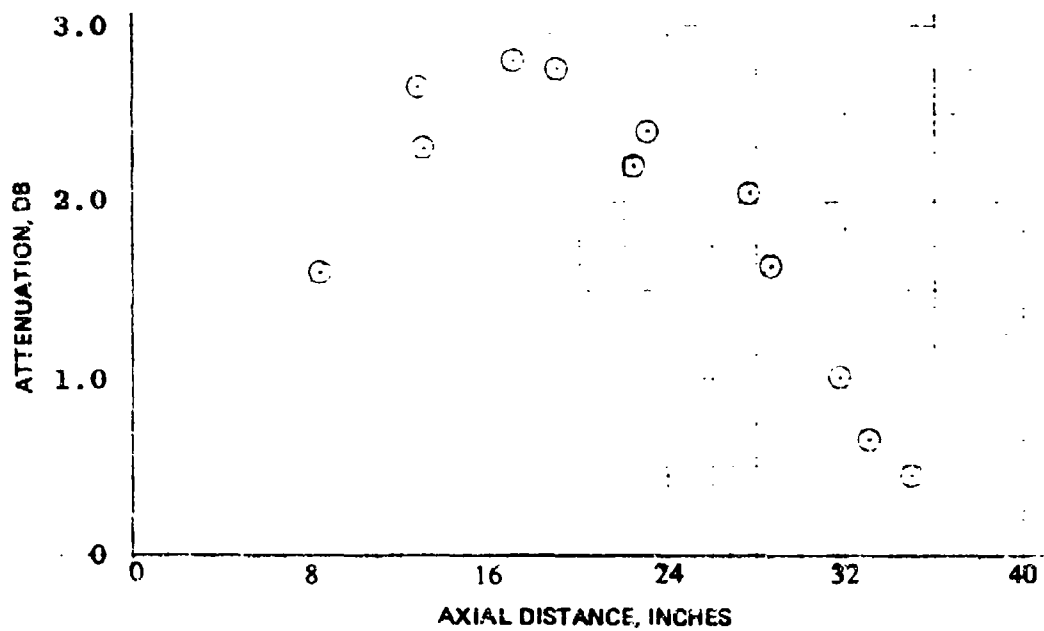


Test No. 13.

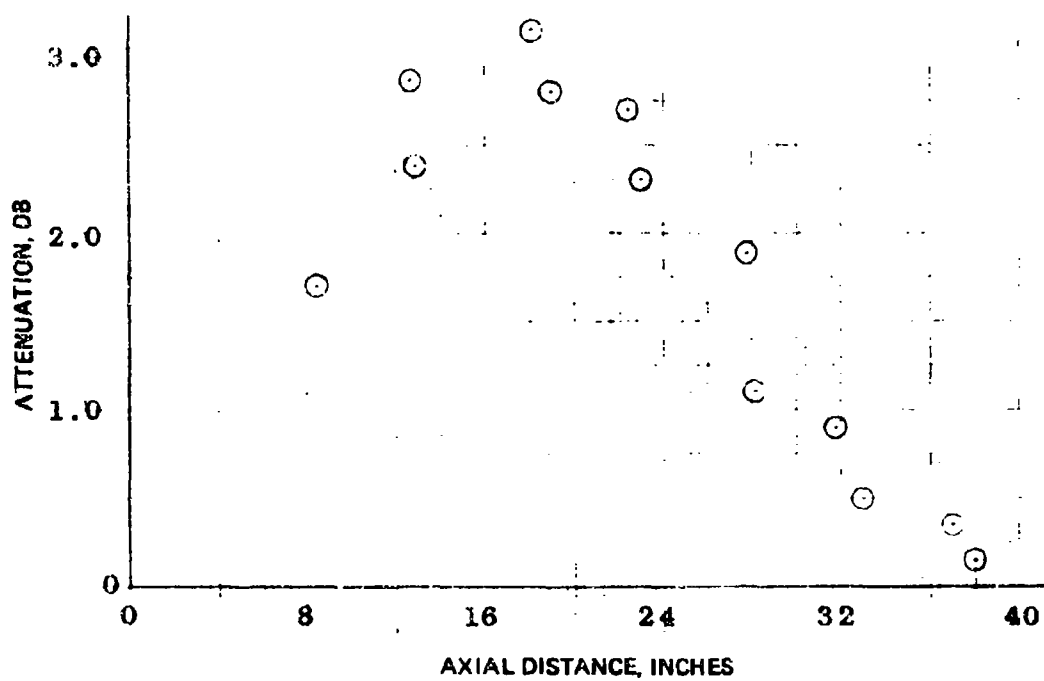


Test No. 14.

NWC TP 5319, Part 1

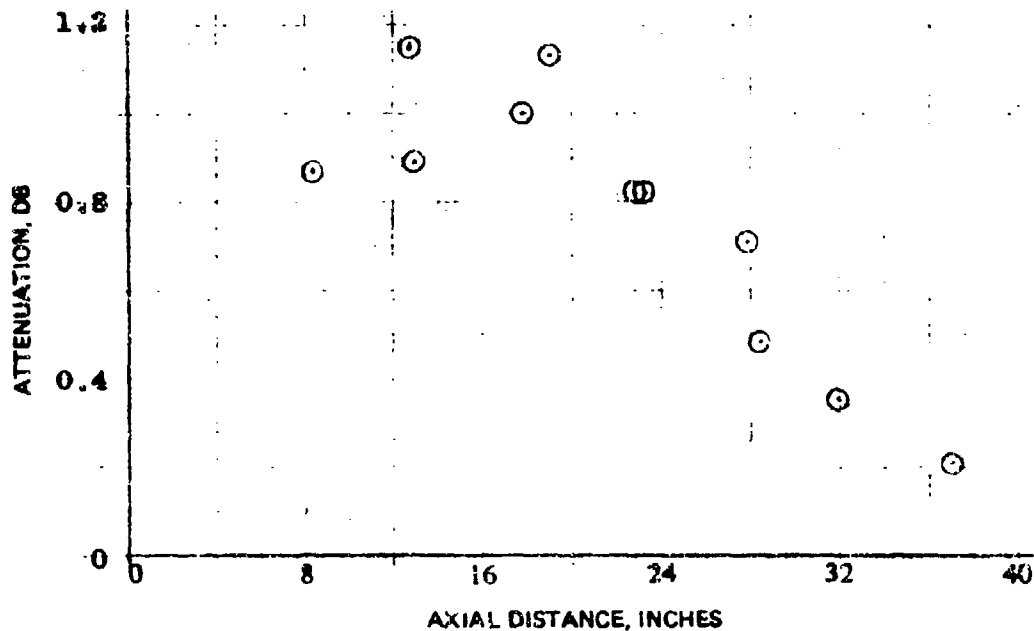


Test No. 15.

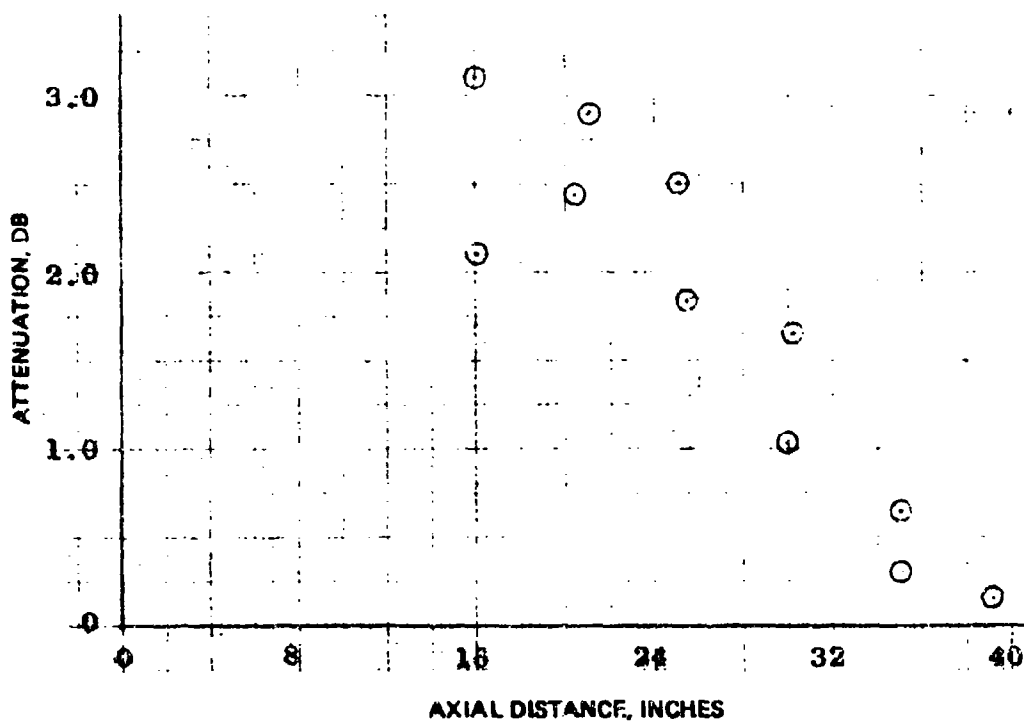


Test No. 16.

NWC TP 5319, Part 1

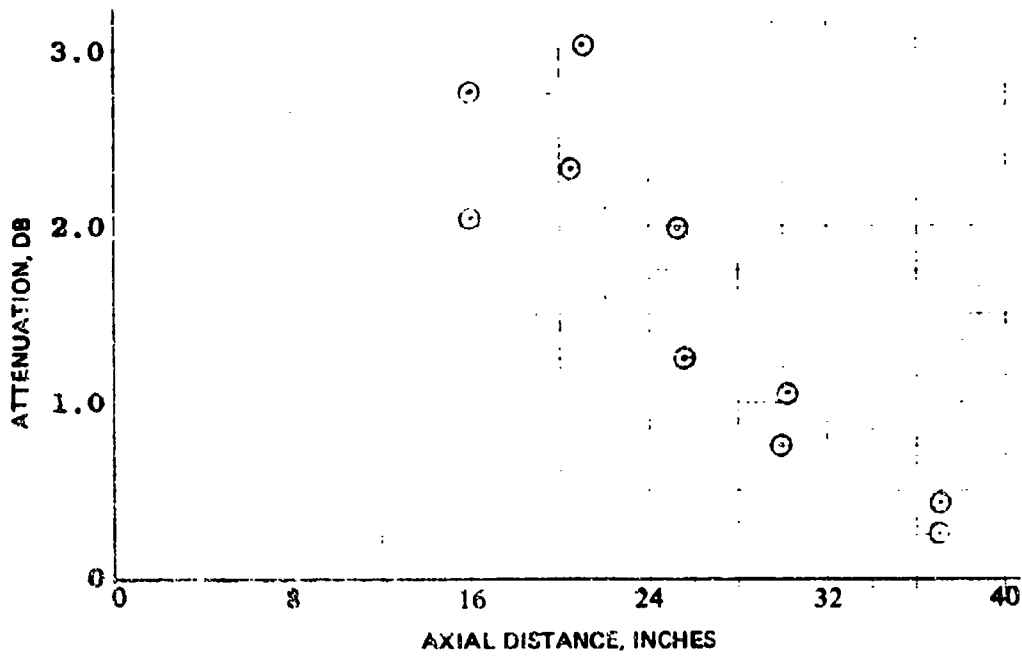


Test No. 17.

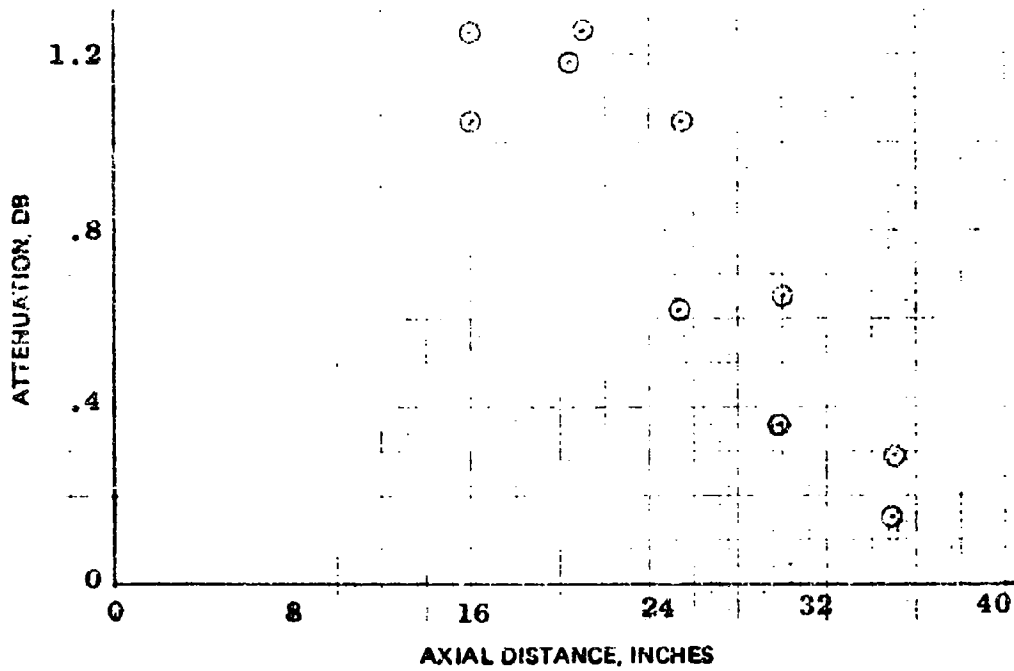


Test No. 18.

NWC TP 5319, Part 1

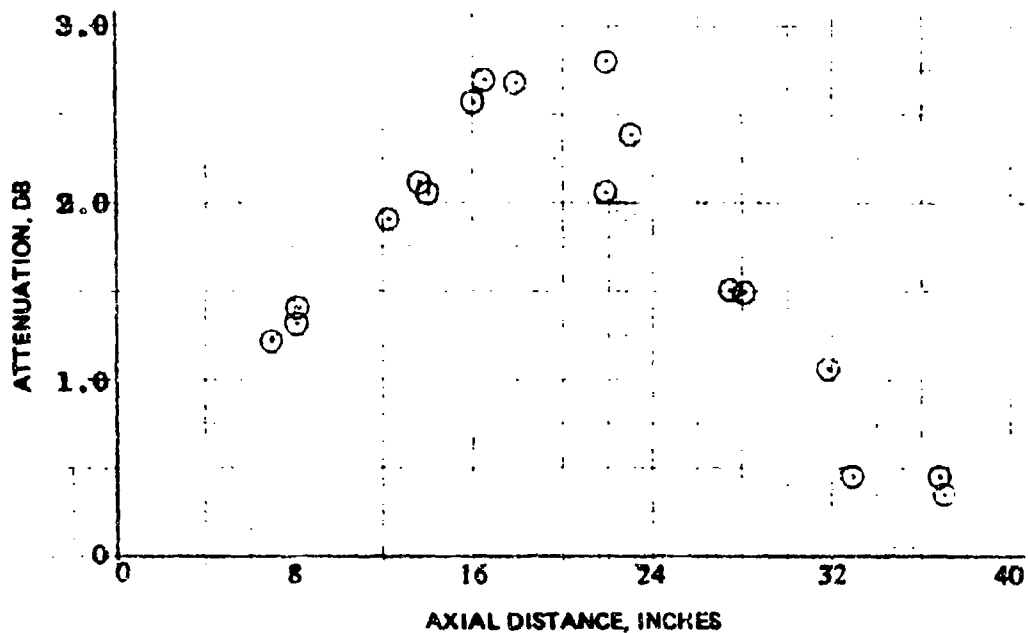


Test No. 15.

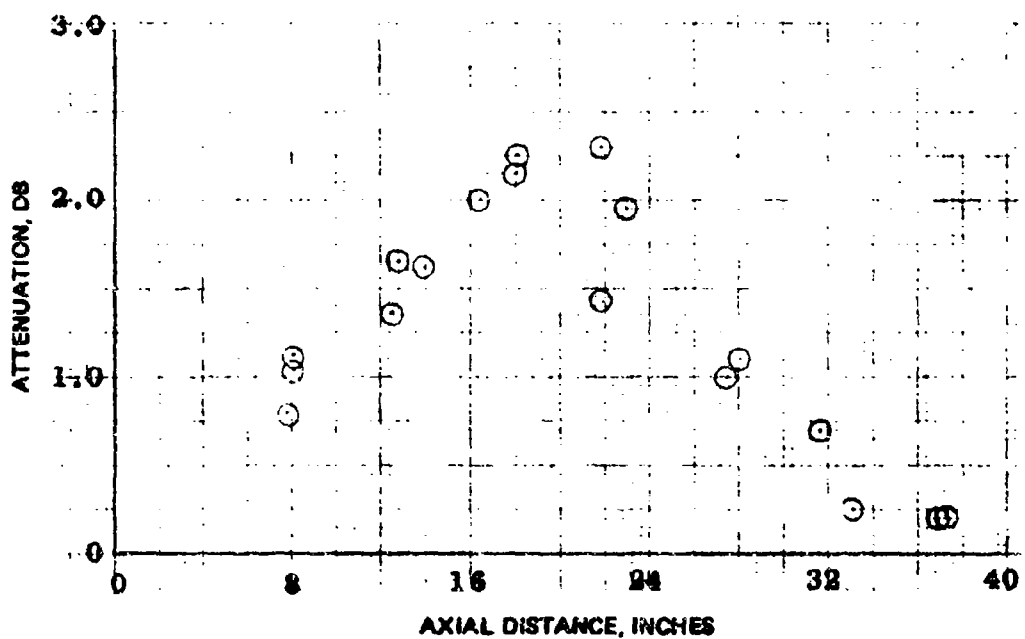


Test No. 20.

NWC TP 5319, Part 1

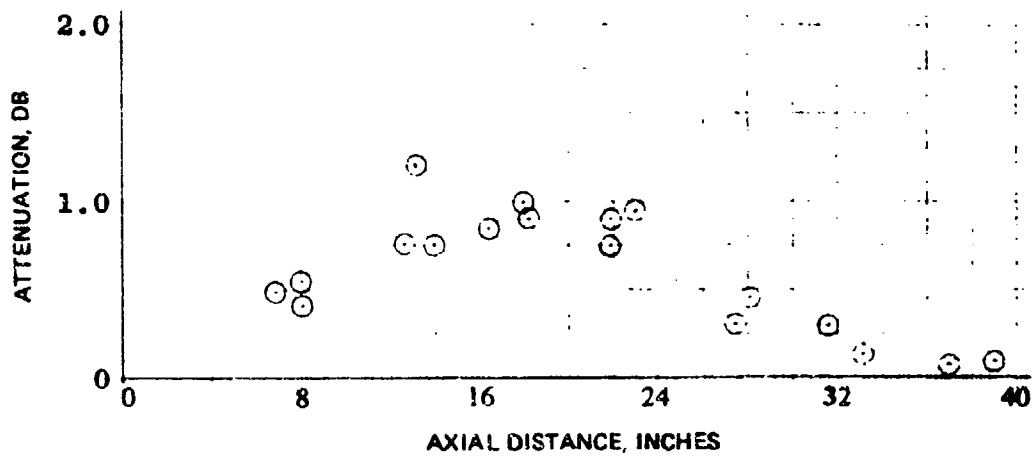


Test No. 21.

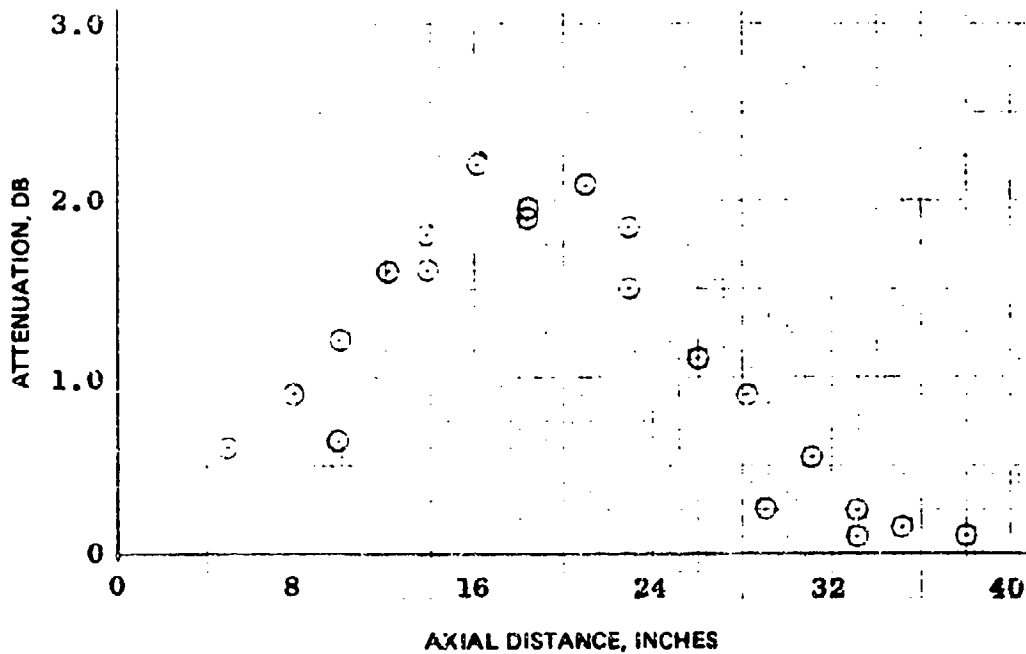


Test No. 22.

NWC TP 5319, Part 1

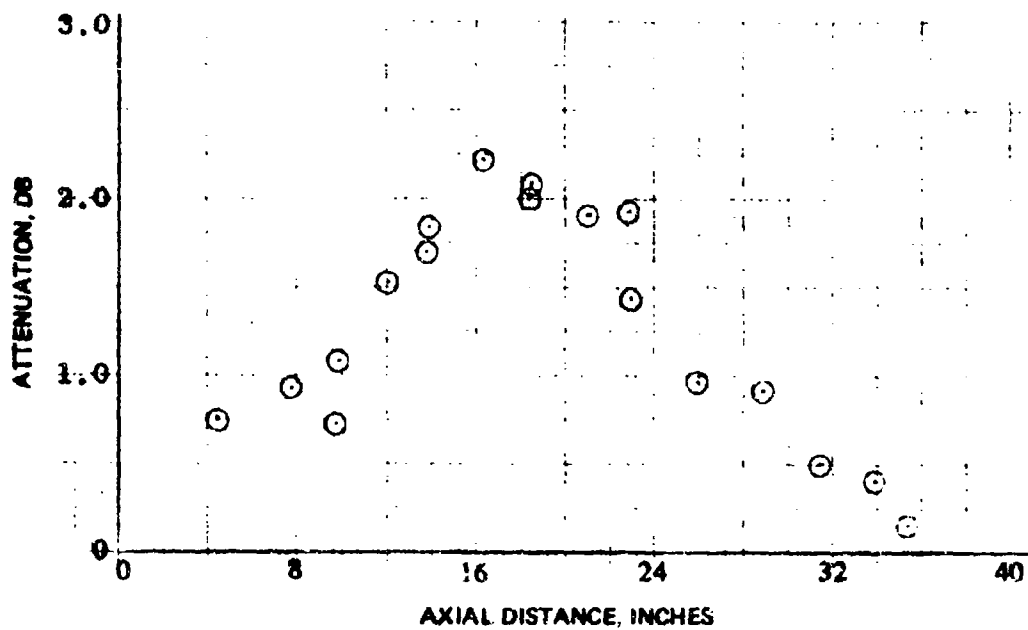


Test No. 23.

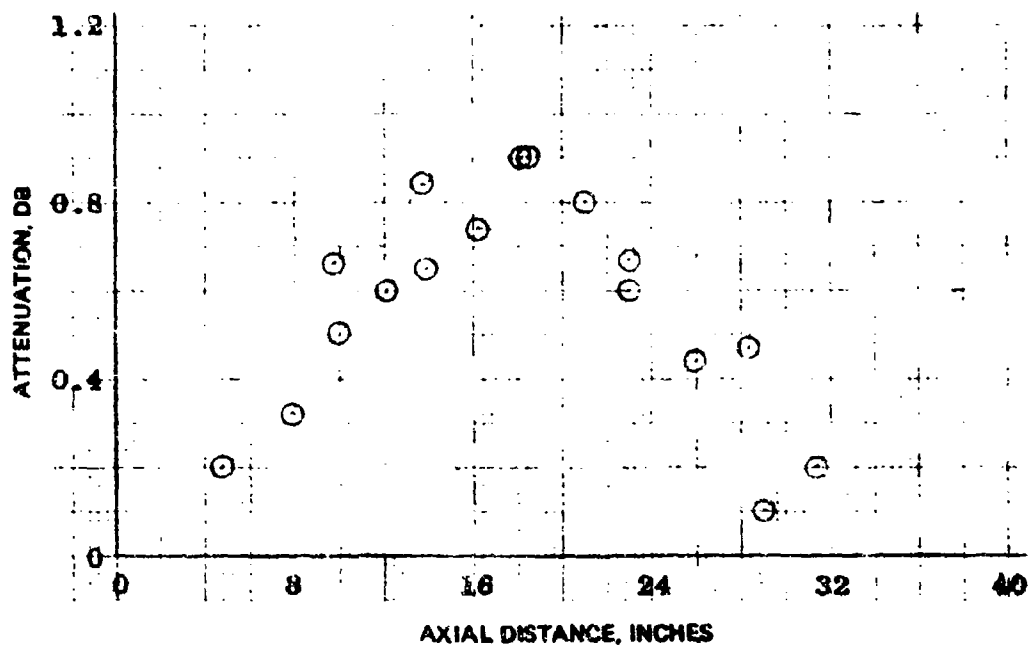


Test No. 24.

NWC TP 5319, Part 1

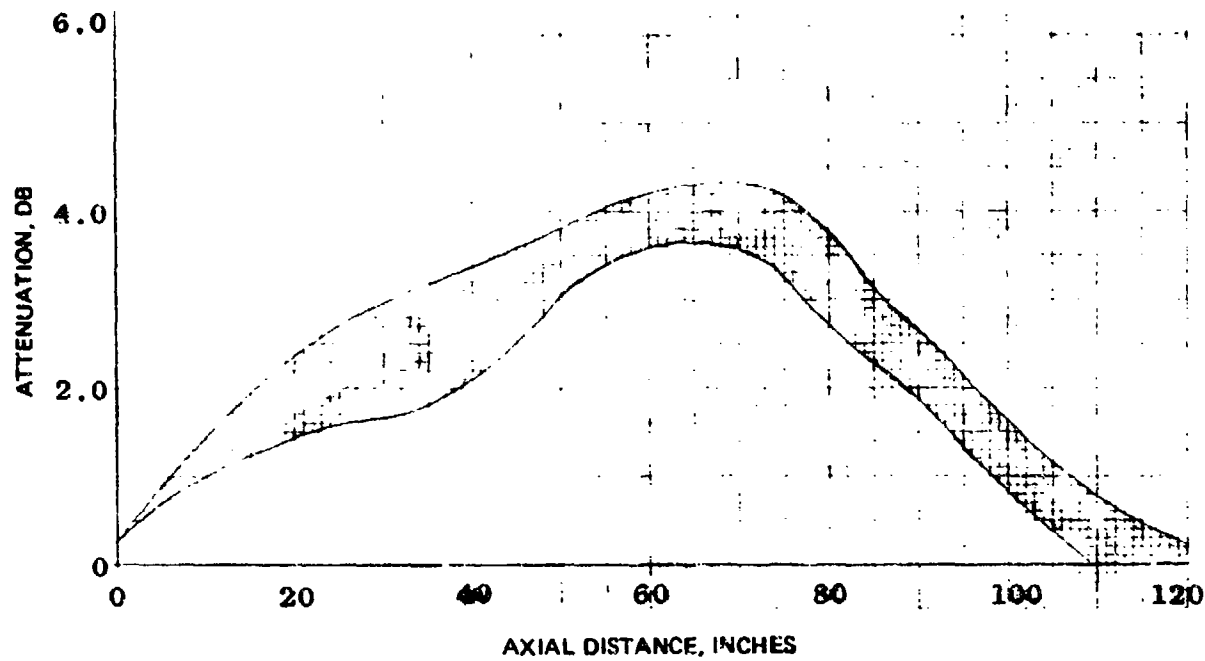


Test No. 25.

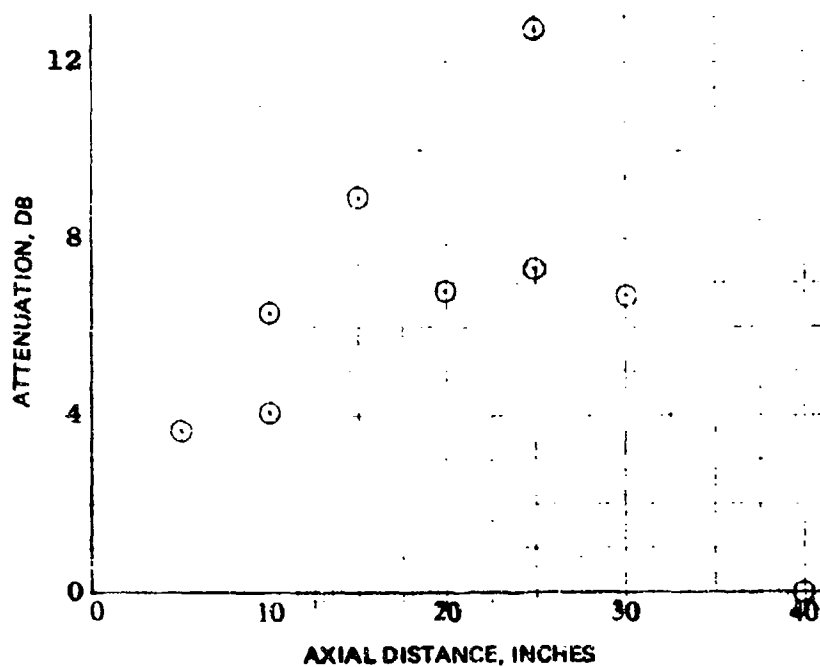


Test No. 26.

NWC TP 5319, Part 1

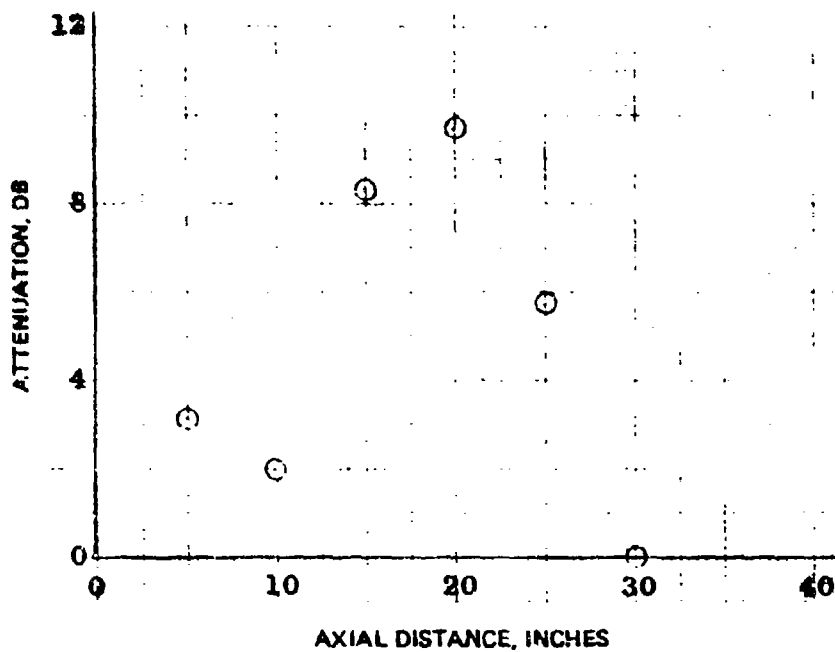


Test No. 27.

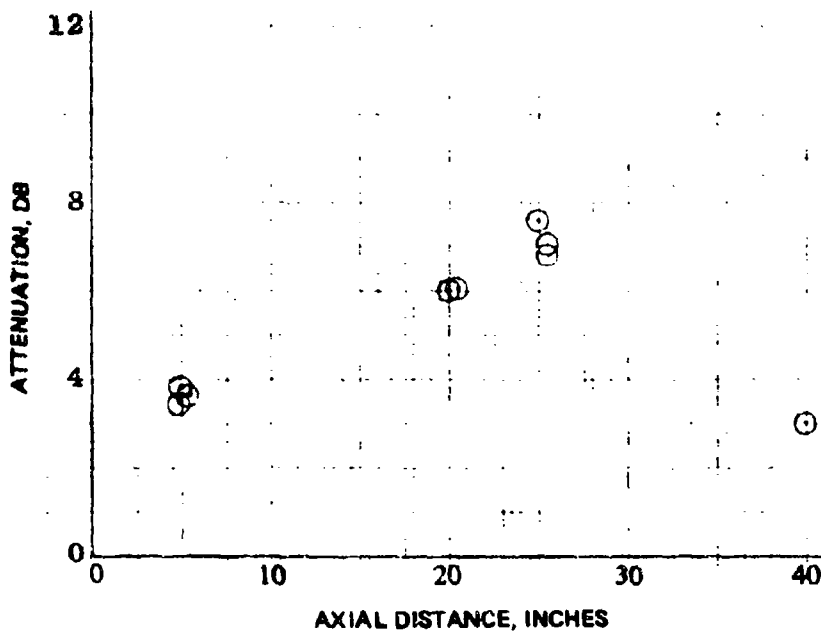


Test No. 28.

NWC TP 5319, Part 1

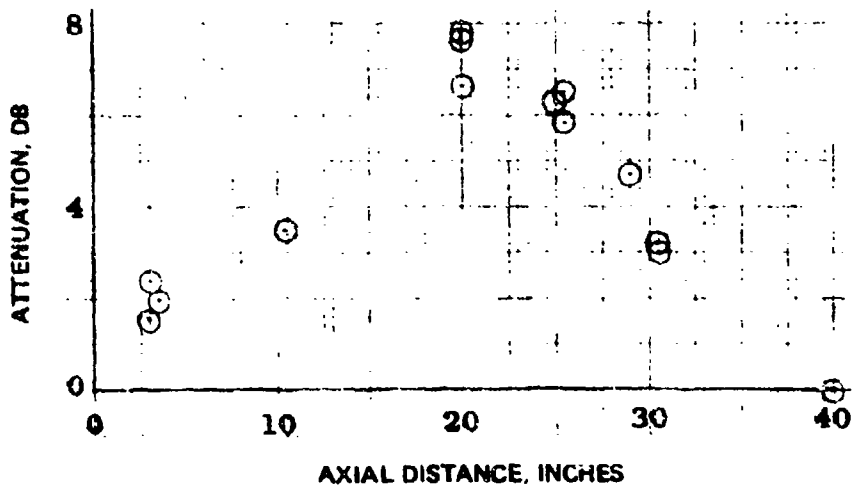


Test No. 29.

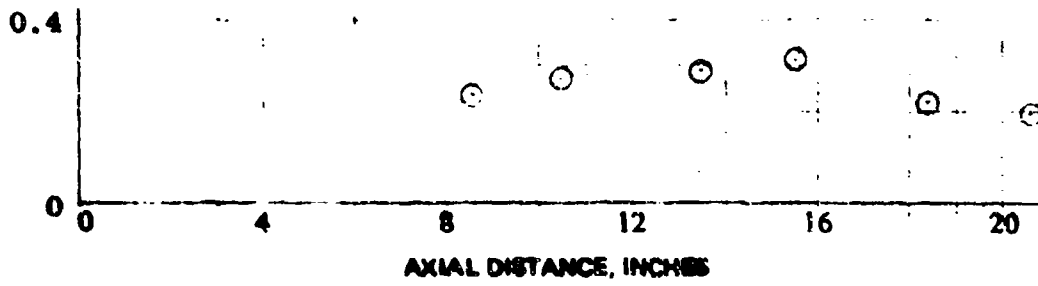


Test No. 30.

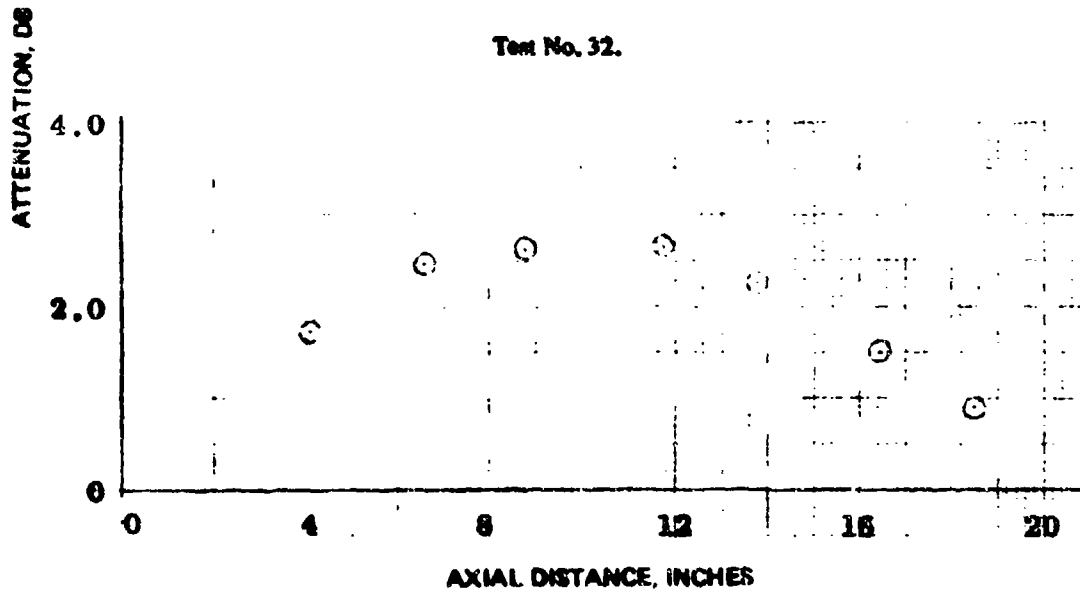
NWC TP 5319, Part 1



Test No. 31.

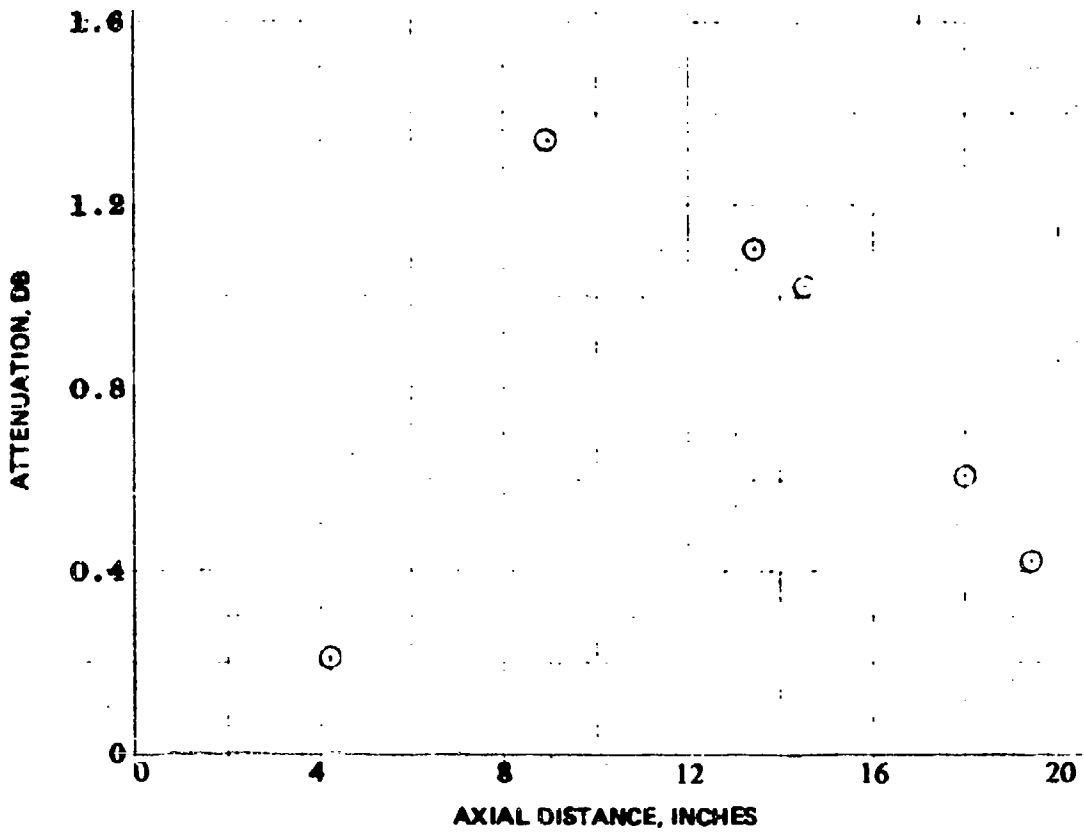


Test No. 32.

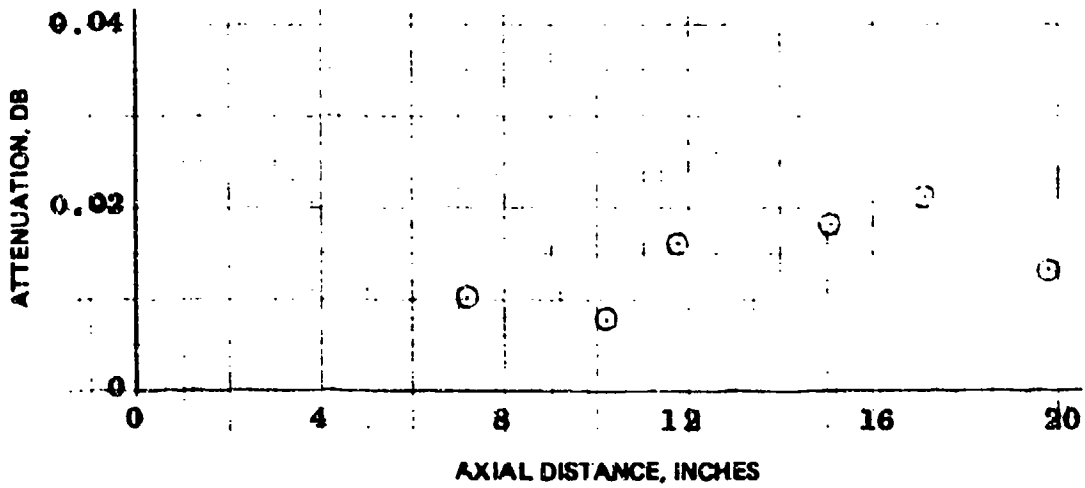


Test No. 33.

NWC TP 5319, Part 1

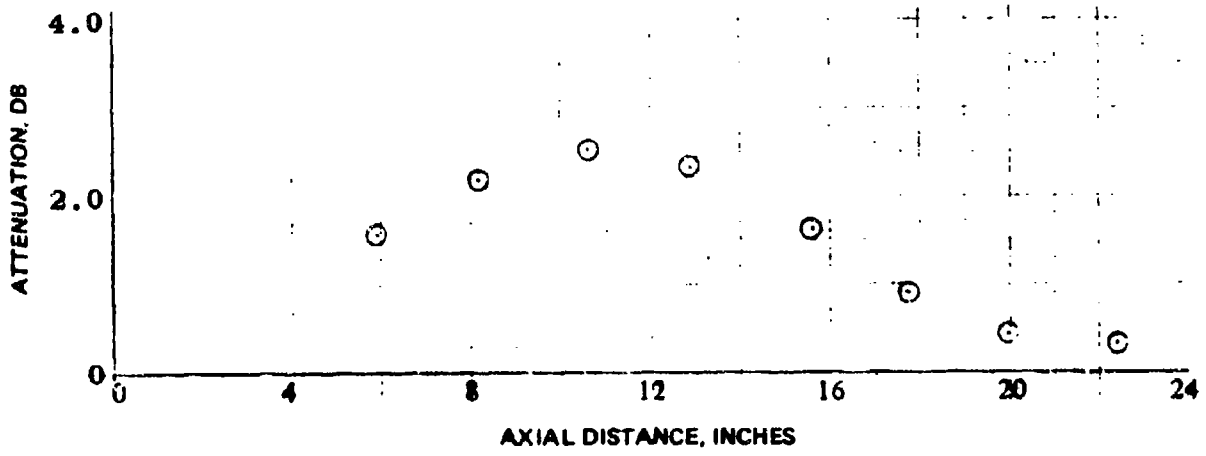


Test No. 34.

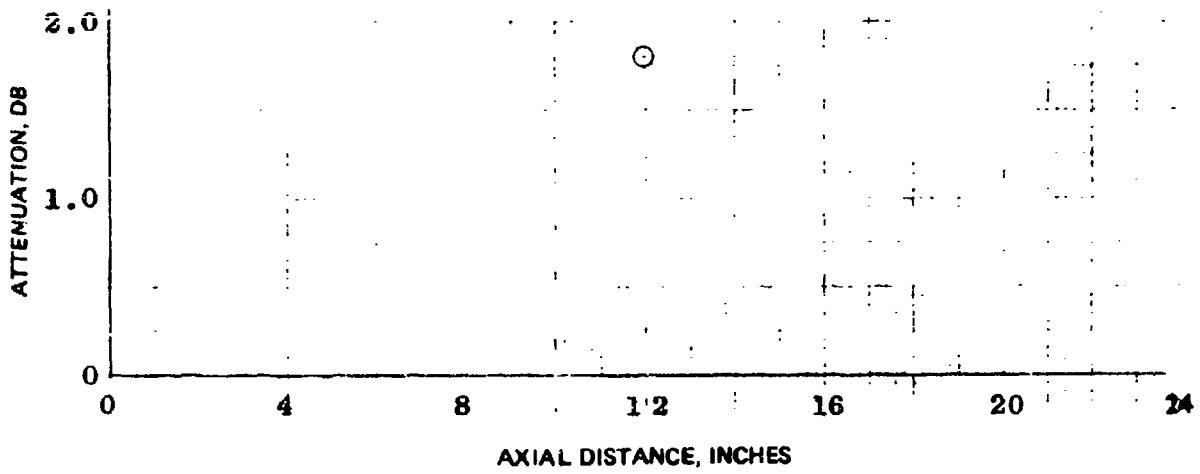


Test No. 35.

NWC TP 5319, Part 1

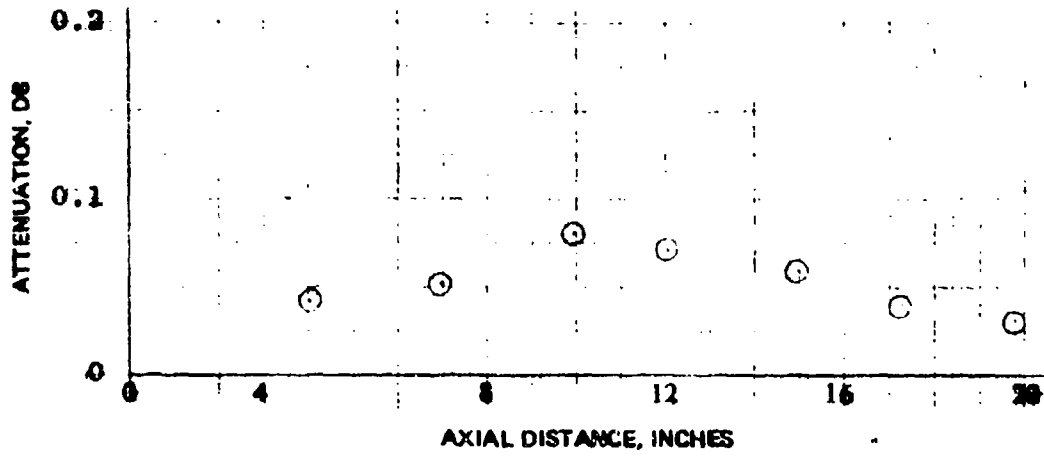


Test No. 36.

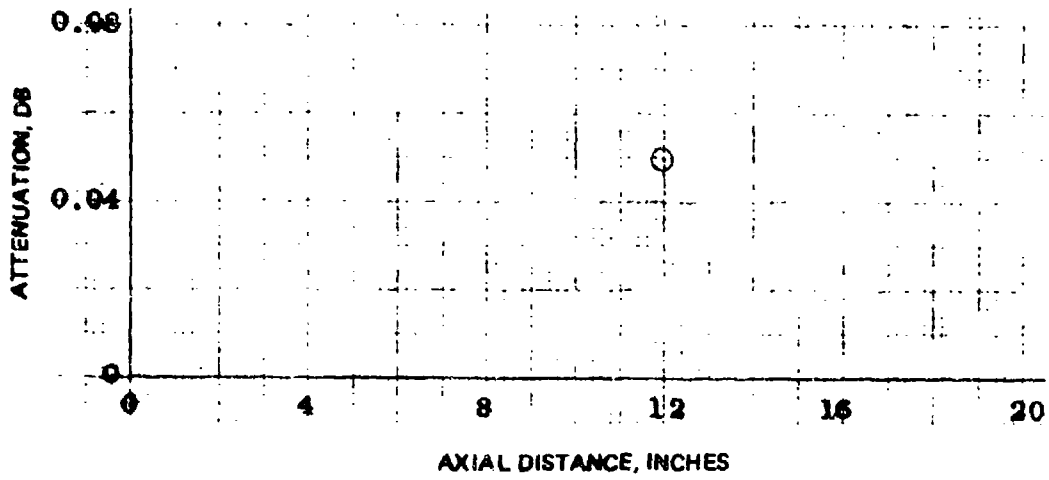


Test No. 37.

NWC TP 5319, Part 1

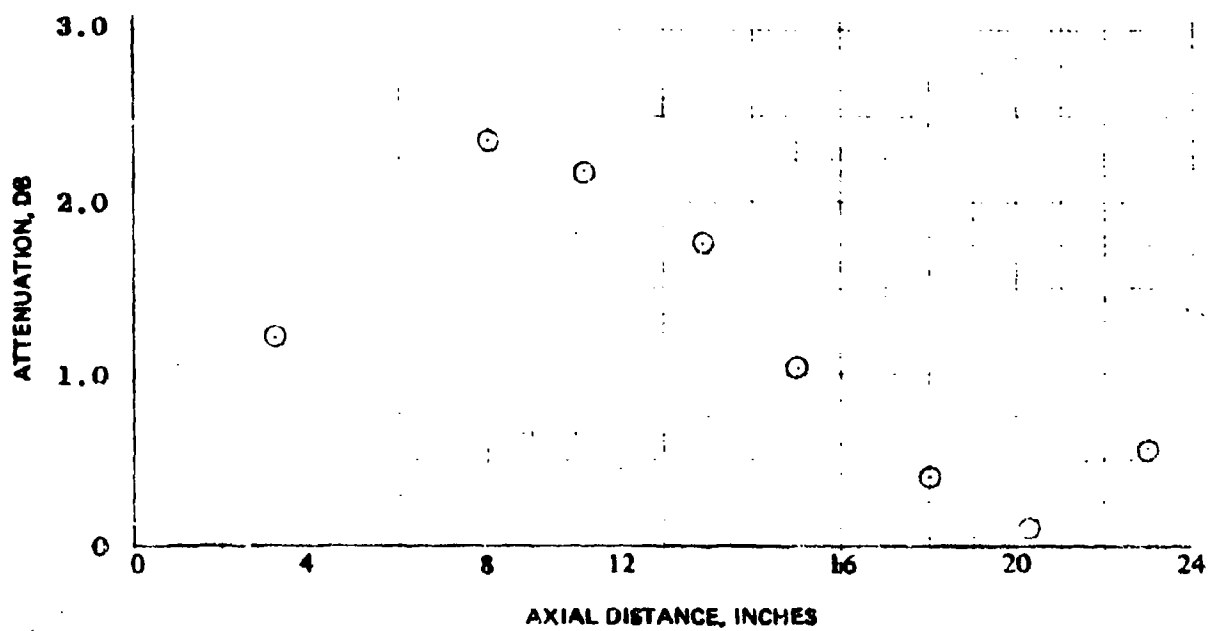


Test No. 38.

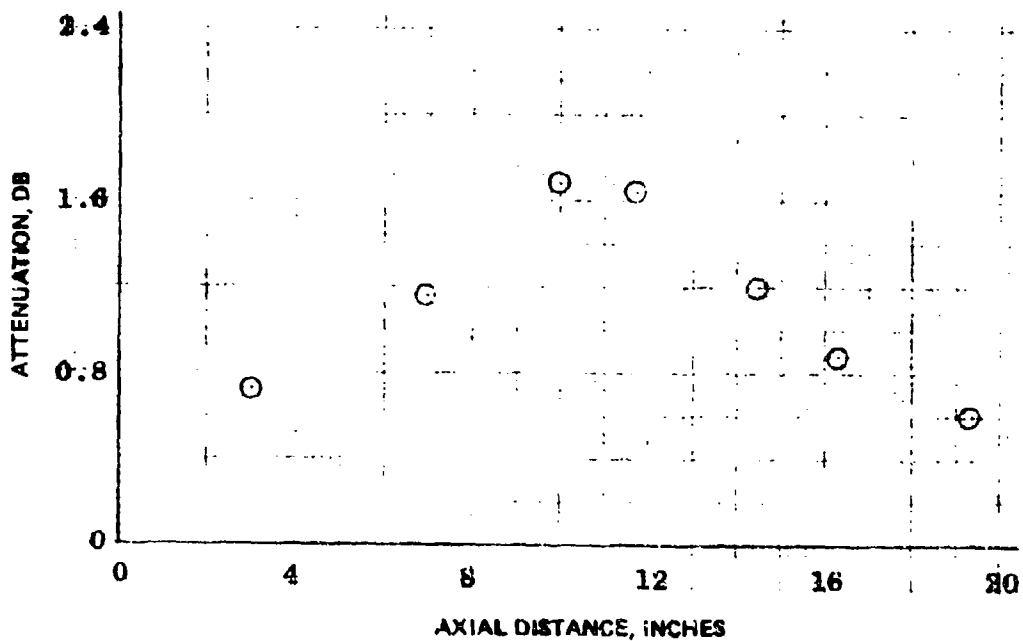


Test No. 39.

NWC TP 5319, Part 1

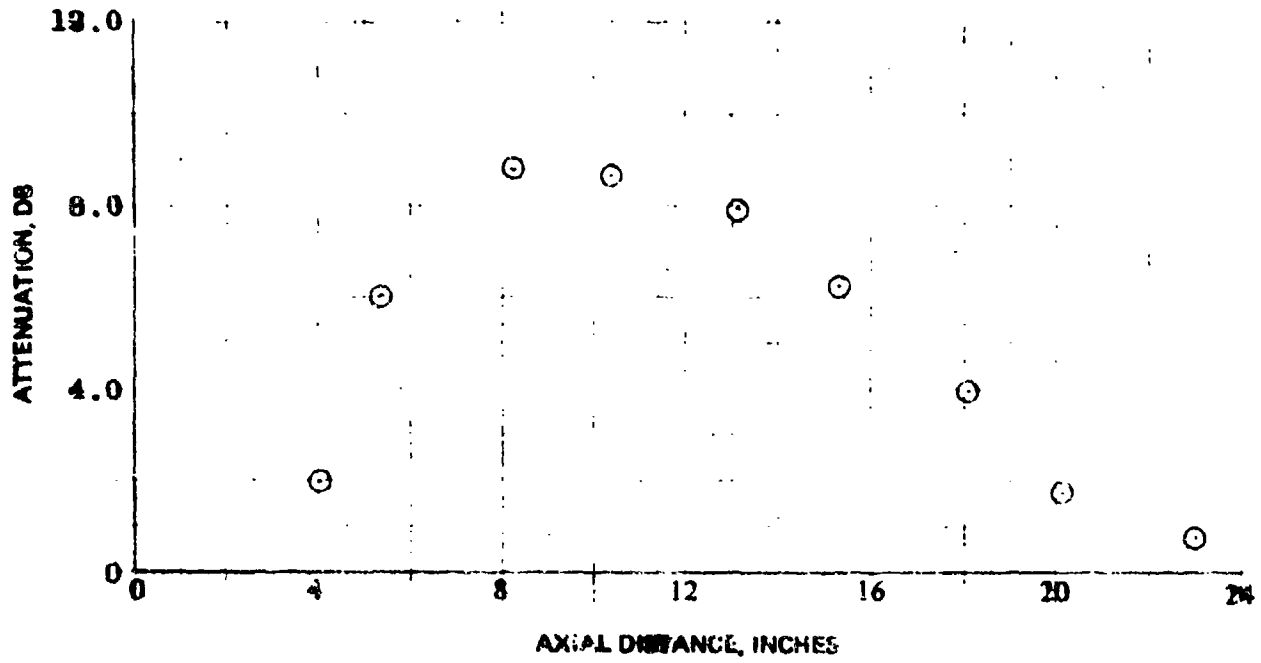


Test No. 40.

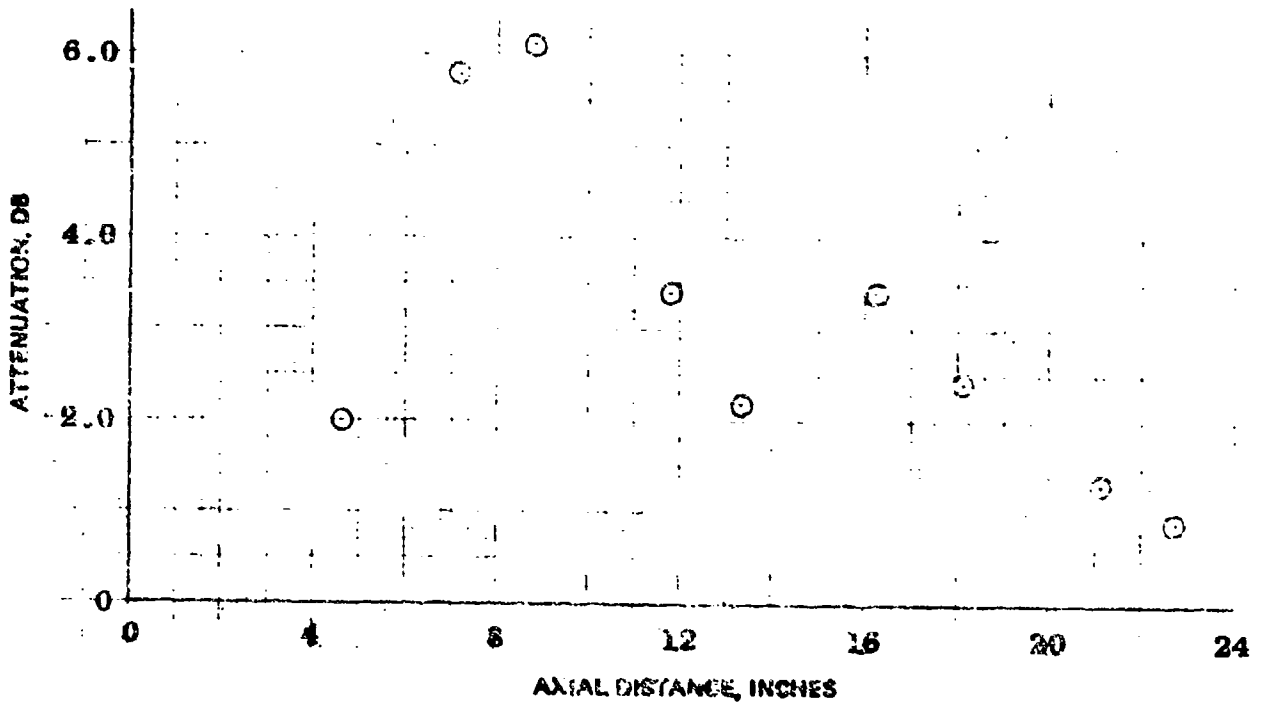


Test No. 41.

NWC TP 5319, Part 1

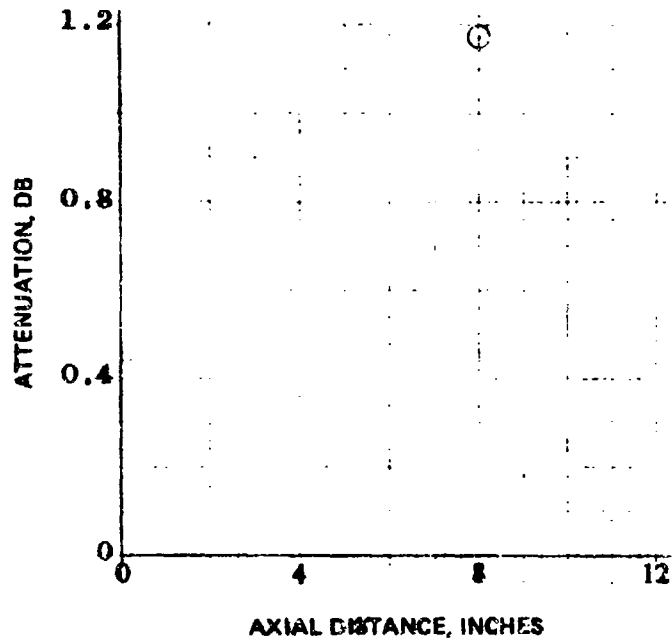


Test No. 42.

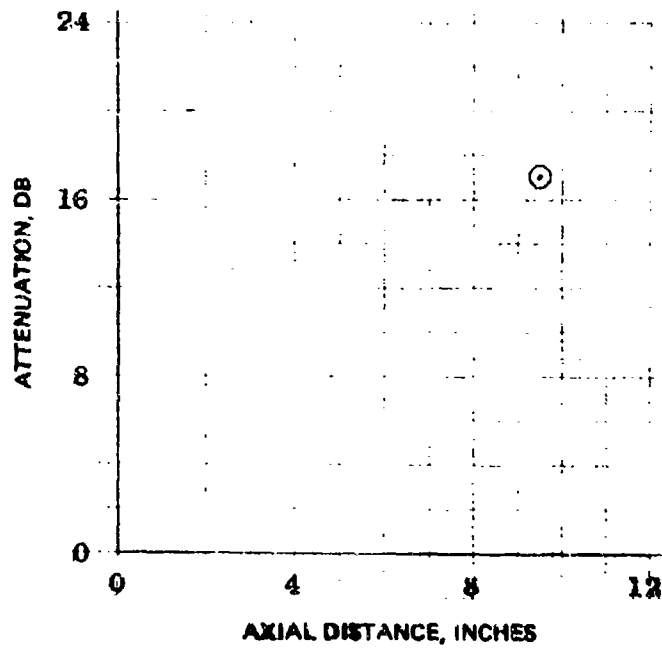


Test No. 43.

NWC TP 5319, Part 1

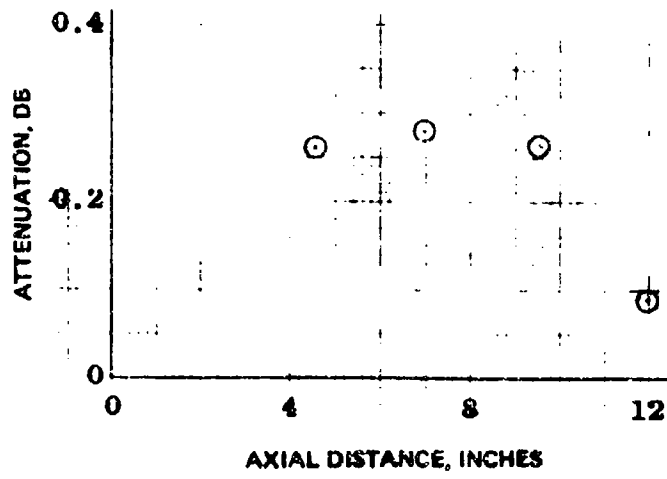


Test No. 44.

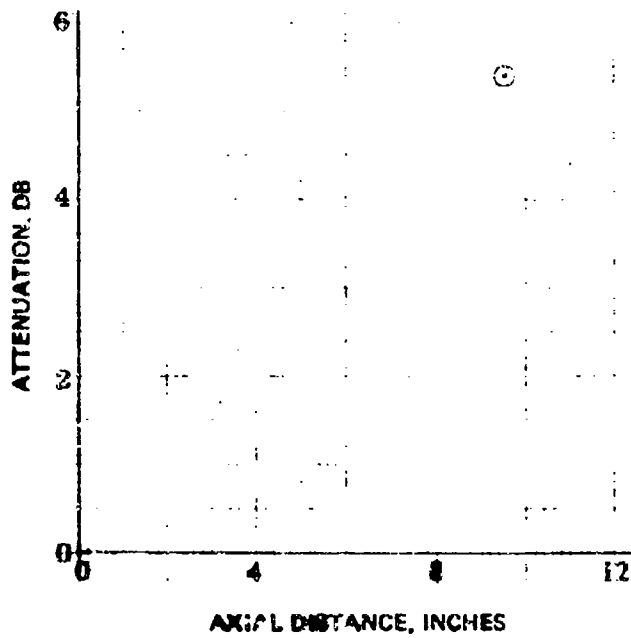


Test No. 45.

NWC TP 5319, Part 1

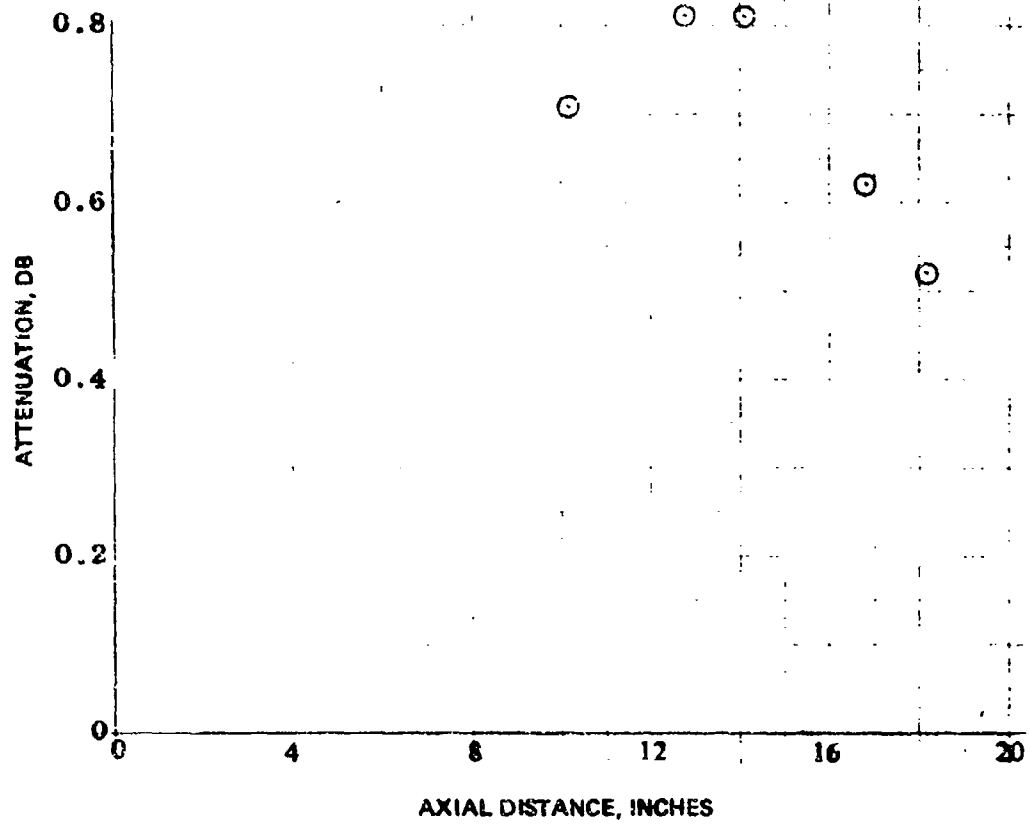


Test No. 46.



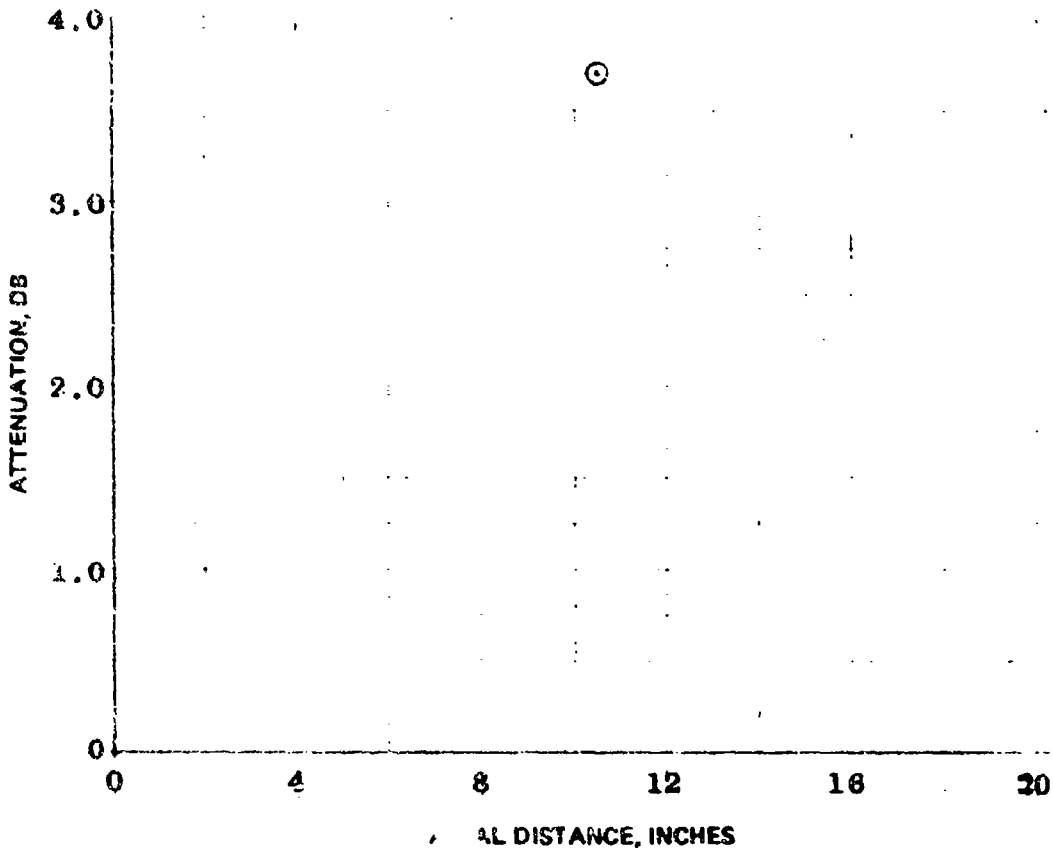
Test No. 47.

NWC TP 5319, Part 1

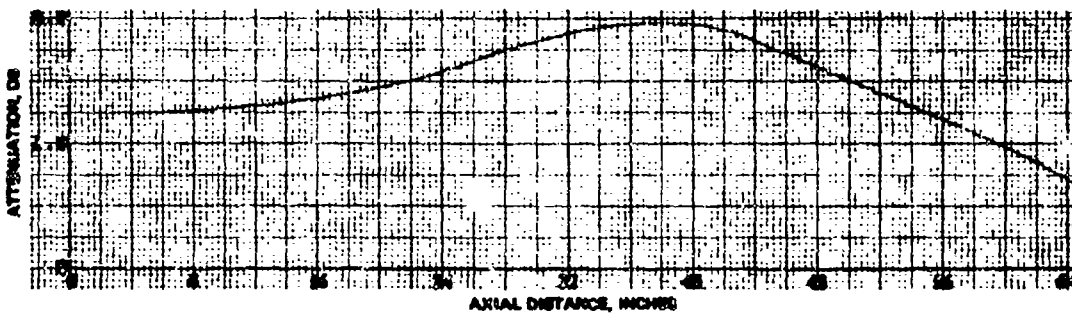


Test No. 48.

NWC TP 5319, Part 1

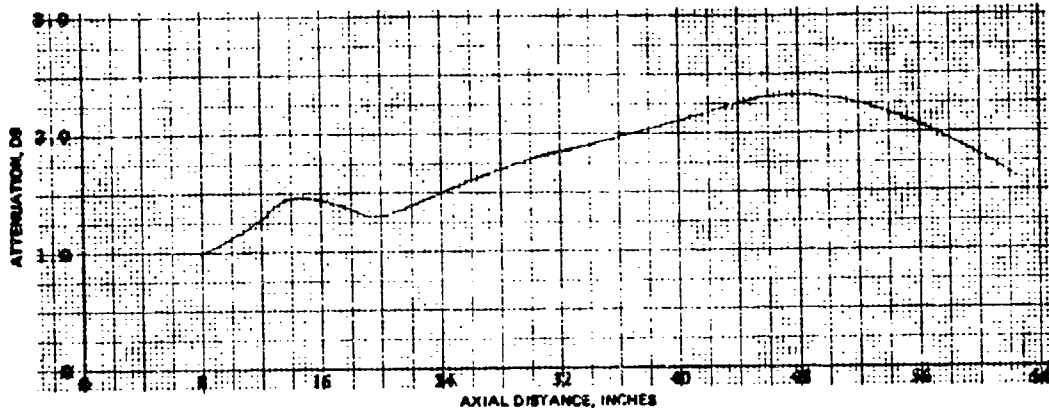


Test No. 49.

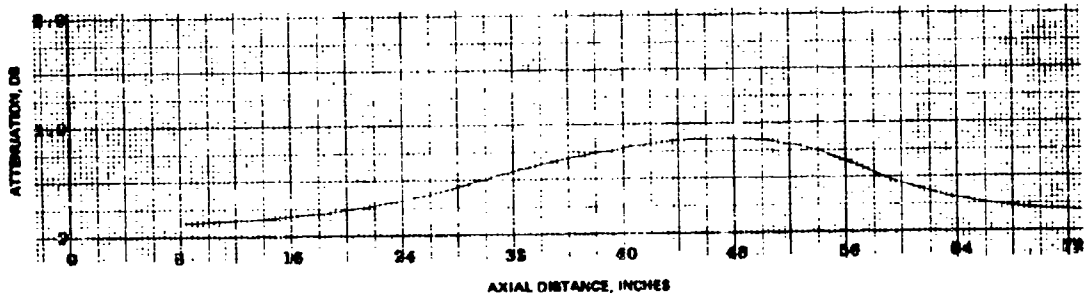


Test No. 50.

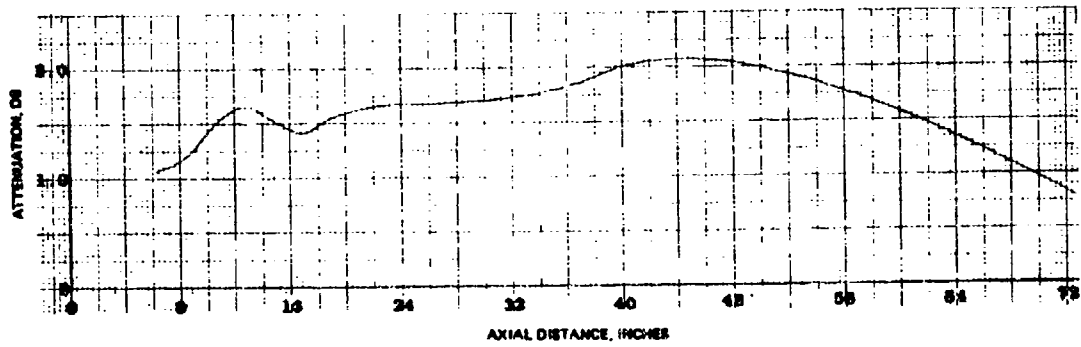
NWC TP 5319, Part 1



Test No. 51.

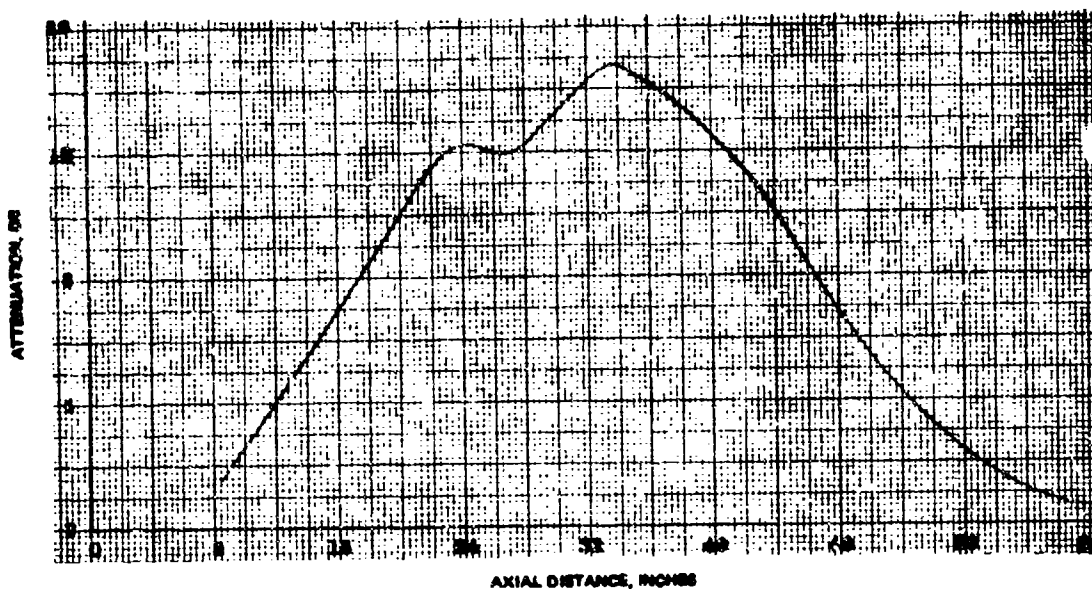


Test No. 52.

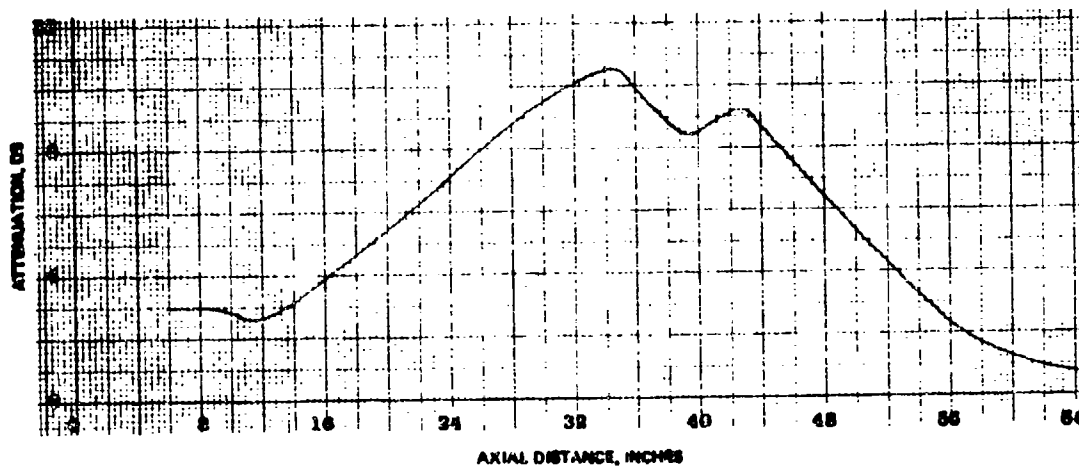


Test No. 53.

NWC TP 5319, Part 1

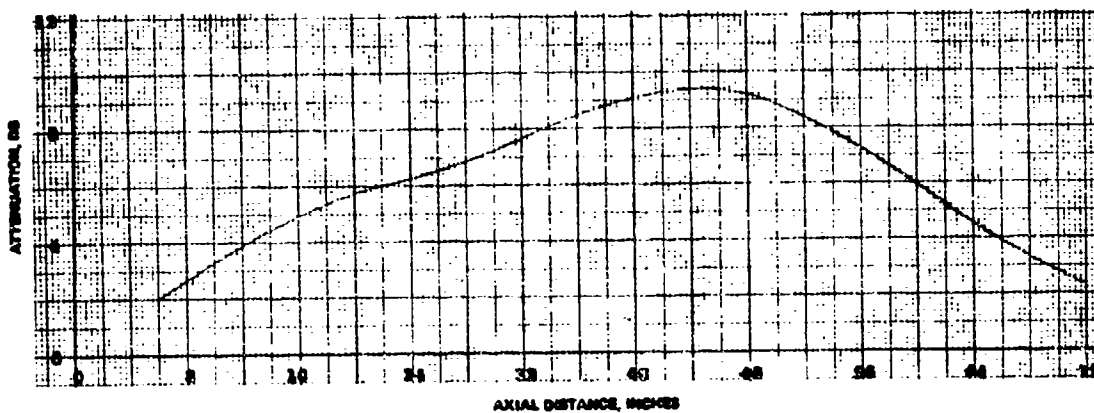


Test No. 54.

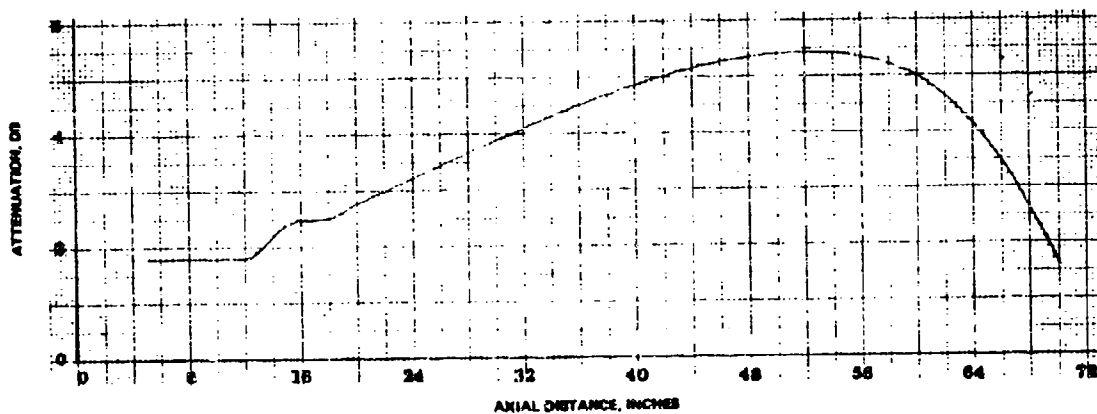


Test No. 55.

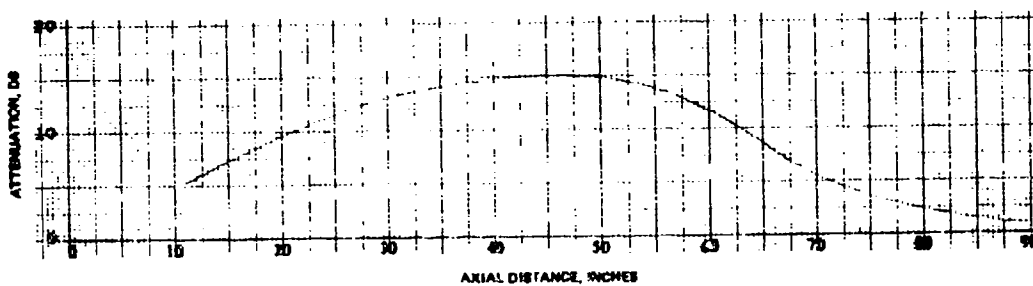
NWC TP 5319, Part 1



Test No. 56.

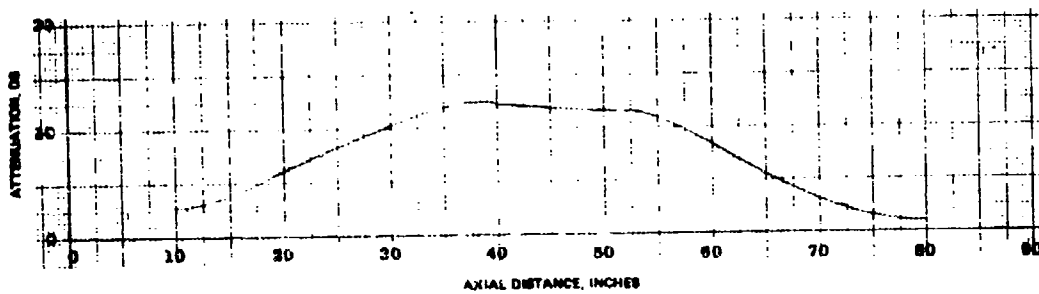


Test No. 57.

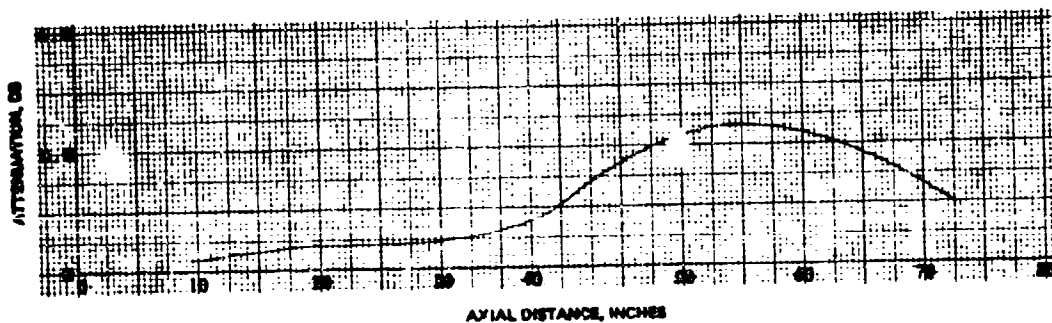


Test No. 58.

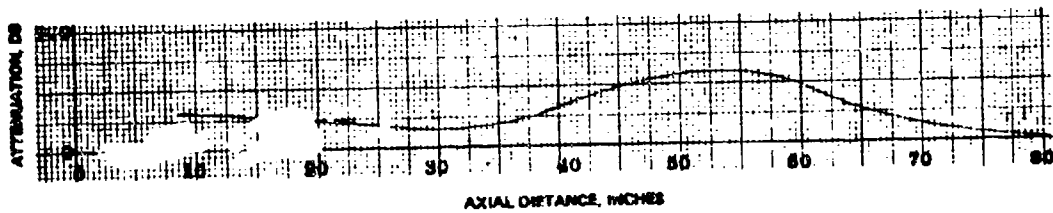
NWC TP 5319, Part 1



Test No. 59.

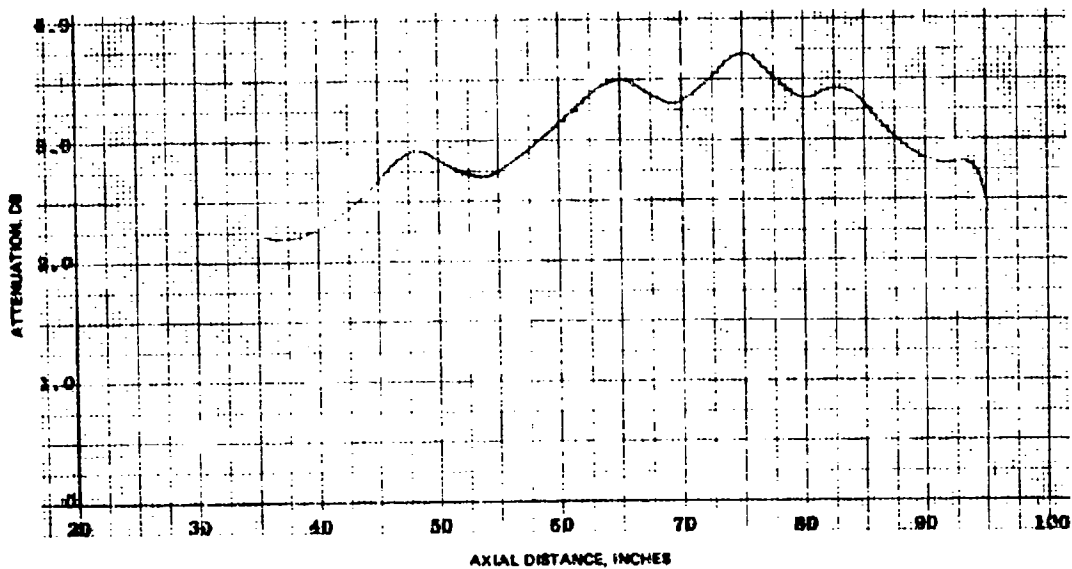


Test No. 60.

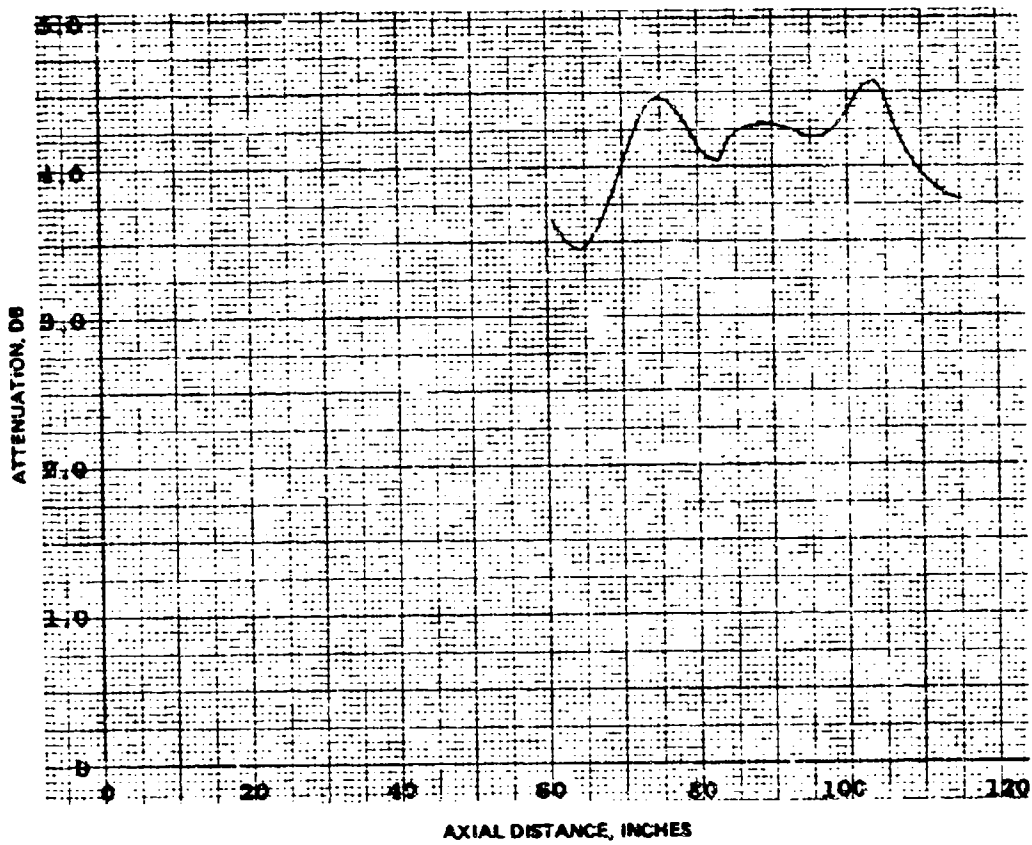


Test No. 61.

NWC TP 5319, Part 1

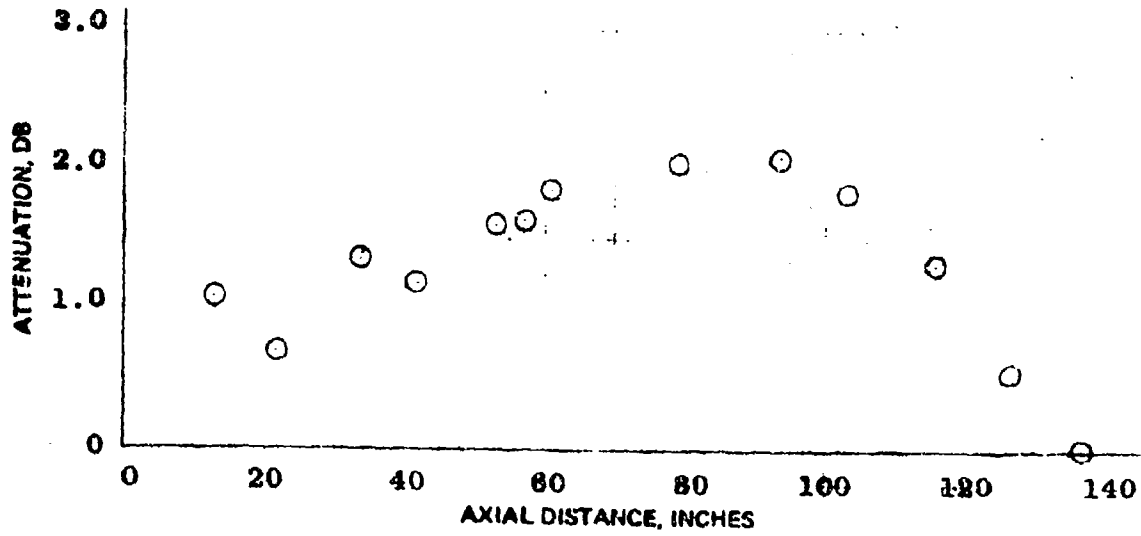


Test No. 62.

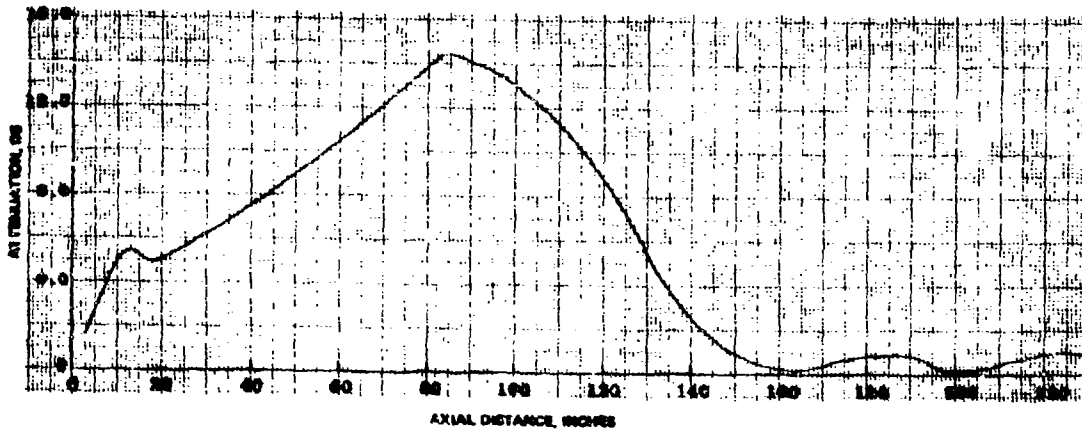


Test No. 63.

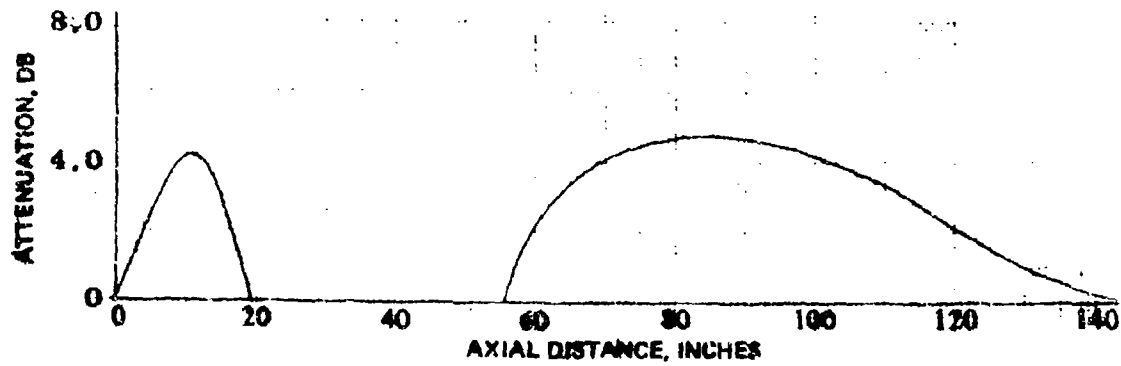
NWC TP 5319, Part 1



Test No. 64.

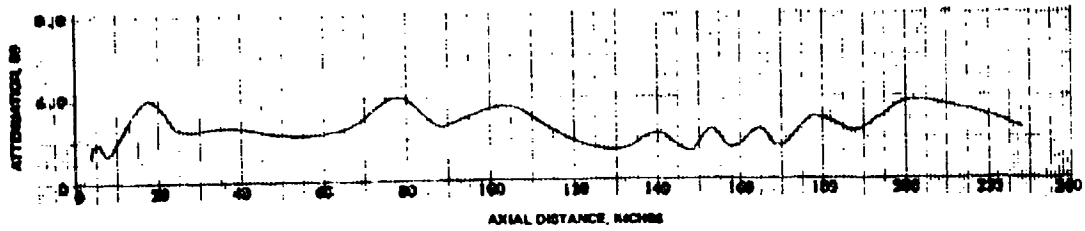


Test No. 65.

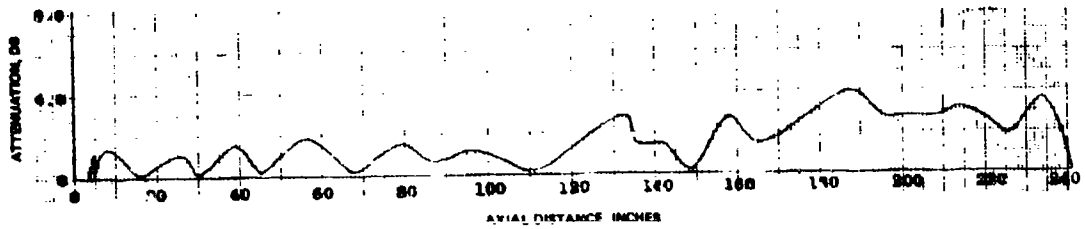


Test No. 66.

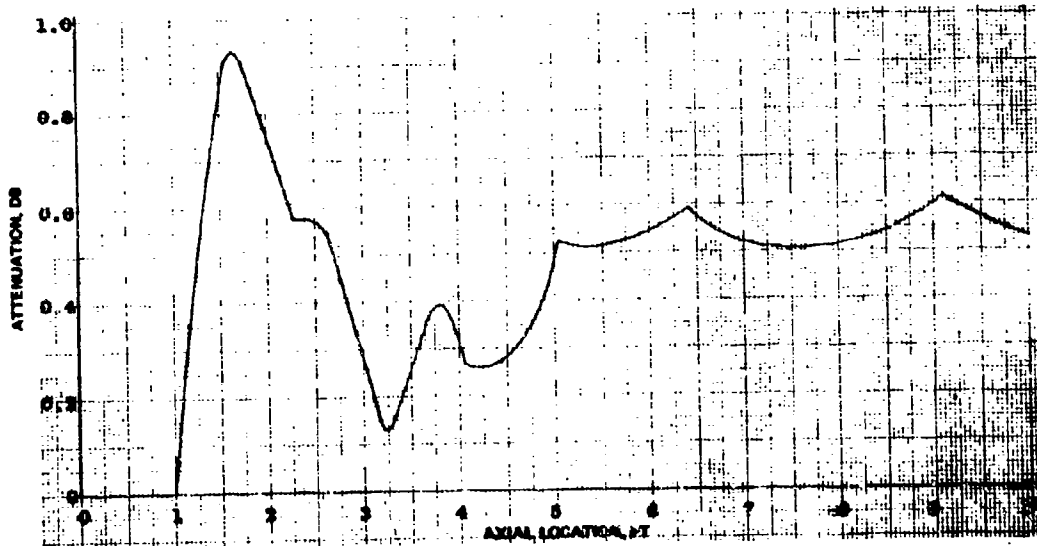
NWC TP 5319, Part 1



Test No. 67.

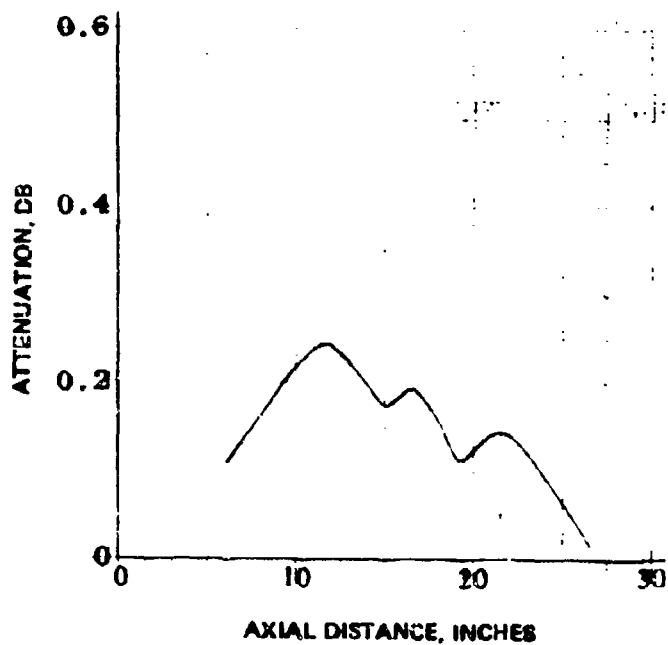


Test No. 68.

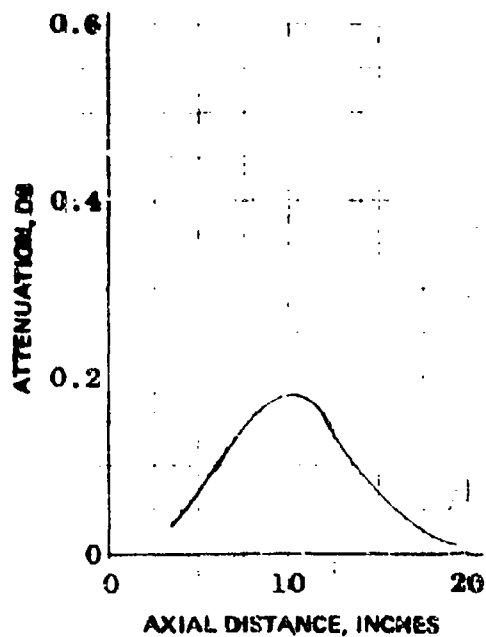


Test No. 69.

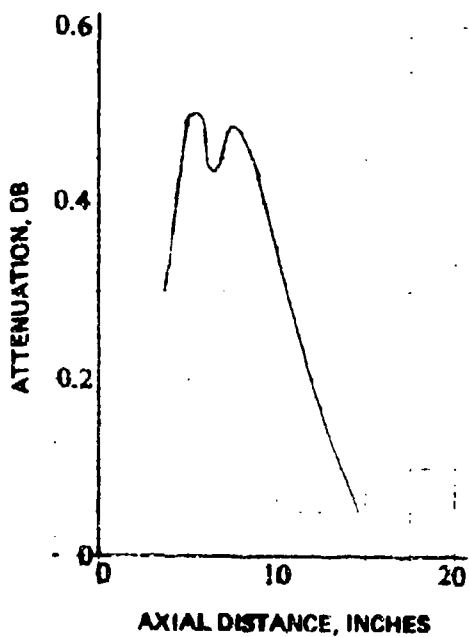
NWC TP 5319, Part 1



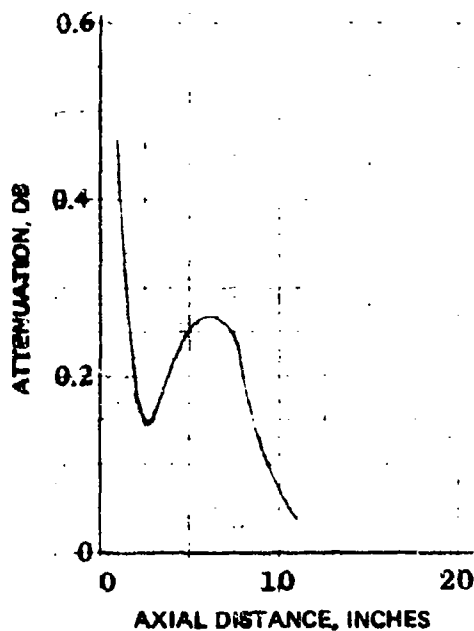
Test No. 70.



Test No. 71.

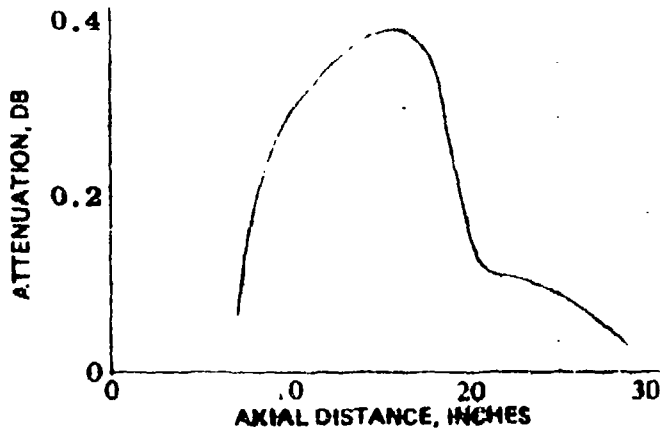


Test No. 72.

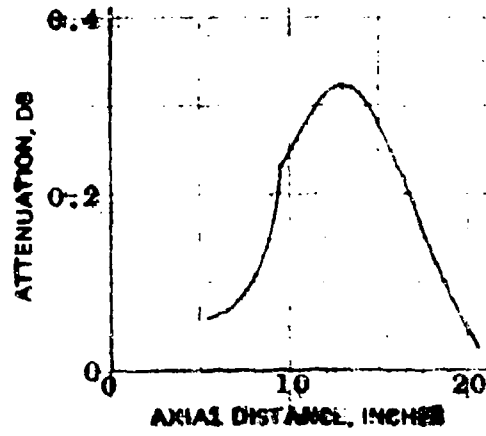


Test No. 73.

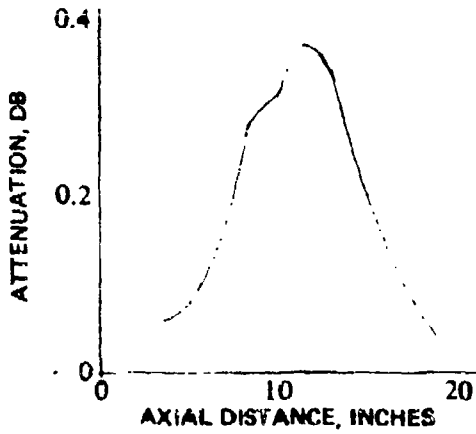
NWC TP 5319, Part 1



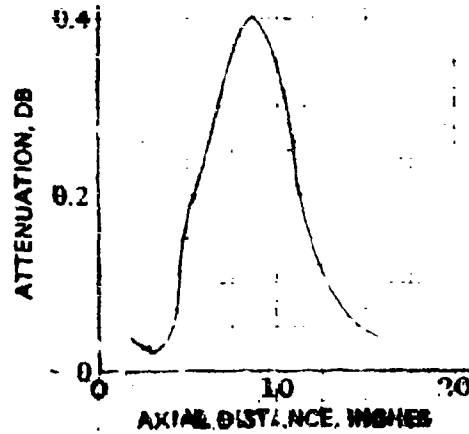
Test No. 74.



Test No. 75.

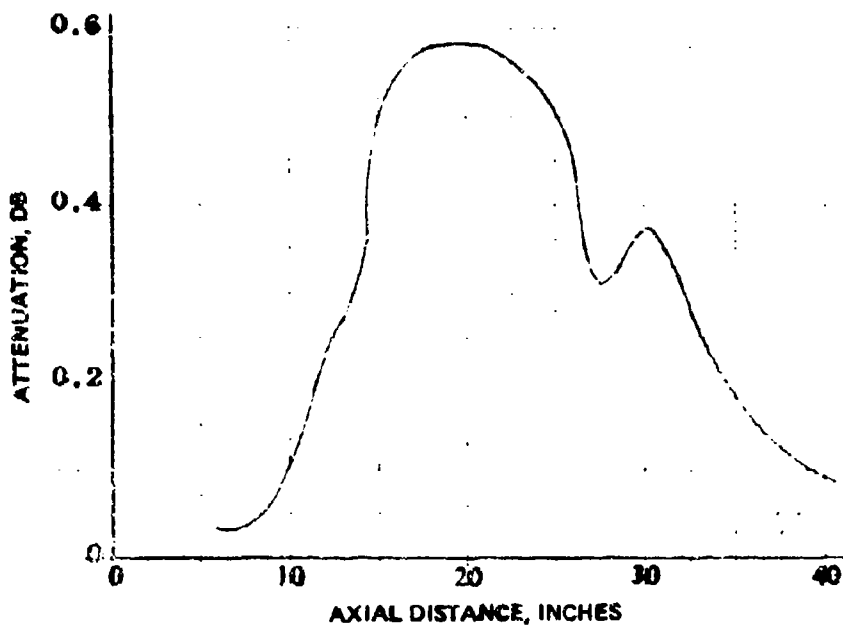


Test No. 76.

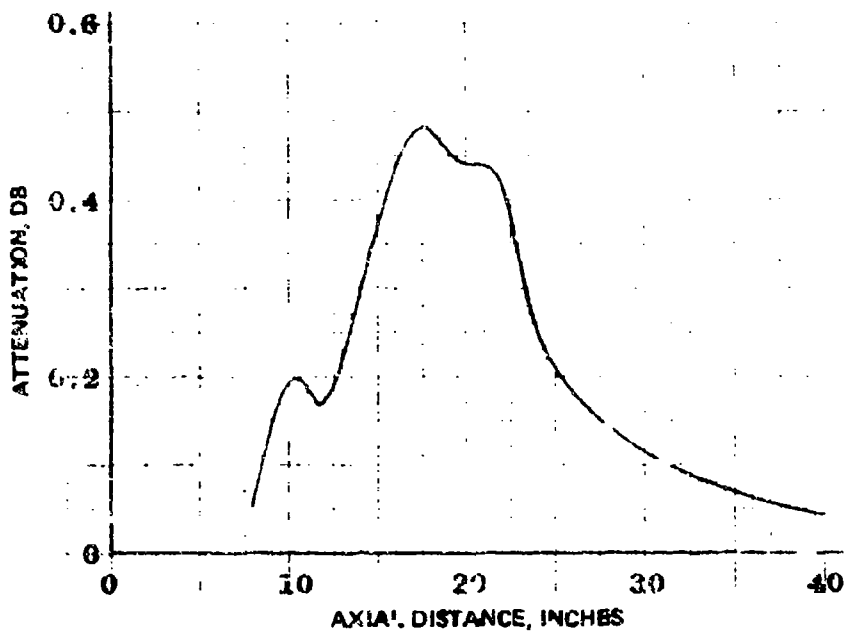


Test No. 77.

NWC TP 5319, Part 1

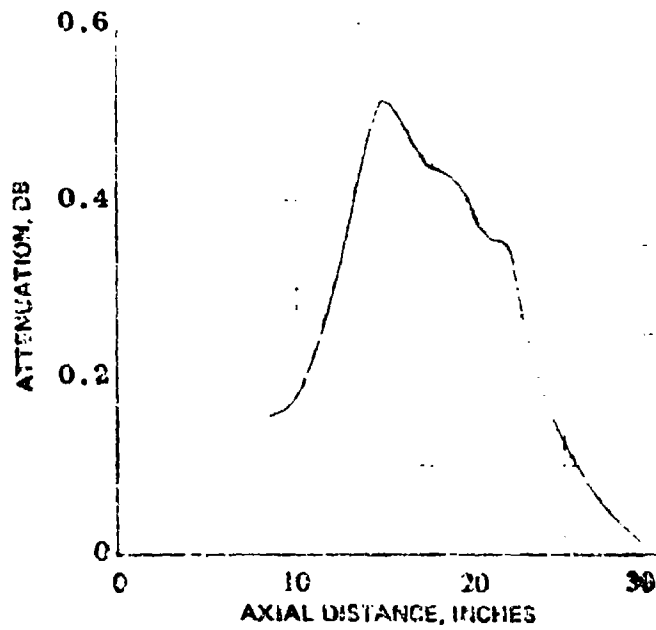


Test No. 78.

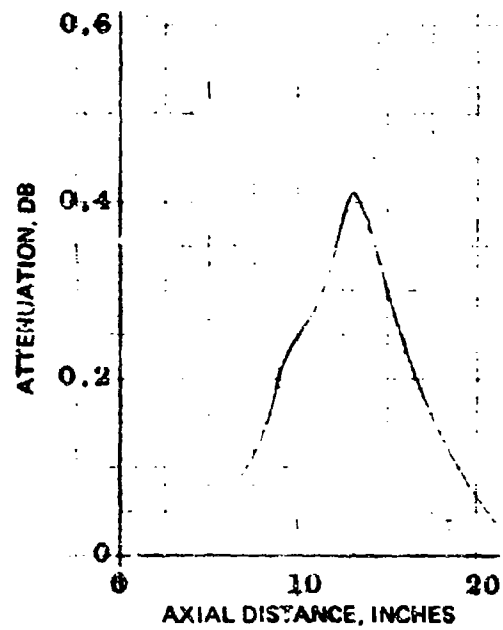


Test No. 79.

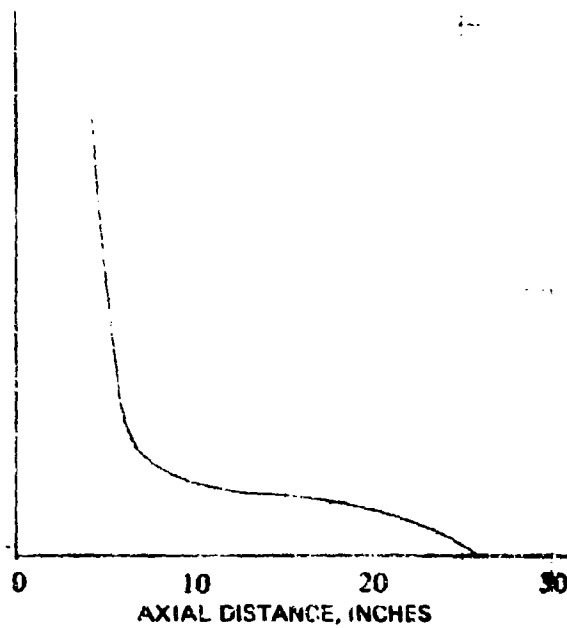
NWC TP 5319, Part 1



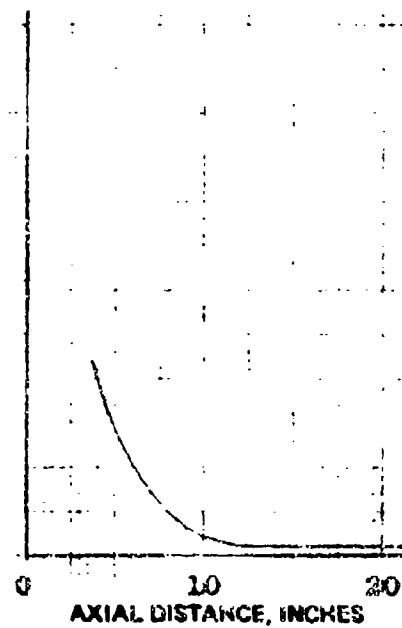
Test No. 80.



Test No. 81.

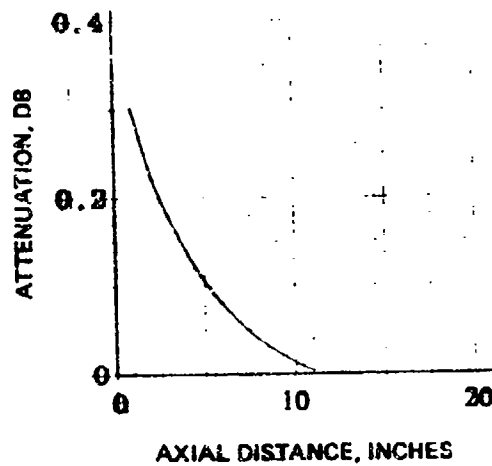


Test No. 82.

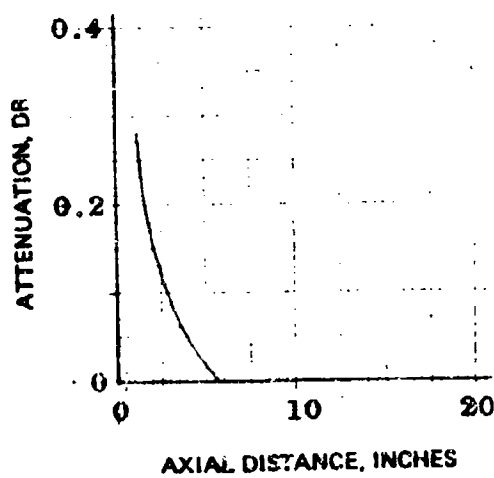


Test No. 83.

NWC IP 5319, Part 1

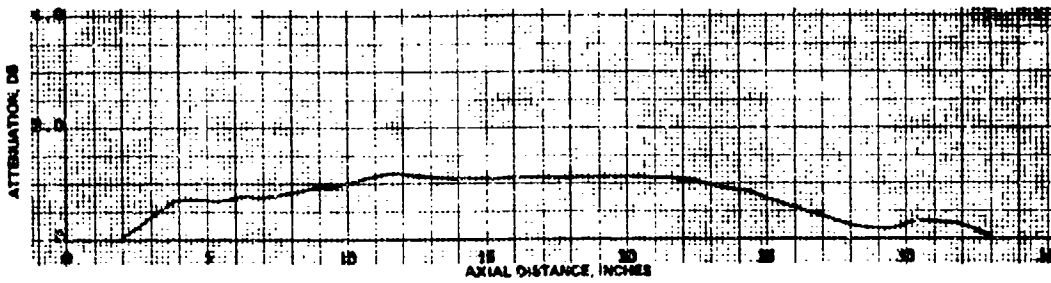


Test No. 84.

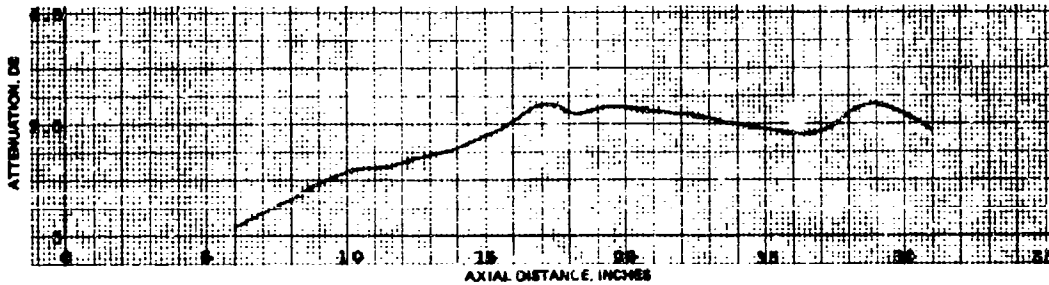


Test No. 85.

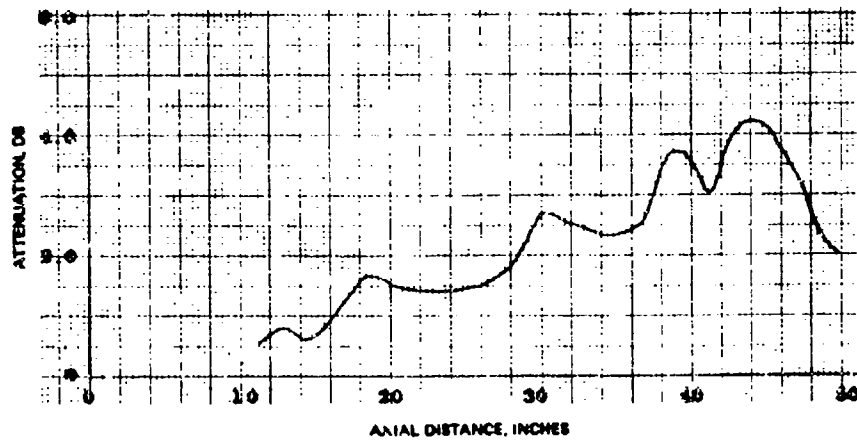
NWC TP 5319, Part 1



Test No. 86.

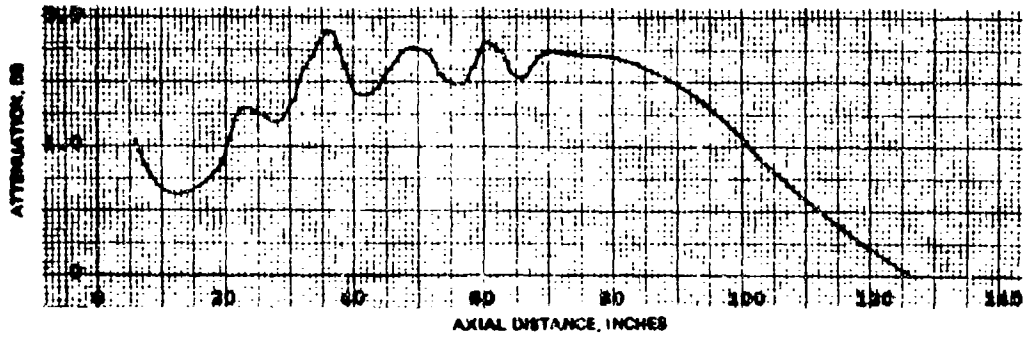


Test No. 87.

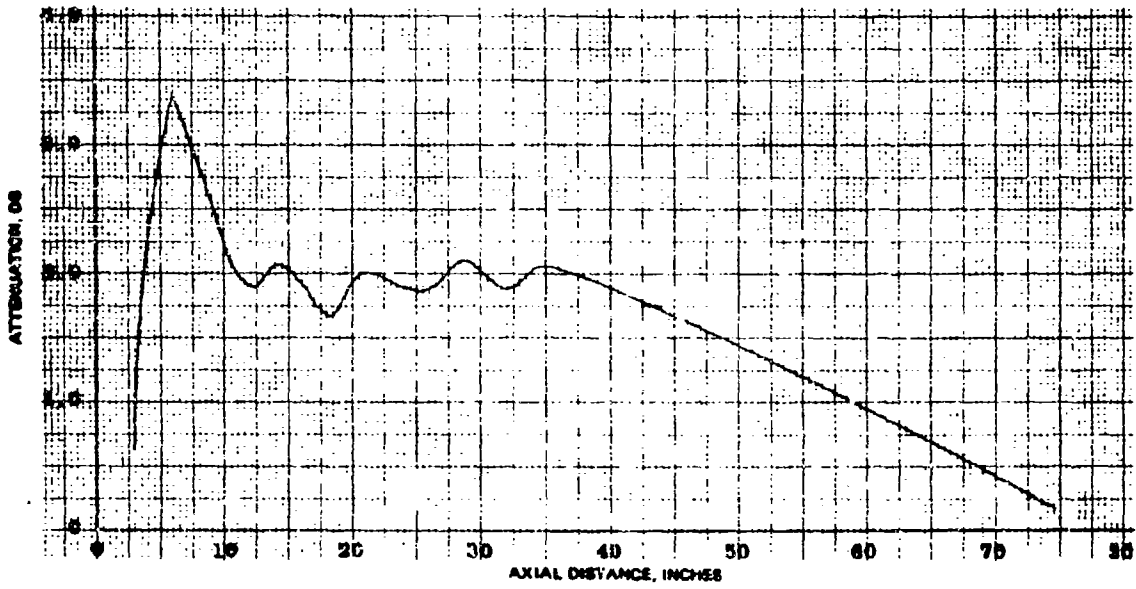


Test No. 88.

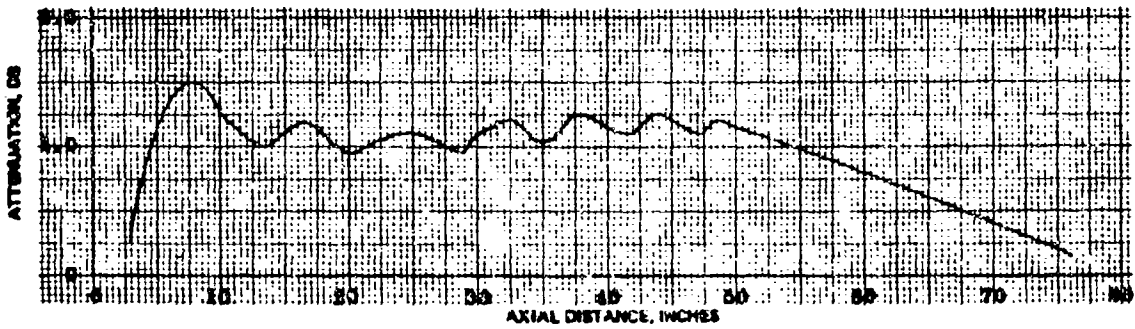
NWC TP 5319, Part 1



Test No. 89.

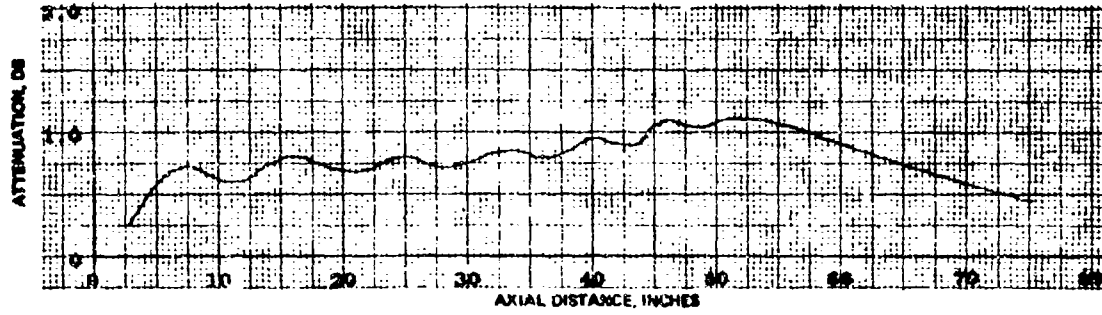


Test No. 90.

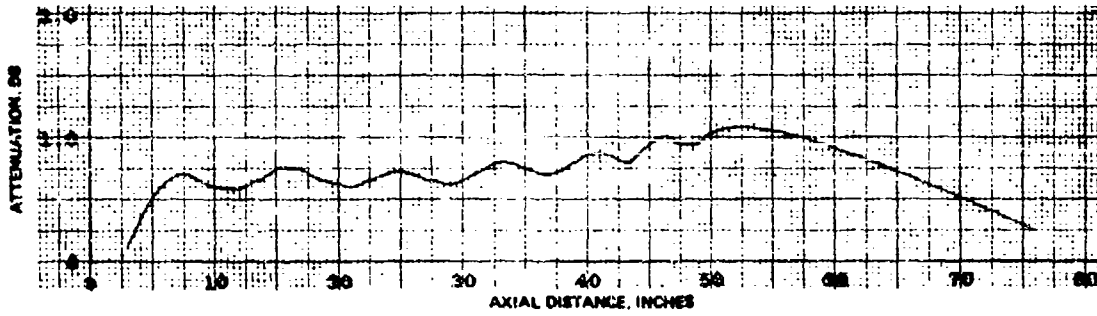


Test No. 91.

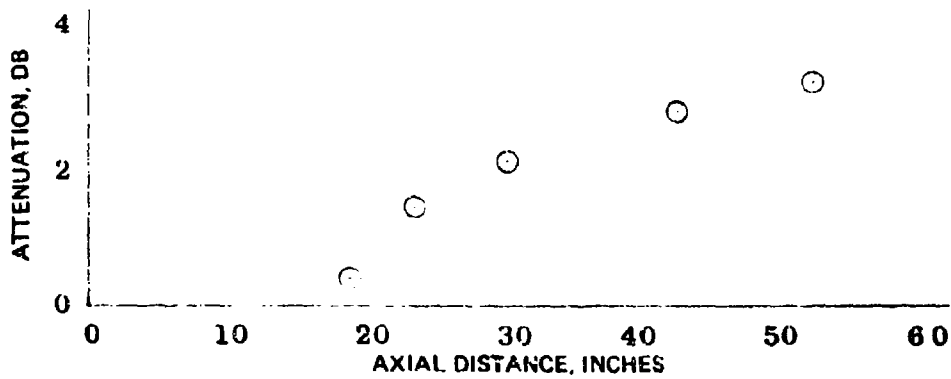
NWC TP 5319, Part 1



Test No. 92.



Test No. 93.



Test No. 94.

NWC TP 5319, Part 1

Appendix D

**PLUME PROPERTIES AND RADAR ATTENUATION FOR
SIX ROCKET MOTOR FIRINGS**



Associated Technical Consultants / P.O. Box 42, University Station, Provo, Utah 84601

Technical Report

**Plume Properties and Radar Attenuation
for Six Rocket Motor Firings**

Prepared by

L. Douglas Smoot
Senior Associate
Associated Technical Consultants
P.O. Box 42, University Station
Provo, Utah

19 February 1974

L.D. Smoot, R.L. Coates, J.M. Simonsen, Sr. Associates

NWC TP 5319, Part 1

INTRODUCTION

Work Statement

At the request of the Naval Weapons Center, under NWC contract N60530-74-4330, (74 January 07), Associated Technical Consultants have completed a series of computer computations for six (6) rocket motor firings. The specific work statement for this project is as follows:

1. The contractor shall perform calculations necessary to fully define the plumes and radar attenuation for the six (6) rocket motor firings described in ATTACHMENT 1. Calculations shall be made to (1) define the flow velocity, pressure, temperature and species in the missile base region using the Base Model Component Computer Program of NWC TP 5521, (2) define internal and external inviscid pressure and velocity using the MOC Model Component Computer Program of NWC TP 5521 and (3) define the velocity, temperature, pressure and species (including free electron density and electron collision frequency) in the aft-plume mixing and afterburning flow using the aft-Plume Model Component Computer Program of NWC TP 5521.
2. Transverse and diagonal attenuation shall be calculated for all plumes at the frequencies indicated in Table 1. There shall be a minimum of ten (10) transverse attenuation calculations for each plume between the fore and aft positions where attenuation is 10% of the transverse maximum. There shall be a minimum of 15 diagonal attenuation calculations approximately equally spaced at angles between minus (-) 4 degrees and plus (+) 25 degrees for the antenna positions shown in Table 1.

NWC TP 5319, Part 1

TABLE 1 (Provided by NWC)
DATA FOR PLUME AND ATTENUATION CALCULATIONS
System Identification Number

Propellant Composition	1	2	3	4	5	6
Nitrocellulose (12.6%)	27.33	28.0	Same	Same		
Nitroglycerine	39.23	38.3				
Al/Mg (70/30) alloy	4.77	4.9				
Triacetin	7.66	7.2				
2-Nitrodiphenylamine	1.0	1.0				
Resorcinol	1.02	1.0				
Ammonium Perchlorate	19.06	19.6			75.0	66.0
Polyurethane					24.0	
Ti O ₂					1.0	
Butarez II						8.4
ZL 496						3.0
HX 868						.26
P Mapo						.34
Aluminum						12.0
Potassium	.002	.002	.002	.002	.007	.0075
Sodium	.005	.005	.005	.005	.022	.005
Radar Freq Hz	5**	9.3**	9.3**	9.3**	4.1**	*
Antenna off axis loc. in.	4.187	2.5	2.5	4.0	5.71	2.5**
Altitude, Kft.	25.	28.	28.	30	32	27+
Velocity ft/sec	1700				2400	
or Mach No.		2.16	2.16	2.17		2.0
Total Temp. TTU, °F		375	370	360		
Nozzle expansion half angle, deg.	12.5	12.5	12.5	12.5	9.3	15
Chamber Pressure, psia	250	260	235	275	573	1243
Nozzle exit diameter, in	6	1.655	1.655	2.628	5.27	2.4
Nozzle throat diameter, in	2.68	.712	.712	1.135	2.54	.8
c	5	5.4	5.4	5.36	4.3	9.
Missile Base Diameter, in	13.2	4.95	7.87	11.72	15.98	12.75
Boattail angle	0	0	0	0	0	0

* For system 6 use 35 GHz for transverse and 9.3 GHz for diagonal.

** For all systems use 9.3 GHz for transverse and for diagonal use frequency shown.

+ Changed from 29 by contractor.

NWC TP 5319, Part 1

3. The distribution of species and temperatures leaving the base region and the X-Y distribution of pressure and velocity which result from the combined calculations 1(1) and 1(2) shall be identified so they can be used as input for other aft-plume calculations at the NAVWPNSCEN.

COMPUTER PROGRAMS

During the six week study, a total of eighteen final computer program computations were completed for the six rocket motor firings with three for each firing. The three computer program codes used in these computations were:

- (1) Missile Base Model Component Program (NWC TP-5048)
- (2) MOC Model Component Program (NWC TP-5521)
- (3) Improved Aft-Plume Model Component Program (NWC TP-5521)

In order to conduct the required computations, the following revisions were required in the referenced programs:

- i. Initial attempts on 2 of the 6 base flow component computations did not converge. The program operated successfully on the remaining 4 cases. For the 2 cases, the base pressure was sufficiently low that negative pressure values were selected during the convergence process, which caused computational termination. The program was modified to provide a positive pressure estimate in the low pressure region. In addition, if the trailing shock pressures failed to converge with the specified accuracy in a set number of iterations (25 in these computations) the final pressure estimate was selected and the computations were continued. Using these new techniques, the remaining two computations were completed with acceptable accuracy.

NWC TP 5319, Part 1

2. Initial run attempts on 4 of the 6 MOC computations failed to converge. The major problem was due to estimated flow turning angles downstream of the trailing shock that were too great for the program to negotiate. The program was modified to permit initial assumptions of smaller turning angles. With relaxation of convergence tolerance, all four of the remaining cases were successfully run with acceptable accuracy. The results of these computations imply that test conditions were at the physical limit of the model to predict the inviscid structure, possibly due to onset of detached shocks.
3. The aft-plume program had never previously been successfully run with MOC input. Development of a subroutine to read and interpolate MOC output for convenient aft-plume input was completed during this study. Several significant changes were also required to the aft-plume program in order to predict plume structure with manually-input MOC data. All required changes were completed and all six aft-plume predictions were completed, including diagonal and transverse radar attenuation predictions.

It should be emphasized that the program decks of these programs supplied to NWC under a previous contractual study cannot be used to compute all of the cases considered in this study since the changes summarized above are not included in the NWC decks.

ADDITIONAL INPUT DATA

Table 1 summarized input data furnished by NWC for the 6 motor firings. Additional input data that were required were located in key references (principally BYU-010F). A summary of all required input data are given in Table 2 for all six cases and all three program components.

TABLE 2
SUMMARY OF INPUT DATA FOR SIX MOTOR FIRINGS

<u>Input Parameter</u>	<u>Units</u>	<u>Case 1</u>	<u>Case 2</u>	<u>Case 3</u>	<u>Case 4</u>	<u>Case 5</u>	<u>Case 6</u>
<u>A. BASE FLOW COMPONENT</u>							
Free Stream Static Pressure	psia	5.45	4.78	4.78	4.36	3.98	4.99
Free Stream Static Temperature	°R	429.90	432.00	429.40	422.30	404.90	302.70
Free Stream Mach Number	--	1.67	2.16	2.16	2.17	2.43	2.00
Free Stream Specific Heat	BTU/lb-°R	0.24	0.24	0.24	0.24	0.24	0.24
Free Stream Molecular Weight	lb/lb mol	28.97	28.97	28.97	28.97	28.97	28.97
Actual Physical Expansion Ratio	--	5.00	5.40	5.40	5.36	4.30	9.00
Chamber Pressure	psia	250.00	260.00	235.00	275.00	573.00	1243.00
Boattail Angle	deg	0.00	0.00	0.00	0.00	0.00	0.00
Nozzle Internal Exit Half-Angle	deg	12.50	12.50	12.50	12.50	9.30	15.00
Missile Base Radius	in	6.60	2.475	3.935	5.85	7.99	6.375
Nozzle Internal Exit Radius	in	3.00	0.8275	0.8275	1.314	2.635	1.2
<u>B. MOC COMPONENT</u>							
*Radial Value of Trailing Shock Intersection Point	ft	0.46	0.15	0.21	0.33	0.55	0.37
*Initial Sillpne Flow Angle	deg	2.68	-0.69	-10.57	-6.27	5.65	-1.03

*From BASE FLOW Program Output

TABLE 2 (Cont.)
SUMMARY OF INPUT DATA FOR SIX MOTOR FIRINGS

Input Parameter	Units	Case 1	Case 2	Case 3	Case 4	Case 5	Case 6
*Initial Pressure Behind Trailing Shock	1bf/ft ²	1046	779	431	505	900	780
*Initial Mach No. of External Flow Downstream of Trailing Shock	--	1.44	1.98	2.25	2.07	1.99	1.63
*Initial Mach No. of Internal Flow Downstream of Trailing Shock	--	2.81	2.91	3.05	3.02	3.28	3.50
*External Flow Heat Capacity Ratio	--	1.40	1.40	1.40	1.40	1.40	1.40
*Internal Flow Heat Capacity Ratio	--	1.20	1.20	1.20	1.20	1.30	1.20
*External Flow Heat Capacity	BTU/lb-°R	0.24	0.24	0.24	0.24	0.24	0.24
*Internal Flow Heat Capacity	BTU/lb-°R	0.408	0.407	0.407	0.407	0.409	0.416
*External Flow Molecular Weight	lb/lb mol	28.97	28.97	28.97	28.97	28.97	28.97
*Internal Flow Molecular Weight	lb/lb mol	28.33	28.49	28.49	28.49	23.22	28.06
*External Flow Static Temperature	°R	430	432	429	422	404	303
*Internal Flow Static Temperature	°R	3210	3186+	3176	3190	2247	3171
*Initial Internal Flow Angle	deg	14.43	15.60	9.25	14.54	21.61	19.17
*Internal Flow Mach No. Upstream of Trailing Shock	--	3.26	3.64	4.09	4.13	4.27	4.82
*Internal Flow Stagnation Temperature	°R	5551	5575	5560	5583	4426	6105

*From BASE FLOW Program Output
+this number was input incorrectly, but stagnation temperature was properly input. Effect on the final result was estimated to be small.

TABLE 2 (Cont.)

SUMMARY OF INPUT DATA FOR SIX MOTOR FIRINGS

Input Parameter	Units	Case 1	Case 2	Case 3	Case 4	Case 5	Case 6
*Base Region Pressure	psia	3.30	1.70	0.67	0.73	1.63	0.96
*Initial External Flow Angle	deg	-12.37	-18.60	-30.92	-28.52	-14.55	-28.25
*External Flow Mach No. Upstream of Trailing Shock	--	1.67	2.16	2.16	2.17	2.43	2.00
*External Flow Stagnation Temperature	°R	670	835	830	820	883	545
C. AFT-PLUME COMPONENT							
*Axial Position Where Aft-Plume Mixing Begins	in	6.245	2.068	2.717	3.936	6.020	4.025
*Radial Position Where Aft-Plume Mixing Begins	in	5.543	1.880	2.486	3.958	6.656	4.481
*Initial Radial Value of Inner Mixing Boundary	in	5.102	1.730	6.262	3.543	6.262	4.018
*Initial External Temperature Behind Trailing Shock	°R	473	467	493	441	493	356
*Flow Velocity External to Trailing Shock	ft/sec	1536	2101	2164	2133	2164	1505
*External Flow Angle	deg	2.689	-0.690	-10.56	-6.263	5.671	-1.051
*Flow Velocity Internal to Trailing Shock	ft/sec	7692	7868	7489	8016	7489	9001
*Internal Flow Angle	deg	2.689	-0.690	-10.56	-6.263	5.671	-1.051

*Output from BASE FLOW Program

TABLE 2 (Cont.)
SUMMARY OF INPUT DATA FOR SIX MOTOR FIRINGS

<u>Input Parameter</u>	<u>Units</u>	<u>Case 1</u>	<u>Case 2</u>	<u>Case 3</u>	<u>Case 4</u>	<u>Case 5</u>	<u>Case 6</u>
Free Stream Static Temperature	°R	430	432	405	422	405	303
*Chamber Enthalpy	Kcal/100G	-54.64	-54.43	-66.91	-54.43	-66.91	-43.74
*Ambient Air Stagnation Enthalpy	BTU/lb-°R	31.80	71.44	82.96	67.83	82.96	1.82
*Ambient Air Molecular Weight	lb/lb mol	29.97	28.57	28.97	28.97	28.97	28.97
*Pressure After Trailing Shock	psia	7.26	5.41	2.93	3.31	6.25	5.41
*Ambient Pressure Before Trailing Shock	psia	5.45	4.78	4.78	4.36	3.98	4.99
*Ambient Air Heat Capacity	BTU/lb-°R	0.24	0.24	0.24	0.24	0.24	0.24
*Initial Density of External Flow Behind Trailing Shock	lb/in ³	0.25 ⁻⁴	0.181 ⁻⁴	0.198 ⁻⁴	0.125 ⁻⁴	0.198 ⁻⁴	0.238 ⁻⁴
Transverse Radar Frequency	GHZ	9.3	9.3	9.3	9.3	9.3	35.0
Diagonal Radar Frequency	GHZ	5.0	5.3	4.1	9.3	4.1	9.3

*Output from BASE FLOW Program

NWC TP 5319, Part 1

Input card decks for each of the motor firings have been furnished under separate cover.

PREDICTED RESULTS

During this contract study, all three model components were successfully run for each of the six motor firings of Table 1. Known limitations of the output include the following:

- (a) For case 1, only transverse attenuation predictions were obtained. A negative argument was obtained for the first diagonal computation. No attempt was made to solve this problem.
- (b) For case 5, some of the thermochemical computations did not converge completely, so thermochemical properties could be somewhat in error. This problem is a basic difficulty with the EAFB Thermochemical program used in this study, and no attempt was made to solve this problem. In addition, only transverse radar computations were obtained for case 5, for the same reason identified above.

Computer output for these 18 computer analysis has been furnished under separate cover. Toward the completion of the computer computations for this contract, the IBM 7030 machine developed input conversion errors. At this point all base component and MGL component runs had been completed. In addition, aft-plume components for cases 1, 2, and 5 were also completed. After waiting for a period of about two weeks, at which time the IBM 7030 machine was still not fully functional, the aft-plume program was converted to the DEC-10 computer. The final three cases (3, 4, 6) were run on this machine. The output for these three cases shows some irregular use of the # symbol.

NWC TP 5319, Part 1

However, the predictions were still readily interpretable.

A summary of selected predicted parameters from each of the model components is shown in Table 3. A computerized graph of the constant weight fraction lines is shown in Fig. 1 for Case No. 2.

This report, together with the input cards and printed computer output, constitute completion of the contract study.

TABLE 3
SUMMARY OF SELECTED PREDICTED PARAMETERS FOR SIX MOTOR FIRINGS

<u>Parameter</u>	<u>Units</u>	<u>Case 1</u>	<u>Case 2</u>	<u>Case 3</u>	<u>Case 4</u>	<u>Case 5</u>	<u>Case 6</u>
<u>A. BASE FLOW COMPONENT</u>							
Chamber Temperature	°K	3084	3097	3089	3102	2459	3392
Wt. Fraction of Exhaust in Base Region	--	0.294	0.484	0.668	0.650	0.514	0.618
Base Temperature	°K	2197	2493	2507	2504	2402	2652
Trailing Shock Point (r,x)	in	6.2,5.5	2.1,1.9	2.7,2.5	3.9,4.0	5.0,6.7	4.0,4.5
Trailing Shock Pressure	psia	7.26	5.41	2.99	3.51	6.25	5.41
Base Pressure	psia	3.30	1.70	0.67	0.73	1.63	0.96
<u>B. MOC FLOW COMPONENT</u>							
Initial Siipline Flow Angle	deg	2.04	1.05	-6.31	-4.06	6.73	6.06
Initial External Trailing Shock Angle	deg	57.74	49.88	57.45	60.14	44.68	57.55
Initial Internal Trailing Shock Angle	deg	-26.72	-26.52	-24.31	-28.42	-24.31	-21.13
Length of MOC Region	ft.	1.25	0.44	0.54	0.84	1.93	1.17
Initial External Velocity (siipline)	ft/sec	1236	1666	1402	1324	1864	1129
Initial Internal Velocity (siipline)	ft/sec	7116	7423	7851	7608	7412	8861
Initial Trailing Shock Pressure	psia	7.31	5.02	2.32	3.01	5.38	3.22

TABLE 3 (Cont.)

Parameter	Units	Case 1	Case 2	Case 3	Case 4	Case 5	Case 6
C. AFT-PLUME COMPONENT							
Concentration Core Length	x/r ₁	26.5	43.8	26.0	34.7	58.2	49.4
Maximum Plume Diameter (at Cr = 0.1)	r/r ₁	4.62	6.27	8.45	8.30	5.62	12.09
Plume Length to Cr=0.1	x/r ₁	239	368	333	458	440	627
Maximum Plume Temperature	°K	2466	2524	2570	2544	2261	2625
Maximum Electron Density	e ⁻ /cc	5.93 ¹⁰	1.10 ¹¹	2.62 ¹¹	1.23 ¹¹	4.79 ⁹	1.72 ¹¹
Maximum Transverse Radar Attenuation	db	5.35	3.31	5.32	5.55	0.11	2.59
Maximum Transverse db Location	x/r ₁	40	60	30	50	40	105
Maximum Diagonal Radar Attenuation	db	--	16.6	57.9	64.6	--	302.0
Maximum Diagonal db Angle	deg	--	3.0	1.0	1.0	--	-1.0

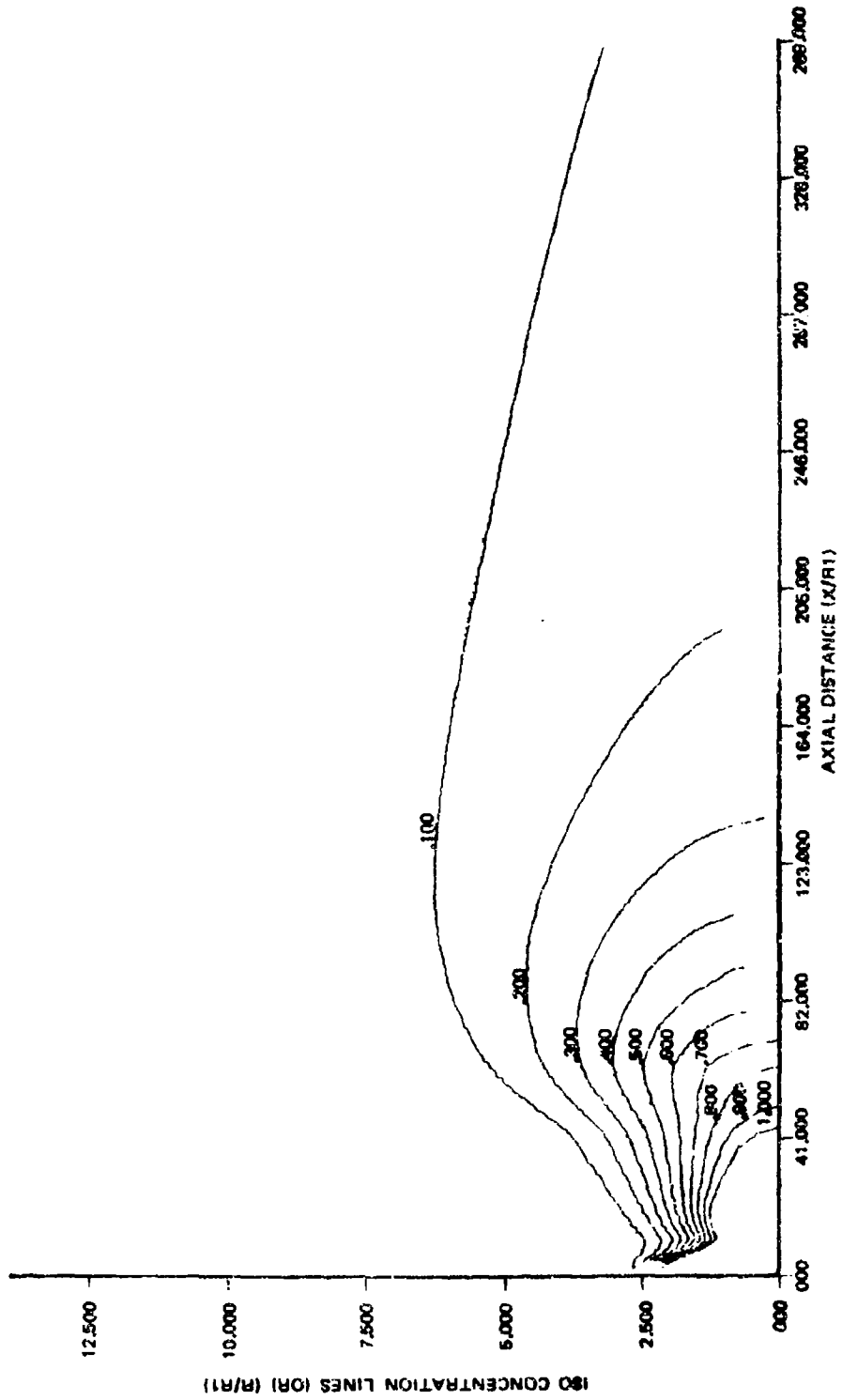


FIGURE 1. Schematic Computer-Produced Diagram of Aft-Plume Structure for Case 2.

INITIAL DISTRIBUTION

21 Naval Air Systems Command	
AIR-03B (1)	AIR-5203 (1)
AIR-03D (1)	AIR-533 (1)
AIR-30212 (2)	AIR-5332 (1)
AIR-330 (1)	AIR-576 (2)
AIR-330B (1)	AIR-5366 (1)
R-140C (1)	AIR-5357 (1)
AIR-503 (1)	AIR-538 (1)
AIR-5106 (1)	AIR-5381 (1)
AIR-520A (1)	AIR-540 (1)
6 Chief of Naval Material	
NSP-00 (1)	NSP-20 (1)
NSP-001 (2)	NSP-27 (1)
NSP-10 ()	
8 Naval Sea Systems Command	
SEA-03 (1)	SEA-034 (1)
SEA-033 (1)	SEA-034 (4)
SEA-0331 (1)	
3 Chief of Naval Research, Arlington	
Dr. Ralph Roberts (1)	
R. Jackel (1)	
ONR-473 (1)	
4 Naval Ordnance Station, Indian Head	
Code 5033H, G. Buckle (1)	
Code DGS (1)	
D. O. H. Dengel (1)	
A Camp (1)	
1 Naval Research Laboratory (W. W. Daivanz)	
1 Naval Undersea Center, San Diego (Code 127)	
1 Naval Surface Weapons Center, White Oak (Code KBM)	
1 Naval Plant Representative Office, Sunnyvale (Code SPL-3124)	
1 Assistant Navy Deputy, SAM-D/ASMS Joint Project, Redstone Arsenal	
4 Army Armament Command, Rock Island (AMSAP-SF)	
1 Army Materiel Command (AMCRD-DS/T)	
1 Picatinny Arsenal (B. Hornstein)	
3 Redstone Arsenal	
AMCPM-MDER (1)	
AMSMI-RDD (1)	
AMSMI-RDK, Dr. B. Walker (1)	
1 White Sands Missile Range (Technical Library)	
1 Air Force Avionics Laboratory, Wright-Patterson Air Force Base (AVWE, P. W. Springer)	
5 Air Force Rocket Propulsion Laboratory, Edwards Air Force Base	
Plans and Program Office (4)	
DYSP, Dr. L. Qulun (1)	
2 Directorate of Armament Development, Eglin Air Force Base	
ESATL-ELQT, Dr. D. Ebooghu (1)	
1 Defense Advanced Research Projects Agency, Arlington	
12 Defense Documentation Center	
1 Explosives Safety Board (GB-270)	
1 National Aeronautics and Space Administration (Code RP)	

- 2 George C. Marshall Space Flight Center
S&E, Aero-AI-7, Greenwood (1)
S&E/STN-21, Van Reed (1)
- 1 AeroChem Research Laboratories, Inc., Fremont, Calif. (Dr. J. J. Meeke)
- 1 Aerodyn, North West Industrial Park, Burlington, Mass. (A. B. B.)
- 1 Aerojet Solid Propulsion Company, Sacramento, Calif. (A. J. Stasick)
- 1 Allegany Ballistics Laboratory, Cumberland, Md. (G. Williams)
- 1 ARO, Incorporated, Keesler, Hanceville, Tenn.
Dr. W. M. McGregor, Research Branch (1)
C. R. Darrington (BTEP) Special Projects (1)
- 1 Atlantic Research Corporation, Alexandria, Va. (Dr. Goetz)
- 2 Brigham Young University, Provo, Utah
Dr. D. L. Smoot (1)
Lane Compton (1)
- 1 Cornell Aeronautical Laboratory, Inc., Buffalo (W. J. Gheeran)
- 1 General Applied Sciences Laboratory, Westbury, New York (Dr. R. Edelman)
- 1 General Dynamics Corporation, Pomona Division, Pomona, Calif. (Dr. Marvin C. Abrams)
- 3 Grumman Aerospace Corporation, Bethpage, New York
C. K. Wiley (1)
H. B. Hopkins (1)
S. Thendrew (1)
- 1 Hercules, Inc., Bacchus Works, Magna, Utah (H. J. Zeamer)
- 1 Hughes Aircraft Company, Inver City, Calif. (Bldg. 5/B-106, Dr. J. Cashen)
- 1 Hughes Aircraft Company, Los Angeles, Calif. (M. S. 4640, Bldg. 366, J. G. Seibold)
- 1 Jet Propulsion Laboratory, CIT, Pasadena, Calif.
- 1 Lockheed-Huntsville, Research & Engineering Center, Huntsville, Ala. (R. R. Mikatanian)
- 1 Lockheed Missiles & Space Company, Sunnyvale, Calif. (R. L. Count)
- 1 Lockheed Propulsion Company, Redlands, Calif. (W. Fuller)
- 1 McDonnell Douglas Astronautics, Huntington Beach, Calif. (R. Hoffman)
- 2 McDonnell Douglas Corporation, Santa Monica, Calif.
Advanced Propulsion Department, Department A-533, Group P-BBFO (1)
D. Chow (1)
- 2 Martin Company, Denver, Colo.
M. Hedrick (1)
R. J. Compton, Jr. (1)
- 1 North American Rockwell Corporation, Columbus, Ohio (B. Steginsky)
- 1 Pan American World Airways, Guided Missile Division, Patrick Air Force Base, Fla.
(Dr. H. A. Poehler)
Raytheon Manufacturing Company, Missile Systems Division, Bedford, Mass. (B. J. Reed)
- 1 Rockwell, Catalina Park, Calif. (R. A. Smith)
- 1 Rocketdyne, McGregor, Tex.
- 1 The Boeing Company, Seattle, Wash. (Dr. G. A. Clark)
- 2 The Martin Company, Orlando, Fla.
J. W. Fisher (1)
Code MP.30, Engineering Library (1)
- 1 Thiokol Chemical Corporation, Huntsville Division, Huntsville, Ala.
- 2 Thiokol Chemical Corporation, Wasatch Division, Brigham City, Utah
R. Lamb (1)
N. Anderson (1)
- 1 TSW Systems, Redondo Beach, Calif. (G. J. MacLeod)
- 1 United Technology Center, Sunnyvale, Calif. (T. A. LaFevre)

98 Chemical Propulsion Mailing List No. 249 dated December 1973 including Categories 1, 2, 3, & 5